

Fakulteit Ingenieurswese, Bou-omgewing & IT
Faculty of Engineering, Built Environment & IT

Investigating the Effect of Adding a Disc Liner to the Mill Shell of a Vertical Stirred Media Mill

by

Elizabeth Maria Ford

Dissertation submitted in partial fulfilment of the
requirements for the degree of
Master in Metallurgical Engineering

Supervisor: Prof. N Naudé

July 2020

School of Engineering
Department of Materials Science and Metallurgical Engineering



UNIVERSITEIT VAN PRETORIA
UNIVERSITY OF PRETORIA
YUNIBESITHI YA PRETORIA
Denkleiers • Leading Minds • Dikgopolo tsa Dihlalefi

ABSTRACT

Comminution processes are used in the metallurgical industry to reduce the particle size of mined ores in order to liberate valuable minerals for downstream separation and extraction. Comminution is a very energy intensive process and an incentive therefore exists for metallurgical operations to optimise the efficiency of the comminution processes employed. Stirred media mills are more efficient for regrinding and fine grinding duties as compared to ball mills that have traditionally been used in these applications. The efficiency of stirred media mills are influenced by both the operating conditions and physical design of the mill. Using the shear based power model, Radziszewski, 2013, hypothesised that the power draw of a vertical stirred media mill operating with pin or disc type stirrers could be increased by adding stationary liners to the mill shell. If this hypothesis holds true this approach might be used to improve the design of stirred media mills for new applications or it might be used to optimise existing mills by modifying the mill internals to improve on the stirrer and mill shell designs. The aim of this investigation was to test the hypothesis and to evaluate the effect of liner addition on the productivity and energy efficiency of the mill.

An experimental test work programme was developed to measure the mill power draw of four different mill geometries under comparative conditions. Two different stirrer designs were evaluated, the first stirrer consisted of a pin type agitator and the second stirrer consisted of a ring type agitator design. Testing was conducted with the two different stirrers operating in both a smooth mill vessel and in a mill vessel fitted with a stationary disc liner. The test work programme also included grinding tests to compare the productivity and energy efficiency of the four different mill configurations. Milling tests were conducted on mono-sized quartz feeds in particle size ranges of around $-150 + 106 \mu\text{m}$ and $-106 + 75 \mu\text{m}$. Results of these tests were used to calculate both the time based specific rate of breakage (S_i) and the energy normalised specific rate of breakage (S_i^E). The breakage rates were used to compare the four different mill geometries in terms of productivity (S_i) and energy efficiency (S_i^E). Further tests were conducted on quartz feed material with a natural feed size distribution. The specific energy requirement (kWh/t) and milling times (minutes) to reach a given target product grind were used to compare the performance of the four different mill geometries. Discrete Element Modelling (DEM) was used to qualitatively study and compare the charge conditions in each of the four geometries.

The experimental results supported the hypothesis and showed that the power draw of the pin and ring stirrer mills increased with the addition of a stationary disc liner to the mill shell. The additional mill power draw resulted in an increase in the productivity of the mill without any negative effect on the energy efficiency. The results of this work shows that there could be a potential to improve the milling performance of stirred media mills by adding stationary discs to the mill shell. Specifically a higher mill power draw could lead to either a smaller equipment footprint in the case of new mills or to a larger throughput capacity or finer product grind in existing mills that have been retrofitted with an improved internal design. Further work would be required to confirm the results of this study on a larger scale and in a continuous milling configuration.


Some general observations were made on the shear based power model proposed by Radziszewski, 2013. When applied to this current investigation the shear based power model correctly predicted that the addition of the disc liner to the mill vessel will result in an increase in the mill power draw. However the model did not correctly predict the relative power draw of the pin versus ring stirrer designs. The shear based power model predicted that the ring stirrer will draw more power than the pin stirrer, but the experimental work showed the opposite result. The pin stirrer had a higher power draw than the ring stirrer. DEM data showed that the pin stirrer resulted in a higher average bead velocity in the mill as compared to the ring stirrer. It is therefore postulated that the reason for the higher power draw with the pin stirrer was that this design provided a better transfer of movement from the mill shaft to the mill charge.

PLAGIARISM DECLARATION

Full names	Elizabeth Maria Ford
Student number	21045772
Topic of work	Master's Thesis - Investigating the Effect of Adding a Disc Liner to the Mill Shell of a Vertical Stirred Media Mill

Declaration

1. I understand what plagiarism is and am aware of the University's policy in this regard.
2. I declare that this report is my own original work. Where other people's work has been used (from a printed source, internet or any other source), this has been properly acknowledged and referenced in accordance with the requirements as stated in the University's plagiarism prevention policy
3. I have not used another student's past written work to hand in as my own.
4. I have not allowed, and will not allow, anyone to copy my work with the intention of passing it off as his or her own work.



Signature

ACKNOWLEDGEMENTS

I would like to acknowledge the contributions and express my gratitude to the following people and organisations:

- My supervisor, Prof. Natasia Naudé, for her input and guidance.
- My employer, Mintek, for making equipment and resources available for executing of the test work programme and DEM modelling.
- Laboratory staff who assisted me during test work execution; Ronny Podile and Onkarabile Songwana.
- My husband, James, for his continued support.

“I can do all things through Christ who gives me strength.” - Philippians 4:13

TABLE OF CONTENTS

1	Introduction	1
1.1	Background.....	1
1.2	The Shear Based Power Model	1
1.3	Value Proposition.....	2
1.4	Hypothesis	2
1.5	Project Objective and Research Questions.....	2
1.6	Scope.....	2
2	Literature Review	4
2.1	Comminution Equipment.....	4
2.2	Stirred Media Mills.....	5
2.2.1	Gravity Induced Stirred Media Mills.....	5
2.2.2	Fluidised Stirred Media Mills	6
2.2.2.1	Glencore IsaMill	7
2.2.2.2	Metso SMD Mill.....	8
2.2.2.3	Outotec HIG Mill.....	10
2.2.2.4	FLSmith VXP Mill	12
2.2.3	Operating Ranges of Different Stirred Media Mills	13
2.2.4	Typical Flowsheet Configurations Utilising Stirred Media Mills.....	13
2.2.5	Energy Efficiency of Stirred Media Mills Compared to Ball Mills	18
2.2.6	Factors That Affect the Energy Efficiency of Stirred Media Mills	21
2.2.6.1	Pulp Solids Concentration	21
2.2.6.2	Media Size	24
2.2.6.3	Media Density	24
2.2.6.4	Stirrer Tip Velocity.....	24
2.2.6.5	Stress Intensity – interrelation of stirrer speed, media density, media size	25
2.2.6.6	Media Filing Level	26
2.2.6.7	Ratio of Beads to Slurry	26
2.2.6.8	Stirrer and Chamber Geometry and Dimensions	26
2.2.6.9	Pulp Viscosity, Dispersants, and Grinding Aids.....	26
2.3	Shear Based Power Model Theory	27
2.4	Particle Breakage Rates	30
2.4.1	Specific rate of Breakage (S_i).....	30
2.4.2	Experimental Determination of Specific Rate of Breakage (S_i)	32
2.4.3	Energy Normalised Rate of Breakage (S_i^E).....	33
2.4.4	Non-first order kinetics	35
2.5	Computational Modelling of Stirred Media Mills	36
2.5.1	Particle Breakage Rates	37
2.5.2	Charge Movement.....	38
2.5.3	Wear Patterns	39
2.5.4	Mill Optimisation.....	40
2.5.5	Novel Modelling Approaches.....	40
2.6	Discrete Element Modelling (DEM)	40
2.6.1	Soft Particle DEM Formulation	41
2.7	Literature Conclusions	43
3	Research Methodology	44
3.1	Overview of Research Methodology	44
3.2	Experimental Design Considerations	45
3.2.1	Quantifying of Results	45
3.2.2	Type of Sample to Use.....	46
3.2.3	Scaling of Geometries.....	46

3.2.4	Batch Operation versus Continuous Operation	46
3.2.5	Design and Fabrication of Stirrers and Mill Vessel	46
3.2.6	Feed Particle Size and Ceramic Bead Size	47
3.2.7	Pulp Solids Concentration	47
3.2.8	Mill Filling Level	47
3.2.9	Ratio of Pulp to Beads	48
3.2.10	Stirrer Speed	49
3.2.11	Grinding Media Density	49
3.3	Batch Milling Test Rig	49
3.3.1	Torque Measurement Calibration	50
3.4	LIGGGHTS Open Source DEM Software	52
3.5	Shell and Stirrer Design Process – DEM Virtual Prototyping	52
3.5.1	DEM Virtual Prototyping Parameter Calibration	53
3.5.2	DEM Virtual Prototyping Simulations	57
3.6	Final Stirrer and Mill Designs Used in Experiments	62
3.7	Shear Volume Calculations of Mill Geometries	63
3.8	Milling Test Feed Material	63
3.8.1	Sample Preparation	64
3.8.2	PSD of Silica Feeds	64
3.8.3	Chemical and Mineralogical analysis of the Silica	64
3.8.4	Specific Gravity of the Silica	65
3.9	Ceramic Grinding Beads Density Characterisation	65
3.10	Experimental Test Work Matrix	65
3.10.1	Bead only tests	65
3.10.2	Beads and water tests	66
3.10.3	Repeatability grinding tests on silica flour	67
3.10.4	Mono-sized feed grinding tests on -150 +106 μm and -106 + 75 μm silica	67
3.10.5	Natural feed size distribution grinding tests on silica flour	67
3.11	Milling Conditions	67
3.12	Mill Product PSD Analysis	68
4	Experimental Results and Discussion	69
4.1	Results of Bead Only Tests	69
4.2	Results of Bead and Water Tests	70
4.3	Results of Repeatability Tests	75
4.4	Results of Mono Sized Feed Grinding Tests	75
4.5	Results of Silica Flour Feed Grinding Tests	78
4.6	Results of DEM Modelling	84
4.7	Discussion of Results	86
4.7.1	Discussion of Results - Research Question 1	86
4.7.2	Discussion of Results – Research Question 2	88
4.7.3	Discussion of Results – Research Question 3	90
4.7.4	Observations on the Shear Based Power Model	92
5	Conclusions and Recommendations	95
6	References	96
7	Appendix	103
7.1	Stirrer and Mill Vessel Designs	103
7.1.1	New Mill Vessel with Disc Liner	103
7.1.2	New ring and pin stirrer design details	106
7.1.3	Existing Stirrer Design Details	111
7.2	Shear Volume Formulas Derivation	115
7.2.1	Shear Volume Formula Derivation for the Pin Tip	115
7.2.2	Shear Volume Formula Derivation for the Pin Bottom Half	116

7.2.3	Shear Volume Formula Derivation for the Pin Top Half.....	117
7.2.4	Shear Volume Formula Derivation for the Outer Ring.....	119
7.2.5	Shear Volume Derivation for the Spoke	119
7.2.6	Formula Derivation for the Spoke Arc Length	120
7.3	Shear Volume Calculations.....	121
7.4	PSD of Silica Feeds	125
7.5	XRD Results	126
7.6	Silica Density Measurement Results.....	127
7.7	Ceramic Grinding Beads Density Measurements.....	128
7.8	Experimental Results – Beads and Water Power Draw	131
7.9	Experimental Results – Repeatability Tests.....	136
7.10	Experimental Results - Mono-size Silica Grinding Tests.....	141
7.11	Experimental Results – Silica Flour Grinding Tests	157
7.12	DEM Virtual Prototyping.....	181
7.12.1	DEM Calibration Model Torque	181
7.12.2	DEM Calibration Model Charge Profiles.....	185
7.12.3	DEM Virtual Prototyping Simulations Model Torque	190
7.12.4	DEM Virtual Prototyping Simulations Charge Profiles	191
7.13	DEM Re-calibrated Model.....	193
7.13.1	DEM Re-calibrated Model Simulations Torque	193
7.13.2	DEM Re-calibrated Model Simulations Charge Profiles	194
7.14	Custom Post Processing Computer Codes Written for DEM modelling	196
7.14.1	Code for Calculating Per Second Average Torque	196
7.14.2	Code for Calculating Velocity Histograms	199
7.15	Silica Flour Data Sheet	204

FIGURES

Figure 1: Picture of a Vertimill installation with four mills, www.metso.com 2018.....	5
Figure 2: General Arrangement Drawing of a Metso Vertimill, Allen 2013	6
Figure 3: General Arrangement Drawing of a Nippion-Eirich tower mill, (www.nippon-eirich , 2018).....	6
Figure 4: Picture of an IsaMill installation, www.isamill.com 2018.....	7
Figure 5: Schematic of IsaMill internals and charge flow, www.isamill.com 2018	8
Figure 6: IsaMill with shell removed and shaft exposed for maintenance, www.isamill.com 2018	8
Figure 7: Picture of an SMD installation with two mills, www.metso.com 2018	9
Figure 8: Schematic showing stirrer arrangement in the SMD, Allen 2013	9
Figure 9: Example of a slurry-media vortex in an SMD mill during operation, Ntsele & Allen 2012.....	10
Figure 10: Picture of a HIG mill installation, HIG mill located on the left, www.outotec.com 2018	10
Figure 11: Cross section schematic of a HIG mill, Astholm 2015.....	11
Figure 12: Schematic of flow through a HIG mill, Lehto et al. 2013.....	11
Figure 13: Picture of an industrial VXP mill installation, FLSmidth 2018	12
Figure 14: Schematic of a VXP mill installation showing mill cross section, FLSmidth 2011.....	12
Figure 15: Open circuit SMD, Metso 2018	13
Figure 16: Open circuit SMD milling a scalped feed, Metso 2018	14
Figure 17: Closed circuit SMD, Metso 2018.....	14
Figure 18: Mount Isa Pb/Zn Concentrator Flowsheet, Xstrata Technology	15
Figure 19: Anglo Platinum Generic Flotation Circuit Layout, Xstrata Technology	16
Figure 20: IsaMill circuit configuration, Pease et al.	16
Figure 21: Typical HIG mill circuit configuration, Keikkala et al. 2015.....	17
Figure 22: Kevitsa Flotation Circuit – HIG mill for Cu regrind, First Quantum Minerals Ltd.	17
Figure 23: HPGR-Vertimill circuit, Metso 2012.....	18
Figure 24: HPGR-ball mill circuit, Wang 2013.....	18
Figure 25: Graphical example of Bond Energy versus Product Size Relationship (Snow et al., 1997) ..	19
Figure 26: Comparison of energy requirement for grinding at various stages, Jankovic 2003.	20
Figure 27: Relative performance of stirred and tumbling mills, Lichter & Davey 2006	21
Figure 28: Grind versus energy required as a function of solids concentration, Jankovic 2003	23
Figure 29: Energy efficiency, E_f , for limestone grinding, Zeng et al 1996	23
Figure 30: Energy required to reach the same target grind at various mill conditions (SI), (Kwade, 2003)	25
Figure 31: Example of shear volume calculation, Radziszewski 2013	28
Figure 32: Various hypothetical geometrical mill arrangements, Radziszewski 2013	29
Figure 33: Example of a first order plot of 1.18 mm x 850 μ m anthracite in a 0.6m diameter ball mill (Austin et al., 1984).....	31
Figure 34: Specific rates of breakage of a South African gold ore as a function of particle size (Austin et al., 1984).....	32
Figure 35: First-order plot for dry grinding of 1.18 mm x 850 μ m petroleum coke in a 200mm i.d. ball mill (Austin et al., 1984).....	33
Figure 36: Example of a first order plot on an energy normalised basis (reproduced in part from Herbst and Fuerstenau, 1973).....	34
Figure 37: Illustrations showing deviation from first order kinetics, (Austin et al., 1984)	36
Figure 38: PEPT Occupancy plots for different impeller types at 520 rpm, (Conway-Baker et al., 2002).....	38
Figure 39: Energy absorption rates a) tower mill normal b) pin mill normal c) tower mill tangential d) pin mill tangential, (Sinnott, 2006).....	39
Figure 40: Wear of IsaMill disc holes a) new disc b) 4 months c) 8 months d) wear pattern on actual mill disc (Jayasundara et al., 2011b).....	39
Figure 41: Variation in media speed and distribution at a) 70% filling b) 80% filling c) 90% filling, (Cleary et al., 2015).....	40
Figure 42: Diagrammatic representation of normal and tangential forces used in DEM, Cleary 1998 ...	41

Figure 43: Four geometries evaluated in this investigation a) 12-pin – smooth vessel, b) 12-pin – disc vessel, c) ring – smooth vessel, d) ring – disc vessel.....	45
Figure 44: Stirred media milling test rig.....	49
Figure 45: Torque arm and load cell installed on milling test rig.....	51
Figure 46: Calibration mass suspended from torque arm a) top view b) side view	51
Figure 47: Torque transducer during calibration a) zero calibration b) span calibration	51
Figure 48: Initial conceptual stirrer designs a) 18-pin stirrer b) 3-disc stirrer	52
Figure 49: Existing pin stirrer used for DEM model calibration purposes	53
Figure 50: Range of coefficient of restitution and friction values evaluated during DEM model calibration	55
Figure 51: Effect of coefficient of restitution on DEM model torque.....	56
Figure 52: Effect of friction coefficient on DEM model torque	56
Figure 53: DEM simulations of conceptual stirrers in smooth vessel a) 18-pin stirrer b) 3-disc stirrer ...	57
Figure 54: Turbulent DEM charge movement observed with the conceptual 3-disc stirrer	58
Figure 55: Revised conceptual stirrer designs a) 12-pin stirrer b) 2-disc stirrer c) ring stirrer	58
Figure 56: Turbulent DEM charge movement observed with the conceptual 2-disc stirrer	59
Figure 57: Disc Vessel design.....	59
Figure 58: Final stirrer design DEM simulations a) 12-pin - smooth vessel, b) 12-pin - disc vessel, c) ring stirrer - smooth vessel, d) ring stirrer - disc vessel.....	60
Figure 59: Torque Predicted from DEM Virtual Prototyping Model.....	61
Figure 60: DEM Virtual Prototyping Model Velocity Histogram for different mill geometries	61
Figure 61: Ring and pin stirrers fabricated for this investigation.....	62
Figure 62: Disc liner mill vessel a) two half pieces b) assembled.....	62
Figure 63: Smooth mill vessel a) side view b) top view	62
Figure 64: Milling test feed a) silica sand, b) silica flour	63
Figure 65: PSD of silica feeds	64
Figure 66: Results of Bead Only Tests.....	69
Figure 67: Comparison of Actual and Predicted Relative Power Draw	70
Figure 68: Test W-1 Pin in Smooth Bead and Water Power Draw	71
Figure 69: Test W-2 Pin in Disc Bead and Water Power Draw	71
Figure 70: Test W-3 Ring in Smooth Bead and Water Power Draw.....	71
Figure 71: Test W-4 Ring in Disc Bead and Water Power Draw	72
Figure 72: Normal mixed charge conditions observed during tests.....	72
Figure 73: Charge with ring stirrer in smooth vessel and 2 mm beads at speeds above 400 rpm	72
Figure 74: Bead and Water Tests Power Draw Comparison of Geometries with 3 mm Media	73
Figure 75: Bead and Water Tests Power Draw Comparison of Geometries with 2 mm Media	73
Figure 76: Bead and Water Tests Power Draw Comparison of Geometries with 1 mm Media	74
Figure 77: Power Draw Increase due to Addition of Disc Liner – Pin Stirrer	74
Figure 78: Power Draw Increase due to Addition of Disc Liner – Ring Stirrer	74
Figure 79: Picture of a milling test conducted on the mono-sized silica	76
Figure 80: Picture of a milling test conducted with the silica flour	78
Figure 81: DEM simulations a) 12-pin - smooth vessel, b) 12-pin - disc vessel, c) ring stirrer - smooth vessel, d) ring stirrer - disc vessel.....	85
Figure 82: DEM Model bead velocity histogram for the different mill configurations	86
Figure 83: Pin Stirrer Increase in Power Draw due to Addition of Disc – Various Tests.....	87
Figure 84: Ring Stirrer Increase in Power Draw due to Addition of Disc – Various Tests	88
Figure 85: Pin Stirrer Increase in Milling Productivity due to Addition of Disc – Various Tests.....	89
Figure 86: Ring Stirrer Increase in Milling Productivity due to Addition of Disc – Various Tests	90
Figure 87: Pin Stirrer Increase in Milling Energy Efficiency due to Addition of Disc – Various Tests	91
Figure 88: Ring Stirrer Increase in Milling Energy Efficiency due to Addition of Disc – Various Tests ...	92
Figure 89: Smooth Mill Vessel Comparative Power Draw – Pin versus Ring stirrer at 400 rpm.....	93
Figure 90: Disc Mill Vessel Comparative Power Draw – Pin versus Ring stirrer at 400 rpm	94

Figure 91: The two disc mill vessel half pieces - 3D drawing	103
Figure 92: Assembled disc mill vessel – 3D drawing	103
Figure 93: Cross section drawing of disc mill vessel showing dimensions	104
Figure 94: Top view of disc mill vessel showing spout arrangement details	105
Figure 95: Ring stirrer – 3D drawing	106
Figure 96: 12-pin stirrer – 3D drawing	106
Figure 97: Ring stirrer arrangement drawing	107
Figure 98: Ring stirrer cross section drawing	108
Figure 99: 12 pin stirrer arrangement drawing	109
Figure 100: 12 pin stirrer cross section drawing	110
Figure 101: Existing stirrer – 3D drawing	111
Figure 102: Existing stirrer pin detail top view	112
Figure 103: Existing stirrer cross section drawing – view 1	113
Figure 104: Existing stirrer cross section drawing – view 2	114
Figure 105: Quantitative XRD results of silica sand	126
Figure 106: Quantitative XRD results of silica flour	126
Figure 107: Simulation 1 Charge Profile a) view of x-axis b) view of y-axis	185
Figure 108: Simulation 2 Charge Profile a) view of x-axis b) view of y-axis	185
Figure 109: Simulation 3 Charge Profile a) view of x-axis b) view of y-axis	185
Figure 110: Simulation 4 Charge Profile a) view of x-axis b) view of y-axis	186
Figure 111: Simulation 5 Charge Profile a) view of x-axis b) view of y-axis	186
Figure 112: Simulation 6 Charge Profile a) view of x-axis b) view of y-axis	186
Figure 113: Simulation 7 Charge Profile a) view of x-axis b) view of y-axis	187
Figure 114: Simulation 8 Charge Profile a) view of x-axis b) view of y-axis	187
Figure 115: Simulation 9 Charge Profile a) view of x-axis b) view of y-axis	187
Figure 116: Simulation 10 Charge Profile a) view of x-axis b) view of y-axis	188
Figure 117: Simulation 11 Charge Profile a) view of x-axis b) view of y-axis	188
Figure 118: Simulation 12 Charge Profile a) view of x-axis b) view of y-axis	188
Figure 119: Simulation 13 Charge Profile a) view of x-axis b) view of y-axis	189
Figure 120: Simulation 14 Charge Profile a) view of x-axis b) view of y-axis	189
Figure 121: Simulation 15 Charge Profile a) view of x-axis b) view of y-axis	189
Figure 122: Pin in Smooth Virtual Prototyping Simulation a) view of x-axis b) view of y-axis	191
Figure 123: Ring in Smooth Virtual Prototyping Simulation a) view of x-axis b) view of y-axis	191
Figure 124: Pin in Disc Virtual Prototyping Simulation a) view of x-axis b) view of y-axis	191
Figure 125: Ring in Disc Virtual Prototyping Simulation a) view of x-axis b) view of y-axis	192
Figure 126: Pin in Smooth DEM Charge Profile a) view of x-axis b) view of y-axis	194
Figure 127: Ring in Smooth DEM Charge Profile a) view of x-axis b) view of y-axis	194
Figure 128: Pin in Disc DEM Charge Profile a) view of x-axis b) view of y-axis	194
Figure 129: Ring in Disc DEM Charge Profile a) view of x-axis b) view of y-axis	195

TABLES

Table 1: Factors that influence stirred media milling as investigated by various authors	22
Table 2: Shear volume for various hypothetical mill geometries, Radziszewski 2013	30
Table 3: Computational Modelling of Stirred Media Mills by Various Authors	37
Table 4: Torque data for 8-pin stirrer in smooth vessel, 400 rpm, dry operation	54
Table 5: Summarised results of DEM calibration process	55
Table 6: DEM parameters used in the virtual prototyping DEM simulations	57
Table 7: Torque Predicted from DEM Virtual Prototyping Model	60
Table 8: Average DEM Virtual Prototyping Model bead velocities	61
Table 9: Radziszewski shear volume calculated for the various geometries	63
Table 10: Experimental Test work Matrix	66
Table 11: Milling conditions	68
Table 12: Results of Bead Only Tests	69
Table 13: Milling Test Repeatability	75
Table 14: Breakage Rates for Mono-sized Silica Grinding Tests	77
Table 15: Power Draw Comparison for Mono-sized Silica Grinding Tests	77
Table 16: Power Draw Comparison for Silica Flour Grinding Tests	79
Table 17: Silica Flour Milling Test Results – Pin Stirrer Smooth Vessel versus Disc Vessel	80
Table 18: Silica Flour Milling Test Results – Ring Stirrer Smooth Vessel versus Disc Vessel	81
Table 19: Silica Flour Milling Test Results – Pin versus Ring Stirrer Smooth Vessel	82
Table 20: Silica Flour Milling Test Results – Pin versus Ring Stirrer Disc Vessel	83
Table 21: DEM Model Parameters Used for Revised DEM Simulations	84
Table 22: DEM Model Torque versus Actual Measured Torque	84
Table 23: DEM model average bead velocities for the different mill configurations	85
Table 24: Mill Power Draw Increase Due to Addition of Disc to Mill Vessel – Various Tests	87
Table 25: Mill Production Rate Increase Due to Addition of Disc to Mill Vessel – Various Tests	89
Table 26: Mill Energy Efficiency Increase Due to Addition of Disc to Mill Vessel – Various Tests	91
Table 27: Comparative Power Draw Data - Pin Stirrer versus Ring Stirrer	93
Table 28: PSD of -150 + 106 μm Mono-Sized Silica Feed	125
Table 29: PSD of -106 + 75 μm Mono-Sized Silica Feed	125
Table 30: PSD of Natural Size Silica Feed	125
Table 31: Specific gravity measurements - silica feed for mono-sized feed tests	127
Table 32: Specific gravity measurements - silica feed for natural particle distribution tests	127
Table 33: Bulk density measurement on 3 mm ceramic beads	128
Table 34: Material density measurement on 3 mm ceramic beads	128
Table 35: Beads fractional voidage calculation – 3 mm beads	128
Table 36: Bulk density measurement on 2 mm ceramic beads	129
Table 37: Material density measurement on 2 mm ceramic beads	129
Table 38: Beads fractional voidage calculation – 2 mm beads	129
Table 39: Bulk density measurement on 1 mm ceramic beads	130
Table 40: Material density measurement on 1 mm ceramic beads	130
Table 41: Beads fractional voidage calculation – 1 mm beads	130
Table 42: Test W-1 Data	131
Table 43: Test W-2 Data	132
Table 44: Test W-3 Data	133
Table 45: Test W-4 Data	134
Table 46: Test W-1 to W-4 Comparison	135
Table 47: Test R-1 Data	136
Table 48: Test R-2 Data	137
Table 49: Test R-3 Data	138
Table 50: Test R-4 Data	139

Table 51: Test R-5 Data	140
Table 52: Test M-1 PSD Data	141
Table 53: Test M-2 PSD Data	142
Table 54: Test M-3 PSD Data	143
Table 55: Test M-4 PSD Data	144
Table 56: Test M-5 PSD Data	145
Table 57: Test M-6 PSD Data	146
Table 58: Test M-7 PSD Data	147
Table 59: Test M-8 PSD Data	148
Table 60: Test M-1 Breakage Rates	149
Table 61: Test M-2 Breakage Rates	150
Table 62: Test M-3 Breakage Rates	151
Table 63: Test M-4 Breakage Rates	152
Table 64: Test M-5 Breakage Rates	153
Table 65: Test M-6 Breakage Rates	154
Table 66: Test M-7 Breakage Rates	155
Table 67: Test M-8 Breakage Rates	156
Table 68: Test N-1 PSD Data	157
Table 69: Test N-2 PSD Data	158
Table 70: Test N-3 PSD Data	159
Table 71: Test N-4 PSD Data	160
Table 72: Test N-5 PSD Data	161
Table 73: Test N-6 PSD Data	162
Table 74: Test N-7 PSD Data	163
Table 75: Test N-8 PSD Data	164
Table 76: Test N-9 PSD Data	165
Table 77: Test N-10 PSD Data	166
Table 78: Test N-11 PSD Data	167
Table 79: Test N-12 PSD Data	168
Table 80: Test N-1 Milling Data.....	169
Table 81: Test N-2 Milling Data.....	170
Table 82: Test N-3 Milling Data.....	171
Table 83: Test N-4 Milling Data.....	172
Table 84: Test N-5 Milling Data.....	173
Table 85: Test N-6 Milling Data.....	174
Table 86: Test N-7 Milling Data.....	175
Table 87: Test N-8 Milling Data.....	176
Table 88: Test N-9 Milling Data.....	177
Table 89: Test N-10 Milling Data.....	178
Table 90: Test N-11 Milling Data.....	179
Table 91: Test N-12 Milling Data.....	180

1 Introduction

1.1 Background

Comminution processes are employed to reduce the particle size of mineral ores in order to liberate the valuable minerals for downstream recovery and concentration. By its nature comminution is a very energy intensive operation. It is estimated that the energy required for comminution contributes to about 2% of the world wide electrical power demand. For a typical mining operation the comminution energy is estimated to contribute to about 34% to 52% of the direct electrical energy usage (Napier-Munn, 2015). A recent trend in the metallurgical industry is that many of the new ores being mined consist of minerals that are characterised by a fine intergrowth with other minerals or gangue. In order to ensure sufficient liberation for the downstream separation process it is then required to mill the ore to very fine particle sizes (Lichter & Davey, 2006). This comes at an additional comminution energy cost. It is therefore important for mining operations to reduce the cost of comminution and one way to do this is to optimise the equipment used for size reduction so that it is more energy efficient.

Stirred media mills are used for fine grinding of particles, and these types of mills are applied in various different industries. Typical industrial applications include the milling of minerals, ceramic materials, paint pigments, chemical products and microorganisms (Kwade, 1999). It has been shown that stirred media mills are more energy efficient for the re-grinding of ore in the minerals processing industry as compared to traditional ball milling processes (Lichter & Davey, 2006). For product grinds below 75 μm stirred media mills exceed ball mills with regard to energy efficiency, requiring less specific energy input (kWh/t) to produce a targeted grind size. Stirred mills have therefore become the preferred option for regrinding and fine grinding in minerals processing circuits (Jankovic, 2003). The design and operating parameters of a stirred media mill does have an effect on the efficiency of the grinding process occurring in the mill. There are many factors that can influence the energy efficiency, some of the main factors are the physical mill design, the choice of grinding media size and density, the speed of the stirrer and the slurry density (Jankovic, 2003). The comminution energy required for a milling application is therefore not a fixed value but is influenced by the mill configuration.

1.2 The Shear Based Power Model

Radziszewski, 2013, proposed that the power draw of a stirred media mill might be calculated using equation 1:

$$P_{\tau} = \mu \omega^2 V_{\tau} \quad (1)$$

Where P_{τ} is the power draw in units of Watt, μ is the viscosity with units of Ns/m^2 of the mill charge which consists of the fluidised slurry and media mixture, ω is the rotational speed of the stirrer in units of rad/s , and V_{τ} is a term that is called the shear volume with units of m^3 . Radziszewski evaluated various hypothetical vertical stirred media mill geometries and calculated the shear volume for each of these hypothetical geometries. The impeller types evaluated included pins, discs, screws, and cylinders. With the pin and disc type of agitators it was postulated that the shear volume of the mill could be increased by the addition of liners to the stationary mill shell. The liners took the form of either pins or discs installed on the shell in such a way that it protrudes into the space between consecutive sets of stirrer agitators. It was further postulated that the shear volume could be significantly increased by the addition of liners to the mill shell. In the case of the pin stirrer the shear volume could potentially be increased by 32% using pin liners and up to 211% using disc liners. In the case of the disc stirrer the shear volume could be potentially be increased by 28% using pins as liners and by 55% by adding discs as liners. According to the shear based power model the power draw of the mill is proportional to the shear volume under similar operating conditions. Based on this Radziszewski, 2013, then postulated that the power draw of a mill operating with pin or disc type stirrers might be increased by adding liners to the mill shell. However no experimental work was presented to evaluate this hypothesis.

1.3 Value Proposition

If the Radziszewski, 2013, hypothesis holds true this approach might be used to improve the design of stirred media mills for new applications or it might be used to optimise existing mills by modifying the mill internals to improve on the stirrer and mill shell designs. Specifically a higher mill power draw could lead to either a smaller equipment footprint in the case of new mills or to a larger throughput capacity or finer product grind in existing mills that have been retrofitted with an improved internal design. However a question that also arises is if the energy efficiency of the comminution process will be affected by the change in mill internal geometrical design.

1.4 Hypothesis

During this research investigation a hypothesis postulated by Radziszewski, 2013, was tested. The hypothesis states that the power draw of a stirred media mill operating with pin or disc type stirrers could be increased by adding stationary liners to the mill shell.

1.5 Project Objective and Research Questions

Radziszewski, 2013, presented no experimental work to evaluate this hypothesis therefore the objective of this investigation was to design and execute an experimental programme that will provide data for a first attempt at evaluating the hypothesis. For this investigation the following specific research questions were formulated:

Research question 1: Will the power draw of a pin or disc type fluidised vertical stirred media mill be increased by the addition of shear surface area, in the form of added mill shell liners?

Research question 2: Will the additional mill power draw increase the productivity of the mill?

Research question 3: Will the addition of the liner surfaces affect the energy efficiency of the mill?

Productivity relates to the amount of product at a desired grind size that is produced in a unit of time. In industrial terms it relates to the throughput rate (tonne/hour) that can be achieved with a given size of equipment. Energy efficiency relates to the amount of energy required to produce a given amount of product at the required grind size (kWh/tonne). Both of these factors influences the economics of a comminution operation as it impacts on both the capital and operating costs of the plant.

1.6 Scope

As part of this investigation an experimental test work programme was developed to generate data in order to answer the research questions formulated in section 1.5. The programme included the design and fabrication of stirrer and mill equipment components to be used during the test work. The tests were aimed at generating comparative power draw and milling performance data. Discrete Element Modelling (DEM) was used during the equipment design and data analysis phases of the project as a virtual prototyping tool and also to provide insight into test work observations.

In Industrially available stirred mill units there is a distinction made between two types of stirred media mills based on the design and charge movement. These two types of mills are the gravity induced and fluidised type of mills. Fluidised stirred media mills can either be designed in a horizontal or a vertical arrangement of the stirrer shaft. The scope of this investigation will only focus on the experimental testing of vertical fluidised stirred media milling configurations.

The dissertation is structured as follows:

- Section 2: Literature Review. This section provides relevant background regarding stirred media mills, comminution energy requirements, the shear based power model, and Discrete Element Modelling (DEM) .
- Section 3: Research Methodology. In this section the focus is on the experimental test work programme and experimental design considerations as well as on the virtual prototyping process employed to design the stirrer and mill geometries used during test work.
- Section 4: Experimental Results and Discussion. The results of the bead and water, mono-sized silica, and silica flour grinding tests are presented in this section. DEM results of the various geometries were used to qualitatively compare the charge movement in each of the mill configurations.
- Section 5: Conclusions and Recommendations. Main findings of the test work programme are summarised and recommendations are made for further work.
- Section 6: References
- Section 7: Appendices

2 Literature Review

2.1 Comminution Equipment

Comminution is a term applied to the process of particle size reduction. Comminution processes are typically employed in the minerals industry to reduce the particle size of mined ore in order to liberate the minerals of interest for downstream metallurgical separation processes. Comminution is a very energy intensive operation and can contribute up to around 34% to 52% of the direct electrical energy usage of a metallurgical operation (Napier-Munn, 2015). There are many different types of comminution equipment used in the industry and the different types of equipment are suitable for different types of duties based on the feed and product particle size requirements. A comminution circuit usually consists of a number of different equipment operating in series to reduce the particles from the run of mine (ROM) particle size distribution down to the grind size required by the separation process. Comminution equipment are generally divided into two main categories namely crushers and mills. Typical types of crushers used in the minerals industry include jaw, cone and gyratory crushers as well as High Pressure Grinding Rolls (HPGR). Tumbling mills include Autogenous (AG), Semi-Autogenous (SAG), Rod, and Ball mills.

In autogenous (AG) mills the feed ore is used as the grinding media, no steel media is added to the mill. In order to provide sufficient energy for breakage, AG mills need to receive a coarse feed material with feed F_{80} particle sizes typically around 200 mm for these types of operations. Semi-autogenous (SAG) mills also use the feed ore as grinding media but steel balls are added to the mill to assist with particle breakage. The typical F_{80} feed size to a SAG mill is around 110 mm. Rod mills utilise steel rods as grinding media in the mill. The particle feed sizes to rod mills typically vary from F_{80} of between 4 mm to 20 mm but the ideal feed size is around 15 mm to 17 mm. When operating in primary milling duties, ball mills can typically accept feed particles of less than 12 mm with typical F_{80} sizes of 8 mm to 10 mm (Outokumpu). However when ball mills are operating in secondary milling and re-grinding applications the feed sizes will be smaller. Typical feed sizes for ball mills in secondary milling applications range from F_{80} of around 1 mm to 4 mm. For ball mills operating in re-grind duties the feed sizes often range from F_{80} of around 100 μm to 150 μm (Callow & Moon, 2002).

Depending on the comminution circuit configuration SAG and AG mills produce product grinds ranging from P_{80} of around 4000 μm to 150 μm . In primary and secondary grinding duties ball mills can produce grinds down to around P_{80} of 100 μm to 200 μm , and when operating in re-grind duty product grinds as fine as P_{80} of 20 to 40 μm can be achieved (Callow & Moon, 2002). Rod mills are not used industrially for fine milling but are used to generate a relatively coarse products. The optimum feed sizes to rod mills are typically in the range of 15 to 17 mm operating with a reduction ratio of around 15:1 (Outokumpu). Hence product grinds of less than 1 mm would rarely be generated on an industrial scale with a rod mill.

Stirred media mills are used for fine milling applications and employ small diameter ceramic grinding media to produce fine product grinds. Various different types of stirred media mills are used in metallurgical operations for fine grinding duties (Wills, 2005). It has been shown that stirred media mills are more energy efficient for the re-grinding of ore in the minerals processing industry as compared to traditional ball milling processes (Lichter & Davey, 2006). For product grinds below 75 μm stirred media mills exceed ball mills with regard to energy efficiency, requiring less specific energy input (kWh/t) to produce a targeted grind size. Stirred mills have therefore become the preferred option for regrinding and fine grinding in minerals processing circuits (Jankovic, 2003).

2.2 Stirred Media Mills

Stirred media mills can generally be classified into two types based on the type of flow pattern of the charge in the mill. The two types of mills are gravity induced and fluidised. Gravity induced mills that are available industrially include the Metso Vertimill and the Nippon-Eirich tower mill. Industrially used fluidised stirred media mills include the IsaMill, stirred media detritor (SMD), VXP mill, and HIG mill among others (Ntsele and Allen, 2012).

2.2.1 Gravity Induced Stirred Media Mills

A picture of a Vertimill installation is presented in Figure 1. General layout drawings of the Metso Vertimill and Nippon-Eirich tower mills are shown in Figure 2 and Figure 3. The design of these types of mills are characterised by a horizontally mounted central screw agitator driven by a top mounted electrical motor and gearbox. Steel balls are usually used as grinding media. The media sizes used typically range from 5 to 38 mm in diameter (Allen, 2013). The rotation of the screw agitator lifts the media to the top of the mill vessel. Once at the top the media then cascades down the sides of the screw back to the bottom of the mill. These type of mills are characterised by a low rotational speed of the screw agitator, typically around 3 m/s (Hasan et al., 2016). Due to the slow rotational speed of the agitator the slurry and the media does not remain completely suspended, or fluidised, but rather settles under the influence of gravity (Ntsele and Allen, 2012), hence the term gravity induced stirred media mill. The mill operates in an overflow mode where the feed slurry is introduced via a feed chute at one end of the top of the mill. The slurry product is collected as overflow at a different location on the top of the mill vessel. The Nippon-Eirich tower mill sizes ranges from installed motor capacity of 15 to 1120 kW ([www.nippon-eirich](http://www.nippon-eirich.com), 2018). The Metso Vertimill product range is much larger with installed capacities ranging from 11 to 3352 kW (Metso, 2018).



Figure 1: Picture of a Vertimill installation with four mills, www.metso.com 2018

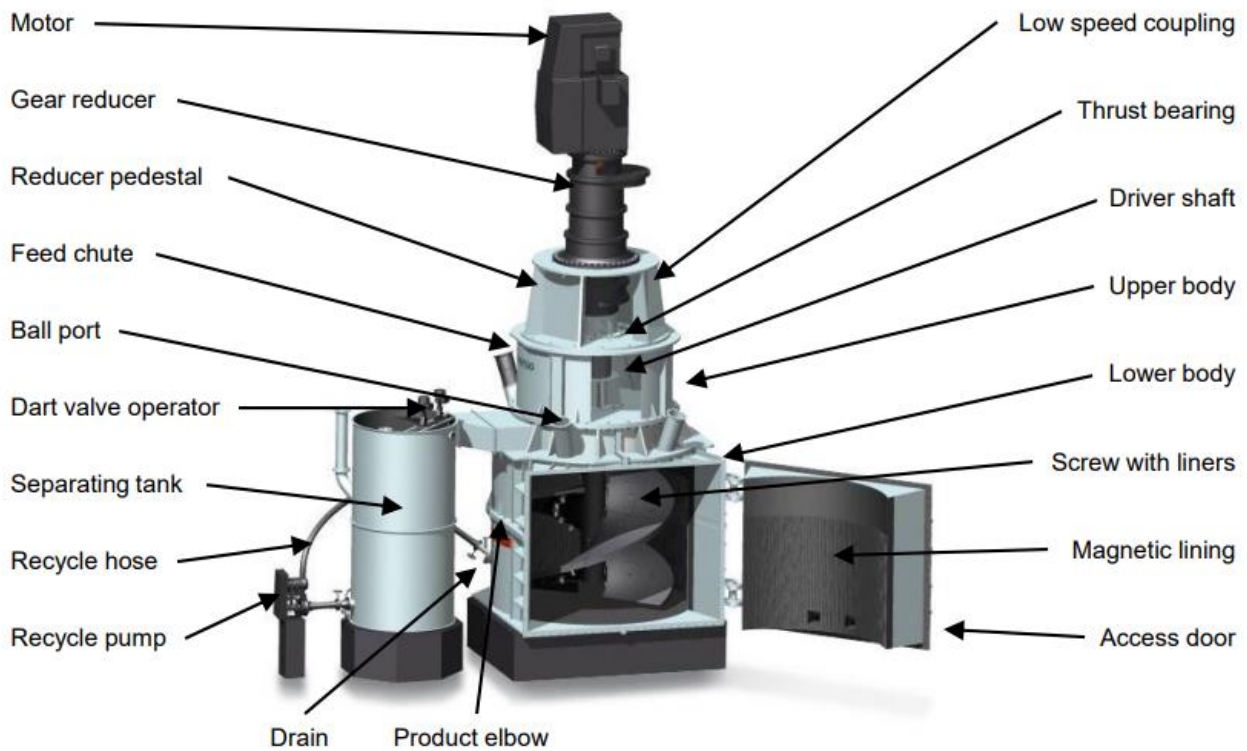


Figure 2: General Arrangement Drawing of a Metso Vertimill, Allen 2013

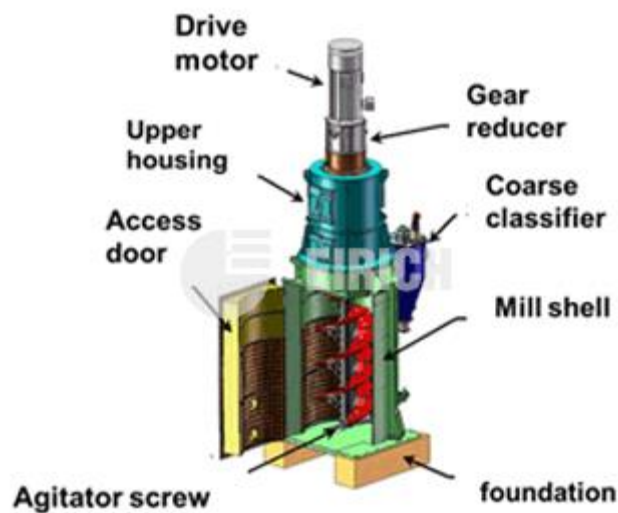


Figure 3: General Arrangement Drawing of a Nippon-Eirich tower mill, ([www.nippon-eirich](http://www.nippon-eirich.com), 2018)

2.2.2 Fluidised Stirred Media Mills

In contrast to the gravity induced type of mills, the rotational speeds of the fluidised type of mills are much higher. Tip velocities for these types of mills range from 10 to 23 m/s depending on the mill design (Hasan, 2016). The fluidised mills also utilise small diameter ceramic beads as grinding media, as opposed to the larger steel ball charge used in gravity induced type mills. The size of ceramic media differs based on mill design and application

but generally ranges in size from 1 to 6 mm (Hasan, 2016). Ceramic grinding beads typically used in stirred media milling applications are also significantly lighter than steel media. The SG of beads typically employed in the minerals processing industry ranges from around 2.6 to 4.2 g/cm³ (Moore et al., 2016; Lehto, 2105) and the typical density of steel is in the region of 7.8 to 8.0 g/cm³ (www.matweb.com, 2018). As a consequence of these factors the charge and slurry in a fluidised type of stirred media mill becomes completely suspended, or fluidised, during mill operation and the slurry and the media mixes completely (Ntsele and Allen, 2012). Fluidised type stirred media mills are divided into two general categories based on the configuration of the stirrer. For horizontal mills the stirrer shaft axis is arranged horizontally relative to the ground level, while for vertical mills the stirrer shaft is arranged vertically relative to the ground. The main type of horizontal stirred media mill being used in the minerals industry is the IsaMill manufactured by Glencore. The most notable examples of vertical fluidised stirred media mills used in the minerals processing industry are the Metso stirred media detritor (SMD), the Outotec high intensity grinding mill (HIG), and the FLSmidth VPX mill formerly called the Knelson-Deswik mill. These mills will be discussed in more details.

2.2.2.1 Glencore IsaMill

An example of a horizontal fluidised stirred mill is the IsaMill pictured in Figure 4. The cutaway schematic in Figure 5 shows the internal configuration of this type of mill. The shaft is fitted with disc type stirrers that rotate at tip speeds ranging from 19 to 22 m/s. The mill vessel is completely closed and feed slurry is pumped in at the non-drive end of the mill. The slurry and media flows through the mill in a plug flow pattern. When the slurry and media reach the discharge end of the mill it is subjected to classification by means of an internal classifier. The classifier acts to centrifuge the media out towards the mill shell. The media along with some slurry is then pumped back in the direction of the feed end of the mill. This is done in order to retain the media inside of the mill. Milled product slurry exits the mill through the centre of the classifier. The IsaMill is available in different mill sizes with installed capacity ranging from 335 to 8000 kW (Glencore Technology, 2015). Figure 6 shows an aerial view of a mill that has been opened for maintenance purposes. The mill vessel is mounted on tracks that enables operators to slide it away from the drive-end to access the mill internals. In Figure 6 the shaft, discs, and internal classifier is visible.



Figure 4: Picture of an IsaMill installation, www.isamill.com 2018

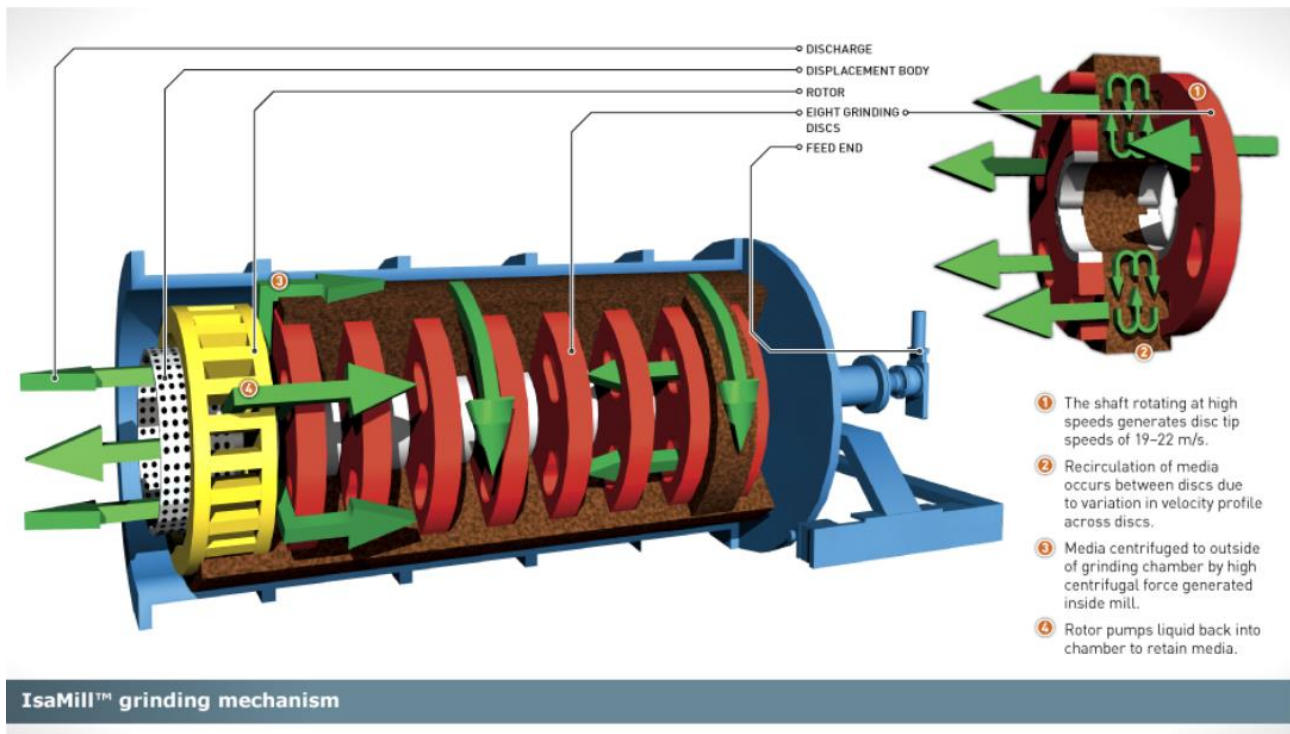


Figure 5: Schematic of IsaMill internals and charge flow, www.isamill.com 2018

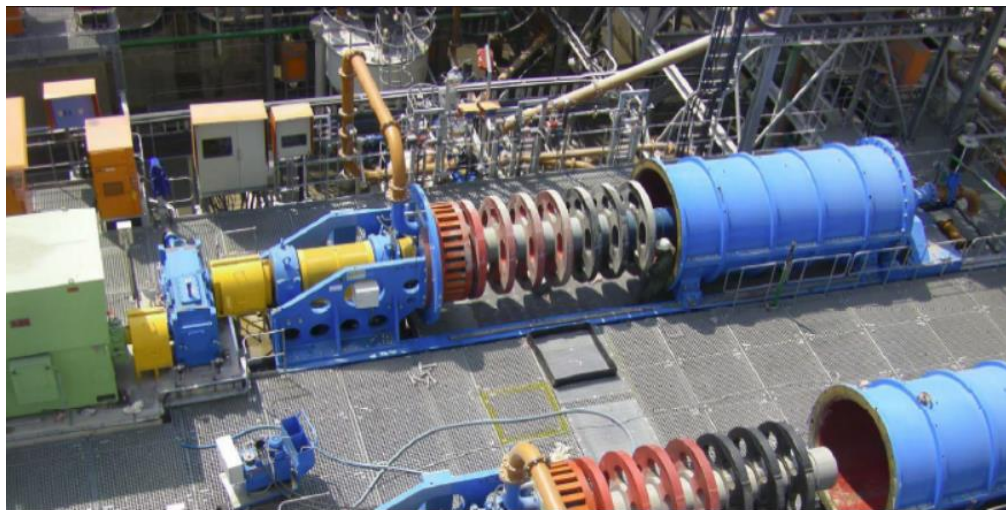


Figure 6: IsaMill with shell removed and shaft exposed for maintenance, www.isamill.com 2018

2.2.2.2 Metso SMD Mill

Figure 7 shows an example of an industrial SMD mill installation. The SMD mill uses pin type agitators mounted on the stirrer shaft as illustrated in Figure 8. The feed slurry is introduced at the top of the mill via a feed spout. The feeding system is arranged in such a way as to direct the feed slurry directly into the bottom of the slurry-media vortex that forms due to the action of the stirrer when the mill is operational. The product overflows at the top of the mill through the media retention screens and is collected in a launder (Metso, 2018). The media retention screens are used to prevent media from leaving the mill. Make up media is added at the top of the mill

through a dedicated chute. As mentioned the charge in the mill forms a vortex when in operation. An example of a vortex formed during milling in a pilot scale SMD mill is pictured in Figure 9. The SMD is available in different sized units with installed capacities ranging from 90 to 1100 kW (Metso, 2018).



Figure 7: Picture of an SMD installation with two mills, www.metso.com 2018



Figure 8: Schematic showing stirrer arrangement in the SMD, Allen 2013

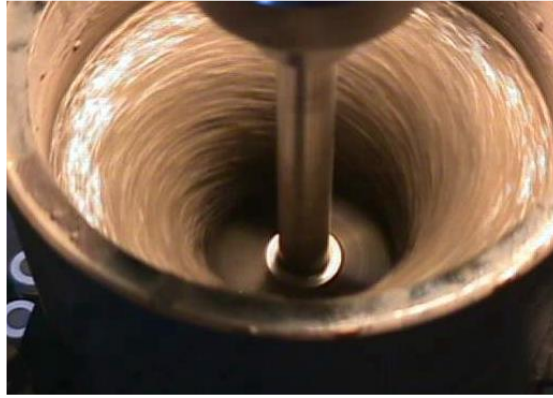


Figure 9: Example of a slurry-media vortex in an SMD mill during operation, Ntsele & Allen 2012

2.2.2.3 Outotec HIG Mill

The Outotec HIG mill is another example of a vertical fluidised stirred media mill, Figure 10. In this design the feed slurry is pumped into the mill through an inlet located at the bottom of the mill, refer to the schematic in Figure 11. Make up beads are added to the feed slurry, and are then pumped into the mill along with the new feed. The stirrer is fitted with disc type agitators and the mill vessel is fitted with stationary liners which are called stationary counter discs. The slurry flows upwards through the mill and as it does so it passes through the rotating discs and the space formed between the shell wall and the static counter discs, refer to Figure 12. The number of stationary and rotating disc sets used in the mill can vary up to a maximum of around 30 depending on the application. According to Outotec the flow paths of the larger and smaller particles through the mill differ due to an internal classification effect brought about by centrifugal forces. The larger particles spend more time at the peripheral area of the mill in the so-called high intensity grinding zone formed close to the stationary discs. The fine particles move closer to the mill shaft at the centre of the mill in what is called the lower intensity grinding zone. The product slurry discharges from the mill at the top while the grinding media are retained by a screen (Lehto et al., 2013). The HIG mill is also available in different sizes with installed capacities ranging from 132 to 5000 kW (Astholm, 2015).



Figure 10: Picture of a HIG mill installation, HIG mill located on the left, www.outotec.com 2018

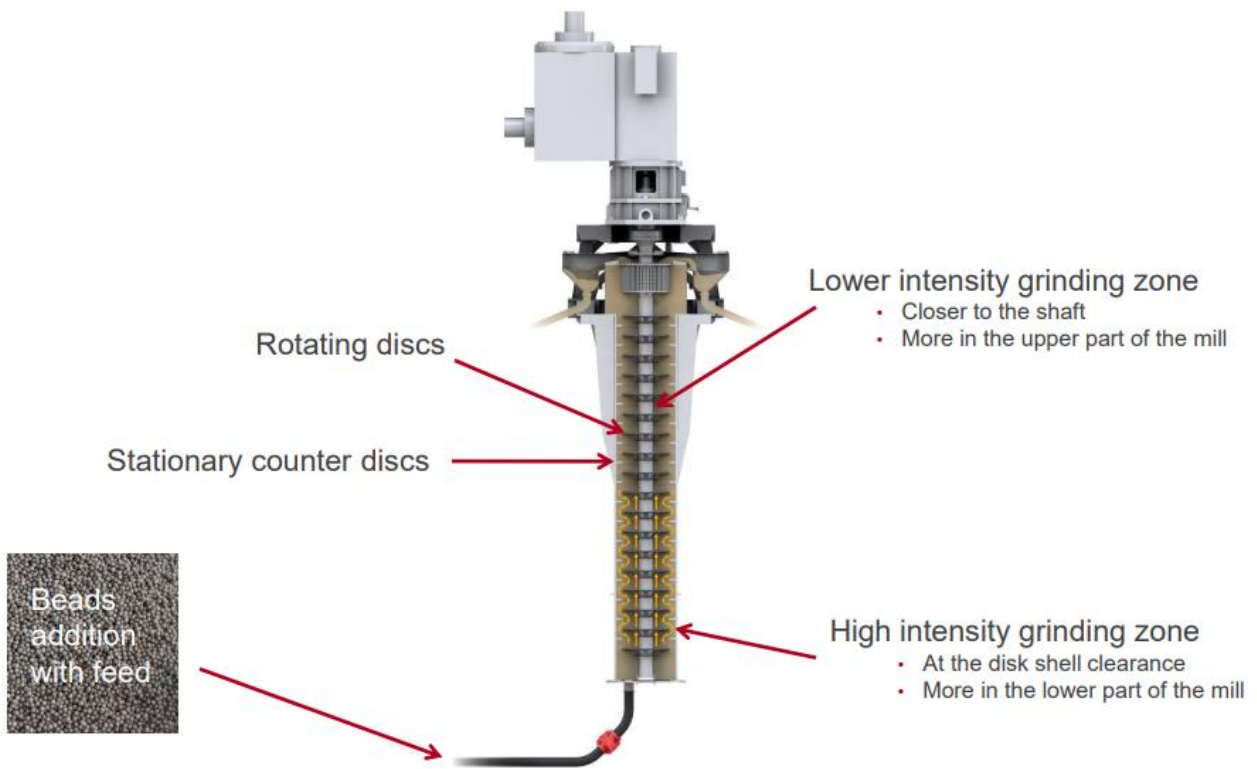


Figure 11: Cross section schematic of a HIG mill, Astholm 2015

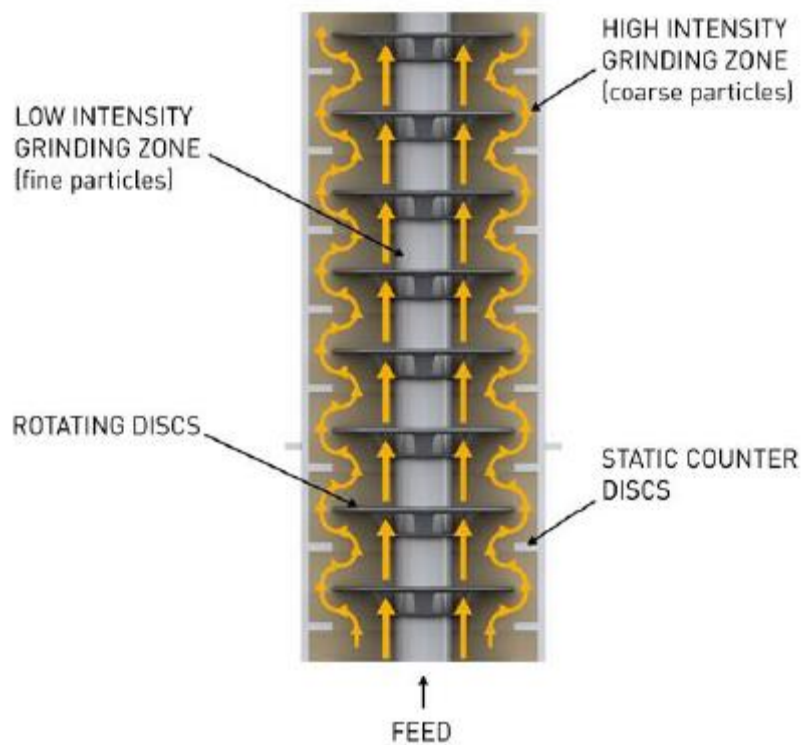


Figure 12: Schematic of flow through a HIG mill, Lehto et al. 2013

2.2.2.4 FLSmidth VXP Mill

The FLSmidth VXP mill is a vertical fluidised stirred media mill and was previously known as the Knelson-Deswik mill, Figure 13. Slurry enters the mill from the bottom, refer to Figure 14. The slurry then flows up towards the top of the mill where it overflows at the top through a media retention screen. The shaft is fitted with polyurethane disc type agitators. The mill is designed with a modular impeller shaft that allows for the addition of discs and spacers. Various sizes of mills are available and installed capacity ranges from 110 to 3000 kW for industrial sized units (FLSmidth, 2011).



Figure 13: Picture of an industrial VXP mill installation, FLSmidth 2018

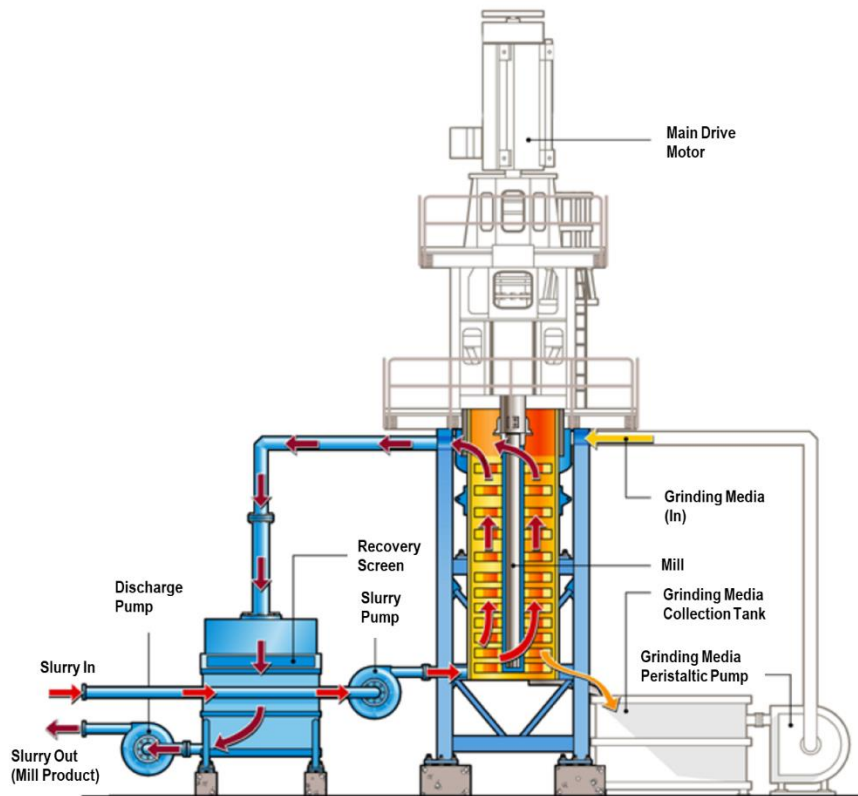


Figure 14: Schematic of a VXP mill installation showing mill cross section, FLSmidth 2011

2.2.3 Operating Ranges of Different Stirred Media Mills

The gravity induced type of mills can generally accept a coarser particle feed size as compared to the fluidised type of mills. The reason for this is that due to the larger steel balls, the media in the gravity induced mills are capable of adequately breaking coarser sized particles, as opposed to the small and lighter ceramic beads used in the fluidised mills. The top-size of feed is influenced by the application, but the Vertimill can accommodate a maximum feed size of up to 6 mm (Metso, 2018). The Nippon-Eirich tower mill can receive feed material up to a maximum particle size of 10 mm (www.nippon-eirich.co.jp, 2018). For the fluidised mills the recommended feed size is significantly less than this. The VXP disc mill has been designed to accept feed particles no coarser than about 300 μm to 400 μm on an 80% passing basis (Rahal, 2011). The Metso SMD is typically used with feed particles of 200 μm and smaller, (Metso, 2018). The Outotec HIG mill can typically accept feeds as coarse as around 100 to 300 μm on an 80% passing basis, depending on the application (Lehto et al., 2011). The horizontal IsaMill can receive feed particles up to 500 μm in size (Glencore Technology, 2015).

2.2.4 Typical Flowsheet Configurations Utilising Stirred Media Mills

A stirred media mill does not operate in isolation but rather in combination with ancillary equipment and other mills or comminution equipment as part of a larger flowsheet. Stirred media mills can operate either in open circuit or in closed circuit. An example of an open circuit operation is shown in Figure 15. In this configuration the entire process stream passes through the mill for size reduction in a single pass. On some cases it is desirable to not mill the entire stream, sometimes it is only required to mill the coarser particles. In these cases a different type of open circuit configuration can be used as shown in Figure 16. In this configuration the process stream is firstly passed through a classifier, in this case a cyclone, to separate coarse and fine particles. The fine particles bypass the mill, cyclone overflow, while the coarse particles are sent to the mill, cyclone underflow, for size reduction. This type of circuit is typically used in minerals flowsheets when coarser particles needs to be milled for liberation purposes but at the same time the production of excessive fines needs to be limited. Stirred media mills can also operate in closed circuit configuration as the example in Figure 17 shows. In closed circuit operation the process stream is firstly passed through a classifier. The fine particles are sent to the downstream process and the coarse particles are sent to the mill for size reduction. The mill product is returned to the classifier to separate the fines from the coarse particles. Coarse particles are sent back to the mill for further grinding.

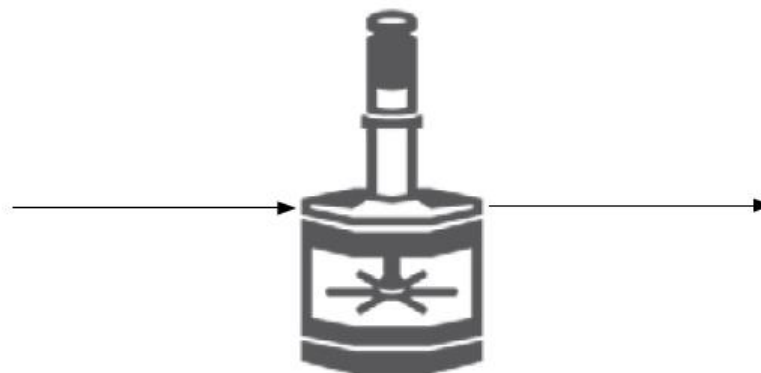


Figure 15: Open circuit SMD, Metso 2018

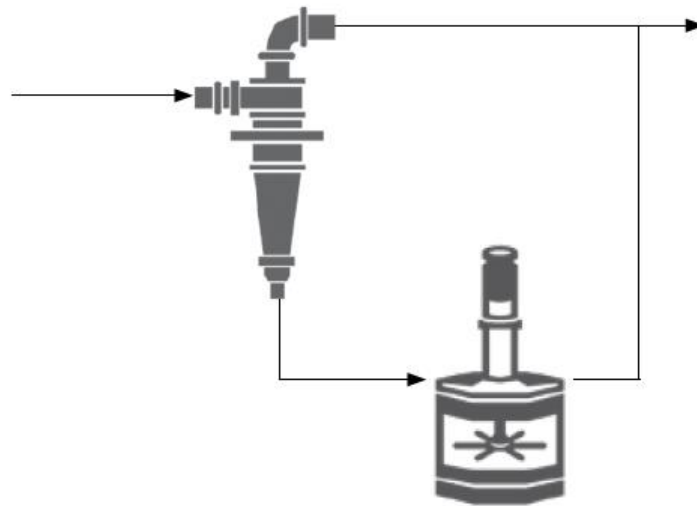


Figure 16: Open circuit SMD milling a scalped feed, Metso 2018

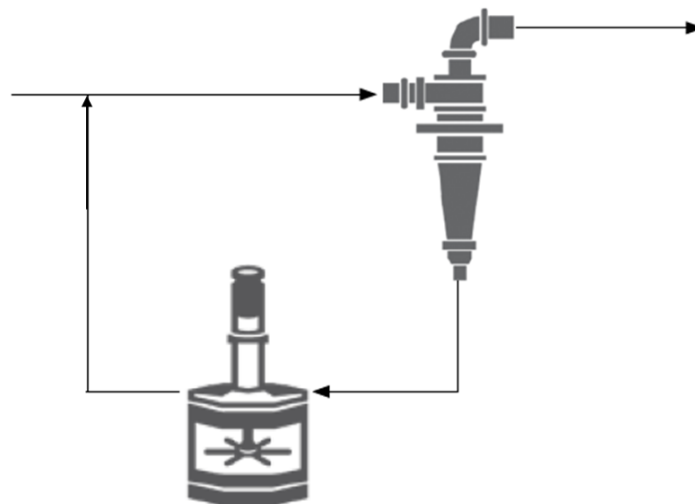


Figure 17: Closed circuit SMD, Metso 2018

IsaMills are usually operated in open circuit configuration and this is the recommended configuration but they can also operate with a scalped feed configuration if densification of the mill feed slurry is required (Pease et al.). These types of mills are commonly used for flotation concentrate re-grinding particularly in copper and lead zinc operations (de Waal et al., 2013), and platinum group metals (PGM), (Rule, 2010). However due to the large size of the units available they can also be suitable for mainstream grinding applications like tailings regrind (Anyimadu et al., 2007; Burford and Clark; Rule, 2010). In these type of circuits the initial milling is conducted using tumbling mills and the re-grinding to finer sizes are done using the IsaMill. Examples of flowsheets incorporating the IsaMill are shown in Figure 18 and Figure 19. Figure 19 shows the process flowsheet for the Mount Isa Mines Pb/Zn concentrating circuit. IsaMills are used for re-grind of both the Pb and Zn flotation concentrate streams. The Pb concentrate is re-grinded to a size of around 12 μm while the Zn concentrate is grinding to 12 μm and then to 7 μm . Figure 19 shows the positions in the Anglo Platinum flotation flowsheet where IsaMills are incorporated in their operations. The schematic shows fine grinding at two different duties in the circuit. The mainstream inert grinding (MIG) duty refers to the regrinding of the primary rougher tailings stream and is positioned after the secondary ball mill stage. This is aimed to liberate locked PGM and to improve recovery in the secondary rougher circuit. The second type of duty is the Ultra-Fine Grinding (UFG) duty and here the IsaMill is used to re-grind the rougher concentrate. The IsaMill is also used in the Albion process that

finds application in gold, copper, cobalt, lead and zinc operations for the treatment of refractory ores. In the Albion process the concentrate is firstly re-grinded in an IsaMill to particle sizes of around 10 to 20 μm depending on the relevant minerals. The milling stage is then followed by a proprietary oxidative leaching process (Stieper, 2018).

The VXP mill, formerly known as the Deswik mill, has had some application in tailings retreatment operations for the regrinding of chrome, gold, and PGM tailings in UFG and MIG grinding duties (Rule, 2010; Rahal et al., 2011; Reddick et al., 2014). The stirred media detritor (SMD) has been installed in metallurgical operations to prepare fine feed for leaching and flotation processes. Due to the fact that the maximum feed size that this unit can accept is only around 200 μm it is more suited for ultrafine grinding applications where a very fine product is required. This coupled with the fact that the largest unit only has an installed capacity of 1100kW, limits its range of applications in mainstream grinding (Moore et al., 2016). Due to the smaller sizes of mills available as compared to the other vertical fluidised mills it is often required to install multiple SMD units to perform a grinding duty. SMD mill circuits are often arranged with the SMD mills configured in series. In this configuration the product from the one mill becomes the feed to the next mill. A benefit of this is that each mill can be equipped with media and conditions that are most suitable to the feed size being milled (de Bakker, 2014). Although it is more suited for ultrafine grinding of concentrates, it has however been used in some mainstream applications (de Bakker, 2014; Rule, 2010).

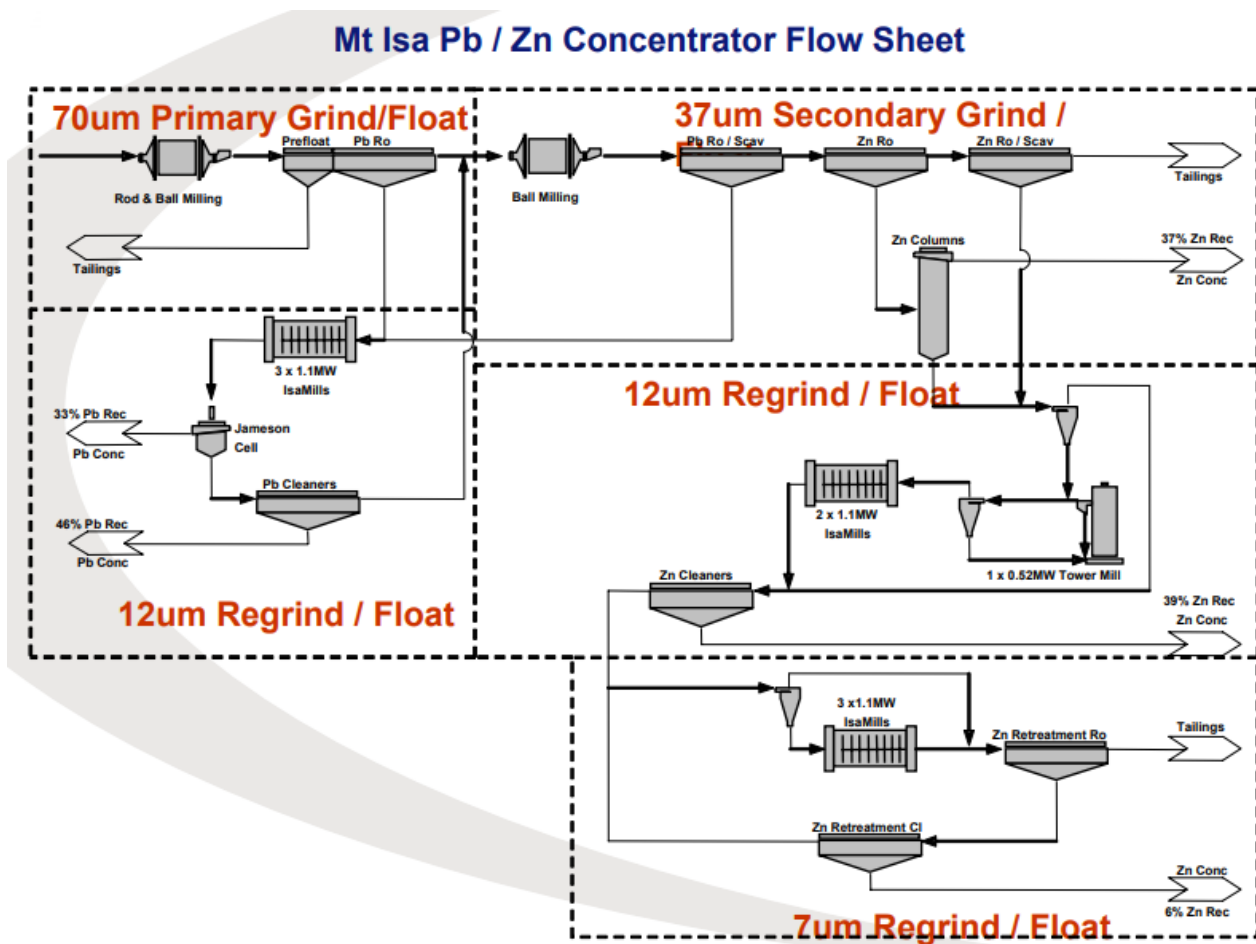


Figure 18: Mount Isa Pb/Zn Concentrator Flowsheet, Xstrata Technology

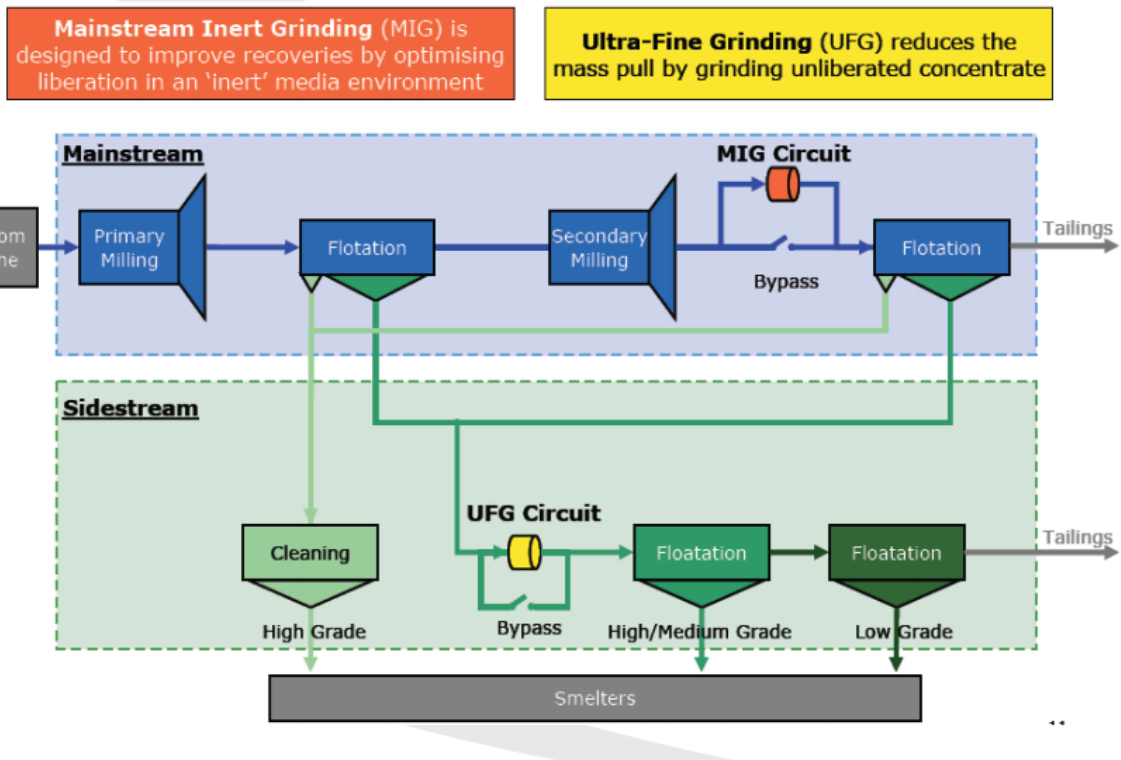


Figure 19: Anglo Platinum Generic Flotation Circuit Layout, Xstrata Technology

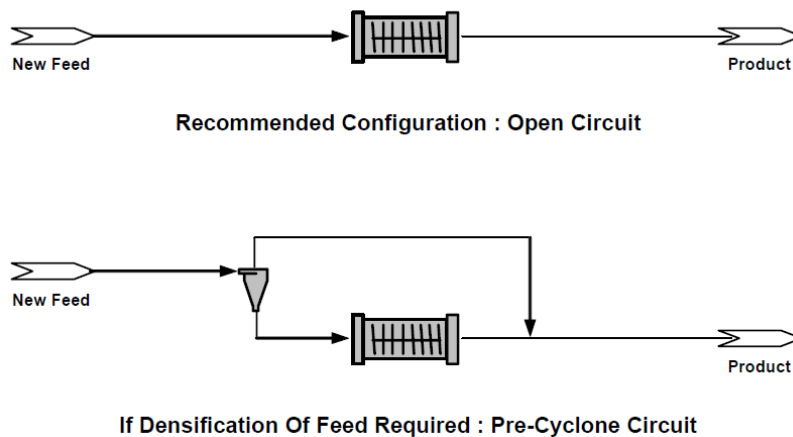


Figure 20: IsaMill circuit configuration, Pease et al.

The high intensity grinding (HIG) mill from Outotec has mainly been applied in concentrate regrinding duties, but due to the large sizes of the units available it can also be used for mainstream grinding duties. The HIG mill usually operates in open circuit with a scalped feed, Figure 21. A cyclone is typically used for scalping of the feed to the mill circuit. The fines are collected in the cyclone overflow and this bypasses the mill to prevent overgrinding. Excess water is also removed in the cyclone overflow. The cyclone underflow is subjected to milling in the HIG mill. However before it enters the mill water is added to produce the required slurry density (40% to 60% solids by mass) for the grinding process. The cyclone overflow and mill products then join to be sent to next stage in the process (Keikkala, 2015). An example of a concentrate regrind duty is at the Kevitsa mine in Finland. A HIG mill is used to regrind the rougher and scavenger flotation copper concentrates to particle sizes of below 20 µm to improve liberation prior to further flotation stages (First Quantum Minerals Ltd., 2016).

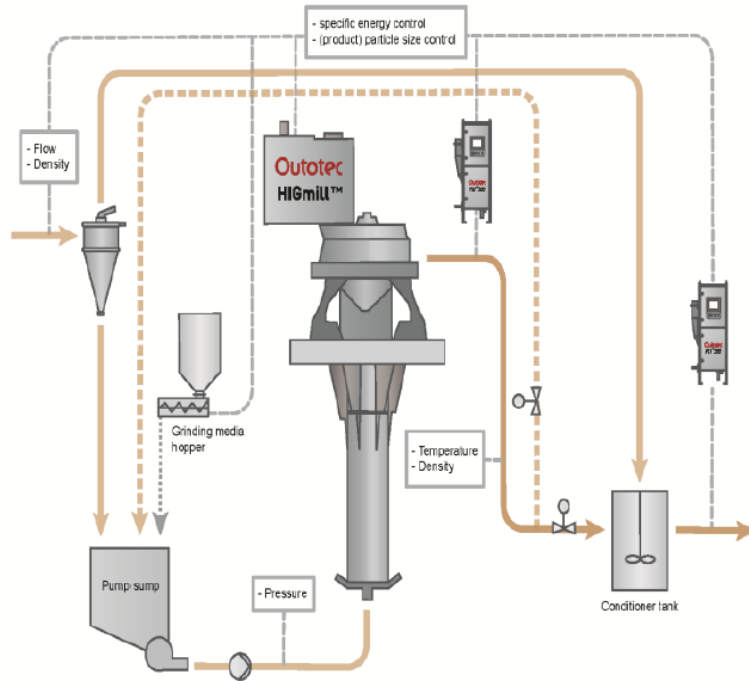


Figure 21: Typical HIG mill circuit configuration, Keikkala et al. 2015

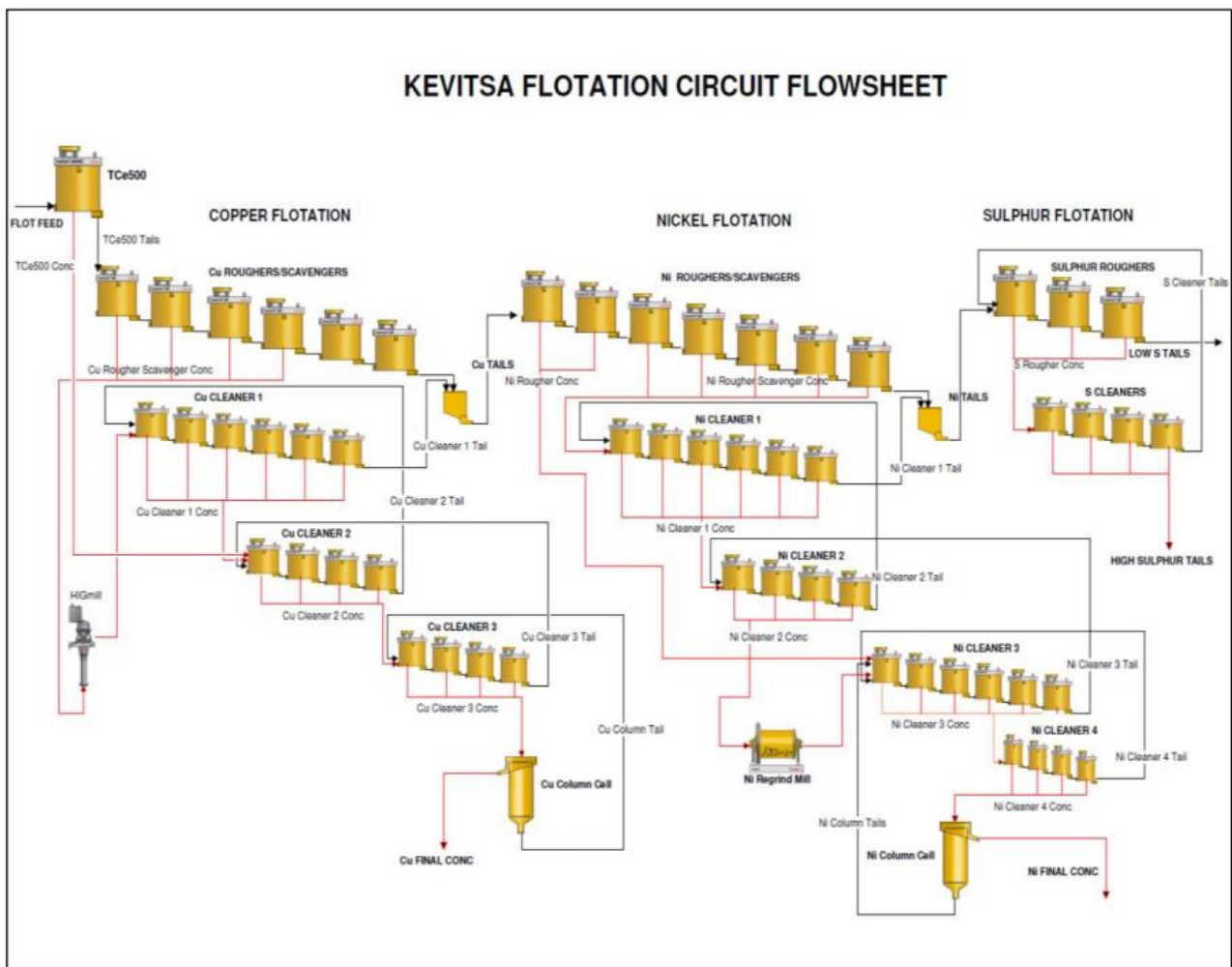


Figure 22: Kevitsa Flotation Circuit – HIG mill for Cu regrind, First Quantum Minerals Ltd.

Similar to the fluidised mills the gravity induced type of mills like the Vertimill are usually used to regrind products from AG, SAG, or ball mills (Samayamutthirian et al., 2015). These type of mills can be used in mainstream or concentrate regrind duties. However due to the fact that these types of mills can accept coarser feed sizes, as compared to the fluidised types of mills, they are also considered for other types of circuits where they can replace ball mills. An example of an alternative type of circuit is the HPGR-Vertimill circuit shown in Figure 23 (Metso, 2012). This circuit consists of a crushing stage followed by an HPGR. The HPGR is closed with a screen to control the transfer size to the Vertimill which operates in closed circuit with a classifier. This type of circuit is similar to that of an HPGR-ball mill circuit, Figure 24 (Wang, 2012), but differs in that the ball mill has been replaced by a Vertimill.

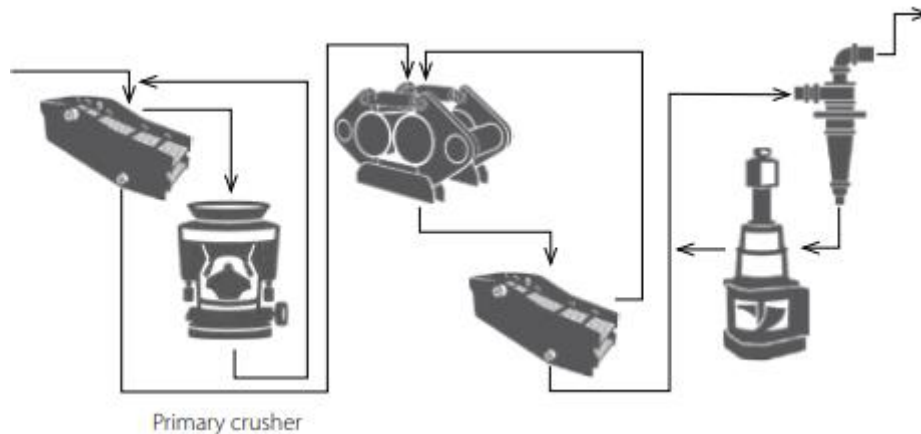


Figure 23: HPGR-Vertimill circuit, Metso 2012

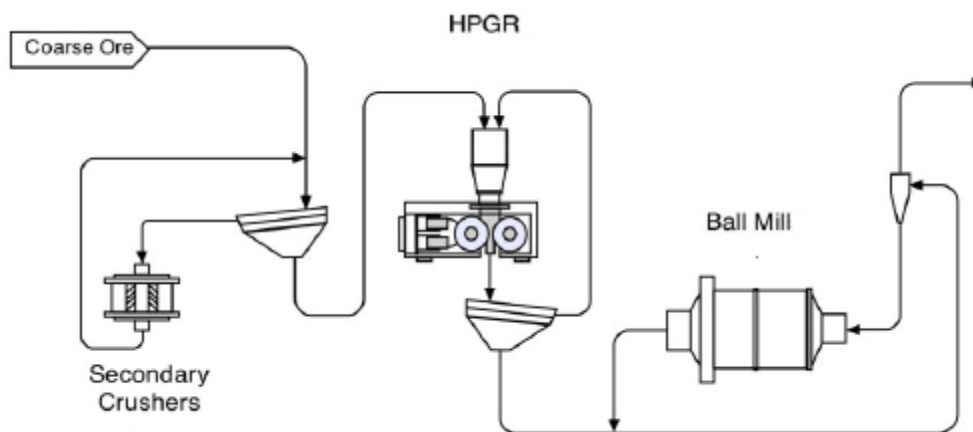


Figure 24: HPGR-ball mill circuit, Wang 2013

2.2.5 Energy Efficiency of Stirred Media Mills Compared to Ball Mills

The energy required for a comminution process is among other factors a function of the feed and product particle sizes of the material being subjected to breakage. As the required product fineness increases so too does the amount energy that is required in the process. An exponential relationship exists between the size of the product that is produced and the amount of energy that is required to produce these product sizes. The following basic empirical differential equation is often used to describe this energy requirement (Richardson et al., 2002).

$$\frac{dE}{dL} = -CL^p \quad (2)$$

This equation states that the incremental amount of energy (dE) required to produce a small change in particle size (dL) of a unit mass of material is a power function of the particle size. In this formula C is a proportionality constant and the power (p) is treated either as a constant or a variable of particle size. Historical work in the field of comminution has produced various suggestions as to the value to be used for p. According to Rittinger's law, that was first postulated in 1867, p = -2, while according to Kick's law, dating from 1885, p = -1. It has been found that neither of these two laws are able to provide an accurate calculation of energy requirement across the full range of particle sizes. Rittinger's law has been found to be more accurate at fine particle sizes and Kick's law has been found to be more accurate at coarser particle sizes. At a later stage in 1952 Bond proposed a third theory of comminution. Bond suggested the use of p = -1.5. This is an intermediate value between those proposed by Rittinger and Kick. Hukki, 1962, suggested that the value of p should not be considered constant, but should rather be treated as a variable and a function of particle size. This approach has more recently been confirmed in work conducted by Morrell (2004). However this work has shown that C should also be treated as a variable. The current more modern approach therefore is to treat both p and C as a function of particle size and various formulas have been proposed to relate p to particle size (Morrell, 2004^b, 2008, 2009, 2010). However Bond's third theory of comminution is also still applied commonly (Bond, 1961). Bond's formulation has found extensive use in industrial practice for sizing of comminution equipment, especially ball and rod mills. It is usually applied in the following simplified form (Rowland, 2002).

$$E = 10 \cdot W_i \left(\frac{1}{\sqrt{P}} - \frac{1}{\sqrt{F}} \right) \quad (3)$$

Where E is the predicted mill energy consumption, kWh/t. W_i is the Bond work index, kWh/t. P and F are the 80% passing sizes of the mill circuit product and feed respectively in units of μm . The Bond work index differs for different ores and is determined using a standard laboratory test. A graphical illustration of the type of energy versus particle size relationship described by equation 3 is presented in Figure 25. In this example a softer gypsum ore with a work index of 8 kWh/t is compared to a harder basalt ore with a work index of 20kWh/t (Snow et al., 1997).

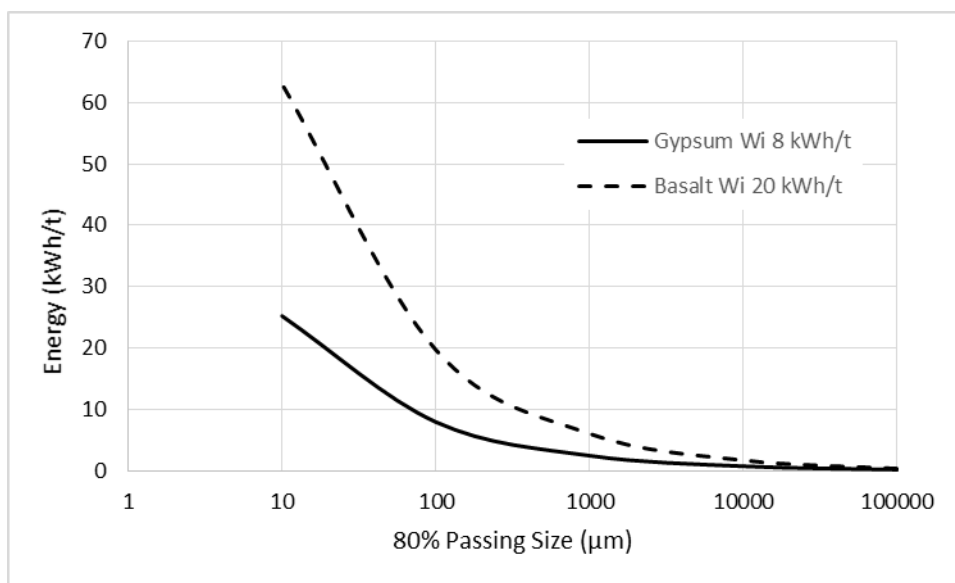


Figure 25: Graphical example of Bond Energy versus Product Size Relationship (Snow et al., 1997)

It should be noted that since the relationship presented in equation 2 is empirical in nature, the appropriate values for the proportionality constant (C) and the power (p) are influenced by amongst other things the properties of the material being broken, the particle size, and the comminution environment. This is evident in

the practical application of the Bond equation. When applying this formula to the sizing of ball or rod mills for example, a number of correction factors need to be applied to convert the energy prediction from the standard conditions to the actual operating conditions. For ball milling the standard conditions are wet, closed circuit grinding in a 2.44m diameter ball mill. For rod milling the standard conditions are wet, open circuit grinding in a 2.44m diameter rod mill. The correction factors used with the Bond equation are more commonly called efficiency factors. The value of E calculated using equation 2 is multiplied by various efficiency factors based on the specific conditions related to the application being evaluated. A detailed discussion of the application of the factors is outside of the current scope. However the factors are listed below for information (Rowland, 2006):

- EF1 – Dry grinding
- EF2 – Open circuit grinding
- EF3 – Mill diameter efficiency factor
- EF4 – Oversize feed
- EF5 – Fineness of grind
- EF6 - High or Low Ratio of Reduction Rod Milling
- EF7 - Low Ratio of Reduction Ball Milling
- EF8 - Rod Milling feed preparation technique

The list of efficiency factors highlights the fact that the energy required for a comminution operation is not fixed but is also dependent on the conditions employed. What is of special interest to the current investigation is the correction factor that needs to be applied to ball mills for fine grinding applications. EF5 acts to increase the energy prediction when ball mills are used in grinding duties to produce products smaller than 80% passing 75 μm . It has long been known that ball mills are not very energy efficient at producing very small product sizes. It has in fact been shown in numerous texts that stirred media mills are more energy efficient for the re-grinding of ore in the minerals processing industry as compared to traditional ball milling processes. Jankovic, 2003 indicated that for product grinds below 75 μm stirred media mills exceed ball mills with regard to energy efficiency, requiring less specific energy input (kWh/t) to produce a targeted grind size, refer to Figure 26. The graph also shows that with an increase in product fineness ball milling becomes significantly more in-efficient compared to the stirred media milling technology. According to Jankovic (2003) ball milling to particle sizes below 30 μm becomes uneconomical. A similar relationship was presented by Lichter and Davey (2006) and is shown in Figure 27. This indicates that at fine product grind sizes stirred media mills are more energy efficient as compared to traditional tumbling mills, since they required less energy to produce a given product grind size.

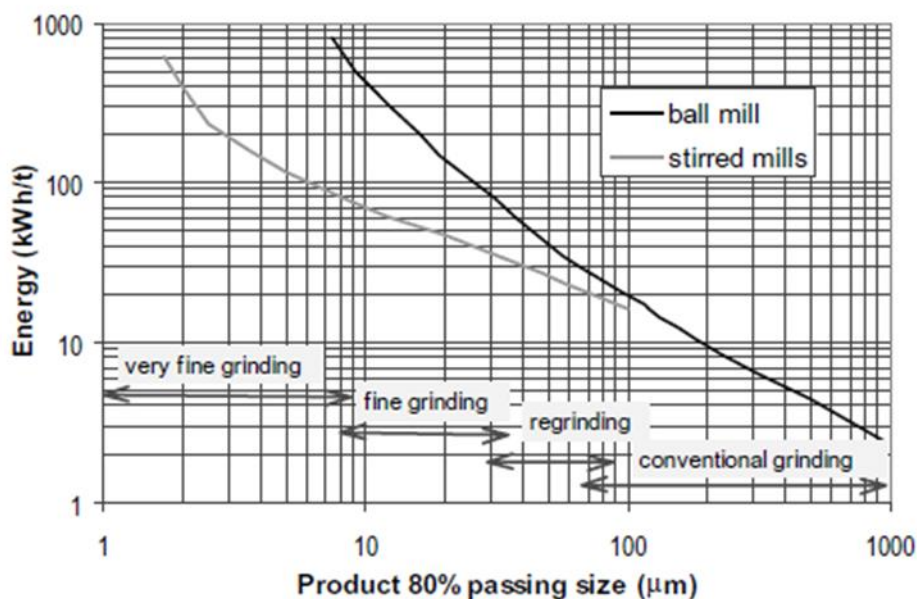


Figure 26: Comparison of energy requirement for grinding at various stages, Jankovic 2003.

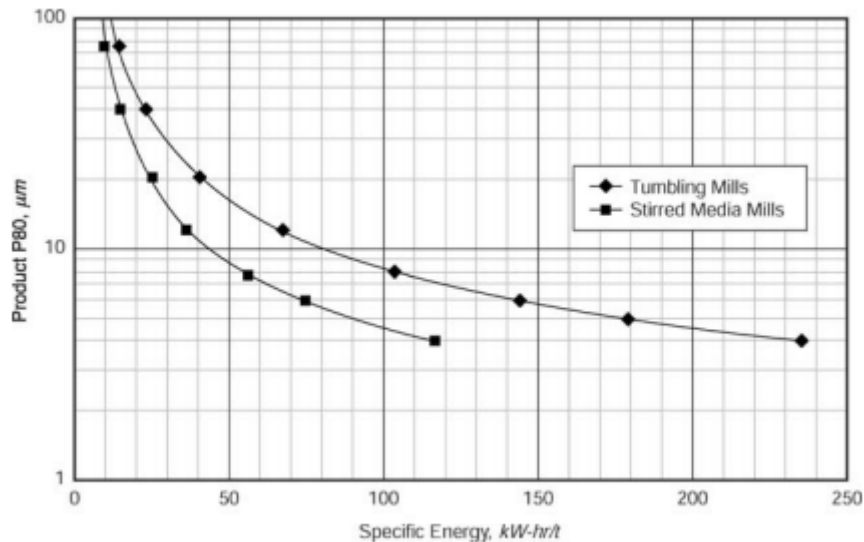


Figure 27: Relative performance of stirred and tumbling mills, Lichter & Davey 2006

2.2.6 Factors That Affect the Energy Efficiency of Stirred Media Mills

The energy required for a stirred media mill duty is not fixed but rather is dependent on the operating conditions and physical design of the specific mill. The choice of these parameters therefore have an influence on how energy efficiently a stirred mill operates. Numerous studies have been conducted to investigate the effect of operating conditions on the efficiency of the grinding process in stirred media mills. A summary of the effects studied by various authors is presented in Table 1. From this summary the most studied parameters seem to be the pulp solids concentration and the media stress intensity which is a function of stirrer speed, media size and media density. Other factors were also investigated to a lesser extent. The next sections will provide a summarised discussion on the observed effects of various factors on the stirred media milling process.

2.2.6.1 Pulp Solids Concentration

The solids concentration of the pulp being milled is usually measured as the mass percentage of solids present in the slurry. The typical trend observed is that for a given application there is an optimum range of solids concentration where the specific energy requirement is at a minimum. Solids concentrations that are either too low or too high negatively affects the energy efficiency. It has been postulated that the improvement in efficiency at higher solids concentrations is due to the higher particle density in the mill charge leading to a higher probability of particles being broken. The drop in the efficiency at very high solids concentrations is generally attributed to the increase in slurry viscosity that then leads to poor flowability of the slurry in the mill (Jankovic, 2003). The optimum solids concentration ranges vary based on the application. For coarser product grind applications the optimum solids concentration is often higher than for very fine applications. When very fine products are being targeted in the mill lower solids concentrations typically provides better results.

Jankovic, 2003 conducted grinding tests on calcium carbonate with a feed size of around 80% passing 65 µm. Comparative testing at 40%, 55% and 65% solids by mass showed that an increase in solids concentration resulted in an improvement of energy efficiency, refer to Figure 28. However it was observed that the relative increase in efficiency from 40% to 55% solids concentration is larger than the relative increase from 55% to 64% solids.

Table 1: Factors that influence stirred media milling as investigated by various authors

Author	Stress Intensity	Stirrer speed	Pulp solids concentration	Ratio of beads to slurry	Media size	Media density	Stirrer dimensions/geometry	Chamber dimensions/geometry	Pulp viscosity/rheology	Grinding aid /dispersant	Ratio of bead size to particle size	Media filling level	Grinding limit
Mankosa et al 1986					x	x					x		
Tuzun 1993		x	x		x	x	x	x				x	
Cho et al 1996													x
Zheng et al 1996		x	x	x	x	x	x	x	x				
Kwade et al 1996	x												
Zheng et al 1997										x			
Bernardt et al 1999			x							x			
Wang & Forssberg 2000		x			x								
Becker et al 2001	x												
Kwade & Schwedes 2002	x												
Kwade 2003	x												
Stender et al 2004	x							x					
Liu et al 2006		x								x			
He & Forssberg 2007		x	x		x	x			x	x			
Choi et al 2009										x			
Choi et al 2010										x			
Celep et al 2011		x			x						x	x	
Pradeep & Pitchumani 2011		x	x		x	x							
Toraman & Katircioglu 2011		x	x										
Jayasundara et al 2012					x						x		
Patel et al 2012			x		x		x			x			
Breitung-Faes & Kwade 2013	x												
Mucsi 2013		x	x		x							x	
Ohenoja et al 2013		x	x		x	x							
Baker 2014		x	x						x				
Breitung-Faes & Kwade 2014	x												
Patel et al 2014					x								
Ouattara & Frances 2014		x	x										
Ohenoja & Illikainen 2015		x			x	x							
Edwards 2016		x	x		x							x	
Hasan 2016		x	x		x								
Breitung-Faes 2017							x	x					
Hasan et al 2017		x	x		x								
Yang Yang et al 2017		x	x			x	x						
Fraginiere et al 2018		x	x		x	x	x						
Strobel et al 2018					x				x				

During grinding experiments on Limestone with a top-size of 400 μm that was ground to a top-size of about 40 μm it was found that the energy efficiency increased with increasing solids concentration up to about 65% solids and thereafter decreased with increasing solids concentration. Refer to the trend for energy efficiency (E_f) in Figure 29, (Zheng et al., 1996). Grinding tests were conducted on a quartz feed with a particle size of around 80% passing 57 μm . The tests were conducted at 10%, 20%, and 30% v/v pulp densities. For quartz this would typically correspond to 22%, 40%, and 53% on a mass basis. The tests at 40%, and 53% provided better results compared to the lower pulp density. In these tests the product sizes ranged and reach particle sizes down to around 0.3 to 0.4 μm , (Mucsi, 2013). Results of milling tests conducted on a TiO_2 pigment with a feed size of 10 μm and a targeted product grind of 0.3 μm indicated that the optimum solids concentration was around 52% solids by mass, (Ohenoja et al., 2013). However when much finer product targets are required the optimum solids concentration seems to be much lower. A different study investigated milling of TiO_2 particles to finer product grinds of around 120 nm to 160 nm. The findings were that at the lower solids concentration of 5% a finer product grind could be obtained than at higher solids concentrations. A grinding limit was reached during the testing where further size reduction could not be achieved. At solids concentrations higher than 30% the slurry viscosity increased to such an extent that the slurry was not flowable, (Liu et al., 2006). In nanomilling of a BaSO_4 with a feed size of around 20 μm it was found that a solids concentration of 15% solids by mass provided the best results when milling the material down to particle sizes of around 80nm. At the fine product particle sizes targeted the higher solids concentrations resulted in slurry flowability problems in the mill, (Patel et al., 2012).

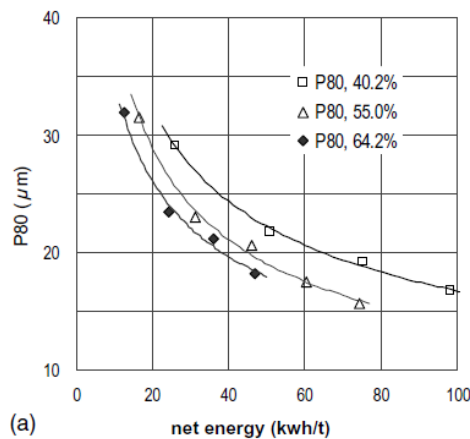


Figure 28: Grind versus energy required as a function of solids concentration, Jankovic 2003

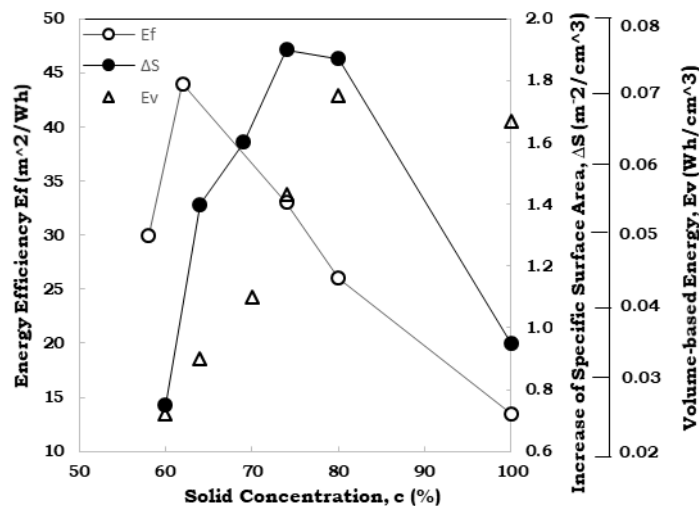


Figure 29: Energy efficiency, E_f , for limestone grinding, Zeng et al 1996

2.2.6.2 Media Size

The choice of media size is influenced by the size of the particles to be milled. The bead sizes need to be larger than the particles and large enough to sufficiently nip the particles to be milled (Tüzün, 1993). It also seems that the optimum bead size depends on the application and the properties of the material being milled. For limestone milling it was reported that a 12:1 ratio of bead size to particle size provided the best milling results (Hogg & Cho, 2000). Results of grinding experiments on a refractory Au/Ag ore found an optimum ratio of 16:1, (Celep et al., 2010). During coal milling experiments it was found that a ratio of 20:1 provided the best breakage properties, (Mankosa et al., 1986). A similar result was found during stirred media mill grinding tests conducted on a quartz feed material, the optimum ratio of bead size to feed particle size was found to be in the region of around 20:1, (Yue & Klein, 2006). Tüzün, 1993, suggested an optimum ratio of bead size to particle size of 26.9 based on nip angle calculations. It therefore seems that the most suitable bead size to particle size ratio might be influenced by the application.

2.2.6.3 Media Density

When a stirred media mill is operated with media of higher densities, the mill will have a higher power draw in comparison to when the mill is operated with lower density media (Tüzün, 1993). However the use of higher bead densities do not necessarily result in more efficient grinding. During a study where limestone was milled with high density steel beads and glass beads, with densities of 7.8 and 2.5 g/cm³ respectively, the glass beads provided better energy efficiency. In this case the steel beads required about double the energy input as compared to the glass beads, (Zheng et al., 1996). An experimental programme conducted on the milling of TiO₂ investigated bead densities of 2.53, 3.87, and 6.10 g/cm³. In this investigation it was also found that lower bead densities results in better energy efficiency as compared to higher bead densities, (Ohenoja et al., 2013). Lower bead densities do however not always result in better performance. During milling experiments conducted on talc with bead densities of 2.53, 3.87, and 6.10 g/cm³ it was found that for the grind target investigated the higher density beads provided better energy efficiency, (Ohenoja & Illikainen, 2015). Also experimental work on quartzite milling showed that beads with densities of 5.4 and 3.7 g/cm³ resulted in more energy efficient grinding than beads with a lower density of 2.5 g/cm³, (He & Forsberg, 2007). The optimal choice of bead density therefore seems to be influenced by the other operating conditions of the mill.

2.2.6.4 Stirrer Tip Velocity

The tip velocity of the stirrer is a function of the stirrer diameter and rotational speed. A higher rotational speed for a given mill will result in a higher power draw (Zheng et al., 1996). Milling experiments were conducted on quartzite at three different stirrer tip velocities of 7.56 m/s, 11.36 m/s and 14.17 m/s and at two different slurry concentrations of 65% and 70% solids by mass. For the 65% solids concentration it was found that the 11.36m/s tip velocity provided the most efficient milling conditions. The tests at higher and lower velocities did not perform as well. However for the higher slurry concentration of 70% solids by mass the higher tip velocity of 14.17m/s provided the most efficient milling conditions. The authors ascribed this observation to the fact that the slurry viscosity at 70% solids was higher than at 65% solids. Due to the higher viscosity the beads needed to be imparted with a higher energy, achieved via the higher tip speed, in order to grind the particles efficiently, (He & Forsberg, 2007). The study by He & Forsberg, 2007, highlighted that for a given mill configuration an optimum stirrer tip velocity can be found. Tip velocities that are either too high or too low will negatively affect the milling efficiency. Other studies that support this observation were presented by (Pradeep & Pitchumani, 2011; Zheng et al., 1996; Ohenoja et al., 2013; Ouattara & Frances, 2014; Ohenoja & Illikainen, 2015; Edwards, 2016; Yang et al., 2017).

2.2.6.5 Stress Intensity – interrelation of stirrer speed, media density, media size

The effects of bead density, bead size, and stirrer tip velocity on the efficiency of the grinding process are interrelated. Work conducted over the course of a number of years at the University of Braunschweig by Kwade and fellow workers has shown that the way in which a stirred media mill is set up has an effect on the amount of energy required to reach a specified target grind. The stress intensity (SI), also called the stress energy (SE), is a way of comparing the energy conditions existing in a stirred media mill (Kwade et al., 1996; Becker et al., 2001; Kwade & Schwedes, 2002; Kwade, 2003; Stender et al., 2004; Breitung-Faes & Kwade, 2013; Breitung-Faes & Kwade, 2014). The stress intensity of the grinding media is proportional to the tip velocity, bead size, and bead density used in the stirred media mill according to equation 4.

$$SI_{gm} \propto v_t^2 \cdot d_{gm}^3 \cdot \rho_{gm} \quad (4)$$

Where SI_{gm} is the stress intensity, v_t is the tip velocity, d_{gm} is the grinding bead diameter and ρ_{gm} is the grinding bead density. Higher tip velocities, larger bead sizes, and higher bead densities has the effect of increasing the magnitude of the energy events in the mill. If the magnitudes of the energy events are too small then the energy conditions are too low in the mill and the grinding is inefficient so a high amount of energy is required. However if the magnitudes of the energy events are too large then a large portion of energy is wasted that does not go into breakage of the ore. In this case the grinding is also inefficient. An optimum stress intensity exists for a given application. This is illustrated in Figure 30. The graph shows the energy (y-axis) required to reach the same grind size with different mill energy conditions or stress intensities (x-axis). As shown an optimum region of mill conditions exist that provides the most energy efficient milling conditions. This observation has significant implications for optimising the energy efficiency of industrially operating stirred media mills.

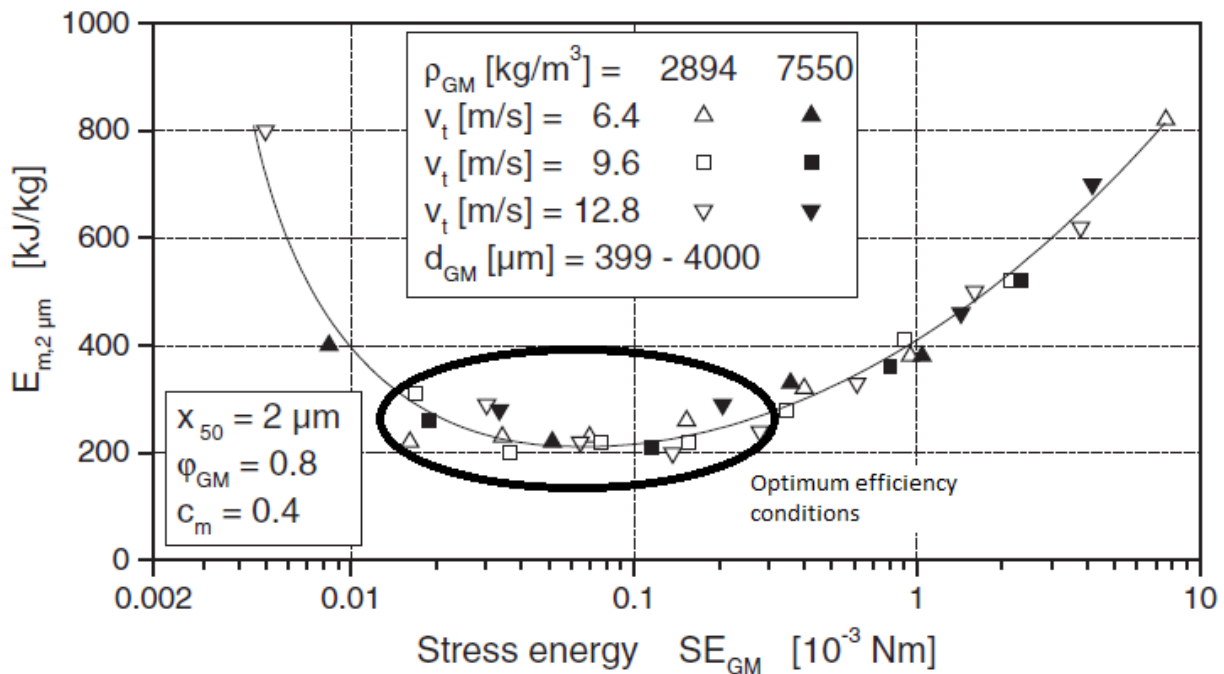


Figure 30: Energy required to reach the same target grind at various mill conditions (SI), (Kwade, 2003)

2.2.6.6 Media Filing Level

A higher level of media filling in the mill will result in a higher mill power draw (Tüzün, 1993). Vertical stirred media mills can operate with media filling levels of up to 80% by volume, (Gupta, 2016). A test work programme conducted on a VXP mill investigated filling levels ranging from 65% to 85%. The study found the effect of the mill filling on grinding efficiency to be minimal. The best efficiency was obtained at 65% filling but lower filling levels were not tested, (Edwards, 2016).

2.2.6.7 Ratio of Beads to Slurry

The effect of the ratio of beads to the ratio of slurry in the mill is a parameter that seems to not have been studied extensively so due to this reason the effect of this parameter might not be fully understood. Experimental milling tests were conducted on limestone where the ratio of particles to beads volume was varied while the solids concentration of the slurry was kept constant. The study found that the best mill performance occurred at a ratio of bead to particle volume of 2.8. This corresponded to a condition where the voids in the grinding media packaging were just filled with the particles, (Zheng et al., 1996).

2.2.6.8 Stirrer and Chamber Geometry and Dimensions

The energy transfer from the stirrer to the mill contents which include the slurry and suspended media is a function of among other factors the mill geometry (Breitung-Faes, 2017). In a study where the effect of changing the ratio of stirrer diameter to tank diameter was evaluated, it was found that a higher ratio of impeller to tank diameter resulted in more efficient milling. If the gap between the stirrer and the vessel was too large the grinding efficiency was negatively influenced, (Zheng et al., 1996). In a similar study milling experiments were conducted with three different lengths of stirrer pins while the mill vessel geometry was kept the same. It was found that the longer pin lengths provided more efficient grinding conditions in the mill, (Patel et al., 2012). In the work by Zheng and Patel it is not clear if the differences in milling performance might have been due to the increase in tip velocity at larger stirrer diameters that resulted in higher stress intensities, or if it was due to a combination of increased tip velocity and change in relative equipment dimensions. The choice of impeller design does seem to have an effect on the milling performance. In a study by Yang Yang et al., 2017, four different types of impeller designs operating in the same vessel were tested and it was found that the differences in design did have a significant influence on the energy efficiency of the milling process. One of the designs tested produced far superior results compared to the other three designs. It was postulated that the efficiency of a mill could be improved by optimising the design of the stirrer.

2.2.6.9 Pulp Viscosity, Dispersants, and Grinding Aids

Some studies have found that milling performance can be improved by modifying the viscosity of the pulp through the addition of chemicals. In a study investigating the effect of adding dispersants to a quartzite slurry milled in a stirred media mill, the addition of dispersant S40 to the milling process had the effect of lowering the viscosity of the pulp at the solids concentration and shear rates employed in the mill. The lowered viscosity resulted in improved grinding efficiency compared to the tests where no dispersant was added, (He & Forssberg, 2007). The effect of grinding aids on limestone milling under various different operating conditions were investigated. The results indicated that in some cases the addition of poly acrylic acid as a grinding aid resulted in an increase of energy efficiency of up to 100% compared with the tests where no grinding aid was added, (Zheng et al., 1997). In a different study the effect of poly acrylic grinding aids for the milling of calcite was investigated. The results showed that when grinding aid was used a 16% to 34% improvement in energy efficiency was obtained, (Choi et al., 2007). The addition of a sodium salt of polyacrylic acid resulted in improved grinding efficiency of barium sulfate, (Patel et al., 2012).

2.3 Shear Based Power Model Theory

Radziszewski, 2013 proposed that the power draw of a stirred media mill might be calculated using the formula shown in equation 5:

$$P_{\tau} = \mu\omega^2V_{\tau} \quad (5)$$

Where P_{τ} is the power draw in units of Watt, μ is the viscosity with units of Ns/m^2 of the mill charge which consists of the fluidised slurry and media mixture, ω is the rotational speed of the stirrer in units of rad/s , and V_{τ} is a term that is called the shear volume with units of m^3 . A general formula for the shear volume is presented in equation 6, (Radziszewski, 2013):

$$V_{\tau} = A \frac{r^2}{y} \quad (6)$$

Where A is the area over which the shear force is acting, r is the radius over which the shear is acting, and y represents that gap over which the shear is acting. The shear volume is calculated from the contribution of all of the parallel shear surface pairs present in the mill geometry. In the calculation only parallel surfaces that are moving past each other when the stirrer is moving are included. A general guideline is that if one parallel surface is found on the rotating impeller and the other parallel surface is found on the chamber then these surfaces would constitute a parallel shear surface pair. Also to be included in the calculation the parallel surfaces must be in full contact with the mill charge, which is the slurry-media mixture. The following example taken from Radziszewski, 2013 is used to describe a typical calculation of shear volume for a smooth shell stirred mill with a stirrer consisting of only one solid disc, refer to Figure 31. In this example the outer mill shell has dimensions of 1 m in diameter and 1 m in height. In this example there are three different shear surface pairs. The first pair of surfaces is the area between the outer circumference of the disc and the walls of the chamber, region a. The second pair of surfaces is between the impeller shaft and the walls of the chamber, region b. The third pair of surfaces is the bottom of the disc and the bottom of the mill chamber, region c. The total shear volume can then be calculated using equation 7, (Radziszewski, 2013):

$$V_{\tau} = A_{disk} \frac{r_{disk}^2}{y_{disk}} + A_{shaft} \frac{r_{shaft}^2}{y_{shaft}} + A_{end} \frac{r_{end}^2}{y_{end}} \quad (7)$$

Note that for region c where the bottom of the disc moves relative to the bottom of the chamber the calculation is not as straightforward as for the other two regions. In this region the shear force is acting concentrically over the circumference of the bottom of the disc. The circumference is a function of the distance from the centre of the impeller, the distance/length over which the force is acting therefore increases as the distance from the centre of the impeller increases. An integration of the shear stress is required over this region. The result of the integration yields equation 8 when simplified, (Radziszewski, 2013):

$$r_{end} = r_{disc} * 2^{-1/2} \quad (8)$$

As indicated previously the surfaces must be in contact with the mill charge fluid to be considered in the calculation. During stirred media milling the shaft might not necessarily be in full contact with the charge, as is evident from the vortex shape formed in an SMD mill. In these cases the contribution of the shaft to the shear volume calculation can be ignored. This contribution is also generally small as the example illustrates. When the shaft shear pair is included the total shear volume is 0.560 m^3 and when it is excluded the shear volume is 0.547 m^3 . The contribution of the shaft is therefore negligible. Due to the large distance between the shaft and the chamber this pair has a very low contribution to the shear forces in the mill. The case presented here was for a simple example with only three shear surface pairs. For geometries with more surface pairs the contribution of each of these pairs will be added to derive the total shear volume. Martins and Radziszewski, 2015 presented generalised formulas for calculating the shear volume of complex types of geometries.

In order to apply the shear based power model the viscosity of the slurry/media fluid in the mill must be known. On an actual operating mill this value can be calculated when the power draw, rotational velocity, and shear volume of the mill is are known. However the viscosity of the fluid is a function of operating conditions. Radziszewski, 2013 identified that the following operating conditions have an influence on the viscosity used in the model:

- Impeller rotational speed
- Media diameter
- Media density
- Slurry density
- Dispersant concentration

A generalised empirical formula was proposed for correcting the apparent viscosity against operating conditions as shown in equation 9, (Radziszewski, 2013):

$$\mu_{est} = k(a\omega^{-b}) \left(\frac{D_b}{D_{bref}}\right)^c \left(\frac{\rho_m}{\rho_{mref}}\right)^d \left(\frac{\rho_{sl}}{\rho_{slref}}\right)^e \left(\frac{100-x}{100}\right)^f \quad [\text{units of } \text{Ns/m}^2] \quad (9)$$

In this formula k,a,b,c,d,e, and f are empirical constants, ω is the angular velocity, D_b and D_{bref} are the actual and reference media diameters respectively, ρ_m and ρ_{mref} are the actual and reference media densities, ρ_{sl} and ρ_{slref} are the actual and reference slurry densities and x is the dispersant concentration. Radziszewski, 2013, fitted this formula to an experimental IsaMill data set that was presented by Gao et al., 1996. The following parameters were obtained from the fitting process: $D_{bref} = 0.00205\text{m}$, $\rho_{mref} = 7.8 \text{ g/cc}$, $\rho_{slref} = 1 \text{ g/cc}$, $k = 0.0199$, $a = 566.04$, $b = 0.571$, $c = 3.5761$, $d = 0.2$, $e = 5$, $f = 4.0188$. It should be noted that since these empirical parameters were fitted to a single data set they might not be applicable to other data sets. Radziszewski, 2013 applied the formula with the Gao parameters to other data sets of experimental data generated on Vertimill and Sala mills. In some cases the predicted power did show some agreement with the experimental data but the correlation was not able to accurately predict power draw in all cases. Hence the parameters to use for estimating the viscosity based on operating conditions seems to be application specific.

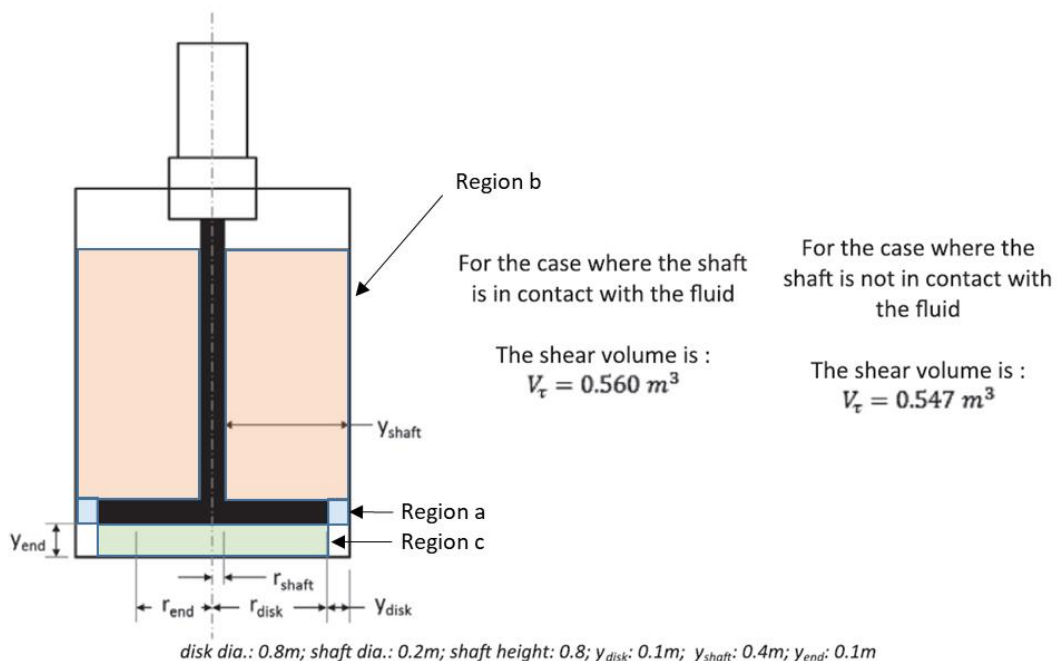


Figure 31: Example of shear volume calculation, Radziszewski 2013

Radziszewski, 2013 evaluated various hypothetical vertical stirred media mill geometries and calculated the shear volume for each of these hypothetical geometries. The impeller types evaluated included pins, discs, screws, and cylinders. With the pin and disc type of agitators it was found that the shear volume of the mill could be increased by the addition of liners to the stationary mill shell. The liners took the form of either pins or discs installed on the shell in such a way that it protrudes into the space between consecutive sets of stirrer agitators. Graphical schematics of the hypothetical geometrical arrangements are shown in Figure 32. The results of the shear volume calculations for the pin and disc stirrers are shown in Table 2. Radziszewski, 2013 found that the shear volume could be significantly increased by the addition of liners to the mill shell. In the case of the pin stirrer the shear volume could be increased by 32% using pin liners and up to 211% using disc liners. In the case of the disc stirrer the shear volume could be increased by 28% using pins as liners and by 55% by adding discs as liners. According to the shear based power model the power draw of the mill is proportional to the shear volume under similar operating conditions. Based on this Radziszewski, 2013 then postulated that the power draw of a mill operating with pin or disc type stirrers might be increased by adding liners to the mill shell. However no experimental work was presented to evaluate this hypothesis. Results obtained from this current work will contribute to providing experimental data to evaluate the predictions made based on the shear power model.

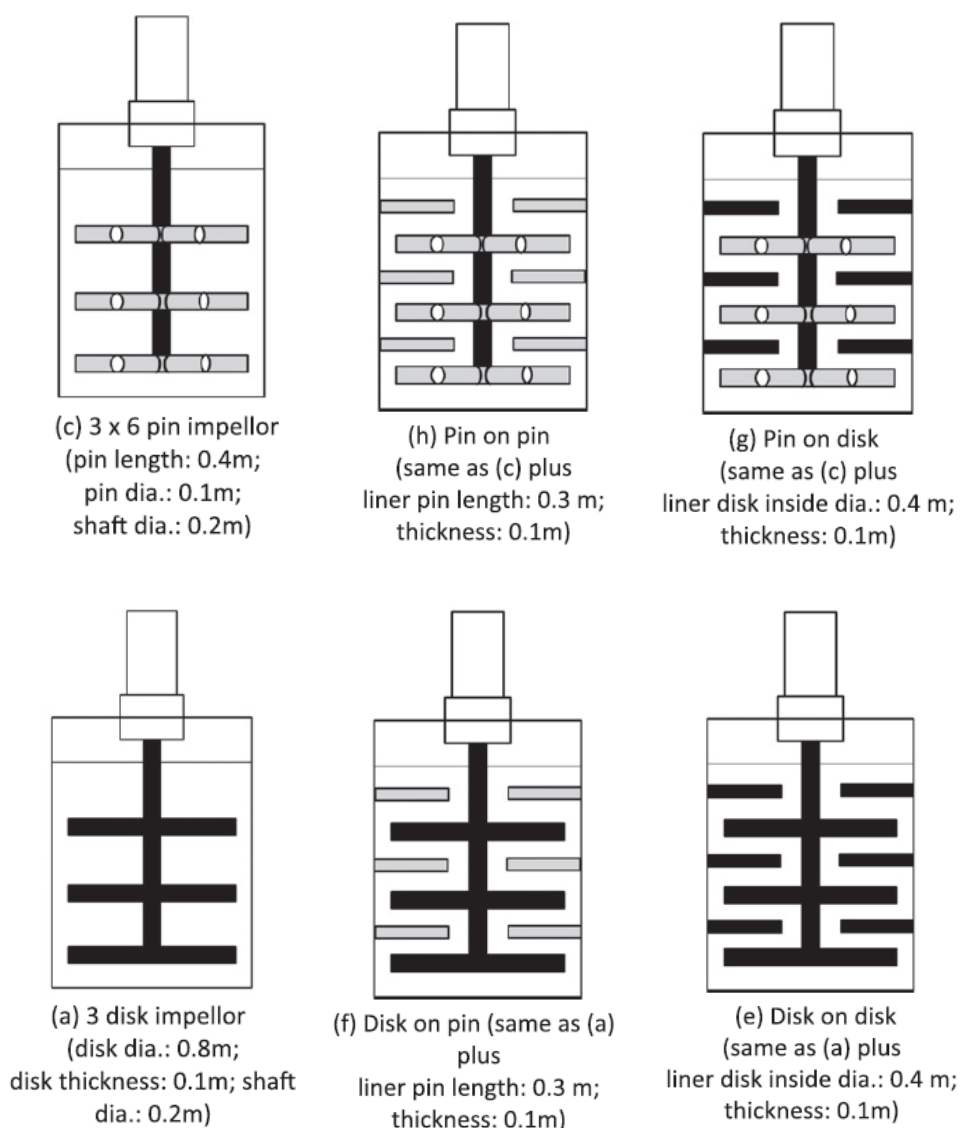


Figure 32: Various hypothetical geometrical mill arrangements, Radziszewski 2013

Table 2: Shear volume for various hypothetical mill geometries, Radziszewski 2013

Geometry	Shear Volume (m ³)	Relative Magnitude of Shear Volume	Increase in Shear Volume due to Shell Liner Addition
Pin type stirrer			
3 x 6 pin stirrer	0.114	1.00	
3 x 6 pin stirrer with pin liners	0.150	1.32	32%
3 x 6 pin stirrer with disc liners	0.355	3.11	211%
Disc type stirrer			
3 disc stirrer	1.618	1.00	
3 disc stirrer with pin liners	2.079	1.28	28%
3 disc stirrer with disc liners	2.503	1.55	55%

2.4 Particle Breakage Rates

The specific rate of breakage function, also called the selection function, was initially developed for use in the modelling of ball milling processes, but it has also found wide application for the modelling and comparative testing of stirred media mills. Various researchers have used the experimental approach of measuring the specific rates of breakage of ores during stirred media milling as part of their investigations (Mankosa et al., 1986; Davis & Dawson, 1989; Tüzün, 1993; Hogg & Cho, 2000).

2.4.1 Specific rate of Breakage (S_i)

The mathematical formulas governing a first-order batch grinding process were presented by Austin et al., 1984 and are related here. Consider the case of a batch milling process grinding a mass of ore W . If the starting feed consists of particles within a narrow size range for instance a $\sqrt{2}$ Taylor series size fraction denoted as size class i then the mass fraction w_i in the feed at time $t = 0$ is $w_i(0) = 1$. According to the first-order law:

Rate of disappearance of size i due to breakage $\propto w_i(t)W$ which can also be written as equation 10:

$$-\frac{d[w_i(t)W]}{dt} = -S_i w_i(t) \quad (10)$$

The total mass W is constant so equation 10 reduces to equation 11:

$$\frac{dw_i(t)}{dt} = -S_i w_i(t) \quad (11)$$

The parameter S_i is called the specific rate of breakage and is expressed in units of time⁻¹. If S_i remains constant with time then equation 12 applies:

$$w_i(t) = w_i(0)\exp(-S_i t) \quad (12)$$

Which can also be expressed in the form shown in equation 13:

$$\log[w_i(t)] = \log[w_i(0)] - S_i t/2.3 \quad (13)$$

If first-order kinetics apply, a plot of $w_i(t)/w_i(0)$ on a log scale versus time will yield a straight line with a slope value equal to $-S_i t/2.3$. An example of such a first-order plot is presented in Figure 33. This shows the specific breakage rate of a single size fraction. In a given feed ore the specific breakage rates differ for different particle size classes. An example of the typical kind of relationship between specific breakage rate and particle size is shown in Figure 34. This relationship is described in detail by Austin et al., 1984 and a summary of their discussion is presented here. The specific breakage rates usually increase with an increase in particle size up to a maximum value. At larger particle sizes the breakage rates are reduced. According to Austin et al., 1984 it is expected for smaller particles to be relatively stronger than larger particles due to the fact that the larger particles should contain larger Griffith flaws. These flaws are broken out as the size is reduced. There also is a geometric effect involved in that for a given media diameter it becomes more difficult to nip smaller particles in comparison to larger particles. However when the particles become very large they are also not properly nipped by a given size of media and the breakage rates are reduced. This is the case with particle sizes falling to the right of the specific breakage rate peak. In this region smaller particles might also interfere with the grinding of the larger particles, reducing the rate of breakage. The particles sizes that fall to the left of the breakage rate peak are said to exhibit normal breakage behaviour in that they usually conform to first-order breakage kinetics. The area on the left of the peak is therefore referred to as the normal breakage region. Particles to the right of the peak often exhibit non first-order behaviour. It has been found that the breakage is often characterised by a faster initial rate and a slower consecutive rate. The area on the right of the peak is referred to as the abnormal breakage region.

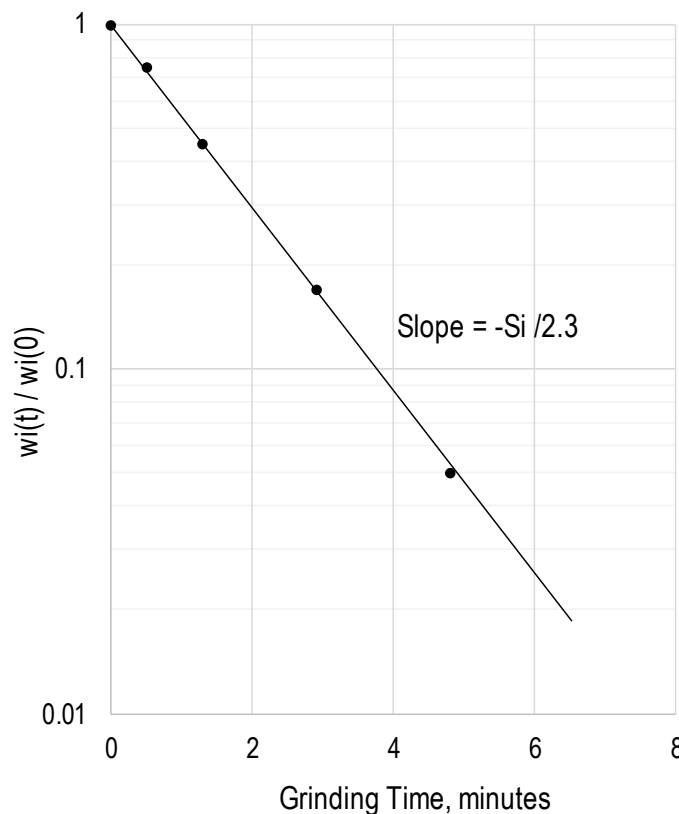


Figure 33: Example of a first order plot of 1.18 mm x 850 μ m anthracite in a 0.6m diameter ball mill (Austin et al., 1984)

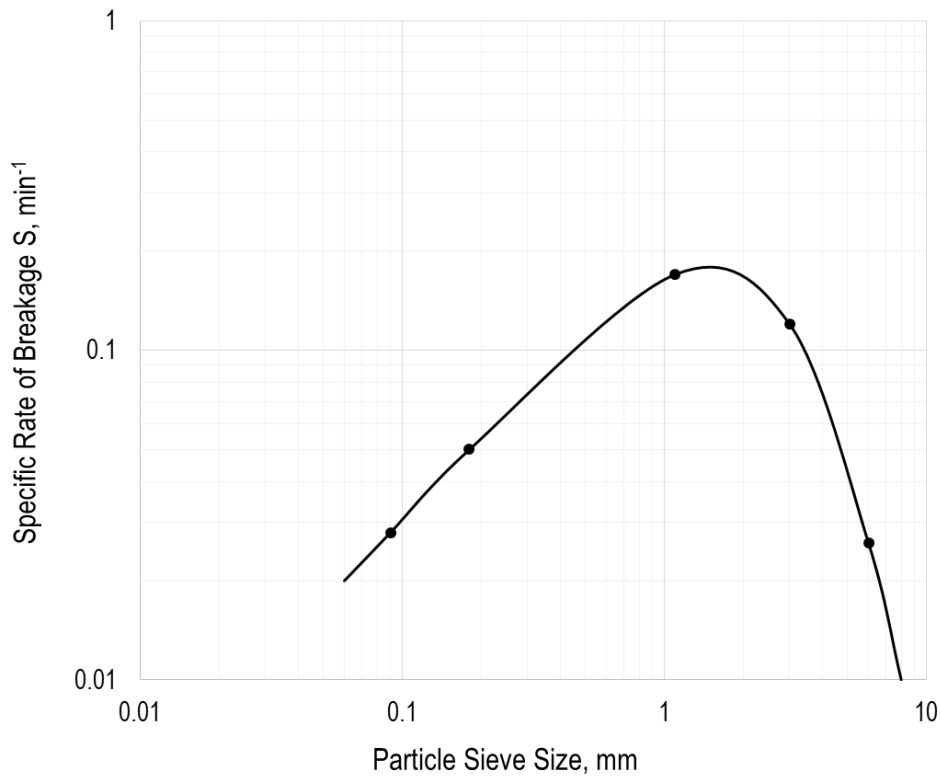


Figure 34: Specific rates of breakage of a South African gold ore as a function of particle size (Austin et al., 1984)

2.4.2 Experimental Determination of Specific Rate of Breakage (S_i)

Austin et al., 1984 describe experimental methods for determining the specific rates of breakage for ores. In the experimental work for this project the one-size-fraction method will be applied, therefore this method as described by Austin et al., 1984 will be related. The one-size-fraction method consists of grinding feed particles consisting of narrowly sized fractions, typically a $\sqrt{2}$ Taylor series size fraction, for various milling times. After each milling interval the mass fraction of particles remaining in the feed particle size fraction is determined by sieve analysis on the mill products. Only the fraction that is left in the top size needs to be determined so it is only necessary to screen at one sieve size. Before starting the tests a blank sieving test needs to be done. This is done by sieving a sub-sample of the feed material on the applicable sieve size representing the bottom size of the fraction. When doing the blank test it is usually found that there is some near-sized material passing through the bottom size sieve. The mass percentage of material passing the bottom sieve is referred to as the incomplete-sieving error, ϵ . It is recommended that this value should be relatively low compared to the material retained on the sieve. Since this represents misplaced material due to incomplete sieving and does not represent breakage products a correction needs to be made. When fitting the specific rate of breakage to the experimental results the line at time zero should extend through a starting point corrected for ϵ , as illustrated in the example in Figure 35. The milling intervals needs to be selected to provide both short and long milling times for fitting of S_i .

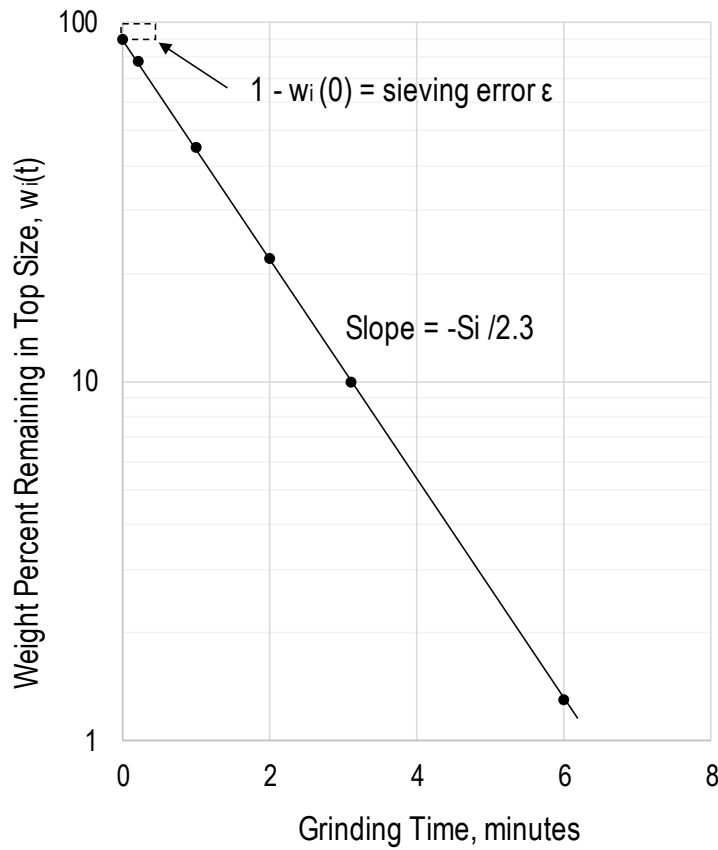


Figure 35: First-order plot for dry grinding of 1.18 mm x 850 µm petroleum coke in a 200mm i.d. ball mill (Austin et al., 1984)

2.4.3 Energy Normalised Rate of Breakage (S_i^E)

Herbst and Fuesternau, 1973 showed that the time based rate of breakage (S_i) can be normalised with regard to specific energy. The mathematical formulas derived by Herbst and Fuesternau, 1973 are related below. It was found that the specific rate of breakage (S_i) is proportional to the specific power input to the mill according to equation 14:

$$S_i = S_i^E \left[\frac{P}{M_p} \right] \quad (14)$$

Where P is the power input to the mill and M_p is the mass of ore particles in the mill. The proportionality constant (S_i^E) therefore has units of $(\text{energy/mass})^{-1}$. Substitution of equation 14 into equation 12 yields equation 15:

$$w_i(t) = w_i(0) \exp \left[-S_i^E \left(\frac{P}{M_p} \right) t \right] \quad (15)$$

The product of specific power and time corresponds to the specific energy input to the mill and can be defined according to equation 16:

$$E = \left[\frac{P}{M_p} \right] t \quad (16)$$

Where E is the specific energy input and this is usually expressed in units of kWh/t. Equation 15 then reduces to equation 17:

$$w_i(E) = w_i(0)\exp[-S_i^E E] \quad (17)$$

Equation 17 is therefore very similar to equation 12. In equation 12 the breakage rate is expressed on a time basis and in equation 17 the breakage rate is expressed on an energy normalised basis. Assuming that S_i^E remains constant with time the equation can be re-written as shown in equation 18:

$$\log[w_i(E)] = \log[w_i(0)] - S_i^E E/2.3 \quad (18)$$

If first-order kinetics apply, a plot of $w_i(E)/w_i(0)$ on a log scale versus specific energy input E will also yield a straight line, in this case with a slope value equal to $-S_i^E E/2.3$ as illustrated in Figure 36.

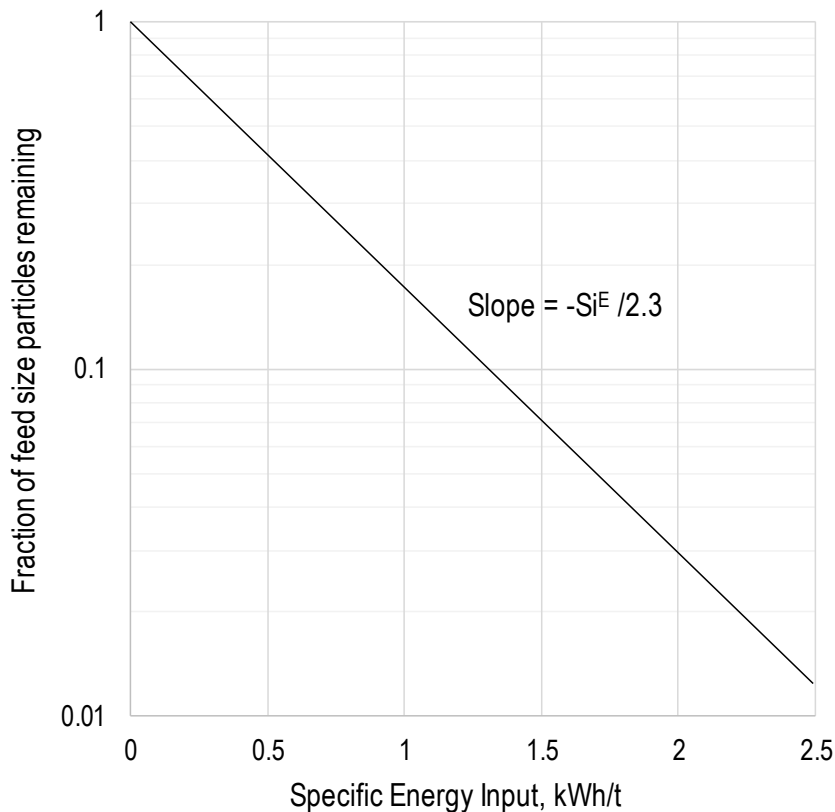


Figure 36: Example of a first order plot on an energy normalised basis (reproduced in part from Herbst and Fuerstenau, 1973)

2.4.4 Non-first order kinetics

The previous sections described cases where the breakage was first-order. However in literature there has been cases documented where non-first order breakage was observed. When non-first order breakage is observed there might be various reasons for why this is happening. Austin et al., 1984 provides a detailed discussion on this phenomenon and their discussion will be related here. Reference will be made to the plot in Figure 37. The discussion will firstly focus on region ab shown in Figure 37. When conducting a breakage test some of the starting material might be abnormally weak. This could be due to fractures introduced during the preparation process or due to an unusual shape, for example flakiness, created by the preparation process. This material will then show an initial faster breakage rate shown in area a. After a short time of grinding when the weaker particles have broken the breakage rate then stabilises into region b. Another reason why the curve ab might be observed is in cases where the top-size of the material being ground is too large to be adequately nipped by the grinding media. The grinding forces are then too small to consistently break the particles. In this case the probability is larger for weaker particles to break so the initial rate of breakage is high. Once the weak particles have broken the breakage rate reduces as shown in area b.

In some cases there is a change in breakage rate after region b. For the case shown by area d the breakage rate reduces again. Possible reasons for this could include the following.

- The remaining unbroken material might contain an accumulation of stronger material
- The fine material produced during milling might have a damping effect on the breakage of larger particles. This type of effect has been observed in the case of the abnormal breakage of large particles, when very fine dry grinding is conducted, and when wet grinding is conducted in a thick paste like slurry.
- The production of fine material might reduce the power draw of the mill due to interference with the mechanical action of the media. This can be identified by a change in the mill power measurements during this period.
- Particles might agglomerate during milling and these agglomerates might not be broken up by sieving

Some cases exhibit an increase in the breakage rate, region c, after the initial decrease in region b. Possible causes of this include:

- Larger particles might shield the breakage of smaller particles. When these larger particles have broken the probability for smaller particles to break will be higher and then the overall breakage rate increases.
- The material being milled might become progressively weaker due to impacts that are not large enough to break the particles but act to weaken them.
- During milling a harder ore component might be liberated and this harder component might act to assist with the grinding of the softer components.
- The increase in fines might act to improve the grinding efficiency of the mill by increasing the power draw.

The causes of the effects observed in region c and d can be divided into two main categories. The effects can be as a result of changes in the milling environment or as a result of changes to the material properties. To distinguish between the two causes it is advised to conduct a grinding rate test with unbroken material left over from region c or d. If the change in breakage rate is due to changes in the properties of the material then the initial breakage rate observed in this test will be the same as that for c or d. However if the change came as a result of changes in the milling environment then the initial breakage rate will be similar to that of region b. This is due to the fact that when the test is done with only unbroken material, the milling conditions are essentially reset to original conditions.

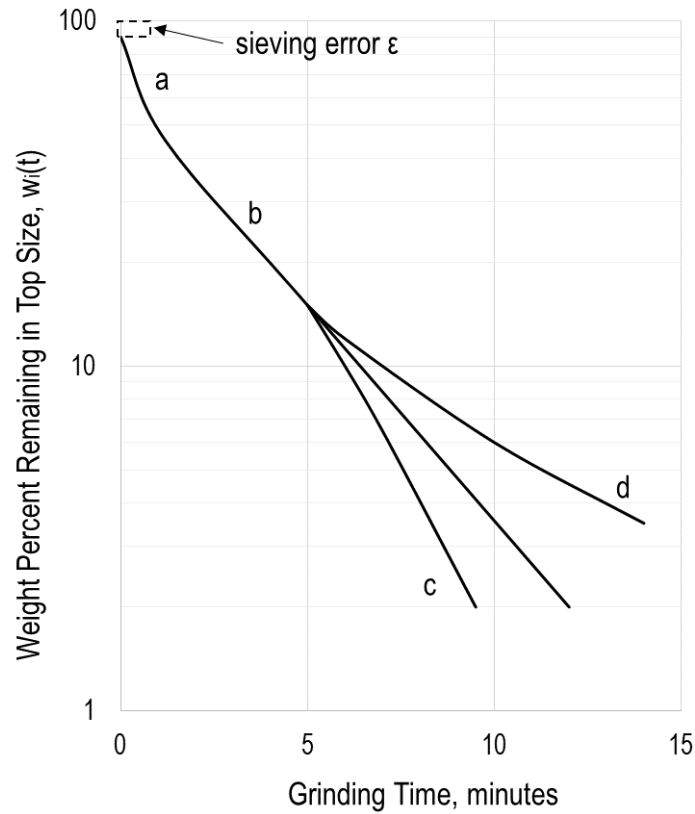


Figure 37: Illustrations showing deviation from first order kinetics, (Austin et al., 1984)

Davis and Dawson, 1989 conducted attrition grinding tests with limestone as the material being milled and with quartz particles used as the grinding medium. In their work they observed non-first order breakage similar to curve ab in Figure 37. They used equation 19 to fit breakage rates to the observed non-first order data.

$$w_i(t) = (1 - \varphi)\exp(-S_{ia}t) + \varphi \exp(-S_{ib}t) \quad (19)$$

Where φ is the fraction of slow-breaking particles in the feed. S_{ia} is the breakage rate constant for the fast-breaking particles (min^{-1}) and S_{ib} is the breakage rate constant for the slow-breaking particles (min^{-1}). This formula is essentially an extension of equation 12. But rather than modelling only one breakage rate this formula allows for handling of faster and slower kinetics. Davis and Dawson, 1989, used a regression technique to fit equation 19 to their data. Equation 19 was developed for time based kinetics. However in this current work use will also be made of energy normalised breakage rates. For this case equation 17 can be extended in a similar way to provide equation 20.

$$w_i(E) = (1 - \varphi)\exp(-S_{ia}^E E) + \varphi \exp(-S_{ib}^E E) \quad (20)$$

Where S_{ia}^E is the energy normalised breakage rate constant for the fast-breaking particles (kWh/t^{-1}) and S_{ib}^E is the energy normalised breakage rate constant for the slow-breaking particles (kWh/t^{-1}).

2.5 Computational Modelling of Stirred Media Mills

Various studies have focused on investigating stirred media milling through the use of computational modelling techniques as summarised in Table 3. The main techniques that were applied were the Discrete Element Method (DEM) and Computational Fluid Dynamics (CFD). These techniques were sometimes used on their own or coupled with each other in the CFD-DEM approach. The DEM approach is used to model the movement

of the beads while the CFD component is used to model the slurry or fluid medium. Some studies also focused on investigating the actual charge movement inside of the mill using Positron Emission Particle Tracking (PEPT). The majority of investigations have focused on evaluating the horizontal laboratory scale IsaMills but there are some studies that considered laboratory scale vertical stirred media mills and full scale IsaMill operation.

Table 3: Computational Modelling of Stirred Media Mills by Various Authors

Author	Mill Orientation (Vertical or Horizontal)	Discrete Element Method (DEM)	Computational Fluid Dynamics (CFD)	DEM-CFD	Positron Emission Particle Tracking (PEPT)	Areas Investigated
Blecher et al. 1996	Horizontal		x			Charge movement
Blecher & Schwedes 1996	Horizontal		x			Charge movement
Conway-Baker et al 2002	Vertical				x	Charge movement
Barley et al 2004	Vertical				x	Charge movement
Gudin et al 2006	Horizontal	x				DEM impact energy versus particle breakage rates
Cleary et al 2006	Vertical	x				Charge movement, wear patterns
Sinnott 2006	Vertical	x				Charge movement, wear patterns
Yang et al 2006	Horizontal	x				Charge movement
Jayasundara et al 2008	Horizontal	x				Charge movement
Kim & Chung 2009	Vertical	x				DEM impact energy versus particle breakage rates
Jayasundara et al 2009	Horizontal			x		Charge movement
Gers et al 2010	Horizontal		x			Charge movement
Jaysandura et al 2010	Horizontal	x				DEM impact energy versus particle breakage rates
Van der Westhuizen et al 2011	Horizontal				x	Charge movement
Jayasundara et al 2011	Horizontal		x		x	Charge movement
Jayasundara et al 2011b	Horizontal	x				Wear patterns
Yamamoto et al 2012	Horizontal	x				Novel computational method
Jayasundara et al 2012	Horizontal			x		Charge movement
Beinert et al 2012	Horizontal			x		Charge movement
Santhanam et al 2013	Vertical	x				Novel computational method
Beinert et al 2014	Horizontal			x		Mill optimisation
Cleary et al 2015	Horizontal	x				Mill optimisation
Beinert et al 2015	Horizontal			x		Mill optimisation
Riley et al 2016	Vertical				x	Charge movement
Beinert et al 2018	Horizontal			x		Mill optimisation
Beinert et al 2018b	Horizontal			x		Mill optimisation

2.5.1 Particle Breakage Rates

Various studies have investigated the correlation between the impact energy modelled by DEM and the particle breakage rates. Gudin et al., 2006, attempted to correlate the breakage rate constant of gibbsite powder milled in a horizontal laboratory stirred media mill to the specific impact energy modelled by the DEM simulation. In a different study DEM simulations and experimental test work were conducted on a laboratory IsaMill operating under dry conditions. The results showed that the breakage of particles followed first order kinetics and that the breakage rate constant of the material can be correlated to the impact energy of the beads predicted from the DEM, (Jaysandura et al., 2010). Experimental tests and DEM modelling of calcite, pyrophyllite, and talc powder grinding in a vertical stirred media mill were conducted. The investigation found that the grinding rate constant for the ore was directly correlated with the magnitude of the forces acting on the media at their contact points, (Kim & Chung, 2009).

2.5.2 Charge Movement

Various studies focused on modelling the charge movement of media in a horizontal IsaMill. Yang et al., 2006, studied the flow of grinding media in an IsaMill using DEM. The effect of DEM parameters on the model predictions were investigated. In a similar study conducted on an IsaMill by a different author, the results showed that the friction coefficient has a significant influence on the charge movement but that the influence of the coefficient of restitution was negligible, (Jayasundara et al., 2008). In addition to DEM other computational modelling techniques has also been used to model horizontal stirred mills. Jayasundara et al., 2009, applied a coupled CFD-DEM approach to model a laboratory IsaMill. Gers et al., 2010, used a CFD approach to model a horizontal stirred media mill. PEPT has been applied to track the motion of grinding media in a laboratory scale IsaMill, (Van der Westhuizen et al., 2011). Predictions from a CFD-DEM model of a laboratory scale IsaMill showed reasonable agreement with the experimental PEPT and power draw results obtained on the actual mill, (Jayasundara et al., 2011; Jayasundara et al., 2012).

Some studies also explored vertical mill configurations. PEPT was used to track the charge movement for different impeller types and stirrer speeds in a vertical laboratory mill, (Conway-Baker et al., 2002; Barley et al., 2004). The investigation showed that the stirrer design and speed has an influence on the charge movement characteristics in the mill, Figure 38. Riley et al., 2016 also used PEPT to study the charge movement in a laboratory pin mill. In a different investigation the media flow patterns and energy absorption of a tower mill were compared against a pin mill using a DEM approach. The results showed that the tower mill has a high degree of media recirculation inside of the mill. Media moves up with the screw and at the top the media then moves down along the side of the mill chamber. The results indicated that the circulation of media in the pin mill was more limited compared to the tower mill. The media tended to circulate in smaller localised areas. Energy absorption by the media in the tower mill was higher as compared to the pin mill, Figure 39. In the pin mill the energy absorption was the highest close to the pins near the base plate and was much lower towards the top of the mill. According to the authors this indicates that in the tower mill a substantial fraction of the media is able to contribute to the size reduction process, whereas in the pin mill a large portion of the grinding media might have energy levels that are too low to contribute significantly to grinding, (Cleary et al., 2006; Sinnott, 2006). This study further highlights the fact that the choice of stirrer design has an influence on the charge motion and consequently the milling conditions generated in the mill.

Effect of impeller type

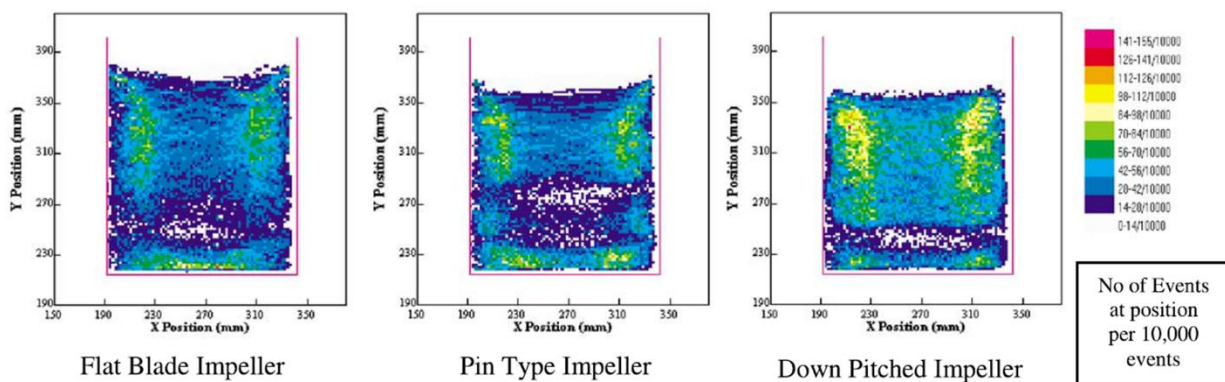


Figure 38: PEPT Occupancy plots for different impeller types at 520 rpm, (Conway-Baker et al., 2002)

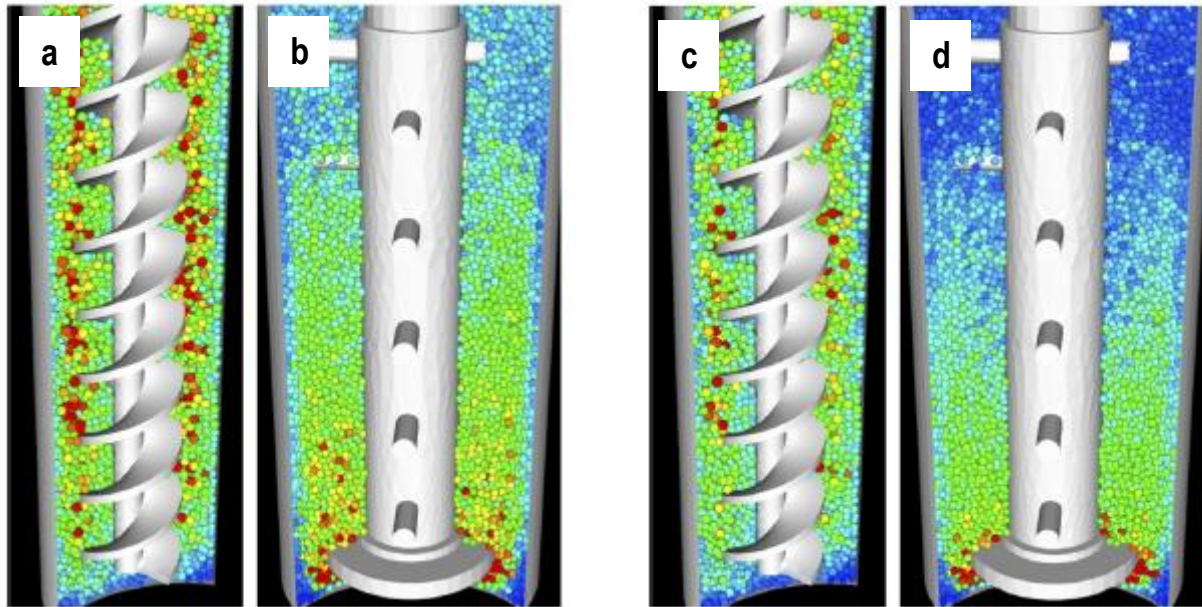


Figure 39: Energy absorption rates a) tower mill normal b) pin mill normal c) tower mill tangential d) pin mill tangential, (Sinnott, 2006)

2.5.3 Wear Patterns

DEM was used to study the wear patterns and wear rates of stirrer discs in an IsaMill. The results predicted by the DEM model showed good agreement with actual wear patterns found in operating mills, Figure 40, (Jayasundara et al., 2011b). In a different study DEM was used to model and compare the expected wear patterns of a tower mill utilising a screw stirrer against that of a similar mill vessel fitted with a pin stirrer design. In the case of the tower mill it was identified that the edge of the screw will be the main wear area. For the pin stirrer design the effect of wear is predicted to generate changes in the pin geometry. The pins will be flattened due to wear and the pin tips will experience rounding, (Cleary et al., 2006; Sinnott, 2006).

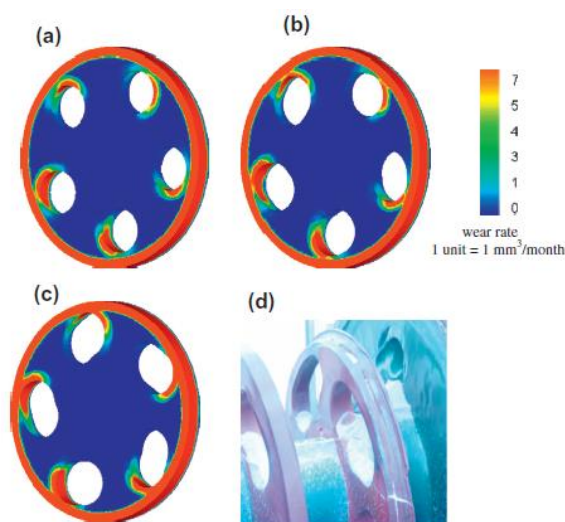


Figure 40: Wear of IsaMill disc holes a) new disc b) 4 months c) 8 months d) wear pattern on actual mill disc (Jayasundara et al., 2011b)

2.5.4 Mill Optimisation

Cleary et al., 2015 used DEM to model a full scale IsaMill in order to better understand the mechanisms acting in the mill with the objective of optimising mill performance. Different mill parameters were investigated including media size, media filling level, Figure 41, angular speed of the impeller, axial pressure gradient, and material properties.

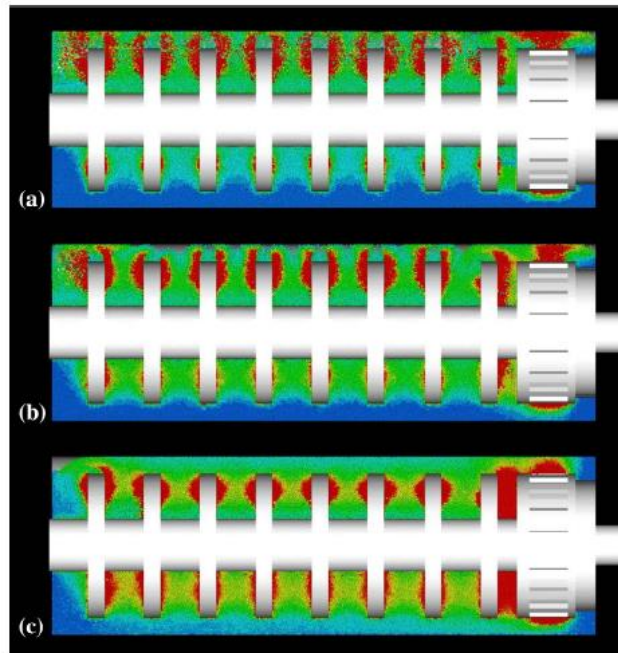


Figure 41: Variation in media speed and distribution at a) 70% filling b) 80% filling c) 90% filling, (Cleary et al., 2015)

The Institute for Particle Technology at the Technical University of Braunschweig developed an approach where the grinding conditions in the stirred mill are described by both the contact frequency and the contact energy spectrum of the grinding media. A CFD-DEM modelling approach is used to quantify the contact frequency and energy spectrum in the mill. Different stirred media mill types and geometries can be compared on this basis, (Beinert et al., 2014; Beinert et al., 2015; Beinert, 2018; Beinert, 2018b).

2.5.5 Novel Modelling Approaches

Some studies examined the use of novel computational approaches. Yamamoto et al., 2012, investigated the modelling of small beads a larger particles in a DEM model. In a different study a novel DEM implementation was developed where the model reacts by changing the rotational speed of the pin mill stirrer based on interactions with the grinding media charge, (Santhanam et al., 2013).

2.6 Discrete Element Modelling (DEM)

For this investigation DEM modelling was applied for two different purposes. Firstly DEM was used for qualitative comparison of the charge conditions of the different geometries. Secondly DEM was also applied in the initial stages of the investigation as a virtual prototyping tool for evaluating conceptual stirrer and mill liner designs. The soft particle DEM formulation was used.

2.6.1 Soft Particle DEM Formulation

The discrete element method is a numerical computational technique that simulates the interaction between a number of individual discrete particles. In the numerical algorithm each particle is identified separately. For particles in contact the normal and tangential contact forces are calculated. The contact forces acting on each particle are then added to calculate the total net force acting on the particle. An integration calculation based on Newton's second law of motion is then applied to each particle to calculate the acceleration, velocity, and position of the particle. This information is then updated for each particle and the calculation process is repeated over a number of time steps (Mishra & Rajamani, 1992). In the soft particle DEM method the particles are allowed to overlap and the amount of overlap determines the magnitude of the contact force acting between the particles. Various types of contact force models can be used but often for the simulation of comminution processes a simple linear spring-dashpot model is used to model the normal and tangential forces occurring between particles in contact (Weerasekara et al., 2013). This model can be visualised with the diagram shown in Figure 42, (Cleary, 1998).

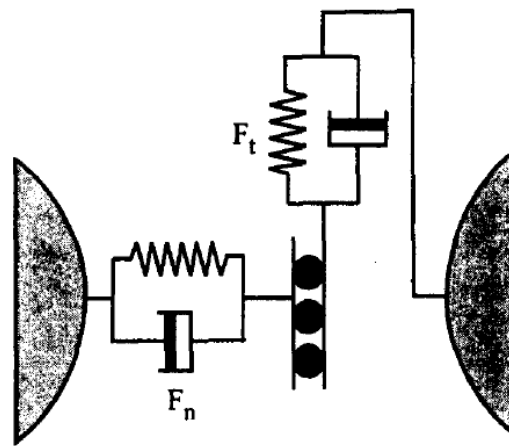


Figure 42: Diagrammatic representation of normal and tangential forces used in DEM, Cleary 1998

The normal force F_n consists of a spring component that models the repulsive force between the particles and a dashpot component that dissipates a portion of the kinetic energy. The normal force F_n is mathematically expressed with equation 21, (Cleary, 1998):

$$F_n = -k_n \delta + C_n v_n \quad (21)$$

Where k_n is the normal spring constant or stiffness, δ is the particle overlap, C_n is the normal damping coefficient, and v_n is the relative velocity in the normal direction. The force acting in the tangential direction, F_t , is calculated using equation 22, (Cleary, 1998):

$$F_t = \min\{\mu F_n, k_t \int v_t dt + C_t v_t\} \quad (22)$$

Where μ is the coefficient of static friction, k_t is the tangential spring constant or stiffness, dt is the time step, C_t is the tangential damping coefficient, and v_t is the relative velocity in the tangential direction. In this formula the integral of the relative velocity, v_t , over the duration of the contact acts as an incremental spring that stores energy originating from the relative tangential motion. This term therefore represents the elastic tangential deformation of the surfaces in contact. The dashpot term is used to model energy dissipation due to plastic deformation occurring at the contact. The tangential force is limited by the Coulomb friction limit at which point the particles will start to slide over each other (Cleary, 1998).

When applying this method of DEM it is typical to use a spring stiffness and time-step that limits the maximum overlap, or maximum penetration depth δ_{max} , of the particles. Different literature sources have provided different guidelines on the recommended maximum overlap. According to Govender et al., 2015 the overlap should be limited to $\delta_{max} \leq 0.05r$ where r is the radius of the smallest particle being simulated. This corresponds to a maximum overlap of 2.5% of the particle diameter. Dragomir et al., 2009 proposes that the maximum overlap should not exceed 0.5% of the particle diameter. Cleary, 1998 indicated that a maximum overlap of between 0.1% to 1.0% of particle diameter is acceptable. The spring stiffness in the normal direction, k_n , can be calculated using equation 23, (Mishra & Murty, 2001).

$$k_n = f^2 m v_0^2 / d^2 \quad (23)$$

Where d is the particle diameter, m is the mass of the particle, v_0 is the estimated maximum velocity of any particle in the system being modelled, f is the penetration factor and is calculated by d/δ_{max} . The spring stiffness is expressed in units of N/m. The tangential stiffness k_t can be calculated as a function of the normal stiffness by using equation 24, (Cummins et al., 2012).

$$k_t = \frac{2(1-\nu)}{(2-\nu)} \cdot k_n \quad (24)$$

Where ν is Poisson's ratio. The damping coefficients, C_n and C_t , in the normal and tangential directions respectively can be calculated as a function of the spring stiffness k , particle masses m , and coefficient of restitution ϵ , using equations 25 to 27, (Govender et al., 2015).

$$C_n = \frac{2 \ln(\epsilon) \sqrt{k_n m_{eff}}}{\sqrt{\ln(\epsilon)^2 + \pi^2}} \quad (25)$$

$$C_t = \frac{2 \ln(\epsilon) \sqrt{k_t m_{eff}}}{\sqrt{\ln(\epsilon)^2 + \pi^2}} \quad (26)$$

$$m_{eff} = \left(\frac{1}{m_1} + \frac{1}{m_2} \right)^{-1} \quad (27)$$

The effective mass of the particles in contact, m_{eff} , is calculated from the masses of the individual particles taking part in the contact, m_1 and m_2 . This is applicable to particle to particle contacts. In the case of particle to wall contacts the mass of the wall can be taken as being much larger than that of the particle. Assuming that m_1 is the mass of the particle and m_2 is the mass of the wall, the ratio of $1/m_2$ approaches zero, so in this case equation 27 simplifies to equation 28, (Mishra & Rajamani, 1992):

$$m_{eff} = \left(\frac{1}{m_1} \right)^{-1} \quad (28)$$

When simulating mills the choice of time step used in the simulation is governed by the rotational speed of the mill and the maximum allowable overlap of particles. Govender et al., 2015, presents the formulas to use for calculating the time-step increment. The distance covered by a mill lifter during a given time step, x_{Lifter} , is calculated by equation 29:

$$x_{Lifter} = R \cdot \omega \cdot \Delta t \quad (29)$$

Where R is the radius of the mill drum and ω is the angular velocity that is calculated using equation 30:

$$\omega = \frac{\pi}{30} \Omega \quad (30)$$

Where Ω is the rotational speed in rpm. The time-step is then chosen based on the maximum penetration distance, $\leq \delta_{max}$ in order to limit the overlap of particles. Equation 31 is used to calculate the time step:

$$\Delta t = \frac{\delta_{max}}{R \cdot \omega} \quad (31)$$

In this example a tumbling mill was simulated so the rotational speed of the rotating drum was used for Ω , but in the case of stirred media mills the outer mill drum is stationary and the stirrer is rotating so the value used for Ω will be the rotational speed of the stirrer. R can then be taken as the distance from the centre of the shaft to the tip of the stirrer.

It should be noted that when using a DEM only approach to model milling processes, it is usually only the media movement and media energy distributions that are simulated with the DEM model. In most cases the ore particles and slurry phases are not modelled. For this reason the parameters used in the DEM simulation are the apparent contact parameters and not the standard physical contact parameters measured experimentally (Tavares, 2017; Mishra & Rajamani, 1992). The presence of the slurry or powder phase has the effect of increasing the apparent static friction coefficient and reducing the apparent coefficient of restitution (Tavares, 2017). It is these two coefficients that are usually tuned during the calibration process. These parameters are commonly selected in such a way as to have the modelled power draw obtained from the DEM match an experimentally determined power draw of the actual mill being simulated. In addition to the power draw the motion of the charge can be used as a factor in the calibration process where the simulated charge movement is compared to the actual charge movement in an experimental mill (Tavares, 2017; Mishra & Rajamani, 1992; Govender et al., 2015; Chagas, 2015; Weerasekara et al., 2013).

2.7 Literature Conclusions

Comminution processes are used in metallurgical operations to reduce the particle size of the mined ore in order to liberate the minerals of interest for downstream separation processes. There are many different types of comminution equipment used in the industry and the different types of equipment are suitable for different types of duties based on the feed and product particle size requirements. A comminution circuit usually consists of a number of different equipment operating in series to reduce the particles from the run of mine (ROM) particle size distribution down to the grind size required by the separation process. Stirred media mills consist of a stationary outer mill chamber and central rotating shaft fitted with a stirrer, also called an impeller. The rotation of the stirrer agitates the grinding media in the mill chamber. The movement of the grinding media creates breakage of the ore particles introduced to the mill for processing. Stirred media mills can be classified into two general types namely gravity induced or fluidised. In the gravity induced type of design relatively large and heavy steel media balls are used as grinding media. During operation the media settles in the mill under the influence of gravity and is lifted up again by the stirrer. In the case of fluidised mills much lighter and smaller ceramic beads are used as grinding media. During operation the entire mill contents are fluidised so the grinding media and slurry act as a single phase. This current investigation focuses on the fluidised type of mill design.

Fluidised stirred media mills are used for fine grinding applications to produce products with particle sizes typically below 75 μm . Depending on the type of stirred media mill, the feed sizes that can be accepted ranges from around 500 μm to 200 μm . Comminution requires a significant amount of energy and as such there is a need to reduce the energy requirement in comminution processes. Ball mills have traditionally been used for fine grinding applications. However stirred media mills are more energy efficient than ball mills for producing product grinds smaller than 75 μm . Stirred mills have therefore become the preferred technology for fine grinding duties in the minerals industry. There are various different designs of fluidised stirred media mills in use. The stationary mill chamber can be orientated either horizontally or vertically. An example of a horizontal mill is the IsaMill. Vertically orientated mills are more common with examples including the HIG, SMD, and VXP mills. Various types of stirrer designs are employed with the disc types of designs being the most common and variations of this design are used in the IsaMill, HIG, and VXP mills. The SMD mill utilises a pin design.

There are various factors that influence the efficiency of the grinding process in a stirred media mill. The main operating variables include, stirrer speed, pulp solids concentration, media size, including ratio of bead size to particle size, and media density. The optimum selection of operating parameters is application specific. Parameter selection that is either too high or too low will result in in-efficient milling. The physical mill design and geometry also has an influence on the grinding efficiency. The type of stirrer used and the ratio of impeller diameter to chamber diameter has been shown to have an effect. When the ratio of impeller to chamber diameter is too low the gap between the impeller and the chamber is large and this leads to lower grinding forces acting against the chamber wall. Various studies have also found that the addition of grinding aid chemicals can improve the grinding process in stirred media mills.

Using the shear based power model Radziszewski, 2013, postulated that the power draw of a vertical stirred media mill operating with pin or disc type stirrers might be increased by adding liners to the mill shell. However no experimental work was presented to evaluate the hypothesis. The objective of this current investigation is to conduct an experimental programme to test this hypothesis.

The rates at which particles break in a comminution process can be quantified by means of the specific rate of breakage. Particle breakage rates can be expressed either on a time basis or on an energy normalised basis. Both the time based, S_i , and energy normalised, S_i^E , breakage rates can be measured experimentally during batch grinding tests conducted with mono-sized feed material. The approach of measuring breakage rates are commonly used in the study of stirred media mills. This technique will also form part of the experimental test work programme for the current study.

Computational modelling techniques have been applied to study the conditions present in stirred media mills. The main techniques that were applied were the Discrete Element Method (DEM) and Computational Fluid Dynamics (CFD). These techniques were sometimes used on their own or coupled with each other in the CFD-DEM approach. The DEM approach is used to model the movement of the beads while the CFD component is used to model the slurry or fluid medium. Some studies also focused on investigating the actual charge movement inside of the mill using Positron Emission Particle Tracking (PEPT). In the current study DEM will be used to obtain a qualitative insight into the grinding media conditions present in the various different stirred media mill configurations tested. The soft particle DEM formulation will be used as this method is most commonly applied to comminution simulations.

3 Research Methodology

3.1 Overview of Research Methodology

To answer research question 1 an experimental programme was developed to measure the mill power draw of four different mill geometries under comparative conditions. To answer questions 2 and 3 a grinding test programme was developed to compare the breakage rates of a silica feed material when milled in the four different mill geometries under similar operating conditions. Since productivity relates to mill throughput rate (tonne/hour) the comparison of equipment productivity needs to be made using a time based measure, while the comparison of energy efficiency needs to be made using an energy based measure. In this regard the time based specific rate of breakage (S_i) and the energy normalised specific rate of breakage (S_i^E) provides a useful way of comparing different mill geometries and were used as measures for comparison in this investigation. Testing was therefore conducted on mono-sized feed material in order to measure the breakage rates. Further tests were also conducted on silica feed material with a natural feed size distribution. The specific energy requirement (kWh/t) and milling times (minutes) to reach a given target product grind were used to compare the performance of the four different mill geometries.

The four different geometries evaluated are pictured in Figure 43. Two types of stirrer designs and two types of mill vessel designs were used. The pin stirrer consisted of two sets of 6 pins for a total of 12 pins. The ring stirrer consisted of two sets of rings. Each ring set was made up of an outside annular ring connected to the

shaft with four spokes. A 180 x 230 cm smooth shell vessel and a 180 x 230 cm vessel fitted with a disc liner were used. All of the equipment were manufactured from steel. The stirrers and disc vessel used for the experimental work were designed and fabricated specifically for this investigation.

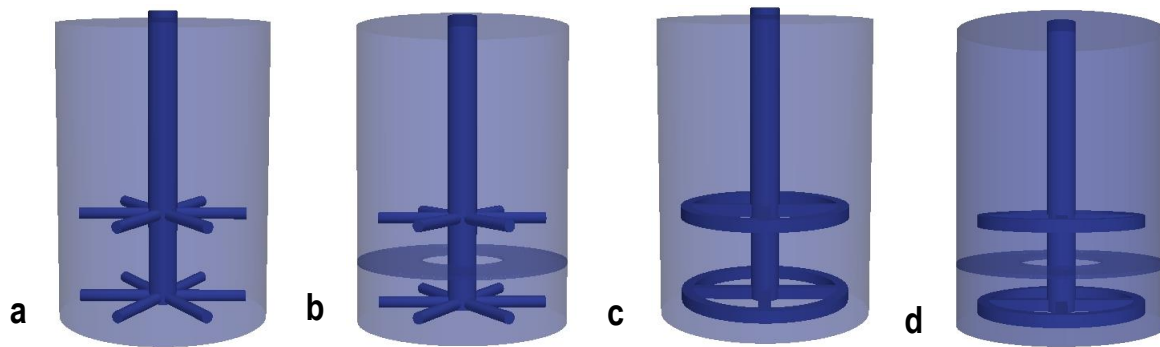


Figure 43: Four geometries evaluated in this investigation a) 12-pin – smooth vessel, b) 12-pin – disc vessel, c) ring – smooth vessel, d) ring – disc vessel

In this work DEM modelling was applied to study the different mill geometries under comparative conditions. The aim of the DEM work was not to quantify the exact physics occurring in the stirred mill, for this a coupled DEM-CFD approach would have been required due to the presence of the slurry phase in the mill. The aim was rather to gain some qualitative insight into the conditions present when different geometries are used under comparative conditions. For this the simpler DEM only approach was used, as the complexities involved with a DEM-CFD approach was outside of the scope of the current investigation. However the experimental results generated during this work might lend itself to future study using coupled DEM-CFD modelling.

3.2 Experimental Design Considerations

During the design of the experimental programme consideration had to be given to identify suitable test conditions. The content in section 3.2 is intended as a discussion of some of the general philosophies adopted in the experimental design process.

3.2.1 Quantifying of Results

The aim of this investigation is to compare the performance of different mill geometries based on two criteria namely equipment productivity and equipment energy efficiency. Productivity relates to the amount of product at a desired grind size that is produced in a unit of time. In industrial terms it relates to the throughput rate (tonne/hour) that can be achieved with a given size of equipment. Energy efficiency relates to the amount of energy required to produce a given amount of product at the required grind size (kWh/tonne).

The comparison of productivity therefore needs to be made using a time based measure, while the comparison of energy efficiency needs to be made using an energy based measure. In this regard the time based specific rate of breakage (S_i) and the energy normalised specific rate of breakage (S_i^E) will provide a useful way of comparing the different mill geometries and will be used as measures for comparison in this investigation. Experimental tests should therefore be focused on providing data to calculate S_i and S_i^E for the different mill geometries under similar operating conditions. An experimental programme of this nature will require the use of mono-sized feed material. It also follows that the test equipment used should provide information on the power draw and energy input during the milling tests to allow calculation of the energy normalised specific rate of breakage S_i^E . In practice a stirred media mill will rarely accept mono-sized feed material, the feed would rather consist of a wide range of particle sizes. For comparative purposes it would also be necessary to conduct testing with a feed material consisting of a natural distribution of particle sizes. For this type of feed the specific

energy requirement (kWh/t) and milling times (minutes) to reach a given target product grind can be used to compare the performance of the four different mill geometries.

3.2.2 Type of Sample to Use

Since the conclusions of the study will rely on comparing the breakage rates of material when milled using different geometries, the level of homogeneity of the material being milled is of importance. The material should behave consistently and the use of a single mineral type is expected to provide more consistent breakage behaviour than a mixture of different mineral types might provide. In this regard it was decided to use silica sand as feed material for the milling experiments as it consists mainly of one type of mineral.

3.2.3 Scaling of Geometries

The theoretical geometries evaluated by Radziszewski, 2013, were based on a 1 m diameter by 1 m height size of mill chamber. While this size of unit would be suitable for pilot scale testing it is impractical for the laboratory scale test work to be conducted during this investigation. For this study a laboratory mill vessel with a chamber diameter of 180 cm and a height of 230 cm was available. The geometries used for this project were therefore selected to conform to a mill chamber dimension of 180 cm x 230 cm.

3.2.4 Batch Operation versus Continuous Operation

The research questions that will be investigated relate to the addition of extra shear surfaces in the mill. The effect of the additional shear surfaces on the breakage rates of material milled will be measured. It is therefore important to set the test up in such a way that the effect of the additional shear surfaces can be isolated. In this regard a batch test will provide more reliable conditions for measuring this effect. Compared to continuous testing the conditions present in the batch mill chamber are easier to control. The amount of solids and water in the mill can be measured accurately and added to the mill. Whereas in a continuous mill operation the slurry density in the mill and feed rate to the mill are always subject to some degree of variation. In continuous operation the slurry flow through the mill and the inherent classification effect present also complicate the comparison of test results. Another case for using batch testing is that the quantification of particle breakage rates are normally done during batch testing so doing batch tests for this type of work is the usual practice.

So while stirred media mills are operated industrially on a continuous feed basis, for the purposes of this current investigation a batch milling test approach would be suitable. However having made this statement it should be kept in mind that addition of extra shear surfaces in a mill will have an influence on the flow pattern of slurry and media in the mill when operated under continuous conditions. Therefore if favourable outcomes are observed during this investigation, it might be necessary to investigate the geometries tested in batch under continuous conditions. In this event continuous testing will be outside of the scope of the current investigation and could potentially be addressed in separate future investigations.

3.2.5 Design and Fabrication of Stirrers and Mill Vessel

The stirrer geometries evaluated in this study were based on pin and disc agitator designs. According to the shear power model proposed by Radziszewski, 2013, it might be possible to increase the power draw for these types of stirrer designs by the addition of extra liners on the mill shell. The testing therefore focused on evaluating both the pin and disc stirrers with and without liners on the mill shell.

A smooth mill vessel, without any shell liners, measuring 180 cm in diameter and 230 cm in height was available for test work. Also an existing 8-pin stirrer was available, however the configuration of the pins on the stirrer was not suitable to allow for the addition of a disc liner on the mill vessel as the spacing between the various levels of pins was very close together. It was therefore necessary to design and fabricate two new stirrers for the purposes of this project. The agitator spacing of the new pin and disc stirrers had to be designed in such a

way as to allow for sufficient space for the addition of a liner between the agitators. Also due to practical considerations associated with the installation of liners in the current mill vessel it was necessary to design a new mill vessel for the mill liner tests. The equipment designs are detailed in a subsequent section.

3.2.6 Feed Particle Size and Ceramic Bead Size

According to literature the Metprotech pin mill should preferably be fed with particles with sizes of less than 300 μm and can operate with media sizes ranging from 3 to 12 mm (Lichter and Davey, 2006). The VXP disc mill has been designed to accept feed particles no coarser than about 300 μm to 400 μm on an 80% passing basis, (Rahal, 2011). The VXP mill can operate with beads in the size range 1.5 to 12 mm (FLSmidth). The Metso SMD is typically used with feed particles of 200 μm and smaller (Metso, 2011). This mill typically uses media in the size range of 1 to 3 mm (Lichter and Davey, 2006). The Outotec HIG mill can typically accept feeds as coarse as around 100 to 300 μm on an 80% passing basis, with media sizes ranging from about 0.5 to 6 mm depending on the application (Lehto et al., 2011). In order to accommodate the range of operating conditions of the different types of mills a bead size of around 3 mm was selected for the experimental work. The ratio of bead size to feed particle size is an important parameter that needs to be set in stirred media milling operations. The bead size should be sufficiently large to be able to nip and break the largest particles in the feed. Selection of bead size will therefore influence the selection of feed particle size to use in the tests. In stirred media mill grinding tests conducted on a quartz feed material it was found that the optimum ratio of bead size to feed particle size was in the region of around 20:1, (Yue and Klein, 2006). The current test work programme was conducted on a similar feed material so based on this guideline the feed particle size used during testing was limited to a maximum size of around 150 μm .

3.2.7 Pulp Solids Concentration

Stirred media mills generally operate with relatively low slurry densities as compared to tumbling mills. The optimum slurry density will depend on the application. In fine grinding experiments on magnetite ore using a pin mill Eswaraiah et al., 2015, found that the product grinds improved when the pulp density was increased from 50% to 60% pulp solids concentration, but product grinds deteriorated at pulp density levels higher than 60% by mass. Edwards, 2016, conducted grinding tests on a MG2 reef ore using a Deswick disc stirrer mill. The tests were conducted at solids concentrations of 20%, 30%, and 40%. The conclusion was that increasing the pulp density from 20% to 40% solids by mass improved the product grinds achieved in the tests.

In order to define a suitable condition for the slurry density the recommendations by the equipment suppliers of various industrial vertical fluidised stirred media mills were evaluated. According to literature, SMD mills typically operate in the range of 30% to 60% solids by mass with the optimum slurry density usually in the range of 40% to 50% solids by mass (Metso, 2011; Davey, 2004). Optimum pulp density for the Knelson-Deswik disc type mill is in the range of 1.2 to 1.5 kg/L (Rahal et al., 2011). For a silica feed material with a typical SG of 2.65 this corresponds to a slurry concentration of around 27% to 54% solids by mass. For the HIG mill, Outotec indicates that the optimum slurry concentration is 30% solids on a volume basis, which corresponds to about 50% solids by mass for an ore with an SG of 2.7 (Lehto et al., 2013).

Based on the information presented a solids density of 50% by mass was selected for the experimental work. This solids concentration falls within the range recommended by the suppliers of all three of the major industrial mill types with similar geometries that will be investigated in this project.

3.2.8 Mill Filling Level

According to Outotec the HIG mill typically operates at a grinding media filling level of around 60% of the mill volume (Lehto et al., 2013). The VXP mill usually operates at grinding media loads ranging from 50% to 65% of the mill volume (FLSmidth). Test work conducted by Barley et al., 2004, investigated the motion of beads in an SMD pin mill over a range of media fillings ranging from 40% to 70% by volume. The investigation showed

a difference in bead motion at different filling levels however the work did not advise an optimum filling level. Work reported by Bailey et al., 2016 seems to indicate that the vortex conditions of the charge in an SMD becomes unstable at media filling levels of less than 30%. Gupta, 2016, indicated that vertical stirred media mills can operate with media filling levels of up to 80% by volume. A test work programme conducted in a VXP mill investigated filling levels ranging from 65% to 85%. The study found the effect that the mill filling had on grinding efficiency to be minimal. The best efficiency was obtained at 65% filling but lower filling levels were not tested, (Edwards, 2016). It therefore seems that a high filling level is not necessarily required in these types of mills. This would support the equipment supplier guidelines of using filling levels ranging from 50 to 65%,

For this test work a media filling level of 50% based on the volume of the smooth mill vessel was used. The 50% media filling calculation was based on the bulk density of the media.

3.2.9 Ratio of Pulp to Beads

The media filling level is usually expressed as the percentage of the mill volume occupied by the media that includes the void space between the beads. The media filling level therefore represents the bulk volume that is occupied by the media. This can be expressed with equation 32:

$$V_{bulk_media} = V_f * V_{mill} \quad (32)$$

Where V_{bulk_media} is the bulk volume occupied by media including the voids between beads. V_f is the mill filling level expressed as a fraction. V_{mill} is the total volume of the mill vessel. In this work the volume of the smooth mill vessel was used. The actual volume occupied by the grinding media beads, excluding the voids between beads, is related to the bulk volume of the media by the charge porosity or voidage. This relationship can be expressed by equation 33:

$$V_{beads} = (1 - p) * V_{bulk_media} \quad (33)$$

Where V_{beads} is the actual volume occupied by the material of the beads and this excludes the voids between beads. The charge porosity or voidage, is represented by p and is expressed as a fraction. In work conducted by (Bailey et al., 2016) a 3L SMD was operated in continuous mode at various conditions and after operation the mill was crash stopped. Measurements of the operating volume of the SMD were taken to quantify the operating volume and the ratio between beads and slurry. The operating volume consist of the total bulk volume of the mill occupied by media and slurry. Results from this work found that the ratio between the actual volume occupied by the slurry and the actual volume occupied by beads was around 1:1. Meaning that under continuous operating conditions the volume of slurry in the mill was about equal to the volume of beads in the mill, V_{beads} . The following relationship therefore applied (equation 34):

$$V_{slurry} \approx V_{beads} \quad (34)$$

To set the test conditions for this work the following assumption was made, (equation 35):

$$V_{slurry} = V_{beads} \quad (35)$$

The operating volume of the mill can therefore be calculated as, (equation 36):

$$V_{operating} = V_{beads} + V_{slurry} \quad (36)$$

3.2.10 Stirrer Speed

Stirrer tip velocities in the HIG mill range from 4-8 m/s for the smaller units to 8-12 m/s in the larger units (Lehto, 2011). Industrial VXP mills were designed to operate with tip speeds ranging from 10-12 m/s (FLSmith). Laboratory SMD mills are usually operated at tip speeds of 5-6 m/s but in industrial mills the tip speeds are typically closer to 8 m/s (Bailey, 2016). The equipment that was available for this study provided stirrer tip speeds ranging from 2 m/s to 4 m/s.

3.2.11 Grinding Media Density

The use of bead densities in the range of 2.6 - 3.0 g/cm³ seems to be the optimum for the SMD mill, (Moore et al., 2016). The HIG mill typically operates with media densities ranging from 3.8 – 4.2 g/cm³, (Lehto, 2015). The bead density of 3.25 g/cm³ used in the current test work therefore seems suitable since it represents an average media density for these types of mills.

3.3 Batch Milling Test Rig

A laboratory scale stirred media milling test rig located at Mintek South Africa was used for conducting the experimental work. The rig is pictured in Figure 44. The test rig can be fitted with different stirrers and mill vessels. The stirrer motor is equipped with a variable speed drive used to change the stirrer speed up to a maximum speed of around 530 rpm. The shaft is fitted with a torque arm and load cell arrangement that allows for the measurement of the torque applied to the shaft during operation. The torque and speed readings are logged on a computer system. The torque and speed values are used to calculate the power draw of the mill in real time using equation 37:

$$P = \frac{2\pi T\omega}{60} \quad (37)$$

Where P is the mill power draw (W), T is the shaft torque (N.m), and ω is the angular velocity in units of revolutions per minute (rpm). Instrument data are logged in one second intervals. The power draw (W) for each one second interval is used to calculate the incremental energy input (kWh) to the mill during that one second interval. The accumulated energy input per mass of solids sample in the mill (kWh/t) is tracked over the duration of the test run and recorded. The mass of solid sample being milled is an input by the user before the start of the run.



Figure 44: Stirred media milling test rig

The test rig used for this work is the same rig that was used by Lisso, 2013. Similar laboratory test rigs have been used by numerous investigators for studying stirred media milling (Tüzün, 1993; Edwards, 2016; Norejko, 2018; Bailey, 2016; Tamblyn, 2009; Eswaraiah, 2015; Yang, 2017; Kim, 2008; Conway-Baker, 2002; Barley, 2004; Mankosa, 1986).

3.3.1 Torque Measurement Calibration

The milling test rig is equipped with a torque arm connected to the mill motor and to a load cell. The load cell in turn is connect to a torque transducer to measure the torque acting on the mill shaft during operation. The signal from the torque transducer is relayed to a computer data logging system where the energy input during milling is calculated and recorded. The mill speed and torque readings are also recorded by the system. The torque arm and load cell configuration is pictured in Figure 45. The load cell reading is calibrated by performing a zero when the mill is stationary and then suspending a weight with a known mass from the torque arm and calibrating the span reading of the load cell based on the known mass. In this case a known mass of 7500 gram was used for the span calibration. The suspended mass used during calibration is shown in Figure 46. Pictures of the torque transducer during the zero and span calibration process are shown in Figure 47. The torque measurement was calibrated before the start of the test work campaign and was checked routinely during the execution of the test work programme.

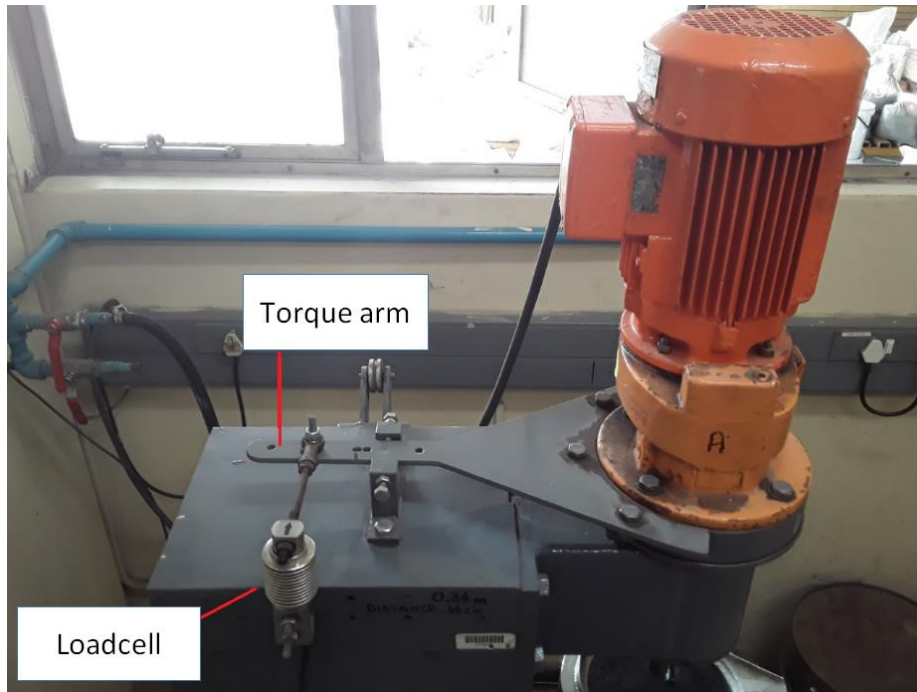


Figure 45: Torque arm and load cell installed on milling test rig

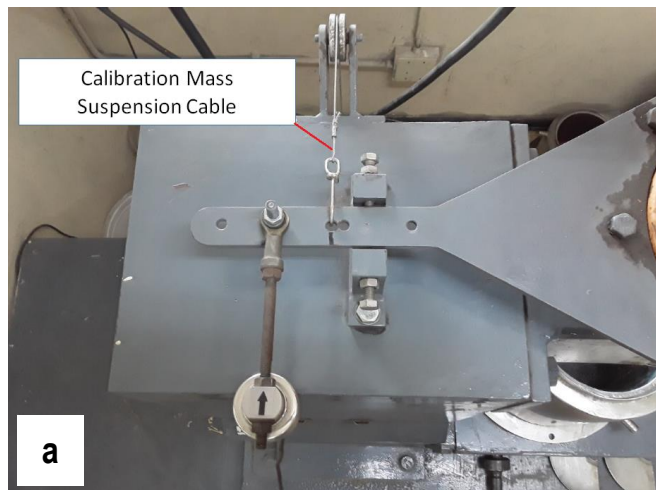


Figure 46: Calibration mass suspended from torque arm a) top view b) side view



Figure 47: Torque transducer during calibration a) zero calibration b) span calibration

3.4 LIGGGHTS Open Source DEM Software

The LIGGGHTS®-PUBLIC version 3.8.0 software was used for conducting the DEM simulations. LIGGGHTS®-PUBLIC is an open source discrete element method particle simulation software, distributed by DCS computing, GmbH, Linz, Austria. LIGGGHTS stands for LAMMPS improved for general granular and granular heat transfer simulations. LAMMPS is a classical molecular dynamics simulator and is widely used in the field of Molecular Dynamics. LIGGGHTS was designed to run on parallel computers using an MPI interface. The LIGGGHTS code offers various different contact models. The Hooke/stiffness contact model can be used to implement the DEM formulation as presented in section 2.6. This model allows users to specify the stiffness and damping constants of the linear spring-dashpot contact model. When implementing this code a keyword selection must be made to limit the force to prevent adhesive forces to develop. Also a keyword selection must be made to allow for the evaluation of the tangential history force (www.cfdem.com, 2019). LIGGGHTS®-PUBLIC does not currently have the functionality to calculate the energy spectra for comminution processes. However it is possible to extract torque data from the simulation. The input script used for the simulations was set up to calculate the torque acting on the stirrer shaft and to dump out the torque data to a text file at regular intervals during the simulation. For this investigation a custom post-processing computer programme was written to calculate per second average torque acting on the stirrer based on the raw torque data output generated during the simulations. The code is presented in Appendix 7.14. The simulation output also provided data on the positions and velocities of the beads at various time steps. A custom post processing computer programme was written to calculate the average bead velocities for the various simulations and also to generate a histogram of the distribution of bead velocities for individual simulations. The code is presented in Appendix 7.14. An open source visualisation programme named Paraview was used to visualise the data generated from the simulations.

3.5 Shell and Stirrer Design Process – DEM Virtual Prototyping

For this investigation two new stirrers and one new mill vessel were designed and fabricated. The equipment design followed an iterative process. Two initial stirrer designs were made based on pin and disc geometries presented by Radziszewski, 2013. The initial conceptual stirrer designs consisted of three sets of pins or discs respectively, spaced equally along the length of the stirrer shaft. Each set of pins consisted of 6 individual pins, for a total of 18 pins. A pin diameter of 10 mm and a disc height of 10 mm was applied. The gap between the disc and pin ends and the mill vessel was 18 mm, based on the scaling ratio from the Radziszewski, 2013, geometries. The distance from the bottom of the shaft to the mill shell bottom was 20 mm. 3D drawings of the initial conceptual stirrer designs are shown in Figure 48.

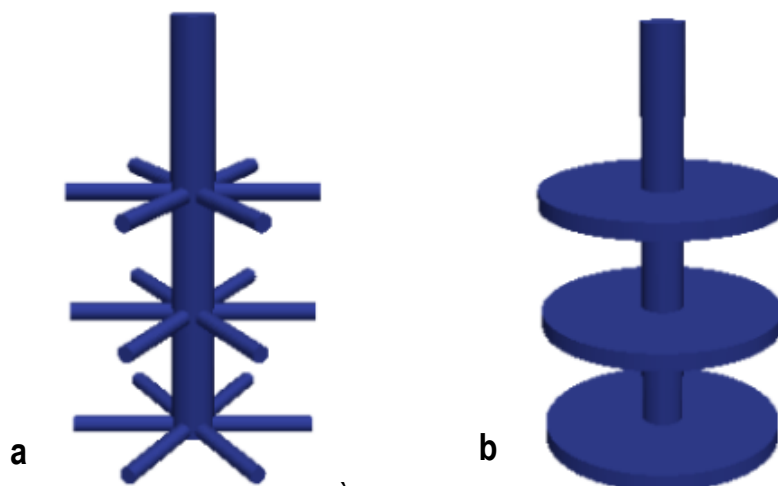


Figure 48: Initial conceptual stirrer designs a) 18-pin stirrer b) 3-disc stirrer

At this stage the stirrer designs were still conceptual and were not yet fabricated. In order to assess how the stirrers might behave during milling, a series of scoping level discrete element method (DEM) simulations were conducted to evaluate the potential charge motion associated with the different stirrer designs.

3.5.1 DEM Virtual Prototyping Parameter Calibration

Before conducting the DEM simulations a set of reasonable DEM model parameters had to be determined for this application. Torque data measured during the operation of an existing 8-pin stirrer, Figure 49, running in the smooth mill vessel was used as a benchmark against which to calibrate the DEM model parameters. The experimental test was conducted with 5706 gram of the 3 mm media and testing was conducted dry with the stirrer operating at a rotational speed of around 400 rpm. The experimental torque data measurements are shown in Table 4. The average torque measured was 1.33 N.m.



Figure 49: Existing pin stirrer used for DEM model calibration purposes

In order to find suitable parameters to use for the virtual prototyping design simulations a series of 15 different DEM simulations were conducted with varying values of the coefficient of restitution and the friction coefficient, refer to Figure 50 and Table 5. For the simulations a total number of 124 200 spherical particles with a diameter of 3 mm and a bead density of 3.25 g/cm³ was used resulting in a total mass of 5706 g of particles which corresponds to the bead properties used during the experiment. For calculating the spring stiffness in the normal direction, k_n , equation 23 was used. The maximum velocity of any particle in the system, v_0 , was assumed to be 2.93 m/s as this corresponds to the tip velocity of a 144 mm diameter stirrer operating at 400 rpm. The maximum overlap δ_{max} was set at 1%. The tangential stiffness k_t was calculated with equation 24 assuming a Poisson ratio of 0.22 which is based on published data for 90% Al₂O₃ ceramic material (www.atcp-ndt.com, 2019). The damping coefficients, C_n and C_t , in the normal and tangential directions respectively for the bead to bead and bead to geometry contacts were calculated using equations 25 and 26 for the various different coefficient of restitution values used during the simulations. The size of the time step was 1.07×10^{-6} s as calculated using equation 31. Each simulation was run for a total number of 18 666 666 time steps, corresponding to around 19 seconds of mill operation. For the DEM simulations the coefficient of friction and coefficient of restitution needs to be specified for the bead to bead and bead to steel contacts. However in order to simplify the parameter calibration process it was assumed that the bead to bead and bead to steel contact parameters were similar, so single values for the coefficient of friction and coefficient of restitution were assumed for each simulation.

Table 4: Torque data for 8-pin stirrer in smooth vessel, 400 rpm, dry operation

Time (sec)	Speed (rpm)	Torque (N.m)	Power (Watt)	Time (sec)	Speed (rpm)	Torque (N.m)	Power (Watt)
1	401	1.31	55.1	31	401	1.33	55.8
2	401	1.32	55.6	32	400	1.31	54.9
3	401	1.36	57.0	33	401	1.31	54.9
4	400	1.34	56.2	34	401	1.34	56.3
5	401	1.30	54.6	35	400	1.35	56.4
6	400	1.33	55.5	36	401	1.32	55.6
7	400	1.35	56.5	37	401	1.31	54.9
8	400	1.34	56.2	38	401	1.31	54.8
9	400	1.31	54.9	39	405	1.33	56.5
10	400	1.32	55.4	40	401	1.35	56.7
11	400	1.36	56.9	41	401	1.36	57.1
12	400	1.35	56.4	42	401	1.33	55.7
13	400	1.31	54.8	43	401	1.31	54.9
14	400	1.31	54.8	44	401	1.29	54.3
15	400	1.34	56.2	45	400	1.31	54.8
16	400	1.36	56.9	46	401	1.34	56.3
17	400	1.33	55.5	47	401	1.34	56.3
18	401	1.31	55.1	48	401	1.36	57.2
19	402	1.32	55.7	49	401	1.34	56.3
20	403	1.34	56.6	50	400	1.31	54.8
21	401	1.36	57.1	51	401	1.28	53.8
22	402	1.33	55.8	52	401	1.29	54.2
23	401	1.31	54.9	53	401	1.33	55.7
24	401	1.32	55.6	54	401	1.34	56.5
25	401	1.35	56.7	55	400	1.33	55.9
26	401	1.34	56.1	56	400	1.31	54.8
27	401	1.31	54.9	57	400	1.28	53.6
28	400	1.31	54.8	58	400	1.31	54.9
29	401	1.36	57.0	59	400	1.34	56.3
30	400	1.35	56.8	60	399	1.34	56.0

Average Torque	1.33	N.m
Average Speed	401	rpm
Average Power	55.7	W

The initial simulation matrix, Figure 50 and Table 5, consisted of 9 individual simulations (Sim 1 to Sim 9) with the friction coefficient ranging from 0.25 to 0.7 (Pasaribu et al., 2005), (Birleanu, 2010), and the coefficient of restitution ranging from 0.38 to 0.88 (Jayasundara et al., 2008). The per second modelled torque acting on the stirrer shaft was evaluated for each condition and compared against the actual torque of 1.33 N.m measured during the experiment. For this selection of parameters the DEM model torque ranged from 2.67 N.m to 1.99 N.m. This was higher than the target value of 1.33 N.m measured during the actual experiment. The results showed that a higher coefficient of restitution resulted in a lower modelled torque, Figure 51, while a higher coefficient of friction resulted in a higher torque, Figure 52. The results showed that the coefficient of friction had a more pronounced effect on the resulting mill torque as compared to the coefficient of restitution. Changes in coefficient of restitution only had a small effect on the overall torque. The next series of simulations (Sim 10 to Sim 15) explored higher values of the coefficient of restitution and lower values of the friction coefficient. A coefficient of restitution of 0.95 was used (Sorace et al., 2009), and the coefficient of friction was varied from 0.08 to 0.2. It was found that a friction coefficient of 0.09 gave a model torque value close to the target of 1.33 N.m, Figure 52. The torque data from all of the simulations are presented in Appendix 7.12.1. Screen dumps of the charge profiles for each simulation are presented in Appendix 7.12.2, the results show that the DEM model exhibited the expected vortex charge profile in all cases.

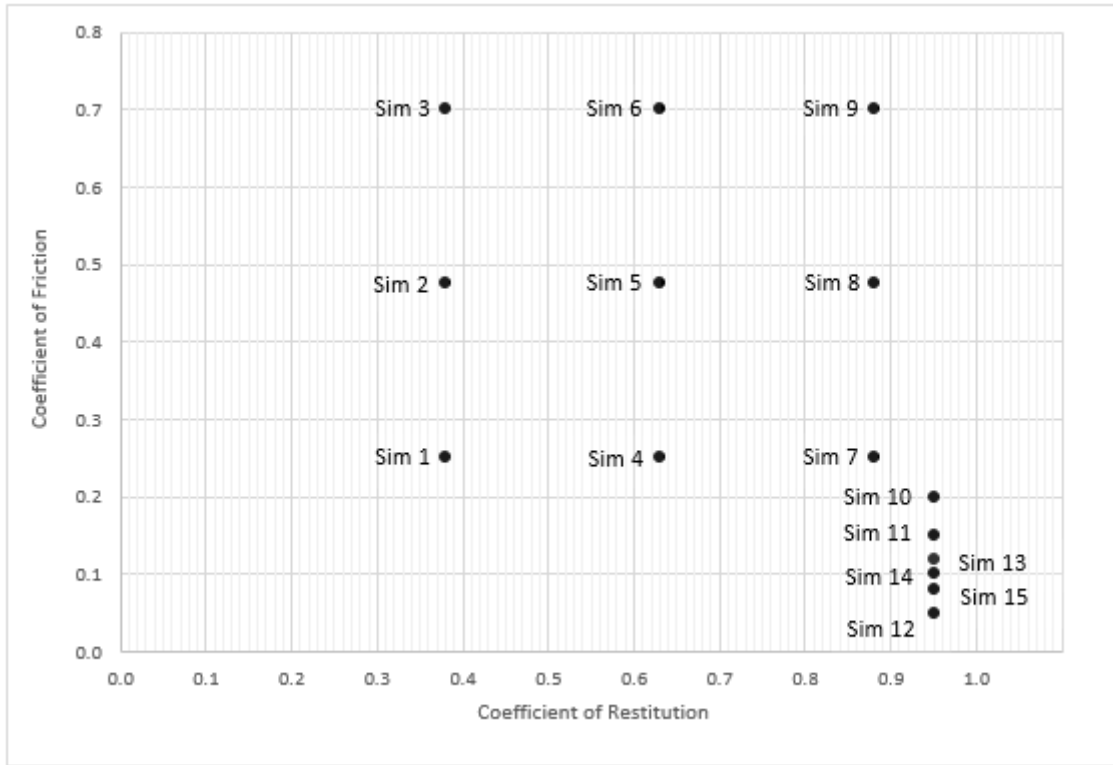


Figure 50: Range of coefficient of restitution and friction values evaluated during DEM model calibration

Table 5: Summarised results of DEM calibration process

Simulation ID	Coefficient of Restitution	Coefficient of Friction	DEM Model Torque (N.m)
Sim 1	0.38	0.250	2.08
Sim 2	0.38	0.475	2.48
Sim 3	0.38	0.700	2.67
Sim 4	0.63	0.250	2.07
Sim 5	0.63	0.475	2.43
Sim 6	0.63	0.700	2.63
Sim 7	0.88	0.250	1.99
Sim 8	0.88	0.475	2.37
Sim 9	0.88	0.700	2.50
Sim 10	0.95	0.200	1.84
Sim 11	0.95	0.150	1.62
Sim 12	0.95	0.050	0.88
Sim 13	0.95	0.120	1.50
Sim 14	0.95	0.100	1.39
Sim 15	0.95	0.080	1.24

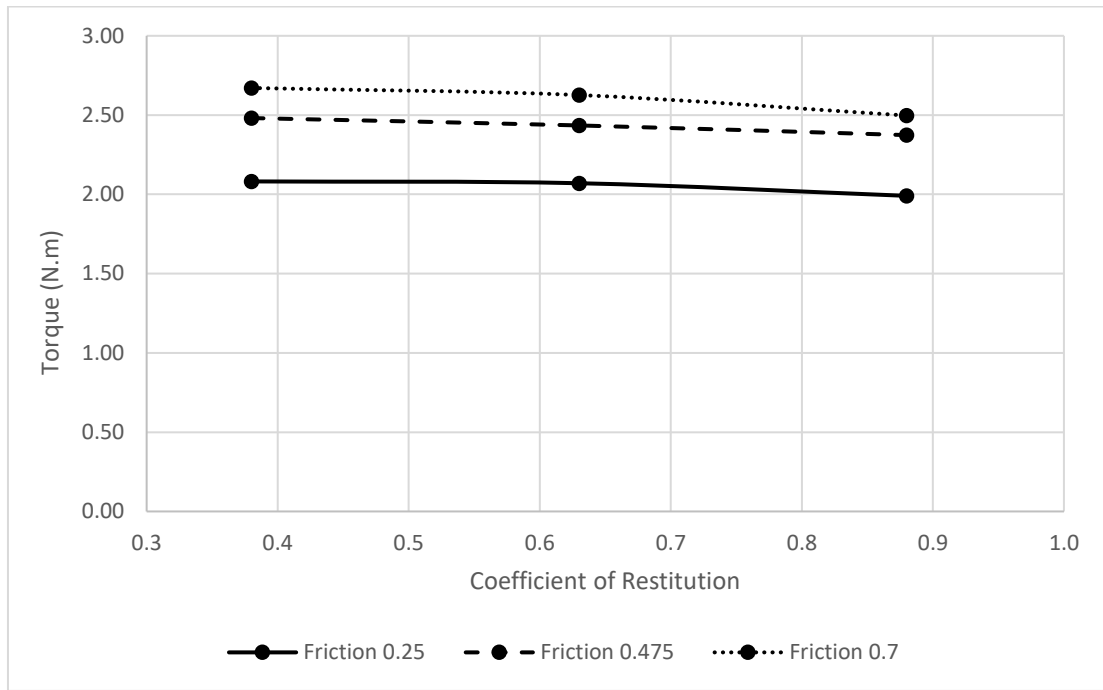


Figure 51: Effect of coefficient of restitution on DEM model torque

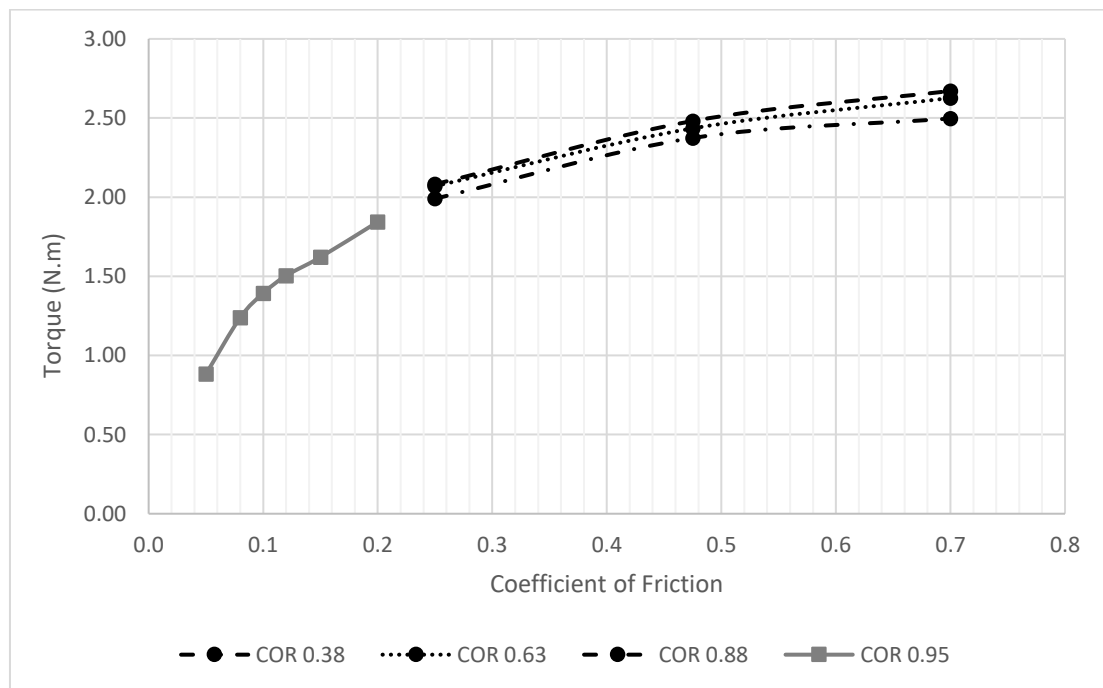


Figure 52: Effect of friction coefficient on DEM model torque

3.5.2 DEM Virtual Prototyping Simulations

Simulations were conducted with the 18-pin and 3-disc conceptual stirrer designs using the DEM parameters obtained from the calibration process. The parameters used are shown in Table 6.

Table 6: DEM parameters used in the virtual prototyping DEM simulations

Parameter	Value Used in DEM	Parameter	Value Used in DEM
Bead density (g/cm ³)	3.25	Coefficient of restitution	0.95
Bead diameter (mm)	3.0	Coefficient of friction	0.09
Poisson Ratio	0.22	Normal spring stiffness (N/m)	438 267
Characteristic velocity (m/s)	2.93	Tangential spring stiffness (N/m)	384 099
Maximum overlap (%)	1.0	Normal Damping (bead-bead)	0.1037
Stirrer speed (rpm)	400	Normal Damping (bead-wall)	0.1466
Number of particles	124 200	Tangential Damping (bead-bead)	0.0970
Number of time steps	18 666 666	Tangential Damping (bead-wall)	0.1372
Time step (seconds)	1.07 x 10 ⁻⁶		

Results of the DEM simulations for the 18-pin and 3-disc conceptual stirrer designs are presented in Figure 53. Note that the height of the mill vessel used during simulations was 280 mm and not the height of 230 mm associated with the physical mill. The height selected for the simulation domain was larger than the actual mill to allow sufficient space for particle insertion into the model. The results for both stirrers show that the top sets of agitators did not adequately contact the charge in the mill. It was also observed that the pin design produced a very consistent vortex charge movement in the mill. However with the 3-disc stirrer design the charge motion was very erratic and turbulent, as shown in Figure 54. The discs acted to throw the beads around the mill chamber and a steady charge profile was not formed.

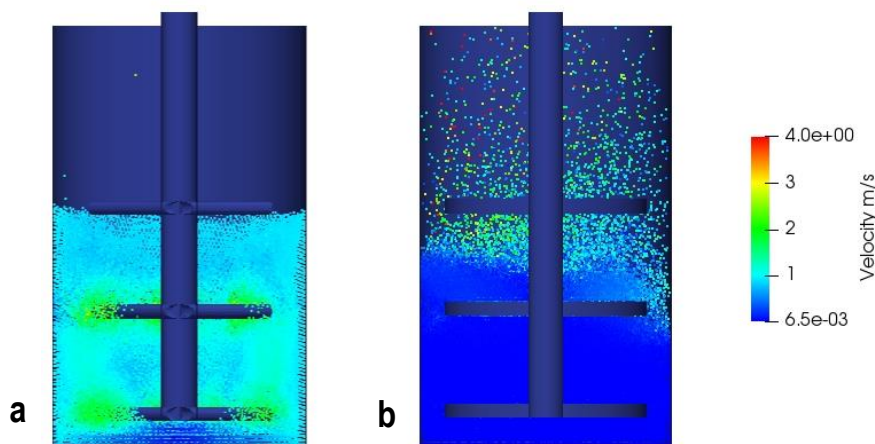


Figure 53: DEM simulations of conceptual stirrers in smooth vessel a) 18-pin stirrer b) 3-disc stirrer

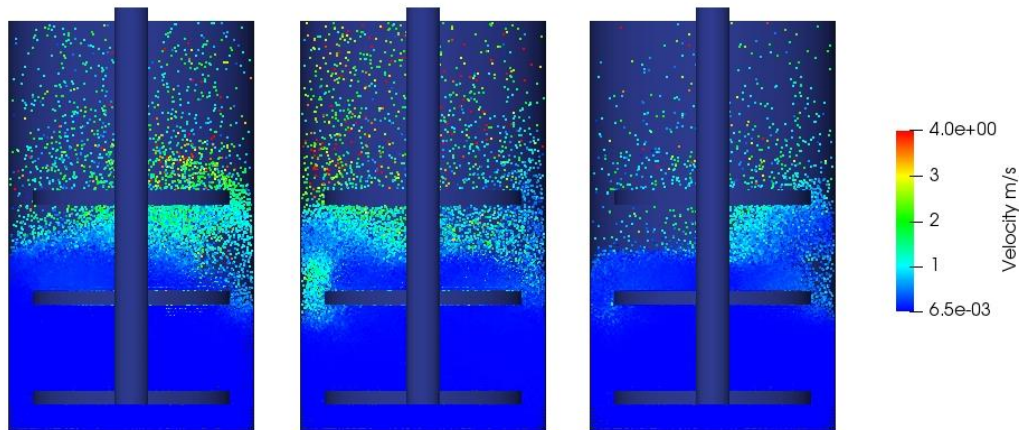


Figure 54: Turbulent DEM charge movement observed with the conceptual 3-disc stirrer

The results of the initial simulations conducted indicated that at the filling level selected the top set of pins or discs on the stirrer would not be in contact with the material in the mill. The stirrer design was then reduced to include only the two bottom sets of agitators as pictured in Figure 55. The simulation results of the 12-pin stirrer showed a very stable charge shape corresponding to the typical vortex shape expected with SMD operation, Figure 58 a. For the disc stirrer however the charge movement was very unsteady and inconsistent as pictured in Figure 56. Once again the discs acted to throw the beads around the mill chamber and a steady charge profile was not formed. An unsteady charge like this will not be useful for the comparative testing purposes of this investigation. The disc design was modified and a hybrid design between the pin and disc stirrer was developed. This revised design consisted of an outer ring connected to the shaft with spokes. This created space for the grinding beads to move through. The hybrid ring stirrer design is pictured in Figure 55 c. Simulations conducted with the ring stirrer showed a stable vortex charge profile similar to that of the 12-pin stirrer, Figure 58 c. For the disc liner vessel a single annular disc was added to the bottom half of the mill shell, Figure 57. This liner is positioned in such a way that the bottom set of pins or ring is located halfway between the mill bottom and the disc. The simulations conducted with the disc vessel are shown in Figure 58 b and d for the pin and ring stirrers respectively. Detailed drawings of the new stirrer and mill vessel designs are presented in Appendix 7.1.

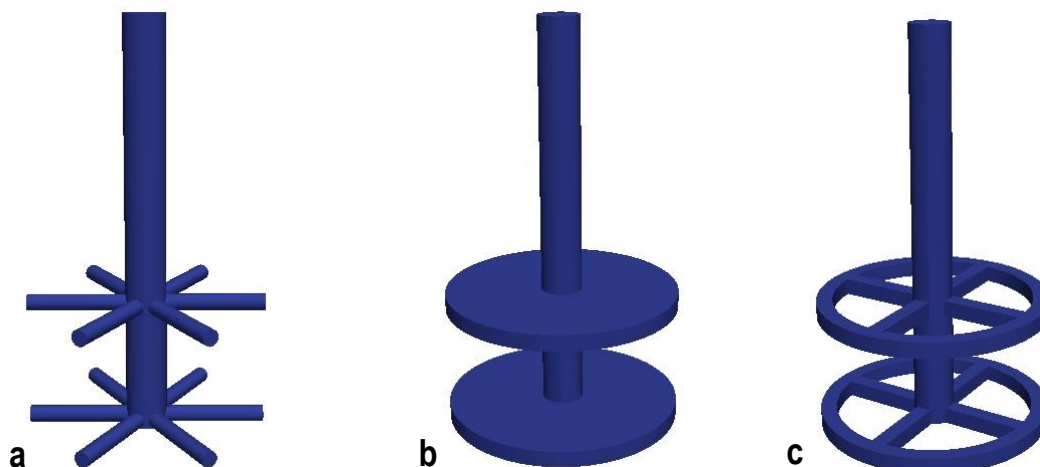


Figure 55: Revised conceptual stirrer designs a) 12-pin stirrer b) 2-disc stirrer c) ring stirrer

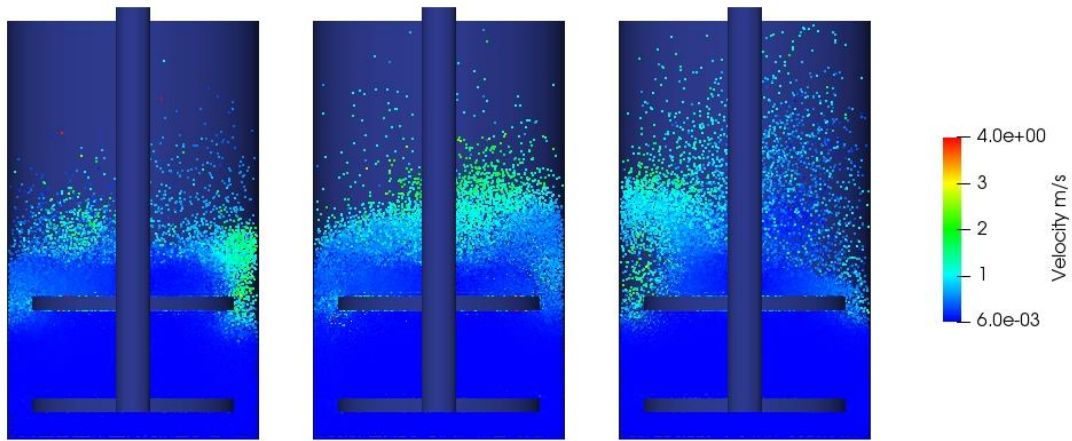


Figure 56: Turbulent DEM charge movement observed with the conceptual 2-disc stirrer

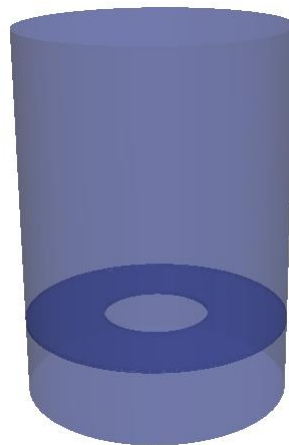


Figure 57: Disc Vessel design

The torque data for the DEM simulations conducted with the final mill designs, Figure 58, are reported in Appendix 7.12.3. The model predicts that the addition of a disc to the mill shell will increase the mill torque with a factor of 1.76 in the case of the pin stirrer and with a factor of 1.42 in the case of the ring stirrer, Table 7 and Figure 59. Also the model predicts that the pin stirrer will result in a higher torque as compared to the ring stirrer when operating in the same mill vessel. The DEM charge profiles exhibited the expected vortex shaped as pictured in Appendix 7.12.4. The average bead velocities predicted by the DEM model for each of the four mill configurations are presented in Table 8. The model predicts that the pin stirrer will result in higher bead velocities as compared to the ring stirrer. For the smooth mill the pin stirrer showed an average bead velocity of 0.94 m/s compared to an average bead velocity of 0.39 m/s for the ring stirrer. For the disc vessel the pin stirrer resulted in an average bead velocity of 0.65 m/s compared to 0.26 m/s for the ring stirrer. The presence of this disc seems to reduce the velocities of the beads but leads to an increase in mill torque due to the additional surface in the mill. Bead velocity histogram data are shown in Figure 60 for the various mill configurations.

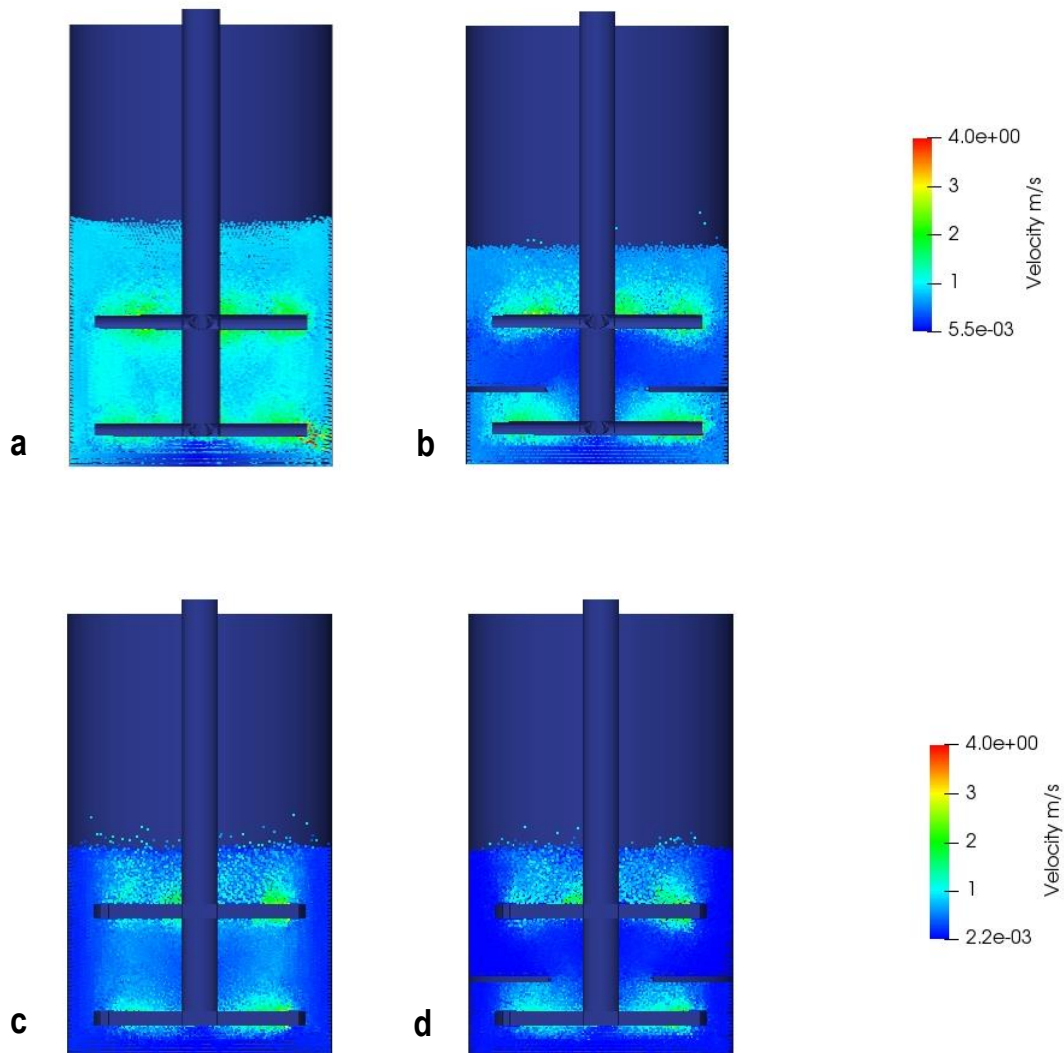


Figure 58: Final stirrer design DEM simulations a) 12-pin - smooth vessel, b) 12-pin - disc vessel, c) ring stirrer - smooth vessel, d) ring stirrer - disc vessel.

Table 7: Torque Predicted from DEM Virtual Prototyping Model

Mill Configuration	Torque (N.m)	Torque (N.m) relative to Pin in Smooth	Torque (N.m) increase due to disc liner
Pin in Smooth	1.88	1.00	
Ring in Smooth	1.25	0.66	
Pin in Disc	3.24	1.72	1.76
Ring in Disc	1.77	0.94	1.42

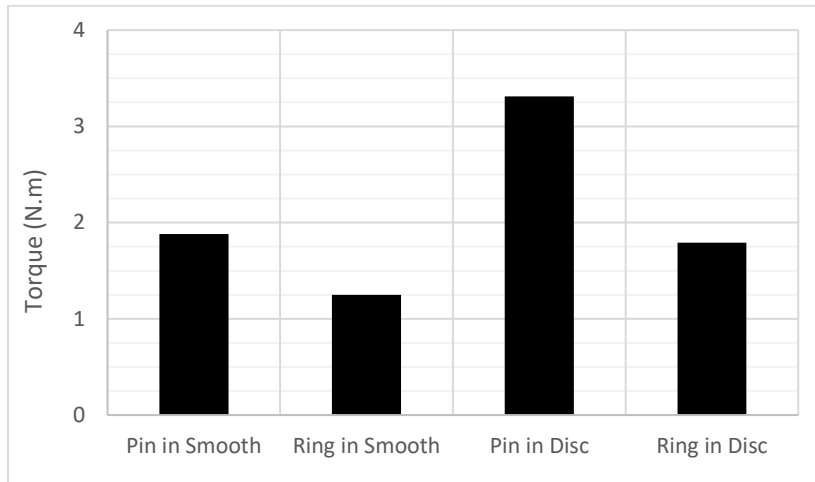


Figure 59: Torque Predicted from DEM Virtual Prototyping Model

Table 8: Average DEM Virtual Prototyping Model bead velocities

Mill Configuration	Average Bead Velocity (m/s)
Pin in Smooth	0.94
Ring in Smooth	0.39
Pin in Disc	0.65
Ring in Disc	0.26

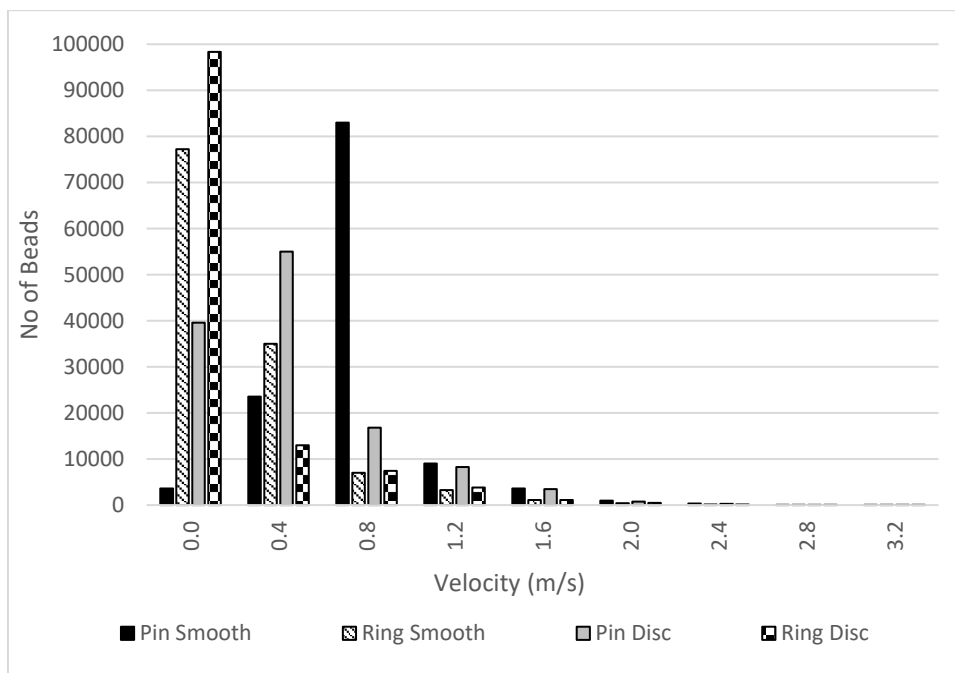


Figure 60: DEM Virtual Prototyping Model Velocity Histogram for different mill geometries

3.6 Final Stirrer and Mill Designs Used in Experiments

Pictures of the stirrers and mill vessels used for the experimental programme are shown in Figure 61 to Figure 63. The ring and pin stirrers and the disc liner mill vessel were specifically made up for this investigation. The disc vessel was constructed as two half pieces that were bolted together. This was done to allow the fitting of the stirrer between the mill bottom and the disc liner. Detailed design drawings for the newly fabricated equipment are presented in Appendix 7.1. For the smooth mill an existing mill vessel was used, Figure 63. This mill chamber measured 180 cm in diameter and 230 cm in height.



Figure 61: Ring and pin stirrers fabricated for this investigation

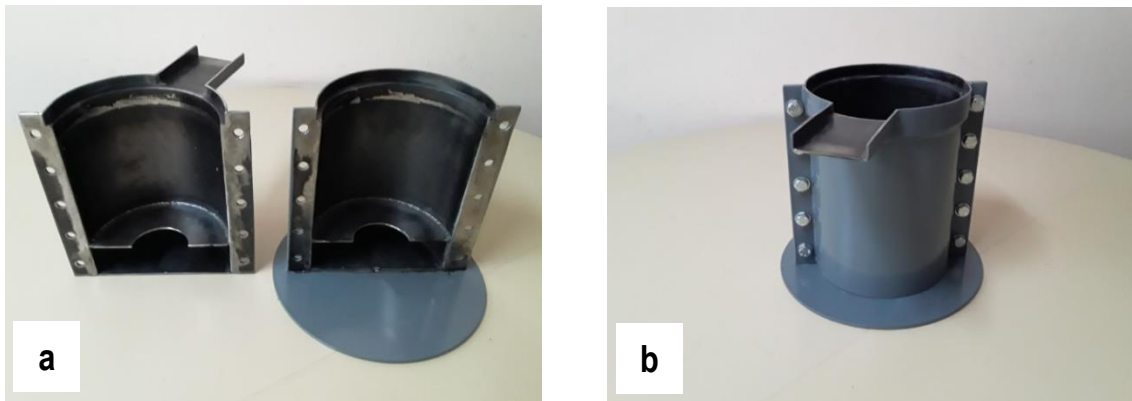


Figure 62: Disc liner mill vessel a) two half pieces b) assembled

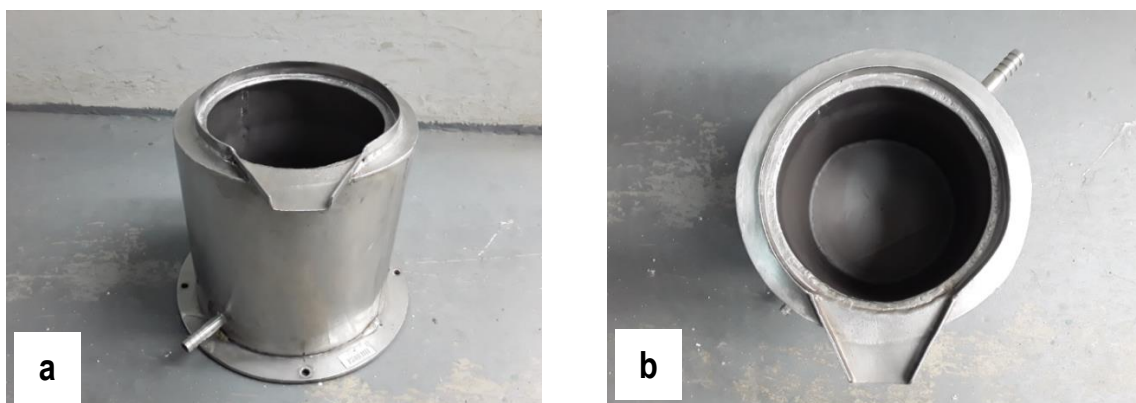


Figure 63: Smooth mill vessel a) side view b) top view

3.7 Shear Volume Calculations of Mill Geometries

The Radziszewski shear volume for each of the four newly designed geometry sets were calculated. In order to calculate the shear volume it was required to derive mathematical formulas for integration of the shear stress over the surface of some of the geometries. The mathematical derivations for the applicable geometries are presented in Appendix 7.2. Numerical integration was applied in cases where an analytical solution to the integral could not be found. The Simpson 1/3 rule was applied for solving the integrals numerically. The shear volume calculations are presented in Appendix 7.3. The shear volumes calculated for each geometry set are shown in Table 9. For the four geometries being evaluated the 12-pin stirrer geometries both have lower shear volumes as compared to the ring stirrer geometries. The addition of a shell liner increases the shear volume with 75% in the case of the 12-pin stirrer and 44% in the case of the ring stirrer.

Table 9: Radziszewski shear volume calculated for the various geometries

Geometry	Shear Volume (m ³)	Relative Magnitude of Shear Volume	Increase in Shear Volume due to Shell Liner Addition
12-pin - smooth vessel	0.000628	1.00	
12-pin – disc vessel	0.001098	1.75	1.75
Ring – smooth vessel	0.003720	5.93	
Ring – disc vessel	0.005342	8.51	1.44

3.8 Milling Test Feed Material

Milling tests were conducted on silica feed material obtained from two different sources, refer to the test matrix in Table 10. For the mono-sized grinding tests the silica was sourced in the form of a filter sand with a particle size of around 2 mm from a company called SA Silica. For the tests on the natural feed size distribution the fine silica was sourced from a company called Omega Fine Products in the form of a silica flour sold under the tradename Silica 150.

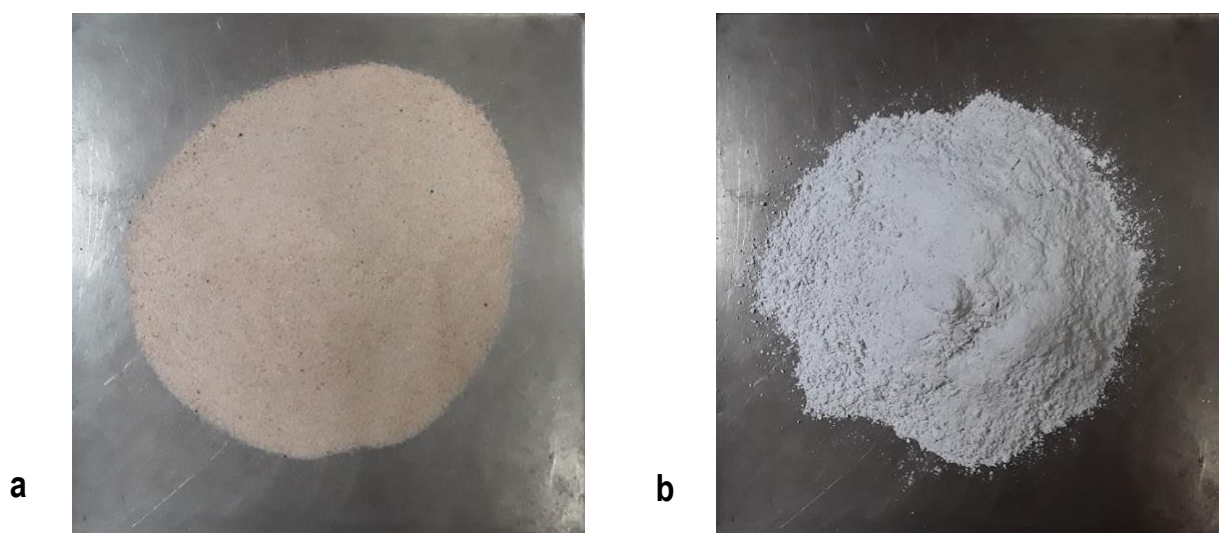


Figure 64: Milling test feed a) silica sand, b) silica flour

3.8.1 Sample Preparation

To prepare the samples for the mono-sized fraction tests a bulk sample of silica at a particle size of around 2 mm was subjected to ball milling to produce fine particles. The ball mill product was then screened to produce test feed material conforming to two different narrow size fractions of approximately $-150 + 106 \mu\text{m}$ and $-106 + 75 \mu\text{m}$. The two size fractions were then split into a number of individual batches of 1277g each using a rotary splitter. One of the batches was further split to produce sub-samples for PSD analysis and sample characterisation via XRD and XRF analysis. For the natural feed size tests the silica flour material was blended and rotary split to produce various individual batches with a mass of 1275g each. One of the batches was further split to produce sub-samples for PSD analysis.

3.8.2 PSD of Silica Feeds

For each of the three feed materials the PSD's were conducted in duplicate according to the procedures described in section 3.12. PSD results are shown in Figure 65 and the full results are tabulated in Appendix 7.4.

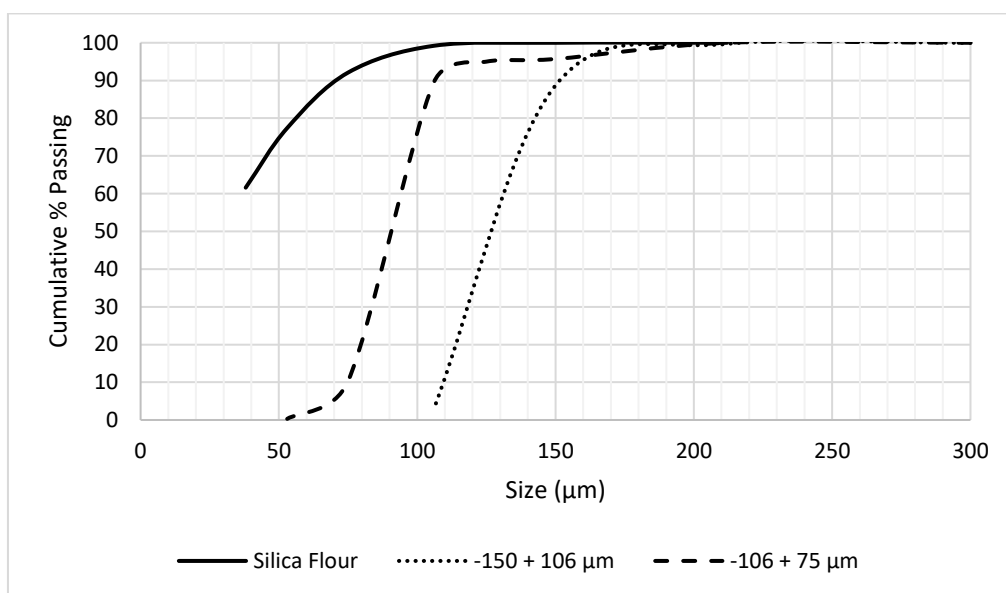


Figure 65: PSD of silica feeds

3.8.3 Chemical and Mineralogical analysis of the Silica

The silica flour material is sold by the supplier Omega Fine Products under the tradename Silica 150. The chemical composition provided by the supplier shows around 98.5% SiO_2 with 0.8% Al_2O_3 and minor amounts of other elements, refer to Appendix 7.15. An XRD analysis conducted by Mintek showed that the sample contained 95% Quartz (SiO_2), 3% Orthoclase (KAlSi_3O_8), 1% Muscovite $\text{KAl}_2(\text{Si}_3\text{AlO}_{10})(\text{OH})_2$, and 1% Montebasite ($\text{LiAl}(\text{PO}_4)(\text{OH})\text{F}$). For the sample used in the mono-sized feed tests there was no information available from the supplier, so a sub-sample of the material was subjected to chemical analysis by the Mintek analytical services laboratory. The results of the XRF method applied showed a SiO_2 concentration of 97.4% by mass. A quantitative mineralogical XRD analysis was also conducted by the Mintek mineralogy department. The results of XRD analysis indicated a Quartz (SiO_2) content of around 99.89%. Trace amounts of Hematite (Fe_2O_3) and Cristobalite (SiO_2) minerals were present at a total concentration of less than 0.1%. The Rietveld XRD results are shown in Appendix 7.5.

3.8.4 Specific Gravity of the Silica

The specific gravity (SG) of the silica test materials were determined using a Micromeritics model AccuPyc II 1340 gas pycnometer. A sub-sample was pulverised and three individual sub-samples of the pulverised material were removed for SG determination. An average SG of 2.67 g/cm³ was measured for the mono-sized feed test material and an average SG of 2.65 g/cm³ was measured for the silica flour, refer to Appendix 7.6.

3.9 Ceramic Grinding Beads Density Characterisation

The ceramic beads used for the experimental work were Minemate CM-320 produced by King's beads. According to the manufacturer the media is composed mainly of Al₂O₃ and SiO₂ and the bead density is around 3.2 g/cm³. Three different bead sizes namely 3 mm, 2 mm, and 1 mm were used during the investigation. The density for each bead size was measured.

A 250ml graduated measuring beaker was filled up to the 250ml level mark with dry beads. The mass of the beads in the beaker was recorded and the bulk density of the beads in units of g/cm³ was then calculated. The next step was to fill the voids between the beads with water up to the 250ml level mark. The total mass of the beads and water in the beaker was recorded. The mass of water in the beaker was calculated by difference. The volume of water in the beaker was then calculated based on a water density of 1 g/cm³. The actual volume of the beads was calculated by subtracting the volume of the water from the volume of the beaker (250 ml). The material density was calculated based on the mass of beads and the actual volume of beads. The measurements were conducted in triplicate.

Results are reported in Appendix 7.7. Average bead densities of 3.25 g/cm³ were measured for the 3 mm and 1 mm beads. The average bead density for the 2 mm beads was measured as 3.24 g/cm³. The fractional voidage or porosity of a particle bed is defined as the fraction of the bulk volume that is not occupied by solid material (Richardson et al., 2002). The fractional voidage was calculated for each measurement. The average fractional voidage measurements were 0.40, 0.39, and 0.39 for the 3 mm, 2 mm, and 1 mm beads respectively. The measured material density of around 3.25 g/cm³ is close to the value of around 3.2 g/cm³ specified by the media supplier. Also the fractional voidage close to 0.4 is typical for spherical particles (Richardson et al., 2002). The measured values therefore show good agreement with expected values and this provides confidence in the results.

3.10 Experimental Test Work Matrix

The test work matrix for the experimental programme is presented in Table 10. The experimental tests were grouped into the following categories:

- Beads only tests
- Beads and water tests
- Repeatability grinding tests on silica flour
- Mono-sized feed grinding tests on -150 +106 µm and -106 + 75 µm silica
- Natural feed size distribution grinding tests on silica flour

3.10.1 Bead only tests

During these tests the mill was filled with beads only, no water or silica were added. The aim of these tests were to measure the torque and power draw of the different mill configurations in order to provide data for the calibration of the DEM models. The mills were operated at a stirrer speed of 400 rpm and a mass of 5706 gram of the 3 mm beads was used.

3.10.2 Beads and water tests

These tests were run at various different stirrer speeds ranging from 270 rpm to 530 rpm and with different bead sizes of 3 mm, 2 mm, and 1 mm. The mill charge consisted of beads with only water added and no silica, detailed test conditions are shown in Table 11. Mill power draw was recorded for each of the mill configurations at the various mill speeds and bead sizes. The data generated were used to evaluate the effect on mill power draw when adding a disc liner to the mill shell.

Table 10: Experimental Test work Matrix

Test ID	Geometry	Stirrer speed (rpm)								
		270	307	343	381	400	418	456	492	530
Beads only										
Test B-1	12-pin stirrer in smooth vessel					X				
Test B-2	12-pin stirrer in disc vessel					X				
Test B-3	Ring stirrer in smooth vessel					X				
Test B-4	Ring stirrer in disc vessel					X				
Beads and water										
Test W-1	12-pin stirrer in smooth vessel	X	X	X	X	X	X	X	X	X
Test W-2	12-pin stirrer in disc vessel	X	X	X	X	X	X	X	X	X
Test W-3	Ring stirrer in smooth vessel	X	X	X	X	X	X	X	X	X
Test W-4	Ring stirrer in disc vessel	X	X	X	X	X	X	X	X	X
Repeatability Tests - Silica Flour										
Test R-1	12-pin stirrer in smooth vessel					X				
Test R-2	12-pin stirrer in smooth vessel					X				
Test R-3	12-pin stirrer in smooth vessel					X				
Test R-4	12-pin stirrer in smooth vessel					X				
Test R-5	12-pin stirrer in smooth vessel					X				
Mono-sized Feed Grinding Tests -150 +106 µm silica										
Test M-1	12-pin stirrer in smooth vessel					X				
Test M-2	12-pin stirrer in disc vessel					X				
Test M-3	Ring stirrer in smooth vessel					X				
Test M-4	Ring stirrer in disc vessel					X				
Mono-sized Feed Grinding Tests -106 +75 µm silica										
Test M-5	12-pin stirrer in smooth vessel					X				
Test M-6	12-pin stirrer in disc vessel					X				
Test M-7	Ring stirrer in smooth vessel					X				
Test M-8	Ring stirrer in disc vessel					X				
Natural Feed Size Grinding Tests - Silica Flour										
Test N-1	12-pin stirrer in smooth vessel	X								
Test N-2	12-pin stirrer in disc vessel	X								
Test N-3	Ring stirrer in smooth vessel	X								
Test N-4	Ring stirrer in disc vessel	X								
Test N-5	12-pin stirrer in smooth vessel					X				
Test N-6	12-pin stirrer in disc vessel					X				
Test N-7	Ring stirrer in smooth vessel					X				
Test N-8	Ring stirrer in disc vessel					X				
Test N-9	12-pin stirrer in smooth vessel									X
Test N-10	12-pin stirrer in disc vessel									X
Test N-11	Ring stirrer in smooth vessel									X
Test N-12	Ring stirrer in disc vessel									X

3.10.3 Repeatability grinding tests on silica flour

Repeatability tests were conducted to measure the degree of variability associated with the experimental grinding procedure. Five variability tests were conducted with silica flour material from batch 2, using the pin stirrer operating at a speed of 400 rpm in the smooth mill vessel with 3 mm beads and test conditions as shown in Table 11. Each test consisted of milling individual batches of the silica flour to three different energy inputs namely 5, 10, and 20 kWh/t. A full particle size distribution was conducted on each of the products. For each of the five repeatability tests the energy (kWh/t) and time (min) required to reach various different grind sizes were determined by means of linear interpolation between the data points. The grind sizes evaluated were 70%, 75%, 80%, and 85% passing 38 μm respectively. For each grind size the coefficient of variation (CV) of the time and energy required to reach the target grind was calculated. The CV was used as a measurement of the experimental variability.

3.10.4 Mono-sized feed grinding tests on -150 +106 μm and -106 + 75 μm silica

Tests were conducted with each of the different mill configurations operating at a stirrer speed of 400 rpm with 3 mm beads to measure the time based and energy normalised breakage rates of the silica. Two different mono-sized silica feeds were used consisting of particles in the approximate size ranges of -150 + 106 μm and -106 + 75 μm respectively. The detailed test conditions employed are presented in Table 11. For each test individual batches of feed material were milled at different energy inputs ranging from 2.5, 5, 10, 15, and 20 kWh/t. A particle size distribution was conducted on each product and the fraction of mass remaining in the parent particle size class was calculated. In this way data points of the fraction remaining in the top size class were generated for each test at energy inputs of 2.5, 5, 10, 15, and 20 kWh/t. The corresponding milling times to reach the different energy inputs were determined from the mill data logs. From this information a set of data points consisting of the mass remaining versus milling time was also generated for each test. The data sets were then used to fit the time based (S_i) and energy based (S_i^E) rates of breakage for each test. The technique used to fit the breakage rates employed the solver routine in Microsoft Excel whereby the sum of squared error between the measured and model fitted data points was minimised by selection of suitable values for S_i and S_i^E . The breakage rates for the different mill configurations were then compared to assess the effect of the added mill shell liner on the milling performance.

3.10.5 Natural feed size distribution grinding tests on silica flour

Testing was conducted for each of the different mill configurations at three different stirrer speeds namely 270, 400, and 530 rpm corresponding to stirrer tip velocities of 2.0, 3.0, and 4.0 m/s respectively. Testing was conducted with 3 mm beads and with other test conditions as shown in Table 11. Each test consisted of milling individual batches of the silica flour to three different energy inputs namely 5, 10, and 20 kWh/t. A full particle size distribution was conducted on each of the products. For each test the energy (kWh/t) and time (min) required to reach various different grind sizes were determined by means of linear interpolation between the data points. The grind sizes evaluated were 70%, 75%, 80%, and 85% passing 38 μm respectively. The data from each test were compared to assess the effect of the addition of a shell disc liner on the mill performance.

3.11 Milling Conditions

The milling conditions employed for the water and beads only tests and for the silica tests utilising the natural and mono-sized particle feeds are presented in Table 11.

Table 11: Milling conditions

	Beads and Water	Silica Flour	Mono-sized
Water S.G (g/cm ³)	1.00	1.00	1.00
Solid mass (g)	0	1275	1277
% Solids	0	50	50
Water mass (g)	1756	1275	1277
Slurry mass (g)	1756	2550	2555
solids S.G (g/cm ³)	-	2.65	2.67
Slurry S.G (g/cm ³)	1.00	1.45	1.46
Slurry volume (cm ³)	1756	1756	1756
Mill Dimensions			
Diameter (cm)	18	18	18
Height (cm)	23	23	23
Mill Volume ($\pi/4$ (D ² /L))	5853	5853	5853
% Loading (fraction)	0.5	0.5	0.5
Ball bulk volume (cm ³)	2926	2926	2926
Ball material volume (cm ³)	1756	1756	1756
Ball S.G (g/cm ³)	3.25	3.25	3.25
Ball Mass (g)	5706	5706	5706

3.12 Mill Product PSD Analysis

After each milling test the product slurry and beads were removed from the mill and separated from each other by rinsing the slurry and bead mixture on a sieve that acted to retain the grinding media. The slurry and wash water were collected in a bucket and then filtered using a pressure filter to separate the solids from the bulk of the water. The filtered solids were placed in an oven for drying. After drying any large lumps that might have formed during the drying process were gently broken apart manually.

A sub-sample from the product was removed by means of a rotary splitter. The sub-sample was then wet screened with a vibratory sieve shaker on either a 38 μm lab sieve in the case of the silica flour tests or a 53 μm lab sieve in the case of the mono-sized silica grinding tests. During the screening process the material on the screen was manually agitated in a gentle way to ensure passage of fines through the screening surface. The screen undersize was collected in a bucket. The wet screening process was continued until visually there were no more fines passing the screen. The screen undersize material was then filtered using a pressure filter. The screen oversize and the filtered screen undersize were dried in an oven. After drying, the screen oversize material was placed on a set of sieves conforming to the Taylor series with sizes ranging from 212, 150, 106, 75, and 53 μm . In the case of the silica flour a 38 μm sieve was also added. The sieves were mounted on a sieve shaker and the sieving process was carried out for 15 minutes. This time was found to be suitable to allow adequate separation of the different particle sizes. The material remaining on each sieve and in the pan was then removed and weighed and the masses were recorded. The dry mass of the screen undersize from the initial wet sieving step was added to the mass of material reporting to the pan. The full PSD was calculated from the masses in each size class.

4 Experimental Results and Discussion

4.1 Results of Bead Only Tests

The results of the bead only tests conducted at 400 rpm with the 3 mm beads are shown in Table 12 and Figure 66. The experimental results indicate that the power draw of the mill is increased by the addition of a disc liner. In the case of the pin stirrer the measured power draw increased with a factor of 1.88 and in the case of the ring stirrer the measured power increased with a factor of 1.73.

Table 12: Results of Bead Only Tests

Test ID	Mill Configuration	Torque (N.m)	Power (W)	Power (W) relative to Pin in Smooth	Power (W) increase due to disc liner
Test B-1	Pin in Smooth	3.09	129.7	1.00	
Test B-3	Ring in Smooth	2.30	96.3	0.74	
Test B-2	Pin in Disc	5.80	243.4	1.88	1.88
Test B-4	Ring in Disc	3.97	166.8	1.28	1.73

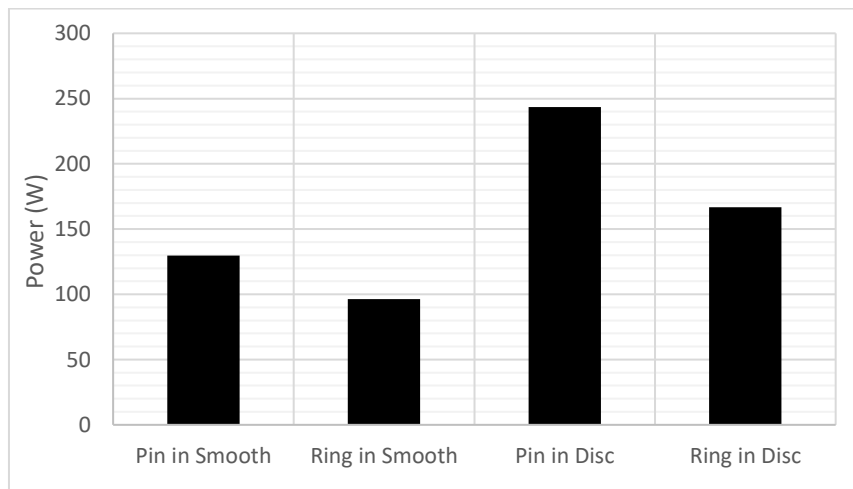


Figure 66: Results of Bead Only Tests

Interestingly the results show a different trend than what was predicted by the shear based power model. According to the shear based power model the ring stirrer was predicted to draw about 5.93 times more power than the pin stirrer when operating in the smooth vessel, refer to Table 9. However in reality this was not the case. The use of the pin stirrer resulted in a higher mill power draw as compared to the ring stirrer. This was observed for both mill vessel designs. The trends observed from the experimental results were in fact more aligned with the trends predicted by the DEM model, refer to Table 7 and Figure 59. Although the magnitude of the torque predicted by the virtual prototyping DEM model was lower than the experimental torque, the relative torque differences showed a similar trend to what was observed in the experiments. A comparison of the trends is shown in Figure 67. The DEM model correctly predicted that the power draw of the ring stirrer will be less than that of the pin stirrer. The shear based power model however overestimated the power draw of the ring stirrer relative to the pin stirrer.

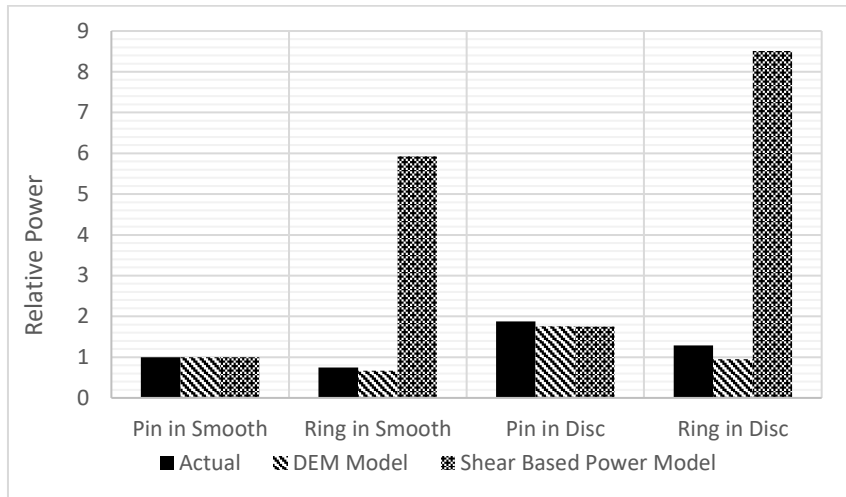


Figure 67: Comparison of Actual and Predicted Relative Power Draw

4.2 Results of Bead and Water Tests

Power draw measurements with beads and water were conducted with the various different mill configurations over a range of different stirrer speeds and bead sizes. The data generated during the tests are reported in Appendix 7.4. Summarised results for each of the mill configurations are shown in Figure 68 to Figure 71. The trends show that the power draw of the mill is a function of stirrer speed and bead size. As expected higher stirrer speeds results in higher power draw and larger bead sizes also result in a higher power draw.

However an anomalous result was observed for Test W-3 which used the ring stirrer operating in the smooth vessel. With the 2 mm beads it was found that the mill power draw drastically increased at stirrer speeds above 400 rpm, as shown in Figure 70. This phenomenon was only observed for the ring stirrer in the smooth vessel with the 2 mm beads, and was not observed in any other configuration. The increase in power draw seemed to be due to a change in the charge profile in the mill. Instead of the normal vortex shape where the water and beads are well mixed it seemed that at speeds higher than 400 rpm some separation between media and water occurred. The typical charge conditions are shown in Figure 72 where the beads and water are well mixed to form a single phase. However during the anomalous power draw conditions the charge did not exhibit the normal characteristics, as shown in Figure 73 the beads separated from the water. In the picture the white beads are clearly visible in the centre bottom of the mill, while the water is pushed up high against the outside of the mill vessel and almost overflows out of the vessel. The increase in the power draw is due to the separation of the beads from the water. Usually the stirrer is in contact with a mixture of beads and water. The presence of the water reduces the resistance of the charge to the movement of the stirrer. However when the localised ratio of water to beads decrease, the resistance to the movement of the stirrer increases and hence the power draw also increase. It is not clear why the phenomenon of charge separation occurred for this specific set of conditions and not for the other conditions. It is also not clear if this phenomenon will be observed during milling where an ore slurry will be used instead of water only. It might therefore be an area that can be explored in a future investigation.

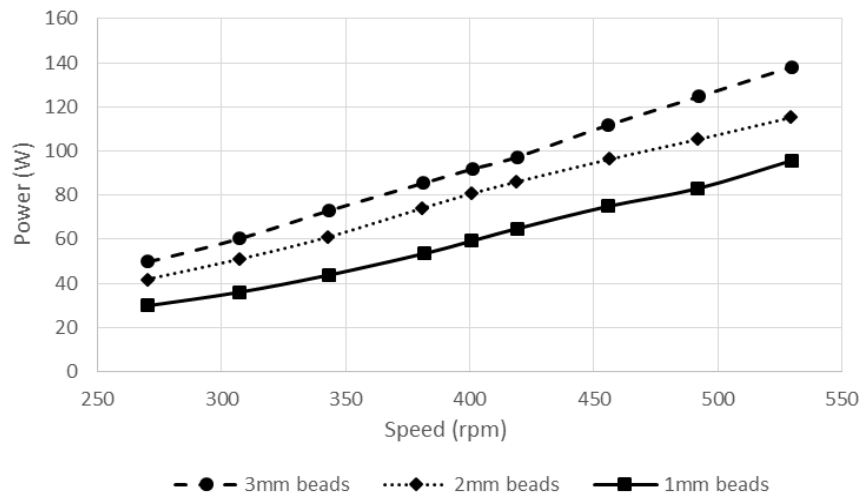


Figure 68: Test W-1 Pin in Smooth Bead and Water Power Draw

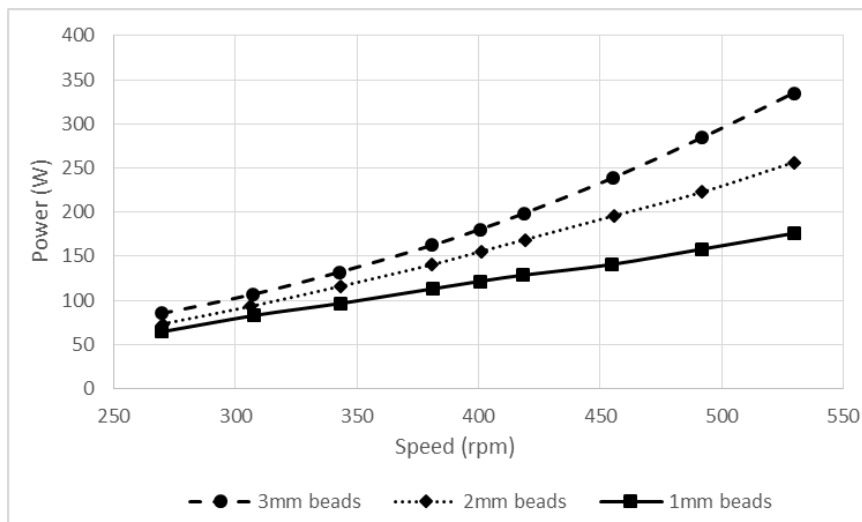


Figure 69: Test W-2 Pin in Disc Bead and Water Power Draw

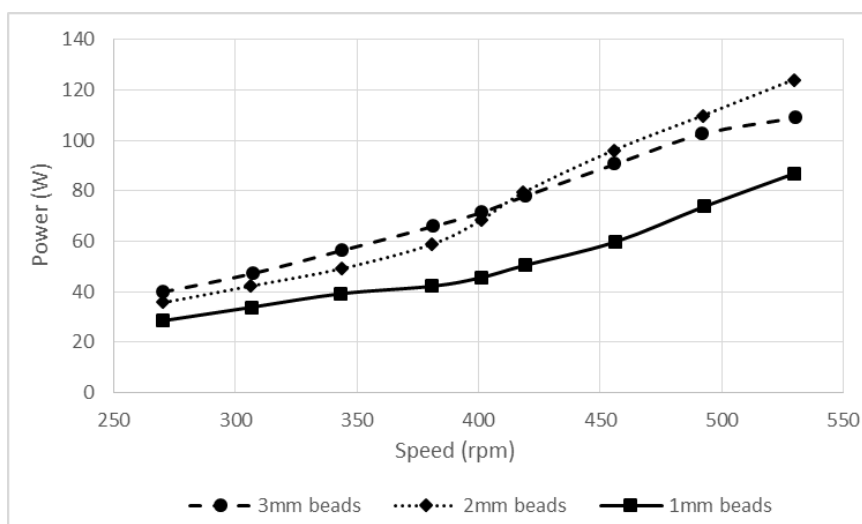


Figure 70: Test W-3 Ring in Smooth Bead and Water Power Draw

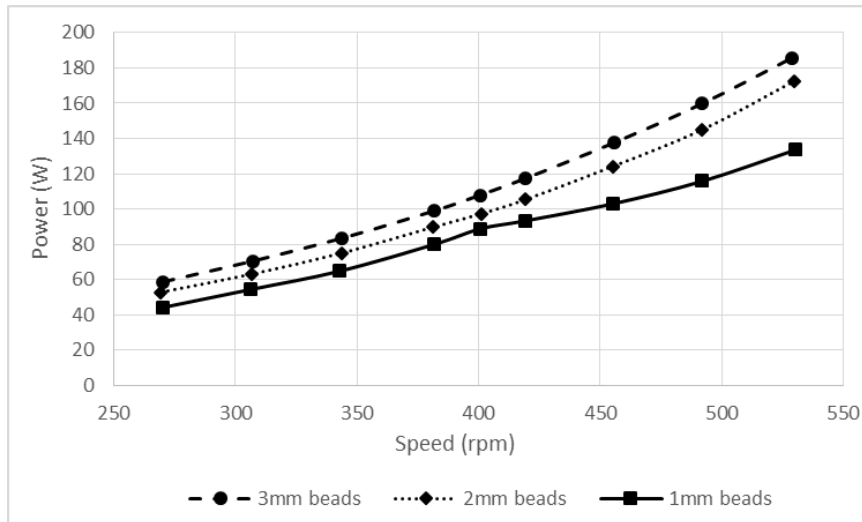


Figure 71: Test W-4 Ring in Disc Bead and Water Power Draw



Figure 72: Normal mixed charge conditions observed during tests



Figure 73: Charge with ring stirrer in smooth vessel and 2 mm beads at speeds above 400 rpm

Comparisons of the power draw for the different mill configurations at various stirrer speeds are shown in Figure 74 to Figure 76 for the 3 mm, 2 mm, and 1 mm beads respectively. The trends show that the pin in disc configuration had the highest power draw and the ring in disc configuration had the second highest power draw. This confirms that the addition of a stationary disc to the mill shell increases the power draw of the mill. A summary of the relative power draw increase due to the addition of the disc is shown in Figure 77 for the pin stirrer and Figure 78 for the ring stirrer. For the pin stirrer the power draw increase with a factor of between 1.71 and 2.42 with an average of 2.00. The power draw increase for the ring stirrer ranged from 1.29 to 1.95 with an average increase of 1.55. For both the smooth vessel and disc vessel configurations the power draw measured with the pin stirrer was higher than the power draw measured when using the ring stirrer. The relative power draw trends are therefore in line with those observed during the bead only tests reported in section 4.1.

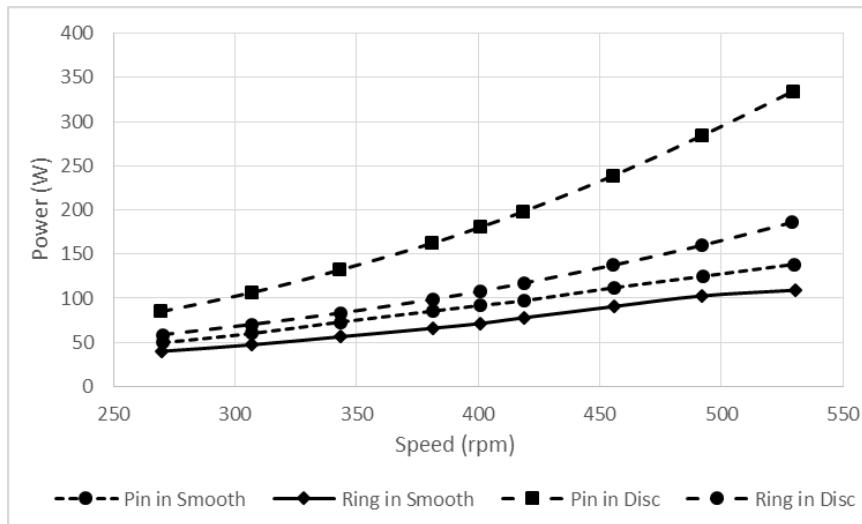


Figure 74: Bead and Water Tests Power Draw Comparison of Geometries with 3 mm Media

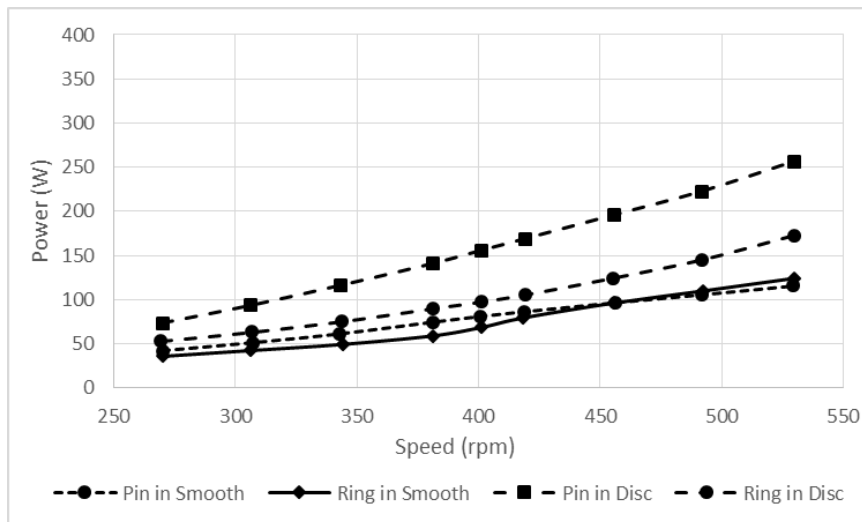


Figure 75: Bead and Water Tests Power Draw Comparison of Geometries with 2 mm Media

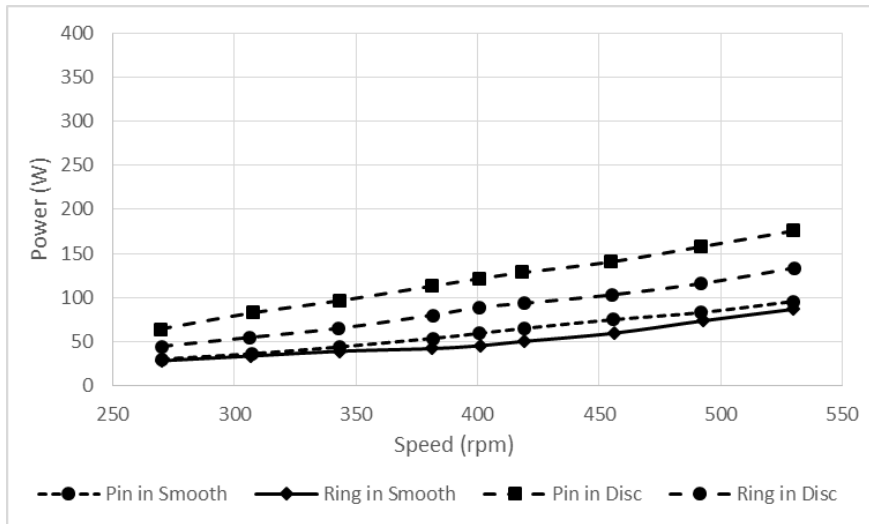


Figure 76: Bead and Water Tests Power Draw Comparison of Geometries with 1 mm Media

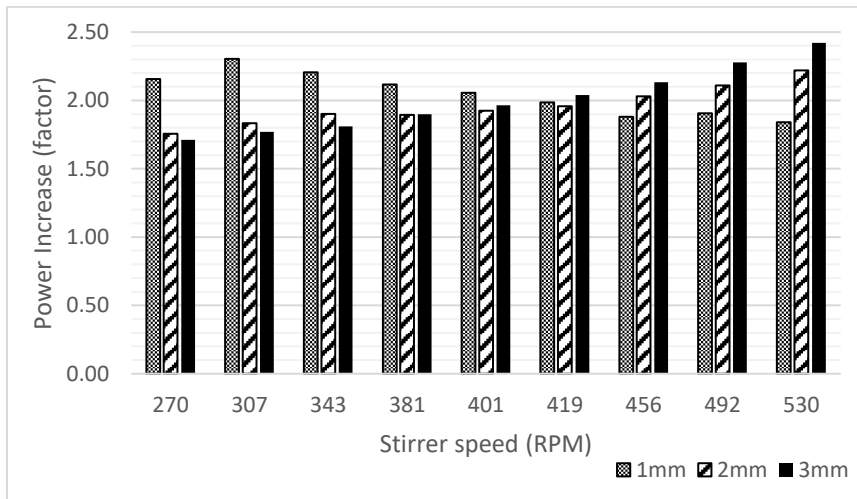


Figure 77: Power Draw Increase due to Addition of Disc Liner – Pin Stirrer

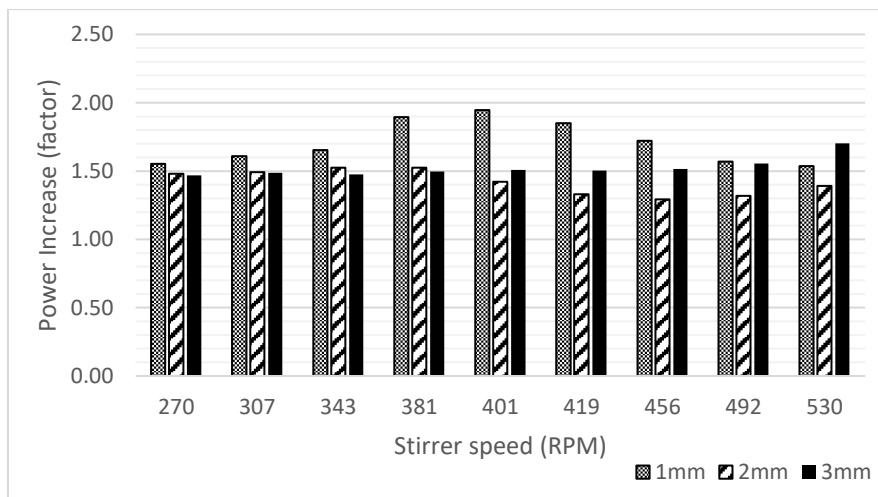


Figure 78: Power Draw Increase due to Addition of Disc Liner – Ring Stirrer

4.3 Results of Repeatability Tests

A set of five repeatability milling tests were conducted on the silica flour material with the pin in smooth mill configuration operating at 400 rpm with 3 mm beads. The data for the tests are reported in Appendix 7.9. The energy based (kWh/t) and time based (min) repeatability of the milling tests were quantified based on the coefficient of variation (CV) % calculated for various different product grinds. The repeatability analysis is shown in Table 13. The energy based repeatability (kWh/t) to reach a given target grind ranged from 2.66% to 5.32% based on the coefficient of variation. On a time basis the repeatability to reach a given target grind ranged from 1.58% to 2.76% measured by the coefficient of variation (CV). It can therefore be concluded that the results are repeatable within a confidence level of around 95%.

Table 13: Milling Test Repeatability

	Test R-1	Test R-2	Test R-3	Test R-4	Test R-5		Standard	Coefficient of
% Passing 38µm	Energy (kWh/t)	Energy (kWh/t)	Energy (kWh/t)	Energy (kWh/t)	Energy (kWh/t)	Mean	Deviation	variation (CV) %
70	3.41	3.25	3.20	2.95	3.10	3.20	0.17	5.32
75	5.48	5.19	5.11	4.72	4.96	5.11	0.28	5.48
80	7.64	7.21	7.20	6.95	7.10	7.20	0.26	3.60
85	9.81	9.22	9.28	9.29	9.25	9.28	0.25	2.66

	Test R-1	Test R-2	Test R-3	Test R-4	Test R-5		Standard	Coefficient of
% Passing 38µm	Time (min)	Time (min)	Time (min)	Time (min)	Time (min)	Mean	Deviation	variation (CV) %
70	2.73	2.81	2.76	2.61	2.76	2.76	0.07	2.68
75	4.43	4.49	4.42	4.18	4.42	4.42	0.12	2.76
80	6.44	6.25	6.30	6.18	6.37	6.30	0.10	1.58
85	8.45	8.01	8.18	8.30	8.34	8.30	0.17	2.03

4.4 Results of Mono Sized Feed Grinding Tests

Milling tests were conducted with the different mill configurations at a stirrer speed of 400 rpm with 3 mm beads on mono-sized silica feeds in the approximate size ranges of -150 + 106 and -106 + 75 µm to measure the time based and energy normalised breakage rates, Figure 79.



Figure 79: Picture of a milling test conducted on the mono-sized silica

The detailed results of the tests performed and the fitting of the breakage rate constants to the experimental data are presented in Appendix 7.10. It was found that first order breakage kinetics applied in all cases. The time based and energy normalised breakage rates for the different mill configurations are compared in Table 14. The results showed that by adding the disc liner to the mill vessel the time based breakage rates were increased significantly. In the case of the pin stirrer the addition of the disc resulted in increased time based breakage kinetics by a factor of 2.81 in the case of the $-150 + 106 \mu\text{m}$ feed and a factor of 2.37 in the case of the $-106 + 75 \mu\text{m}$ feed. For the ring stirrer the time based breakage rates increased with a factor of 1.69 for the $-150 + 106 \mu\text{m}$ feed and with a factor of 1.61 for the $-106 + 75 \mu\text{m}$ feed. As far as the energy efficiency is concerned the addition of the disc liner did not have a detrimental effect on the energy requirement. In fact the tests with the disc liner showed improved energy efficiency. For the pin stirrer the energy normalised breakage rate increased with a factor of 1.26 for the $-150 + 106 \mu\text{m}$ feed and with a factor of 1.08 for the $-106 + 75 \mu\text{m}$ feed. In the case of the ring stirrer the energy normalised breakage rate increased with a factor of 1.09 for the $-150 + 106 \mu\text{m}$ feed and with a factor of 1.02 for the $-106 + 75 \mu\text{m}$ feed. The results for the mono-sized milling test therefore show that an increase in mill productivity can be obtained by adding a disc liner without a negative impact on the energy efficiency of the milling process.

It is also interesting to note that the pin stirrer configuration provided improved energy efficiency as compared to the ring stirrer configuration. Comparing the pin stirrer with the ring stirrer in the smooth vessel the energy normalised breakage rates were $0.123 \text{ (kWh/t)}^{-1}$ for the pin versus $0.098 \text{ (kWh/t)}^{-1}$ for the ring with the $-150 + 106 \mu\text{m}$ feed and $0.138 \text{ (kWh/t)}^{-1}$ for the pin versus $0.120 \text{ (kWh/t)}^{-1}$ for the ring with the $-106 + 75 \mu\text{m}$ feed. In the case of the disc liner vessel the breakage rates were $0.155 \text{ (kWh/t)}^{-1}$ for the pin versus $0.107 \text{ (kWh/t)}^{-1}$ for the ring with the $-150 + 106 \mu\text{m}$ feed and $0.148 \text{ (kWh/t)}^{-1}$ for the pin versus $0.122 \text{ (kWh/t)}^{-1}$ for the ring with the $-106 + 75 \mu\text{m}$ feed.

The average measured power draw data for the different mill configurations are presented in Table 15. The relative power draw for the different configurations exhibited a similar trend to that observed during the bead only and bead and water tests. The tests conducted in the disc vessel were associated with the highest power draws due to the additional surface. For the pin stirrer the addition of the disc increased the power draw with a factor ranging from 2.14 and 2.17 and for the ring stirrer the addition of the disc increased the power draw with a factor ranging from 1.56 to 1.58. The pin stirrer provided a higher power draw compared to the ring stirrer when operating in the same mill vessel.

Table 14: Breakage Rates for Mono-sized Silica Grinding Tests

Breakage Rates: -150 + 106 μm Monosized Silica Feed

Mill Configuration	Si (min^{-1})	Change with addition of disc liner	Si ^E (kWh/t^{-1})	Change with addition of disc liner
Pin in Smooth	0.136		0.123	
Ring in Smooth	0.081		0.098	
Pin in Disc	0.382	2.81	0.155	1.26
Ring in Disc	0.137	1.69	0.107	1.09

Breakage Rates: -106 + 75 μm Monosized Silica Feed

Mill Configuration	Si (min^{-1})	Change with addition of disc liner	Si ^E (kWh/t^{-1})	Change with addition of disc liner
Pin in Smooth	0.149		0.138	
Ring in Smooth	0.097		0.120	
Pin in Disc	0.353	2.37	0.148	1.08
Ring in Disc	0.156	1.61	0.122	1.02

Table 15: Power Draw Comparison for Mono-sized Silica Grinding Tests

Power Draw: -150 + 106 μm Monosized Silica Feed

Mill Configuration	Average Power (W)	Power (W) relative to Pin in Smooth	Power (W) increase due to disc liner
Pin in Smooth	86.4	1.00	
Ring in Smooth	63.9	0.74	
Pin in Disc	184.6	2.14	2.14
Ring in Disc	99.7	1.15	1.56

Power Draw: -106 + 75 μm Monosized Silica Feed

Mill Configuration	Average Power (W)	Power (W) relative to Pin in Smooth	Power (W) increase due to disc liner
Pin in Smooth	81.5	1.00	
Ring in Smooth	61.6	0.71	
Pin in Disc	176.6	2.04	2.17
Ring in Disc	97.5	1.13	1.58

4.5 Results of Silica Flour Feed Grinding Tests

A series of milling tests were conducted with the silica flour feed material at various different stirrer speeds, Figure 80. The detailed results of the milling tests are presented in Appendix 7.11.



Figure 80: Picture of a milling test conducted with the silica flour

Average power draw data for the various mill configurations at different stirrer speeds are presented in Table 16. The data showed similar trends to those observed during the previous testing with bead and water only and with the mono-sized silica grinding tests. The addition of the disc to the mill vessel increased the power draw of the pin stirrer configuration with a factor of around 1.88 to 2.71. In the case of the ring stirrer the addition of the disc increased the power draw with a factor of between 1.53 to 1.80. As with the previous test results, the use of the pin stirrer resulted in a higher power draw as compared to the ring stirrer when operating in the same mill vessel.

Summarised results showing the effect on the grinding performance when adding a disc liner to the mill vessel are presented in Table 17 and Table 18 for the pin and ring stirrers respectively. For both the pin stirrer and the ring stirrer the addition of the disc resulted in significantly increased mill productivity as measured based on the milling time required to reach a given grind size. In the case of the pin stirrer the increase in productivity ranged from around 52.6% to 65.3% and for the pin the productivity increased by around 33.0% to 47.6%. This is due to the higher power draw brought about by adding the additional surface to the mill.

With regard to the energy efficiency, in the case of the pin stirrer the results showed that the energy efficiency of milling improved by the addition of the disc. The results shows that energy efficiency increased by around 6.5% to 17.1%. These measured increases are higher than the coefficient of variation (CV) measured during the repeatability tests. The CV which is an indication of the experimental error ranged from around 2.66% to 5.32% so it seems that the results do indicate an increased efficiency when the disc is added to the pin stirrer configuration. In the case of the ring stirrer the results are not so clear cut. Some data points show an improvement in energy efficiency while other points show a decrease in energy efficiency. The change in energy requirement ranged from around -10.9% to 3.6%. The majority of the data points were however inside of the experimental error range so in the case of the ring stirrer the effect of adding a disc liner on energy efficiency is considered to be negligible.

The milling performance of the ring stirrer is compared against the pin stirrer in Table 19 and Table 20 for the smooth and disc vessels respectively. The pin stirrer provided better results compared to the ring stirrer in both cases. For the smooth vessel configurations the ring stirrer required around 0.7% to 13.4% more energy (kWh/t) and the production rate for a given grind size was around 18% to 55.3% lower compared to the pin stirrer. For the disc vessel the difference in stirrer performance was more pronounced. For this configuration the ring stirrer required around 5.9% to 28.1% more energy than the pin stirrer and the production rate was about 73.9% to

119.5% lower compared to the pin stirrer. This large difference observed with the disc configurations is due to the fact that the energy efficiency performance of the pin stirrer was enhanced by the addition of the disc liner. However in the case of the ring stirrer the energy efficiency remained unchanged when the disc was added. The stirrer performance should therefore not be considered in isolation but rather in conjunction with other mill geometry elements such as the disc liner.

Table 16: Power Draw Comparison for Silica Flour Grinding Tests

Power Draw: 270 RPM

Mill Configuration	Average Power (W)	Power (W) relative to Pin in Smooth	Power (W) increase due to disc liner
Pin in Smooth	43.8	1.00	
Ring in Smooth	31.9	0.73	
Pin in Disc	82.3	1.88	1.88
Ring in Disc	48.9	1.12	1.53

Power Draw: 400 RPM

Mill Configuration	Average Power (W)	Power (W) relative to Pin in Smooth	Power (W) increase due to disc liner
Pin in Smooth	82.3	1.00	
Ring in Smooth	60.2	0.73	
Pin in Disc	171.4	2.08	2.08
Ring in Disc	102.7	1.25	1.71

Power Draw: 530 RPM

Mill Configuration	Average Power (W)	Power (W) relative to Pin in Smooth	Power (W) increase due to disc liner
Pin in Smooth	112.7	1.00	
Ring in Smooth	94.3	0.84	
Pin in Disc	305.0	2.71	2.71
Ring in Disc	170.1	1.51	1.80

Table 17: Silica Flour Milling Test Results – Pin Stirrer Smooth Vessel versus Disc Vessel

12-Pin Stirrer at 270 RPM

	Smooth Vessel	Disc Vessel	Energy Required	Smooth Vessel	Disc Vessel	Productivity
Grind Size % Passing 38µm	Energy (kWh/t)	Energy (kWh/t)	% Change with addition of disc	Time (min)	Time (min)	% Change with addition of disc
70	3.56	2.97	-16.5%	6.14	2.70	-56.0%
75	5.73	4.75	-17.1%	9.95	4.32	-56.6%
80	8.00	7.11	-11.1%	14.07	6.49	-53.9%
85	10.47	9.60	-8.3%	18.52	8.77	-52.6%

12-Pin Stirrer at 400 RPM

	Smooth Vessel	Disc Vessel	Energy Required	Smooth Vessel	Disc Vessel	Productivity
Grind Size % Passing 38µm	Energy (kWh/t)	Energy (kWh/t)	% Change with addition of disc	Time (min)	Time (min)	% Change with addition of disc
70	4.21	3.69	-12.4%	3.84	1.65	-57.0%
75	6.41	5.78	-9.9%	5.88	2.58	-56.2%
80	8.45	7.62	-9.8%	7.79	3.39	-56.5%
85	10.80	9.45	-12.5%	10.04	4.21	-58.1%

12-Pin Stirrer at 530 RPM

	Smooth Vessel	Disc Vessel	Energy Required	Smooth Vessel	Disc Vessel	Productivity
Grind Size % Passing 38µm	Energy (kWh/t)	Energy (kWh/t)	% Change with addition of disc	Time (min)	Time (min)	% Change with addition of disc
70	3.18	2.97	-6.5%	2.19	0.77	-64.9%
75	5.08	4.75	-6.5%	3.50	1.23	-64.9%
80	7.26	6.69	-7.8%	4.92	1.71	-65.3%
85	9.44	8.73	-7.4%	6.34	2.20	-65.3%

Table 18: Silica Flour Milling Test Results – Ring Stirrer Smooth Vessel versus Disc Vessel

Ring Stirrer at 270 RPM

	Smooth Vessel	Disc Vessel	Energy Required	Smooth Vessel	Disc Vessel	Productivity
Grind Size % Passing 38µm	Energy (kWh/t)	Energy (kWh/t)	% Change with addition of disc	Time (min)	Time (min)	% Change with addition of disc
70	3.77	3.51	-6.9%	8.76	5.45	-37.9%
75	6.13	5.84	-4.7%	14.42	9.07	-37.1%
80	8.60	8.75	1.7%	20.57	13.65	-33.7%
85	11.86	12.29	3.6%	28.76	19.26	-33.0%

Ring Stirrer at 400 RPM

	Smooth Vessel	Disc Vessel	Energy Required	Smooth Vessel	Disc Vessel	Productivity
Grind Size % Passing 38µm	Energy (kWh/t)	Energy (kWh/t)	% Change with addition of disc	Time (min)	Time (min)	% Change with addition of disc
70	4.39	3.91	-10.9%	5.48	2.87	-47.6%
75	6.64	6.16	-7.2%	8.39	4.54	-45.9%
80	8.76	8.32	-5.0%	11.18	6.16	-44.9%
85	11.55	10.80	-6.5%	14.82	8.05	-45.7%

Ring Stirrer at 530 RPM

	Smooth Vessel	Disc Vessel	Energy Required	Smooth Vessel	Disc Vessel	Productivity
Grind Size % Passing 38µm	Energy (kWh/t)	Energy (kWh/t)	% Change with addition of disc	Time (min)	Time (min)	% Change with addition of disc
70	3.60	3.68	2.2%	3.09	1.67	-45.7%
75	5.68	5.81	2.2%	4.78	2.64	-44.9%
80	7.59	7.78	2.5%	6.13	3.51	-42.7%
85	9.50	9.75	2.6%	7.48	4.39	-41.3%

Table 19: Silica Flour Milling Test Results – Pin versus Ring Stirrer Smooth Vessel

Smooth Vessel at 270 RPM

	Pin Stirrer	Ring Stirrer	Energy Required	Pin Stirrer	Ring Stirrer	Productivity
Grind Size % Passing 38µm	Energy (kWh/t)	Energy (kWh/t)	% Change Ring vs. Pin	Time (min)	Time (min)	% Change Ring vs. Pin
70	3.56	3.77	6.0%	6.14	8.76	42.7%
75	5.73	6.13	6.9%	9.95	14.42	44.9%
80	8.00	8.60	7.6%	14.07	20.57	46.2%
85	10.47	11.86	13.3%	18.52	28.76	55.3%

Smooth Vessel at 400 RPM

	Pin Stirrer	Ring Stirrer	Energy Required	Pin Stirrer	Ring Stirrer	Productivity
Grind Size % Passing 38µm	Energy (kWh/t)	Energy (kWh/t)	% Change Ring vs. Pin	Time (min)	Time (min)	% Change Ring vs. Pin
70	4.21	4.39	4.2%	3.84	5.48	42.7%
75	6.41	6.64	3.5%	5.88	8.39	42.7%
80	8.45	8.76	3.7%	7.79	11.18	43.5%
85	10.80	11.55	6.9%	10.04	14.82	47.6%

Smooth Vessel at 530 RPM

	Pin Stirrer	Ring Stirrer	Energy Required	Pin Stirrer	Ring Stirrer	Productivity
Grind Size % Passing 38µm	Energy (kWh/t)	Energy (kWh/t)	% Change Ring vs. Pin	Time (min)	Time (min)	% Change Ring vs. Pin
70	3.18	3.60	13.4%	2.19	3.09	41.0%
75	5.08	5.68	11.9%	3.50	4.78	36.7%
80	7.26	7.59	4.6%	4.92	6.13	24.7%
85	9.44	9.50	0.7%	6.34	7.48	18.0%

Table 20: Silica Flour Milling Test Results – Pin versus Ring Stirrer Disc Vessel

Disc Vessel at 270 RPM

	Pin Stirrer	Ring Stirrer	Energy Required	Pin Stirrer	Ring Stirrer	Productivity
Grind Size % Passing 38µm	Energy (kWh/t)	Energy (kWh/t)	% Change Ring vs. Pin	Time (min)	Time (min)	% Change Ring vs. Pin
70	2.97	3.51	18.3%	2.70	5.45	101.6%
75	4.75	5.84	23.1%	4.32	9.07	110.2%
80	7.11	8.75	23.1%	6.49	13.65	110.2%
85	9.60	12.29	28.1%	8.77	19.26	119.5%

Disc Vessel at 400 RPM

	Pin Stirrer	Ring Stirrer	Energy Required	Pin Stirrer	Ring Stirrer	Productivity
Grind Size % Passing 38µm	Energy (kWh/t)	Energy (kWh/t)	% Change Ring vs. Pin	Time (min)	Time (min)	% Change Ring vs. Pin
70	3.69	3.91	5.9%	1.65	2.87	73.9%
75	5.78	6.16	6.7%	2.58	4.54	76.1%
80	7.62	8.32	9.2%	3.39	6.16	81.7%
85	9.45	10.80	14.2%	4.21	8.05	91.4%

Disc Vessel at 530 RPM

	Pin Stirrer	Ring Stirrer	Energy Required	Pin Stirrer	Ring Stirrer	Productivity
Grind Size % Passing 38µm	Energy (kWh/t)	Energy (kWh/t)	% Change Ring vs. Pin	Time (min)	Time (min)	% Change Ring vs. Pin
70	2.97	3.68	24.0%	0.77	1.67	118.1%
75	4.75	5.81	22.4%	1.23	2.64	114.9%
80	6.69	7.78	16.3%	1.71	3.51	105.8%
85	8.73	9.75	11.6%	2.20	4.39	99.4%

4.6 Results of DEM Modelling

The DEM model parameters derived during the virtual prototyping process, Table 6, resulted in an under prediction of the actual torque of the four different mill geometries compared to the actual data from the experiments. The DEM model was re-calibrated to provide torque predictions that are closer to that measured during the experimental programme. The friction coefficient was increased to 0.45 and this resulted in predicted torque values that are closer to the experimental results. The parameters used for the revised simulations are shown in Table 21. A comparison of the modelled versus actual torque is shown in Table 22. This was the best correlation that could be achieved.

Table 21: DEM Model Parameters Used for Revised DEM Simulations

Parameter	Value Used in DEM	Parameter	Value Used in DEM
Bead density (g/cm ³)	3.25	Coefficient of restitution	0.95
Bead diameter (mm)	3.0	Coefficient of friction	0.45
Poisson Ratio	0.22	Normal spring stiffness (N/m)	438 267
Characteristic velocity (m/s)	2.93	Tangential spring stiffness (N/m)	384 099
Maximum overlap (%)	1.0	Normal Damping (bead-bead)	0.1037
Stirrer speed (rpm)	400	Normal Damping (bead-wall)	0.1466
Number of particles	124 200	Tangential Damping (bead-bead)	0.0970
Number of time steps	18 666 666	Tangential Damping (bead-wall)	0.1372
Time step (seconds)	1.07 x 10 ⁻⁶		

Table 22: DEM Model Torque versus Actual Measured Torque

Mill Configuration	Actual Torque (N.m)	DEM Model Torque (N.m)	Difference (%)
Pin in Smooth	3.09	3.25	5.2 %
Ring in Smooth	2.30	2.59	12.6%
Pin in Disc	5.80	4.71	-18.8%
Ring in Disc	3.97	3.80	-4.3 %

Cross sectional views of the DEM simulations of the four different geometries are shown in Figure 81. The charge profiles for the DEM simulations all exhibited the expected vortex shape as pictured in Appendix 7.13.2. Once again the DEM model showed higher bead velocities for the pin stirrer compared to the ring stirrer when

operating in the same vessel. For the smooth mill vessel the pin stirrer resulted in an average bead velocity of 0.71 m/s compared 0.56 m/s when using the ring stirrer, Table 23. With the disc vessel the pin stirrer resulted in an average bead velocity of 0.47 m/s compared to an average velocity of 0.39 m/s when using the ring stirrer. The presence of this disc on the mill shell results in a lower average bead velocity but in a higher mill power draw. Comparative velocity histograms are shown in Figure 82.

Table 23: DEM model average bead velocities for the different mill configurations

Mill Configuration	Average Bead Velocity (m/s)
Pin in Smooth	0.71
Ring in Smooth	0.56
Pin in Disc	0.47
Ring in Disc	0.39

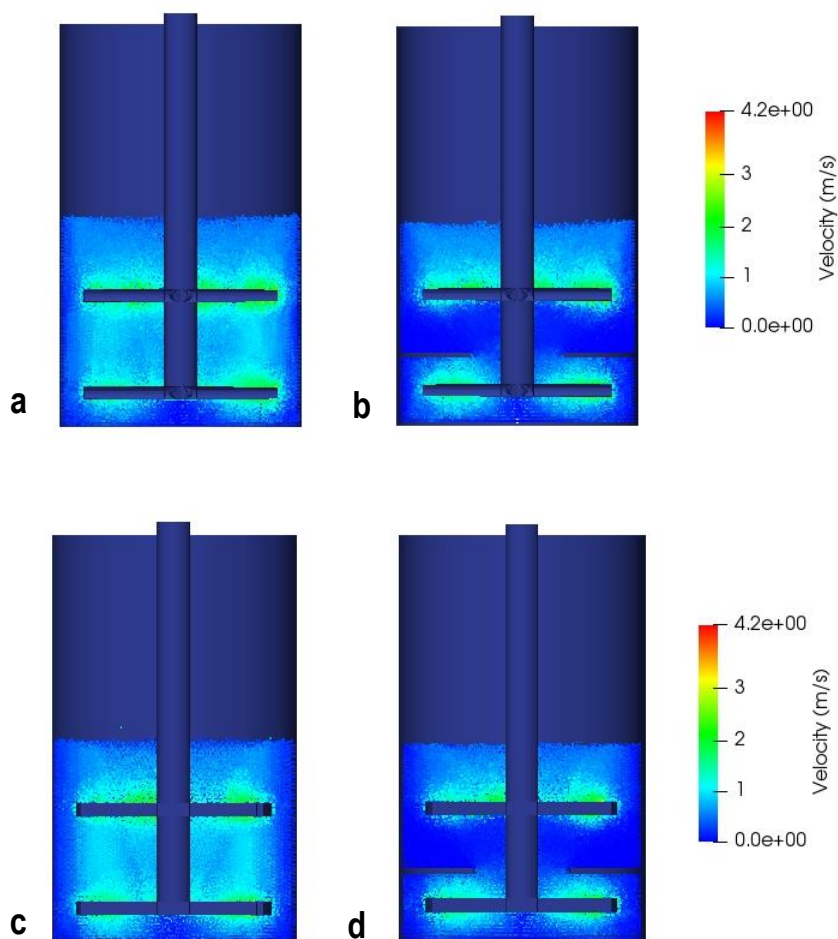


Figure 81: DEM simulations a) 12-pin - smooth vessel, b) 12-pin - disc vessel, c) ring stirrer - smooth vessel, d) ring stirrer - disc vessel.

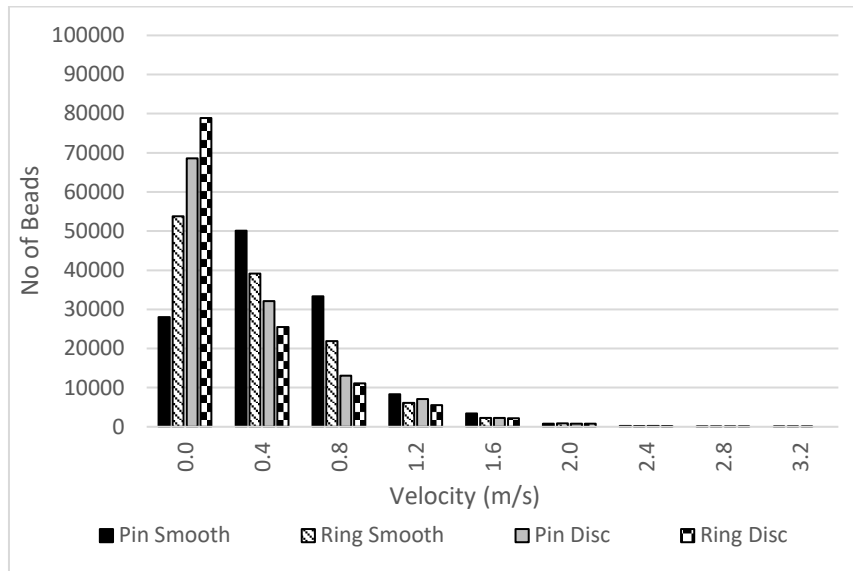


Figure 82: DEM Model bead velocity histogram for the different mill configurations

4.7 Discussion of Results

4.7.1 Discussion of Results - Research Question 1

During this research investigation a hypothesis postulated by Radziszewski, 2013, was tested. The hypothesis states that the power draw of a stirred media mill operating with pin or disc type stirrers could be increased by adding liners to the mill shell. This led to the development of the first research question which was formulated as follows:

Research question 1: Will the power draw of a pin or disc type fluidised vertical stirred media mill be increased by the addition of shear surface area, in the form of added mill shell liners?

The results from all of the tests conducted confirm that the power draw increases with the addition of a disc liner to the mill shell. The relative increase in power draw for various tests are summarised in Table 24 and also shown in Figure 83 and Figure 84 for the pin and ring stirrers respectively. For the pin stirrer the power increase ranged with a factor of 1.71 to 2.71 with an average of increase factor of 2.07. In the case of the ring stirrer the power increase ranged with a factor of 1.39 to 1.95 with an average increase of 1.59.

Table 24: Mill Power Draw Increase Due to Addition of Disc to Mill Vessel – Various Tests

Pin Stirrer - Relative Increase in Power draw due to Addition of Disc

Speed (rpm)	Bead & Water 1 mm	Bead & Water 2 mm	Bead & Water 3 mm	Silica Flour	-150 + 106 μ m	-106 + 75 μ m
270	2.16	1.76	1.71	1.88		
400	2.06	1.92	1.96	2.08	2.14	2.17
530	1.84	2.22	2.42	2.71		

Ring Stirrer - Relative Increase in Power draw due to Addition of Disc

Speed (rpm)	Bead & Water 1 mm	Bead & Water 2 mm	Bead & Water 3 mm	Silica Flour	-150 + 106 μ m	-106 + 75 μ m
270	1.55	1.48	1.47	1.53		
400	1.95	1.42	1.51	1.71	1.56	1.58
530	1.54	1.39	1.70	1.80		

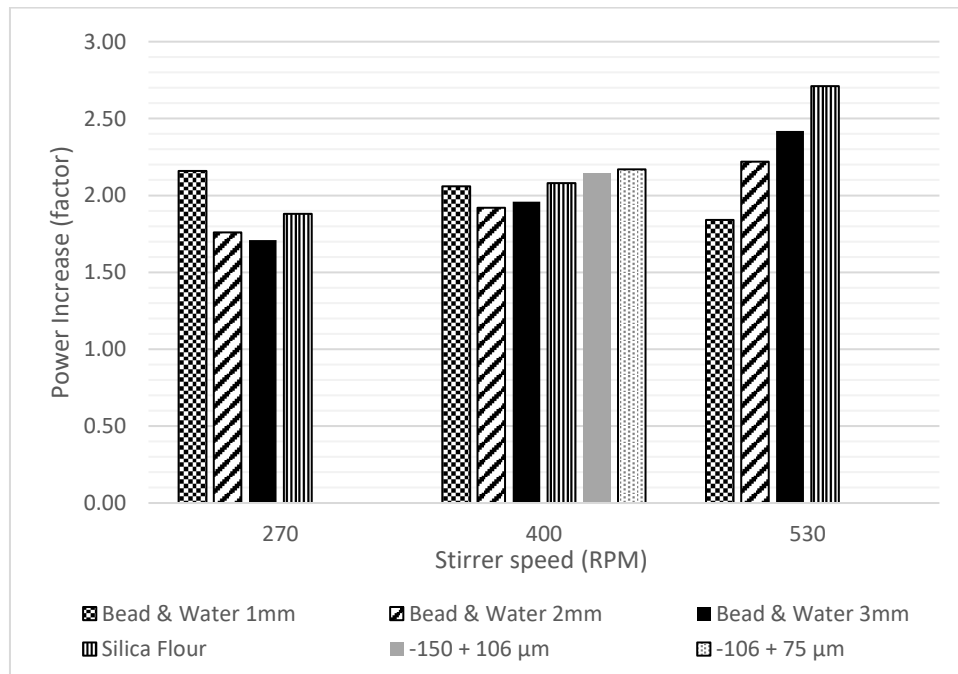


Figure 83: Pin Stirrer Increase in Power Draw due to Addition of Disc – Various Tests

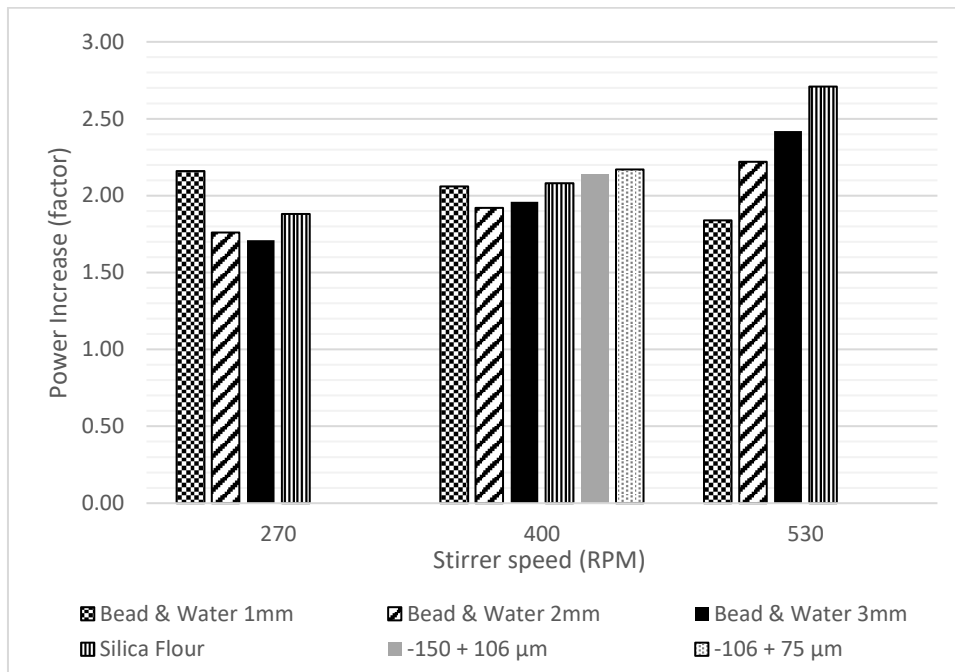


Figure 84: Ring Stirrer Increase in Power Draw due to Addition of Disc – Various Tests

4.7.2 Discussion of Results – Research Question 2

The second research objective was aimed at understanding if there is a potential to increase the mill throughput rates by increasing the mill power draw with the addition of the disc liner to the mill vessel. The research question was formulated as follows:

Research question 2: Will the additional mill power draw increase the productivity of the mill?

In order to answer this question the time based breakage rates were evaluated and compared for the mono-sized silica feed tests. Also the milling times to reach a given grind size were compared for the silica flour grinding tests. The results all showed that the increased power draw, brought about by adding the disc liner, resulted in significantly faster milling rates for both the pin and ring stirrer configurations. Results for various grinding tests are summarised in Table 25 and Figure 85 to Figure 86. For the ring stirrer the productivity increased with a factor of around 1.35 to 1.69 with an average of 1.51. For the pin stirrer the productivity increased with a factor of 1.55 to 2.81 with an average of 1.99. The results indicated that significant productivity improvements could be obtained by adding disc liners to the stationary mill shell of a vertical stirrer media mill. This could lead to a smaller equipment footprint in the case of a new mill installation or in the case of existing mills could lead to increased throughput capacity if the mills are retro-fitted with disc liners on the mill shell.

Table 25: Mill Production Rate Increase Due to Addition of Disc to Mill Vessel – Various Tests

Pin Stirrer - Relative Increase in Mill Productivity due to Addition of Disc

Speed (RPM)	Silica Flour	-150 + 106 μm	-106 + 75 μm
270	1.55		
400	1.57	2.81	2.37
530	1.65		

Ring Stirrer - Relative Increase in Mill Productivity due to Addition of Disc

Speed (RPM)	Silica Flour	-150 + 106 μm	-106 + 75 μm
270	1.35		
400	1.46	1.69	1.61
530	1.44		

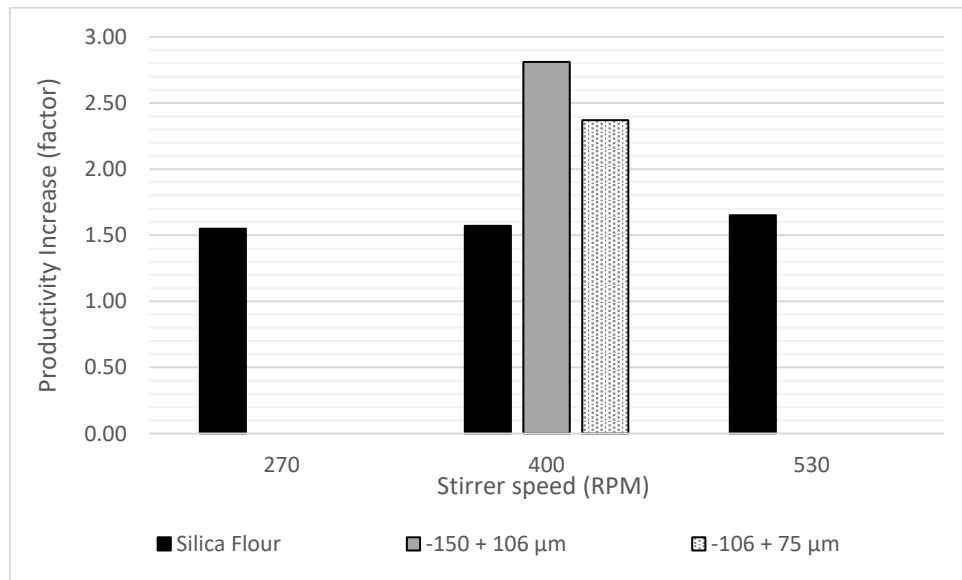


Figure 85: Pin Stirrer Increase in Milling Productivity due to Addition of Disc – Various Tests

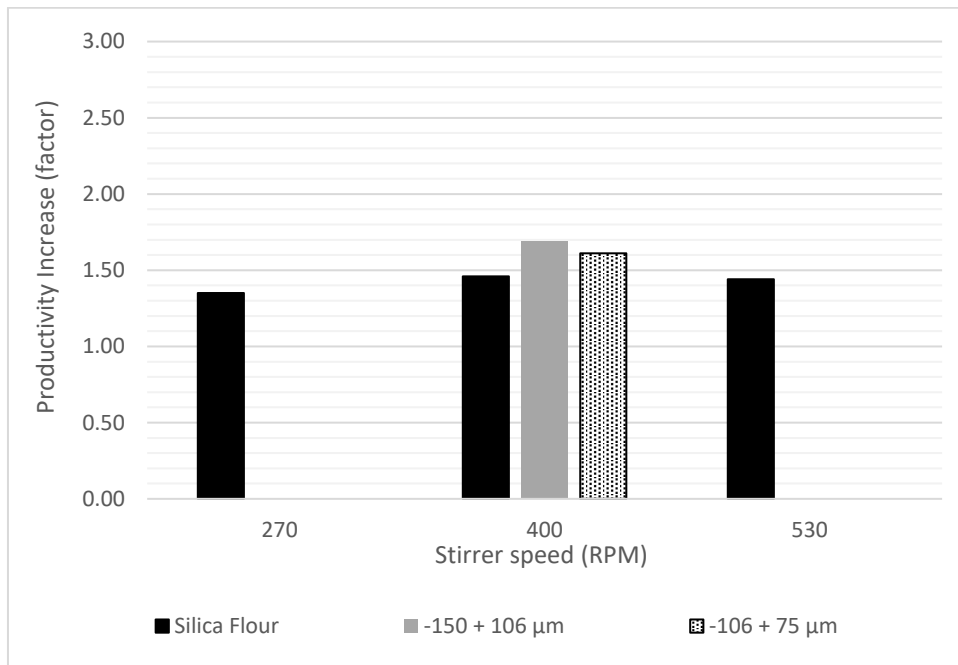


Figure 86: Ring Stirrer Increase in Milling Productivity due to Addition of Disc – Various Tests

4.7.3 Discussion of Results – Research Question 3

The third objective of the investigation was to assess if the addition of the disc to the mill vessel will have an effect on the energy efficiency of the milling operation. The following research question was formulated:

Research question 3: Will the addition of the liner surfaces affect the energy efficiency of the mill?

In order to answer this question the energy normalised breakage rates were evaluated and compared for the mono-sized silica feed tests. Also the specific energy input to reach a given grind size was compared for the silica flour grinding tests. Results for various grinding tests are summarised in Table 26 and also in Figure 87 to Figure 88. In the case of the pin stirrer the addition of the disc resulted in a somewhat improved energy efficiency. The efficiency increased by a factor of around 1.07 to 1.26 with an average of around 1.13 which equates to 13% improvement. For the ring stirrer the addition of the disc did not have a significant impact on the energy efficiency. The relative change in energy efficiency ranged from around -1.02 to 1.09 corresponding to a 2% decrease in energy efficiency to a 9% increase in energy efficiency. However the majority of the data points were inside of the experimental error range so therefore the change in energy efficiency was negligible and not significant.

The results of the tests conducted therefore indicated that the addition of the disc did not have a negative effect on the energy efficiency of the milling process.

Table 26: Mill Energy Efficiency Increase Due to Addition of Disc to Mill Vessel – Various Tests

Pin Stirrer - Relative Increase in Mill Energy Efficiency due to Additon of Disc

Speed (RPM)	Silica Flour	-150 + 106 μm	-106 + 75 μm
270	1.13		
400	1.11	1.26	1.08
530	1.07		

Ring Stirrer - Relative Increase in Mill Energy Efficiency due to Additon of Disc

Speed (RPM)	Silica Flour	-150 + 106 μm	-106 + 75 μm
270	1.02		
400	1.07	1.09	1.02
530	-1.02		

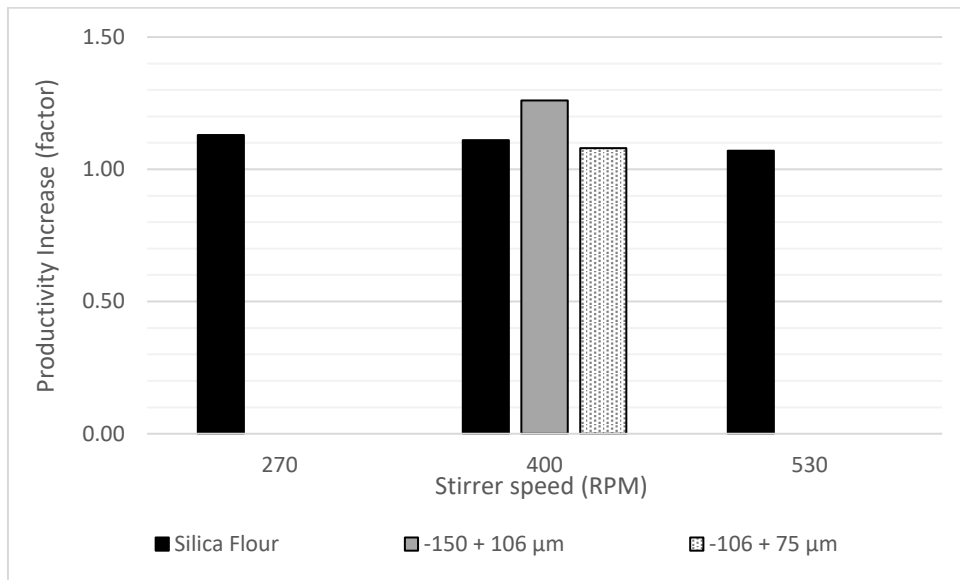


Figure 87: Pin Stirrer Increase in Milling Energy Efficiency due to Addition of Disc – Various Tests

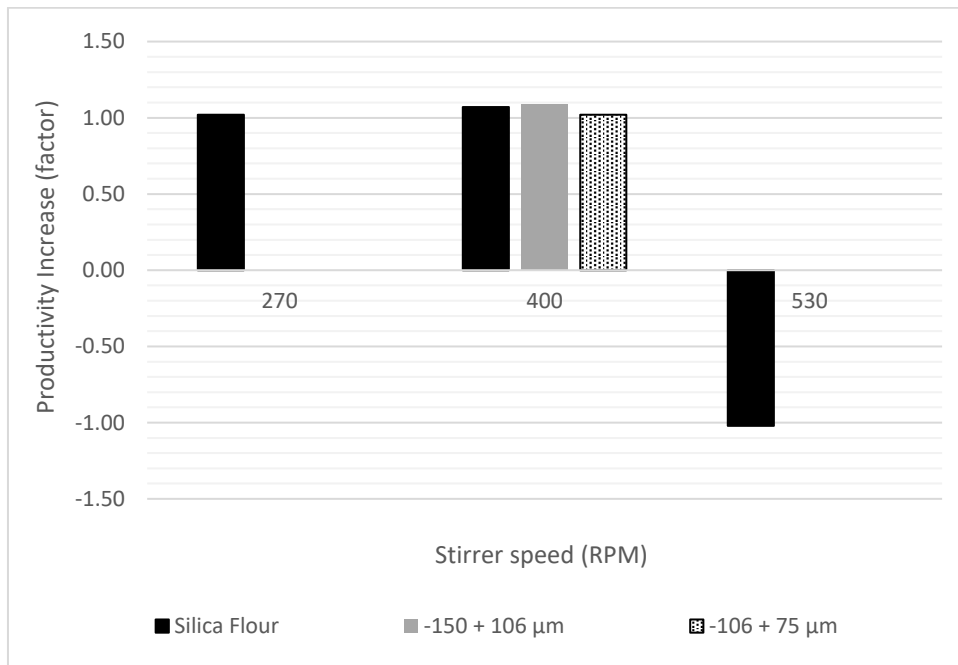


Figure 88: Ring Stirrer Increase in Milling Energy Efficiency due to Addition of Disc – Various Tests

4.7.4 Observations on the Shear Based Power Model

The shear based power model by Radziszewski, 2013, proposes that the power draw of a stirred media mill is proportional to a parameter termed the shear volume. The shear volume is calculated based on the geometry of the stirrer and the mill vessel, details of this concept is provided in the literature review section. The associated shear volume was calculated for each of the four geometries as part of this investigation, refer to Table 9. Based on the shear volume calculations the shear based power model predicted that the pin stirrer in smooth mill configuration will draw the lowest amount of power. The model predicted that the pin stirrer in disc vessel configuration will draw more power than when the pin is operating in the smooth mill, with the relative power draw increasing by a factor of 1.75. The model then predicted that the ring stirrer operating in the smooth vessel will draw 5.93 times the power as compared to the pin stirrer operating in the same vessel. It was predicted that the ring stirrer operating in the disc vessel will draw the most power and that the power draw will be about 8.51 times higher than the pin stirrer operating in the smooth vessel.

Although the shear based power model did predict that the addition of the disc liner to the mill vessel will result in an increase in the mill power draw, the results of the work conducted during this investigation do not support all of the predictions made by the model. Specifically the model predicted that the ring stirrer will draw significantly more power than the pin stirrer, but in reality this was not the case. The use of the pin stirrer did in fact result in a higher mill power draw. Comparative power draw data are presented in Table 27 and in Figure 89 and Figure 90 for the smooth and disc mill vessels respectively.

Interestingly the DEM simulations provided a more realistic indication of the relative power draw trends. An analysis of the DEM results showed that the pin stirrer resulted in a higher average bead velocity in the mill as compared to the ring stirrer. It is therefore speculated that the reason for the higher power draw with the pin stirrer was that this stirrer design provided a better transfer of movement from the mill shaft to the mill charge.

Table 27: Comparative Power Draw Data - Pin Stirrer versus Ring Stirrer

Smooth Vessel: Tests at 400 rpm stirrer speed

Tests	Pin Stirrer (W)	Ring Stirrer (W)
Bead & Water 1 mm	59.2	45.6
Bead & Water 2 mm	80.7	68.4
Bead & Water 3 mm	91.8	71.5
Silica Flour	82.3	60.2
-150 + 106 μm	86.4	63.9
-106 + 75 μm	81.5	61.6

Disc Vessel: Tests at 400 rpm stirrer speed

Tests	Pin Stirrer (W)	Ring Stirrer (W)
Bead & Water 1 mm	121.7	88.8
Bead & Water 2 mm	155.3	97.3
Bead & Water 3 mm	180.4	107.9
Silica Flour	171.4	102.7
-150 + 106 μm	184.6	99.7
-106 + 75 μm	176.6	97.5

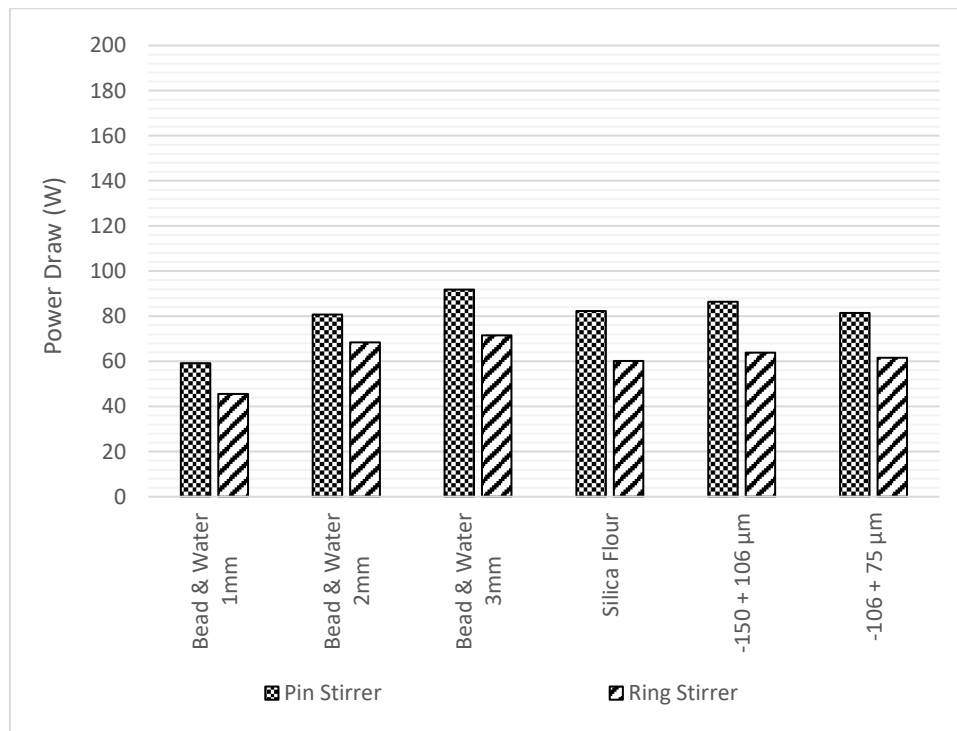


Figure 89: Smooth Mill Vessel Comparative Power Draw – Pin versus Ring stirrer at 400 rpm

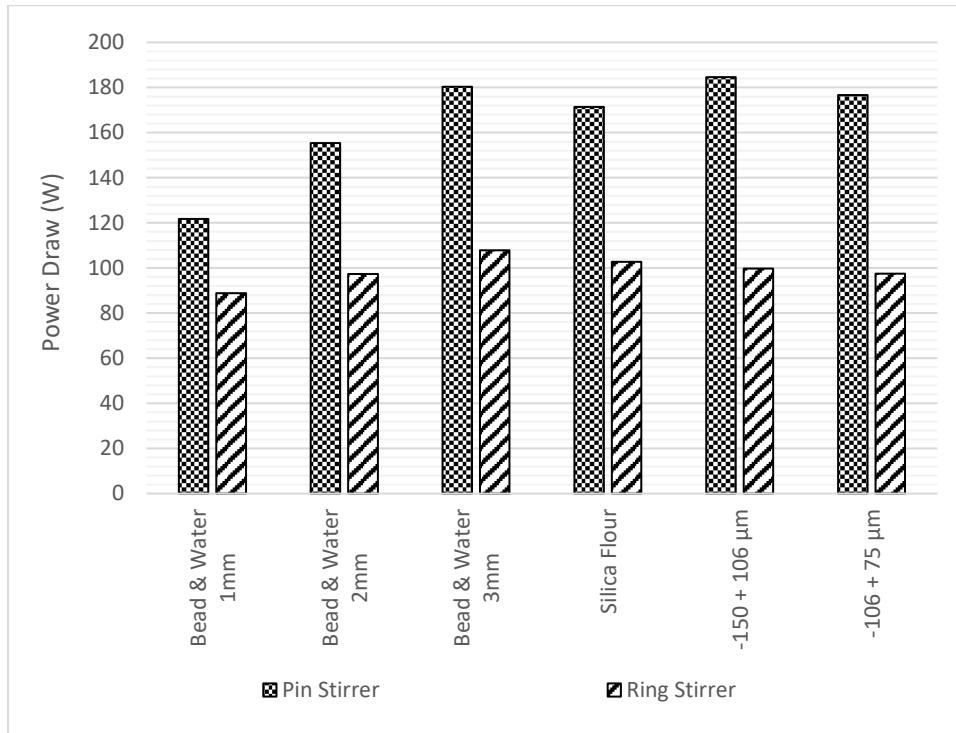


Figure 90: Disc Mill Vessel Comparative Power Draw – Pin versus Ring stirrer at 400 rpm

5 Conclusions and Recommendations

The experimental test work programme was aimed at investigating the hypothesis that the power draw of a stirred media mill operating with pin or disc type stirrers could be increased by adding stationary disc liners to the mill shell. In this regard three different research questions were formulated.

The first research question was aimed at testing the hypothesis by establishing if the power draw of a pin or disc type fluidised vertical stirred media mill will be increased by the addition of shear surface area, in the form of added mill shell liners. The experimental results supported the hypothesis and showed that the power draw of the pin and ring stirrer mills increased with the addition of a disc liner to the mill shell. For the pin stirrer the power draw increased with a factor of between 1.71 to 2.71 with an average of 2.07. For the ring stirrer the power draw increased with a factor ranging from 1.39 to 1.95 with an average of 1.59.

The second question aimed to evaluate if the additional mill power draw will lead to an increase in the productivity of the mill. Grinding test results showed that the time based production rate of mill product increased due to the increased mill power draw brought about by the additional mill disc liner. For the pin stirrer the productivity increased with a factor of between 1.55 to 2.81 with an average of 1.99. For the ring stirrer the productivity increased with a factor ranging from 1.35 to 1.69 with an average of 1.51.

The third research question evaluated whether the addition of the liner surfaces will affect the energy efficiency of the milling operation. Results of grinding tests conducted showed that the addition of the disc liner did not have a negative effect on the energy efficiency. In the case of the pin stirrer the energy efficiency improved with the addition of the disc with a factor of between 1.07 to 1.26 and an average of 1.13. For the ring stirrer the effect on energy efficiency was insignificant.

The results of this work show that there could be a potential to improve the milling performance of stirred media mills by adding stationary discs to the mill shell. Specifically a higher mill power draw could lead to either a smaller equipment footprint in the case of new mills or to a larger throughput capacity or finer product grind in existing mills that have been retrofitted with an improved internal design

The scope of this current investigation was focused on conducting experimental work at a laboratory scale to test the proof of concept. Further work would be required to confirm the results of this study on a larger scale and in a continuous milling configuration. In this regard it should be noted that the Outotec HIG mill already utilises disc liners in the mill design, while the other mills on the market do not use this design element. With this in mind it seems that the idea of utilising discs on the mill shell could be feasible in practice. However the process benefits of such a design compared to the traditional smooth shell design should be assessed at a larger scale and in a continuous feed configuration.

Some general observations were made on the shear based power model proposed by Radziszewski, 2013. The model proposes that the power draw of a stirred media mill is proportional to a parameter termed the shear volume. When applied to this current investigation the shear based power model correctly predicted that the addition of the disc liner to the mill vessel will result in an increase in the mill power draw. However the model did not correctly predict the relative power draw of the pin versus ring stirrer designs. The shear based power model predicted that the ring stirrer will draw more power than the pin stirrer, due to the larger shear volume of the ring design compared to the pin design. However the experimental work showed the opposite result, the pin stirrer had a higher power draw than the ring stirrer. Results of DEM simulations conducted on the different mill configurations matched the experimentally observed power draw trends. An analysis of the DEM data showed that the pin stirrer resulted in a higher average bead velocity in the mill as compared to the ring stirrer. It is therefore speculated that the reason for the higher power draw with the pin stirrer was that this design provided a better transfer of movement from the mill shaft to the mill charge.

6 References

- Allen J., (2013). *Stirred Milling machine development and application extension*. Metso.
- Anyimadu, A.K., Rule, C.M., Knopjes, L. (2007). The development of ultra-fine grinding at Anglo Platinum. *The Journal of The Southern African Institute of Mining and Metallurgy*, Volume 107, pp. 15 – 22.
- Asthalm M., (2015). *Outotec technology for fine and ultra-fine grinding in minerals processing*. Almaty: Outotec.
- Austin, L., Klimpel, R. and Luckie, P. (1984). Process engineering of size reduction. New York: Soc. of Mining Engineers, pp.62 - 189.
- Baker, F., (2014). *Scale-up and Operation of a Vertical Stirred Mill*. Master of Applied Science, University of British Columbia.
- Bailey, S., Hadler, K., Rescorl, T., Wilshaw, N., Lepoint, F., Clermont, B., (2016) The Effect of Media Loading Conditions on Vortex Stability and Grinding Performance in SMD Milling. In: *Comminution 2016 Conference*, Cape Town: MEI.
- Barley, R.W., Conway-Baker, J., Pascoe, R.D., Kostuch, J., McLoughlin, B., Parker, D.J., (2004). Measurement of the motion of grinding media in a vertically stirred mill using positron emission particle tracking (PEPT) Part II. *Minerals Engineering*, 17, pp. 1179 – 1187.
- Becker, M., Kwade, A., Schwedes, J., (2001). Stress intensity in stirred media mills and its effect on specific energy requirement. *Int. J. Miner. Process.*, 61, pp. 189 – 208.
- Bernhardt, C., Reinsch, E., Husemann, K., (1999). The influence of suspension properties on ultra-fine grinding in stirred ball mills. *Powder Technology*, 105, pp. 357 – 361.
- Birleanu, C., (2010). Aspects Concerning the Tribological Behaviour of Engineering Ceramics Type Alumina (Al_2O_3) in Dry Sliding Point, Line and Plane Contacts. In: *Proceedings of the 21st International DAAAM Symposium, Volume 21, No. 1*, Vienna: DAAAM International.
- Bond, F.C., (1961) *Crushing and Grinding Calculations*. Milwaukee: Allis-Chalmers Manufacturing Company.
- Breitung-Faes, S., Kwade, A., (2013). Prediction of energy effective grinding conditions. *Minerals Engineering*, 43 – 44, pp. 36 – 43.
- Breitung-Faes, S., Kwade, A., (2014). Use of an Enhanced Stress Model for the Optimization of Wet Stirred Media Milling Processes. *Chem. Eng. Technol.*, 37, No. 5, 819–826
- Breitung-Faes, S., (2017) Estimation of product relating energy of wet operated stirred media mills in terms of process transfer to other mill geometries and sizes. *Minerals Engineering*, 103–104, pp. 33–42.
- Burford, B.D., Clark, L.W., *IsaMill™ Technology Used in Efficient Grinding Circuits*. Available at https://www.isamill.com/en/downloads/TechnicalPapers/IsaMill_Technology_Used_in_Efficient_Grinding_Circuits.pdf [Accessed 20 Sept. 2019].
- Callow, M., Moon, A., (2002). Types and characteristics of Grinding Equipment and Circuit Flowsheets. In: A. Mular, D. Halbe, D. Barratt, ed., *Mineral Processing Plant Design, Practice, and Control Proceedings, Volume 1*. Colorado: Society for Mining, Metallurgy, and Exploration, Inc. (SME), pp. 698 – 709.

- Celep, O., Aslan, N., Alp, I., Taşdemir, G., (2011). Optimization of some parameters of stirred mill for ultra-fine grinding of refractory Au/Ag ores. *Powder Technology*, 208, pp. 121–127.
- Chagas, A.S., (2015) *Calibration of DEM contact parameters for tumbling mills using PEPT*. BEng Metallurgical, Federal University of Rio de Janeiro, Polytechnic School.
- Cho, H., Waters, M.A., Hogg, R., (1996). Investigation of the grind limit in stirred-media milling. *Int. J. Miner. Process.*, 44-45, pp. 607-615.
- Choi, H., Lee, W., Kim, S., (2009). Effect of grinding aids on the kinetics of fine grinding energy consumed of calcite powders by a stirred ball mill. *Advanced Powder Technology*, 20, pp. 350–354.
- Choi, H., Lee, W., Kim, D.U., Kumar, S., Kim, S.S., Chung, H.S., Kim, J.H., Ahn, Y.C., (2010). Effect of grinding aids on the grinding energy consumed during grinding of calcite in a stirred ball mill. *Minerals Engineering*, 23, pp. 54–57.
- Cleary, P.W., (1998). Predicting Charge Motion, Power Draw, Segregation and Wear in Ball Mills Using Discrete Element Methods. *Minerals Engineering*, Vol.11, No. 11, pp. 1061-1080.
- Conway-Baker, J., Barley, R.W., Williams, R.A., Jia, X., Kostuch, J., McLoughlin, B., Parker, D.J., (2002). Measurement of the Motion of Grinding Media in a Vertically Stirred Mill using Positron Emission Particle Tracking (PEPT). *Minerals Engineering*, 15, pp. 53–59.
- Cummins, S.J., Thornton, C., Cleary, P.W., (2012). Contact Force Models in Inelastic Collisions. In: *Ninth International Conference on CFD in the Minerals and Process Industries*, Melbourne: CSIRO.
- Davey, G., (2004). Fine copper grinding using Metso's Stirred Media Detritor, Mining Engineering. *SciTech Premium Collection*, vol. 56, no. 4, pp. 33 – 35.
- Davis, S.B., Dawson, M.F., (1989). A Laboratory Study of Attrition Grinding. *J. S. Afr. Inst. Min. Metall.*, vol. 89, no. 8, pp. 231-241.
- De Bakker, J., (2014). Energy Use of Fine Grinding in Mineral Processing. *Metallurgical and Materials Transactions E*, Volume 1E, pp. 8 – 19.
- De Waal, H., Barns, K., Monama J., (2013). From base metals and back – IsaMills and their advantages in African base metal operations. In: *Base Metals Conference 2013*, Johannesburg: The Southern African Institute of Mining and Metallurgy.
- Dragomir, S., Sinnott, M., Semercigil, E., Turan, O., (2009). Predicting Energy Dissipation Characteristics of a Tumbling Granular-flow Damper using DEM. In: *Seventh International Conference on CFD in the Minerals and Process Industries*, Melbourne: CSIRO.
- Edwards, G.C., (2016). *Investigation of operating parameters in a vertical stirred mill*. Master of Science in Chemical Engineering, University of Cape Town.
- Eswaraiah, C., Venkat, N. Mishra, B.K., Holmes, R., (2015). A Comparative Study on a Vertical Stirred Mill Agitator Design for Fine Grinding. *Separation Science and Technology*, Vol 50, pp. 2639–2648.
- First Quantum Minerals Ltd., (2016). *Kevitsa Nickel Copper Mine, NI 43-101 Technical Report*.
- FLSmidth, (2011), *FLSmidth® VXPmill*. FLSmidth.

- Fragniere, G., Beinert, S., Overbeck, A., Kampen, I., Schilde, C., Kwade, A., (2018). Predicting effects of operating condition variations on breakage rates in stirred media mills. *Chemical Engineering Research and Design*, 138, pp. 433–443.
- Gao, M., Forssberg, K.S.E., Weller, K.R., (1996). Power predictions for a pilot stirred ball mill. *International Journal of Mineral Processing*, 44–45, pp. 641–652.
- Glencore Technology, (2015). *IsaMill™ Breaking the Boundaries, High Intensity, energy efficient grinding providing versatile solutions to the minerals industry*, Brisbane: Glencore.
- Govender, N., Rajamani, R.K., Kok, S., Wilke, D.N., (2015). Discrete element simulation of mill charge in 3D using the BLAZE-DEM GPU framework. *Minerals Engineering*, 79, pp. 152–168.
- Gupta, A., Yan, D. 2016: *Mineral Processing Design and Operations*. Second Edition, Amsterdam, Elsevier, pp. 287 – 316.
- Hasan, M., (2016). *Process Modelling of Gravity Induced Stirred Mills*. PhD, University of Queensland.
- Hasan, M., Palaniandy, S., Hilden, M., Powell, M., (2016). Investigating internal classification within gravity induced stirred mills. *Minerals Engineering*, 95, pp. 5–13.
- Hasan, M., Palaniandy, S., Hilden, M., Powell, M., (2017). Calculating breakage parameters of a batch vertical stirred mill. *Minerals Engineering*, 111, pp. 229–237.
- He, M., Forssberg, E., (2007). Influence of slurry rheology on stirred media milling of quartzite. *Int. J. Miner. Process.*, 84, pp. 240–251.
- Herbst, J.A., Fuerstenau, D.W., (1973). Mathematical Simulation of Dry Ball Milling Using Specific Power Information. *Society of Mining Engineers, AIME, Transactions*, Vol. 254, pp. 343 – 348.
- Hogg, R., Cho, H., (2000). A Review of Breakage Behaviour in Fine Grinding by Stirred-Media Milling. *KONA*, no.18, pp. 9 – 19.
- Hukki, R.T., (1962). Proposal for a solomonic settlement between the theories of von Rittinger, Kick and Bond. *Trans. AIME*, 223, pp. 403–408.
- Jankovic, A., (2003). Variables affecting the fine grinding of minerals using stirred mills. *Minerals Engineering*, 16, pp. 337–345.
- Jayasundara, C.T., Yang, R.Y., Yu, A.B., (2012). Effect of the size of media on grinding performance in stirred mills. *Minerals Engineering*, 33, pp. 66–71.
- Keikkala, V., Lehto, H., Roitto, I., (2015). Recent progress of regrinding circuits with Outotec HIGmills. *CUPRUM – Czasopismo Naukowo-Techniczne Górnictwa Rud*, 2 (75), p. 37-45.
- Kim, S., Choi, W.S., (2008). Analysis of Ball Movement for Research of Grinding Mechanism of a Stirred Ball Mill with 3D Discrete Element Method. *Korean J. Chem. Eng.*, 25(3), pp. 585-592.
- Kwade, A., (1999). Wet comminution in stirred media mills — research and its practical application. *Powder Technology*, 105, pp. 14 - 20.

- Kwade, A., Blecher, L., Schwedes, J., (1996). Motion and stress intensity of grinding beads in a stirred media mill. Part 2: Stress intensity and its effect on comminution. *Powder Technology*, 86, pp. 69-76.
- Kwade, A., Schwedes, J., (1997). Wet Comminution in stirred media mills. *KONA*, no.15, pp. 91 – 102.
- Kwade, A., Schwedes, J., (2002). Breaking characteristics of different materials and their effect on stress intensity and stress number in stirred media mills. *Powder Technology*, 122, pp. 109–121.
- Kwade, A., (2003). A Stressing Model for the Description and Optimization of Grinding Processes. *Chem Eng. Technol.*, vol. 26, no. 2, pp. 199 – 205.
- Lehto, H., Paz, A., Roitto, I., Åsthalm, M. (2013). Outotec HIGmills; A Fine Grinding Technology. In: *23rd International Mining Congress & Exhibition of Turkey*, Antalya: Chamber of Mining Engineers of Turkey, pp. 245 – 250.
- Lichter, J.K.H., Davey, G., (2006). Selection and Sizing of Ultrafine and Stirred Grinding Mills. In: S., Kawatra, *Advances in Comminution*. Colorado: Society for Mining, Metallurgy, and Exploration, Inc, pp. 69 – 86.
- Lisso, M., (2013). *Evaluating the Effect of Operating Variables on Energy Consumption in Stirred Mills*. Master of Science in Chemical Engineering, University of Cape Town.
- Liu, Y., Yu, Z., Zhou, S., Wu, L., (2006). De-agglomeration and Dispersion of Nano-TiO₂ in an Agitator Bead Mill. *Journal of Dispersion Science and Technology*, 27, pp. 983–990.
- Mankosa, M.J., Adel, G.T., Yoon, R.H., (1986). Effect of Media Size in Stirred Ball Mill Grinding of Coal. *Powder Technology*, 49, pp. 75 – 82.
- Martins, S., Radziszewski, P., (2015). Generalizing a shear–volume power model for stirred mill power prediction. *Minerals Engineering*, 77, pp. 150 – 158.
- Metso, (2011), *Stirred Milling Vertimill® Grinding Mills & Stirred Media Detritor*, Brochure No. 2357-10-11. Metso.
- Metso, (2012). *Energy Efficient Comminution Circuits*, Brochure No. 2791-09-12. Canonsburg: Metso.
- Metso, (2018). *Basics in Mineral Processing, Edition 11*. Metso.
- Mishra, B.K., Murty, C.V.R., (2001). On the determination of contact parameters for realistic DEM simulations of ball mills. *Powder Technology*, 115, pp. 290–297.
- Mishra, B.K., Rajamani, R.K., (1992). The discrete element method for the simulation of ball mills. *Appl. Math. Modelling*, Vol. 16, pp. 598 – 604.
- Moore, A., Gallimore, M., Knorr, B., Radziszewski, P., (2016). Pursuit of Best Practices with the Stirred Media Detritor. In: *Comminution 2016 Conference*, Cape Town: MEI.
- Morrell, S., (2004). An alternative energy–size relationship to that proposed by Bond for the design and optimisation of grinding circuits. *Int. J. Miner. Process.*, 74, pp. 133– 141.
- Morrell, S., (2004). Predicting the specific energy of autogenous and semi-autogenous mills from small diameter drill core samples. *Minerals Engineering*, 17, pp. 447–451.

- Morrell, S., (2008). A method for predicting the specific energy requirement of comminution circuits and assessing their energy utilisation efficiency. *Minerals Engineering*, 21, pp. 224–233.
- Morrell, S., (2009). Predicting the overall specific energy requirement of crushing, high pressure grinding roll and tumbling mill circuits. *Minerals Engineering*, 22, pp. 544–549.
- Morrell, S., (2010). Predicting the specific energy required for size reduction of relatively coarse feeds in conventional crushers and high pressure grinding rolls. *Minerals Engineering*, 23, pp. 151–153.
- Mucsi, G., (2013). Grindability of Quartz in Stirred Media Mill. *Particulate Science and Technology*, 31, pp. 399–406.
- Napier-Munn, T., (2015). Is progress in energy-efficient comminution doomed? *Minerals Engineering*, 73, pp. 1–6.
- Norejko, T., van der Wielen, K., Hadler, K., Wilshaw, N., (2018). Linking Stirred Media Detritor Vortex Stability to Operational Variables. In: *Comminution 2018 Conference*, Cape Town: MEI.
- Ntsele, C., Allen, J., (2012) Technology Selection of Stirred Mills for Energy Efficiency in Primary and Regrinding Applications for the Platinum Industry. In: *Platinum 2012*, Johannesburg: The Southern African Institute of Mining and Metallurgy.
- Ohenoja, K., Illikainen, M., Niinimäki, J., (2013). Effect of operational parameters and stress energies on the particle size distribution of TiO₂ pigment in stirred media milling. *Powder Technology*, 234, pp. 91–96.
- Ouattara, S., Frances, C., (2014). Grinding of calcite suspensions in a stirred media mill: Effect of operational parameters on the product quality and the specific energy. *Powder Technology*, 255, pp. 89–97.
- Outokumpu, *The Science of Comminution*. Outokumpu Técnica Perú SAC.
- Ohenoja, K., Illikainen, M., (2015). Effect of operational parameters and stress energies on stirred media milling of talc. *Powder Technology*, 283, pp. 254–259.
- Pasaribu, H.R., Reuver, K.M., Schipper, D.J., Ran, S., Wiratha, K.W., Winnubst, A.J.A, Blank, D.H.A., (2005). Environmental effect on friction and wear of dry sliding zirconia and alumina ceramics doped with copper oxide. *International Journal of Refractory Metals & Hard Materials*, 23, pp. 386 – 390.
- Patel, C.M., Murthy, Z.V.P., Chakraborty, M., (2012). Effects of operating parameters on the production of barium sulfate nanoparticles in stirred media mill. *Journal of Industrial and Engineering Chemistry*, 18, pp. 1450–1457.
- Patel, C.M., Chakraborty, M., Murthy, Z.V.P., (2014). Enhancement of stirred media mill performance by a new mixed media grinding strategy. *Journal of Industrial and Engineering Chemistry*, 20, pp. 2111–2118.
- Pease, J.D., Young, M.F., Curry, D.C., *Fine Grinding as Enabling Technology – The IsaMill*. Available at https://www.isamill.com/en/downloads/TechnicalPapers/FineGrindingasEnablingTechnology_TheIsaMill.pdf [Accessed 5 Sept. 2019]].
- Pradeep, P.R., Pitchumani, B., (2011). Effect of operating variables on the production of nanoparticles by stirred media milling. *Asia-Pac. J. Chem. Eng.*, 6, pp. 154–162.
- Radziszewski, P., (2013). Assessing the stirred mill design space. *Minerals Engineering*, 41, pp. 9–16.

- Rahal, D., Erasmus, D., Major, K. (2011). Knelson-Deswik Milling Technology: Bridging the Gap Between Low and High Speed Stirred Mills. In: *Proceedings of the 43rd Annual Canadian Mineral Processors Conference*, Ottawa: CIM, pp. 557 – 587.
- Reddick, S., Rahal, D., Hines, B., Shah, I., (2014). VXP2500 Stirred Mill Optimization at Casmyn Mining Turk Mine. In: *46th Annual Canadian Mineral Processors Operators Conference*, Ottawa: CIM.
- Richardson, J.F., Harker, J.H., and Backhurst, J.R. (2002): *Coulson and Richardson's Chemical Engineering, Volume 2, Particle Technology and Separation Processes*. Fifth Edition, Oxford: Butterworth-Heinemann, pp. 192 – 194.
- Rowland, C., (2006) Bond's Method for Selection of Ball Mills. In: S., Kawatra, *Advances in Comminution*. Colorado: Society for Mining, Metallurgy, and Exploration, Inc, pp. 385 – 398.
- Rule, C., (2010). Stirred milling—new comminution technology in the PGM industry. In: *The 4th International Platinum Conference*, Johannesburg: The Southern African Institute of Mining and Metallurgy.
- Samayamutthirian, P., Powell, M., Hilden, M., Allen, J., Kermanshahi, K., Oats, B., Lollback, M., (2015). VertiMill – Preparing the feed within floatable regime at lower specific energy. *Minerals Engineering*, 73, pp. 44–52.
- Snow, R.H., Allen, T., Ennis, B.J., Litster, J.D., (1997). Size Reduction and Size Enlargement. In: Perry, R.H., Green, D.W., *Perry's Chemical Engineers' Handbook*, Seventh Edition, Singapore: Mc Graw Hill, pp. 19-1 – 19-65.
- Sorace, C.M., Louge, M.Y., Crozier, M.D., Law, V.H.C., (2009). High apparent adhesion energy in the breakdown of normal restitution for binary impacts of small spheres at low speed. *Mechanics Research Communications*, 36, pp. 364–368.
- Stender, H., Kwade, A., Schwedes, J., (2004). Stress energy distribution in different stirred media mill geometries. *Int. J. Miner. Process.* 74S, pp. S103–S117.
- Stieper, G., (2018). First Chalcopyrite Copper Concentrate Leaching using Albion Process™ Technology. *10th International Seminar on Process Hydrometallurgy*, Santiago: Gecamin.
- Strobel, A., Schwenger, J., Wiipahl, S., Schmidt, J., Romeis, S., Peukert, W., (2018). Assessing the influence of viscosity and milling bead size on the stressing conditions in a stirred media mill by single particle probes. *Chemical Engineering Research and Design*, 136, pp. 859–869.
- Tamblyn, R.J., (2009). *Analysis of Energy Requirements in Stirred Media Mills*. Doctor of Engineering in Chemical Engineering, University of Birmingham.
- Tavares, L.M., (2017), A Review of Advanced Ball Mill Modelling. *KONA Powder and Particle Journal*, No. 34, pp. 106 – 124.
- Toraman, O.Y., Katircioglu, D., (2011). A study on the effect of process parameters in stirred ball mill. *Advanced Powder Technology*, 22, pp. 26–30.
- Tüzün, M.A., (1993). *A Study of Comminution in a Vertical Stirred Ball Mill*. Doctor of Philosophy in Chemical Engineering, University of Natal.
- Wang, C., (2013) *Comparison of HPGR-Ball Mill and HPGR-Stirred Mill Circuits to the Existing AG/SAG Mill – Ball Mill Circuits*. Master of Applied Science in Mining Engineering, University of British Columbia.

- Wang, Y., Forssberg, E., (2000). Technical Note Product Size Distributions in Stirred Media Mills. *Minerals Engineering*, Vol. 13, No. 4, pp. 459 - 465.
- Weerasekara, N.S., Powell, M.S., Cleary, P.W., Tavares, L.M., Evertsson, M., Morrison, R.D., Quist, J., Carvalho, R.M. (2013). The contribution of DEM to the science of comminution. *Powder Technology*, 248, pp. 3 –24.
- Wills, B.A. and Finch, J.A. 2016: *Will's Mineral Processing Technology, An Introduction to the Practical Aspects of Ore Treatment and Mineral Recovery*. Eight Edition, Oxford, Butterworth-Heinemann, pp. 102-103.
- Xstrata Technology (2019) *Stirred Milling Technology*, Available at www.isamill.com [accessed January 2019].
- Yang, Y., Rowson, N.A., Tamblyn, R., Ingram, A., (2017). Effect of Operating Parameters on Fine Particle Grinding in a Vertically Stirred Media Mill. *Separation Science and Technology*, Vol 52. No.6, pp. 1143 – 1152.
- Yue, J., Klein, B., (2006). Effects of Bead Size on Ultrafine Grinding in a Stirred Bead Mill. In: S., Kawatra, *Advances in Comminution*. Colorado: Society for Mining, Metallurgy, and Exploration, Inc, pp. 87 – 98.
- Zheng, J., Harris, C., Somasundaran, P., (1996). A study on grinding and energy input in stirred media mills. *Powder Technology*, 86, pp. 171-178.
- Zheng, J., Harris, C., Somasundaran, P., (1997). The effect of additives on stirred media milling of limestone. *Powder Technology*, 91, pp. 173-179.

7 Appendix

7.1 Stirrer and Mill Vessel Designs

For this project two new stirrers and one new mill vessel were designed and fabricated for use in the experiments. This section provides detail on the design and dimensions of the new equipment and the existing pin stirrer.

7.1.1 New Mill Vessel with Disc Liner

The mill vessel was constructed in two half pieces that are bolted together with flanges. A two part construction was required since the inside of the mill vessel is fitted with one annular disc (ring). If the mill was constructed from a single assembly it would not be possible to place the stirrers in the mill vessel due to this ring. Both halves of the mill has an identical design except for one that is fitted with a spout at the top of the vessel. The spout is used for directing the discharge of mill contents when the mill is tipped over for emptying. When in operation the top of the mill is covered with a loose two-piece lid. The diameter increases at the top of the mill vessel to provide a ledge for supporting the mill lid. The lid was already available and did not need to be fabricated.

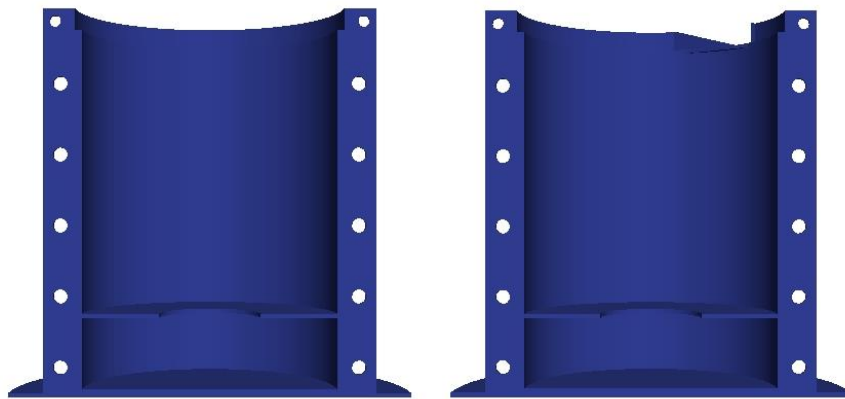


Figure 91: The two disc mill vessel half pieces - 3D drawing

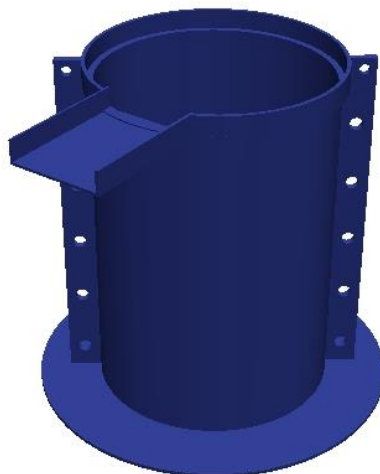


Figure 92: Assembled disc mill vessel – 3D drawing

Mill Vessel Design Detail - Cross section slice (slice view cut through at flange)

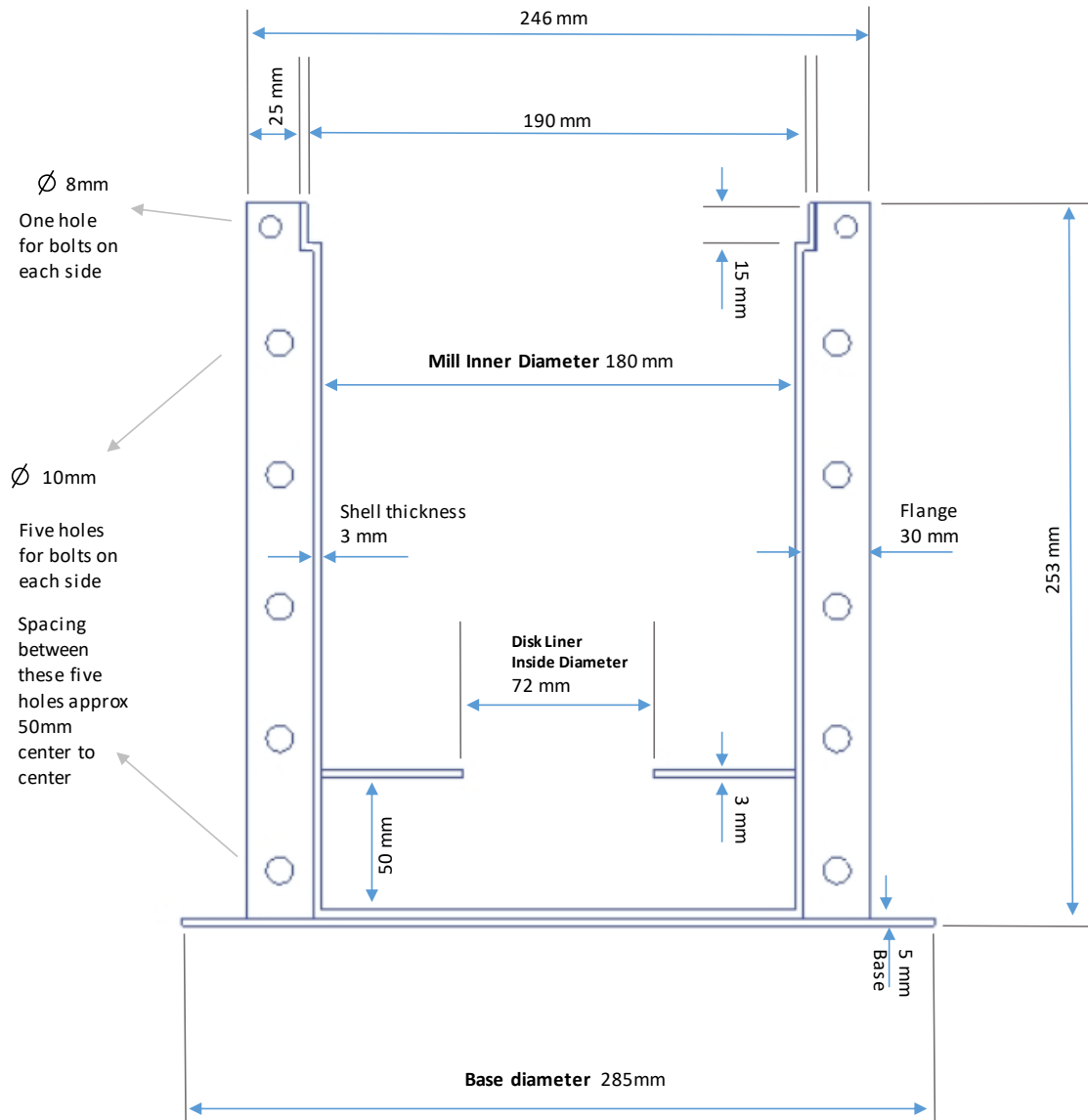


Figure 93: Cross section drawing of disc mill vessel showing dimensions

Mill Vessel Top View showing spout detail and position relative to mill flanges

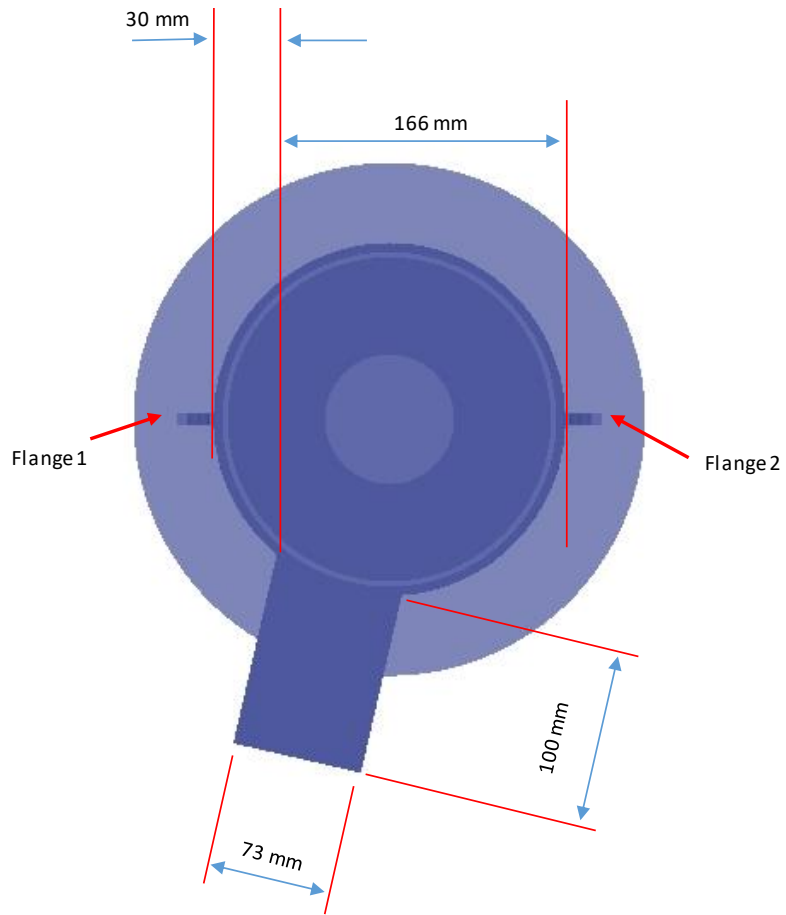


Figure 94: Top view of disc mill vessel showing spout arrangement details

7.1.2 New ring and pin stirrer design details

New ring and pin stirrers were designed for use in the experimental work. The ring stirrer consisted of a shaft fitted with two sets of ring stirrer discs, Figure 95. The pin stirrer consisted of a shaft fitted with two sets of 6 pins, for a total of 12 pins, Figure 96.

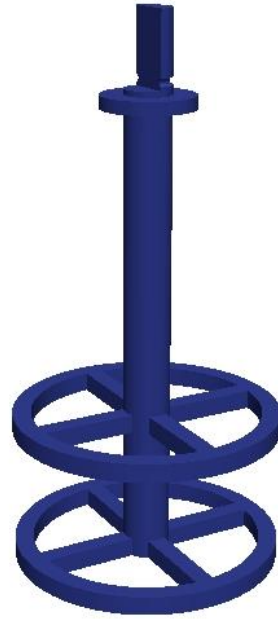


Figure 95: Ring stirrer – 3D drawing

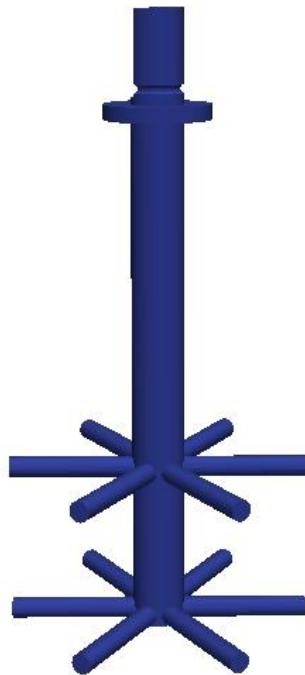


Figure 96: 12-pin stirrer – 3D drawing

Ring Stirrer Design Detail - Top View

This shows detail of one ring

The stirrer will have two of these rings on the shaft

Ring height: 10mm

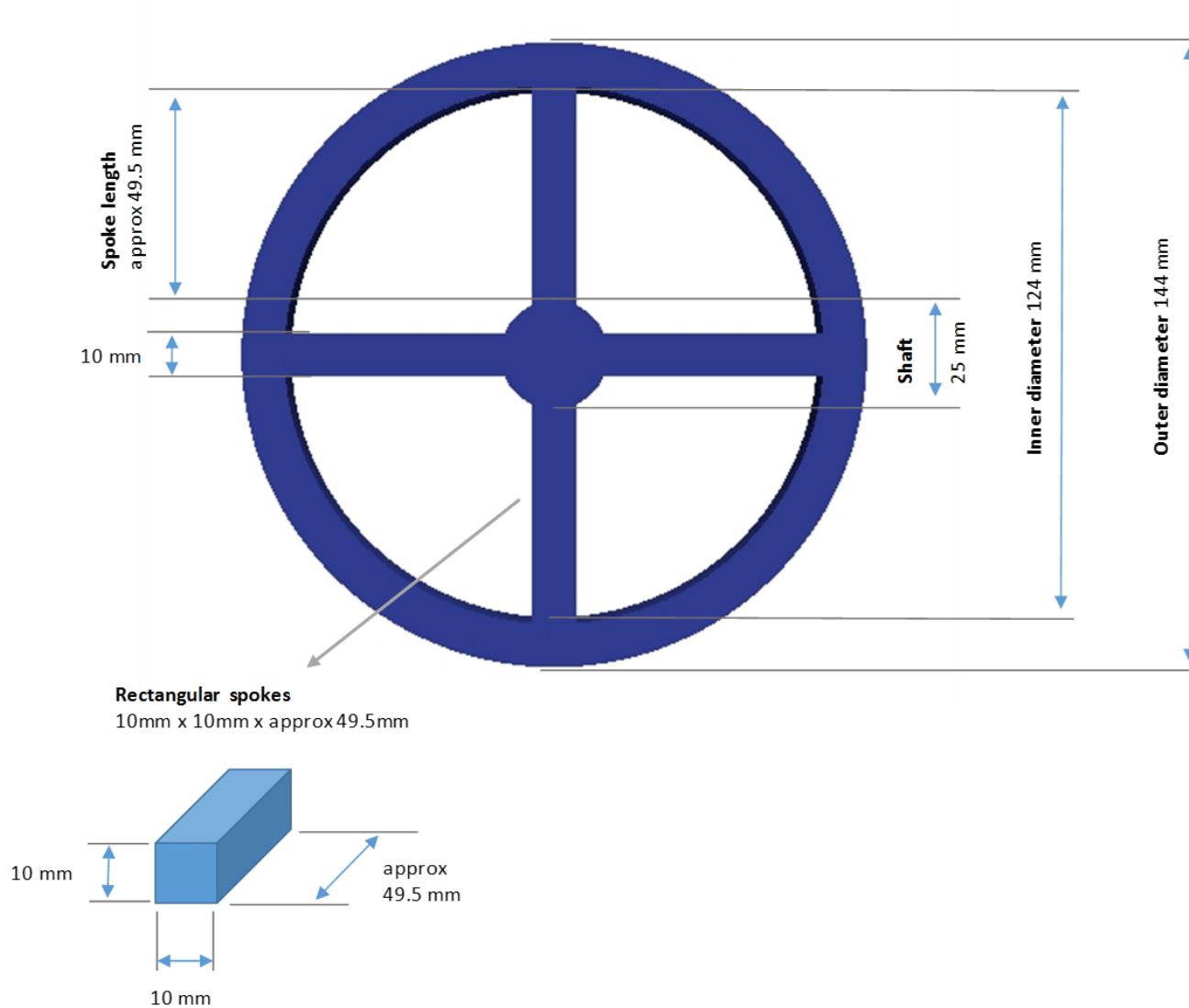


Figure 97: Ring stirrer arrangement drawing

Ring Stirrer Design Detail - Cross section slice (at center)

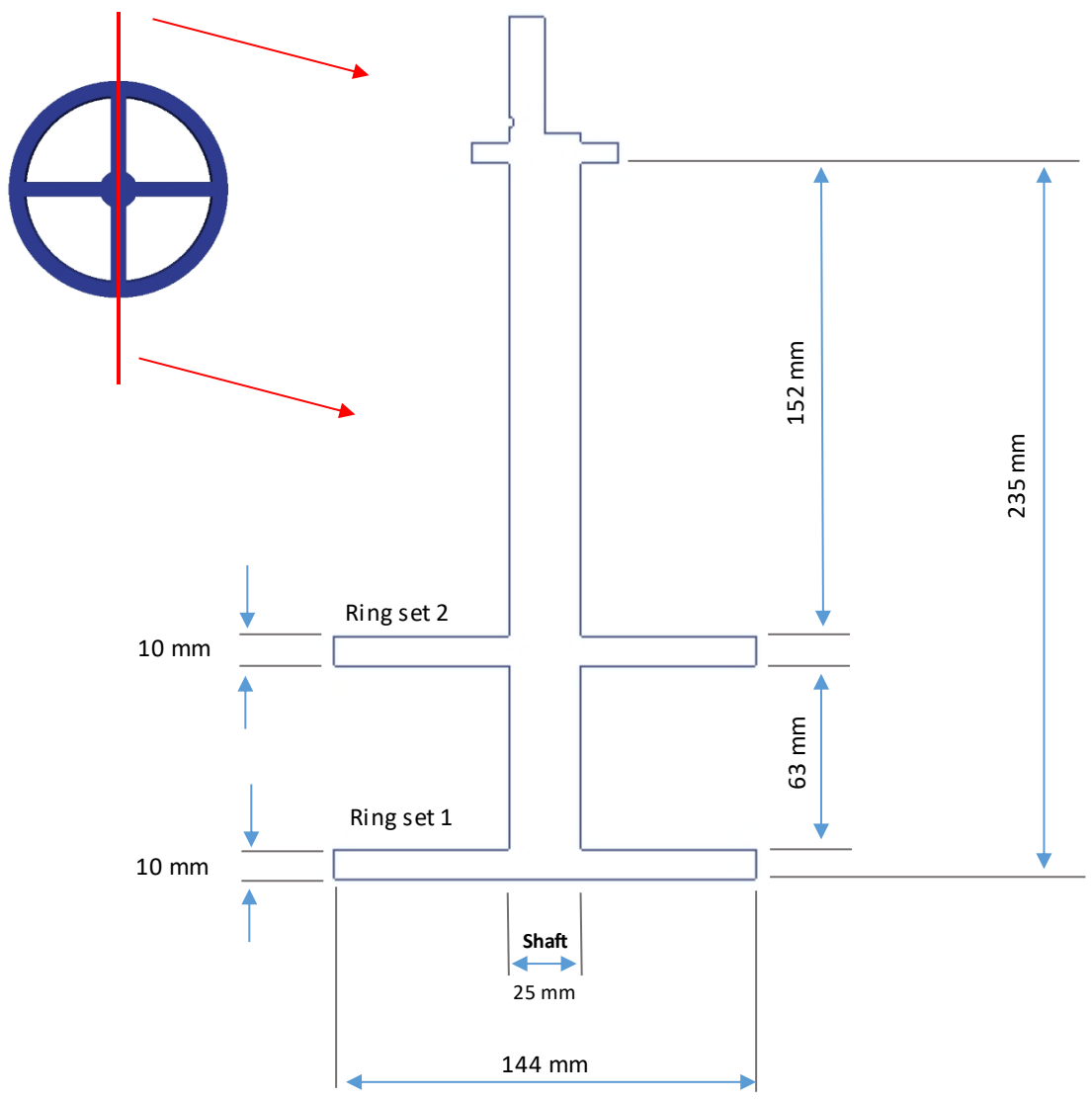


Figure 98: Ring stirrer cross section drawing

Pin Stirrer Design Detail - Top View

This shows detail of one set of pins

The stirrer will have two sets of these pins on the shaft

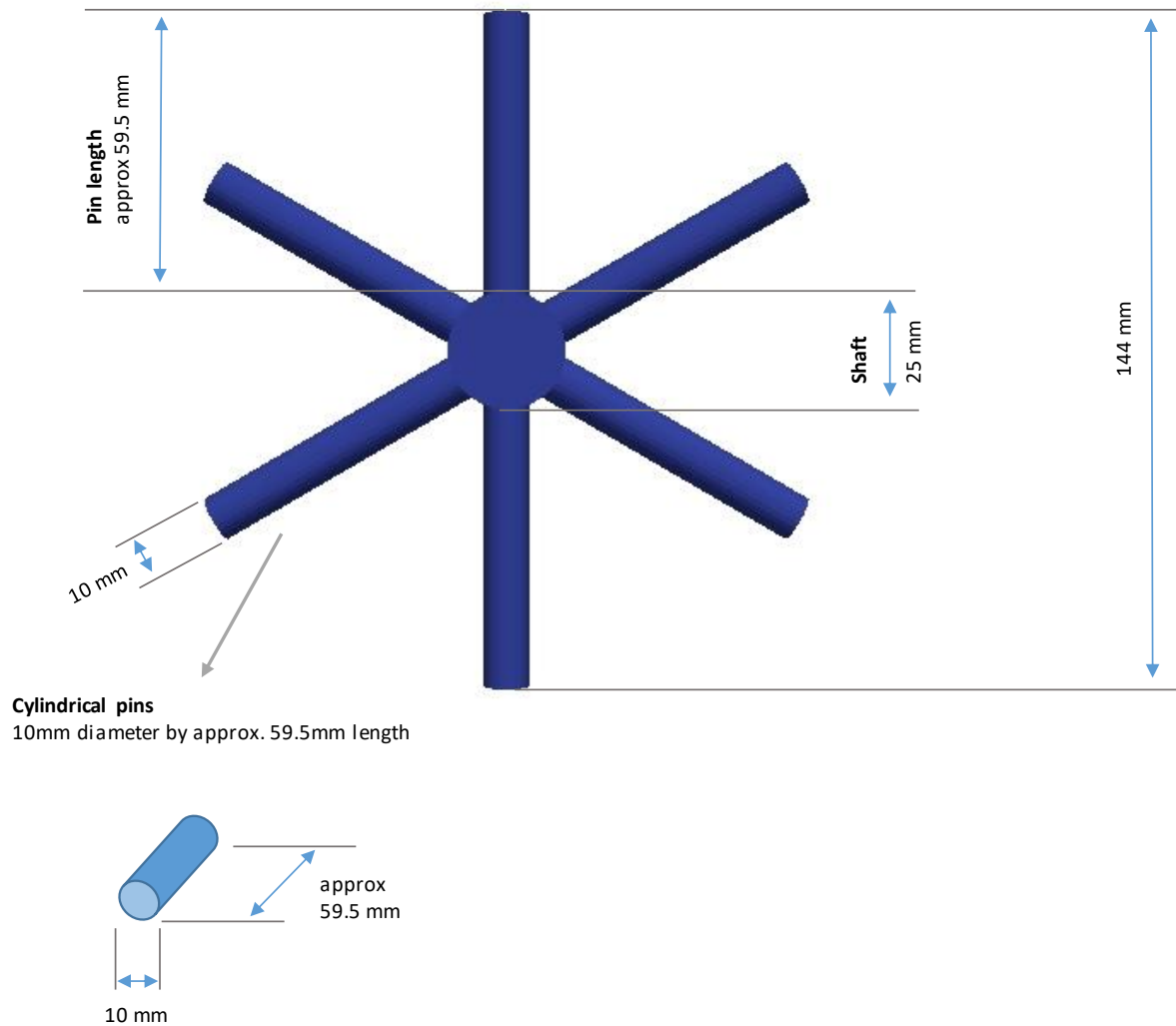


Figure 99: 12 pin stirrer arrangement drawing

Pin Stirrer Design Detail - Cross section slice (at center)

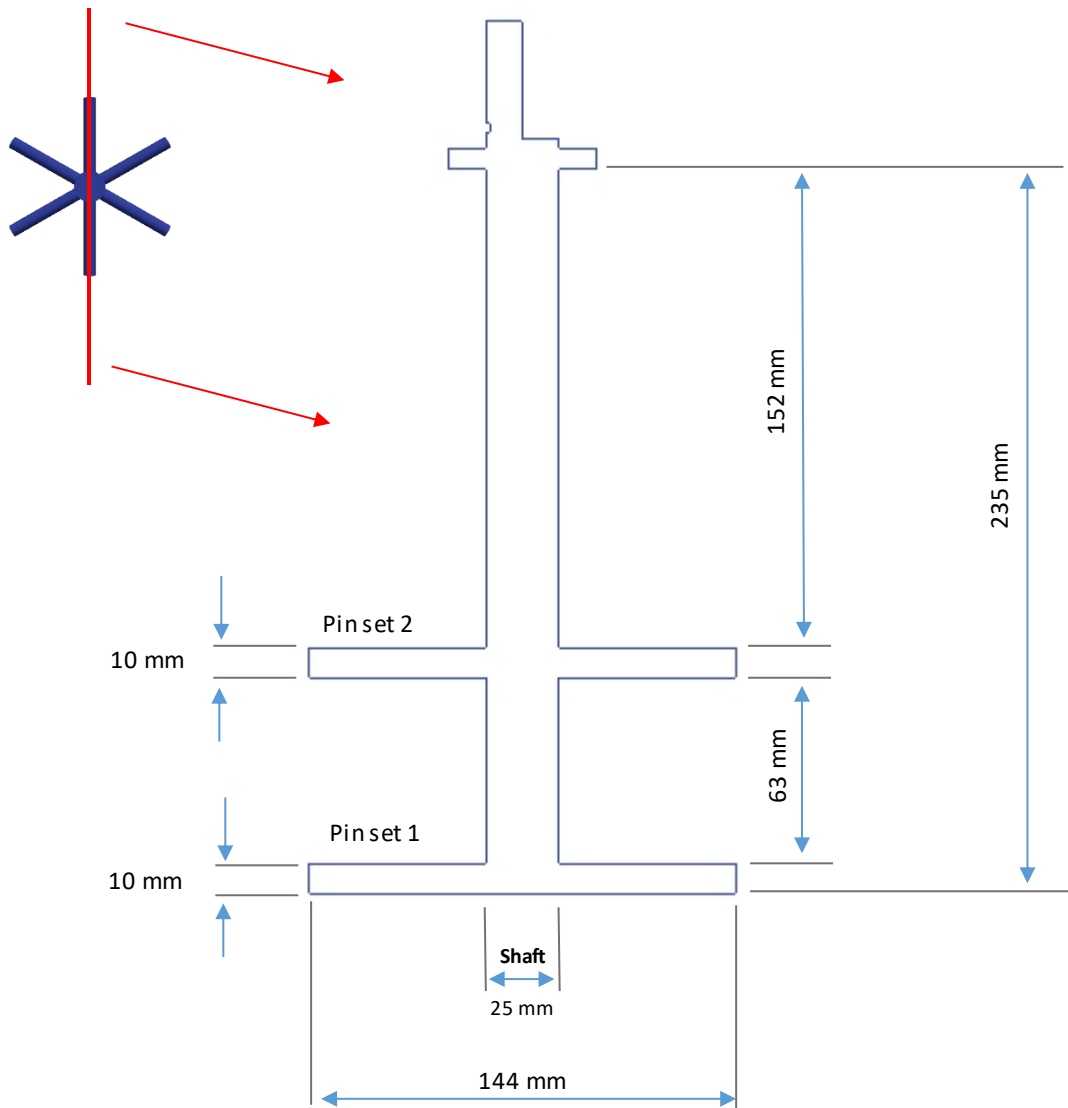


Figure 100: 12 pin stirrer cross section drawing

7.1.3 Existing Stirrer Design Details

An existing mill stirrer was used to generate torque data for DEM calibration purposes during the virtual prototyping process. A 3D drawing of the stirrer geometry is shown in Figure 101. The stirrer is comprised of four sets of pins. Each set of pins consists of two pins located 180° apart. More detail on the stirrer arrangement and dimensions are presented in Figure 102 to Figure 104.

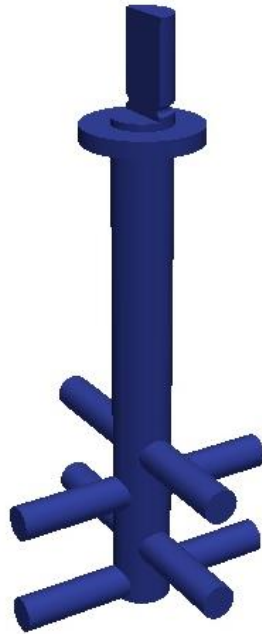


Figure 101: Existing stirrer – 3D drawing

Existing Pin Stirrer Detail - Top View

Note that the pins are located on different heights along the length of the shaft

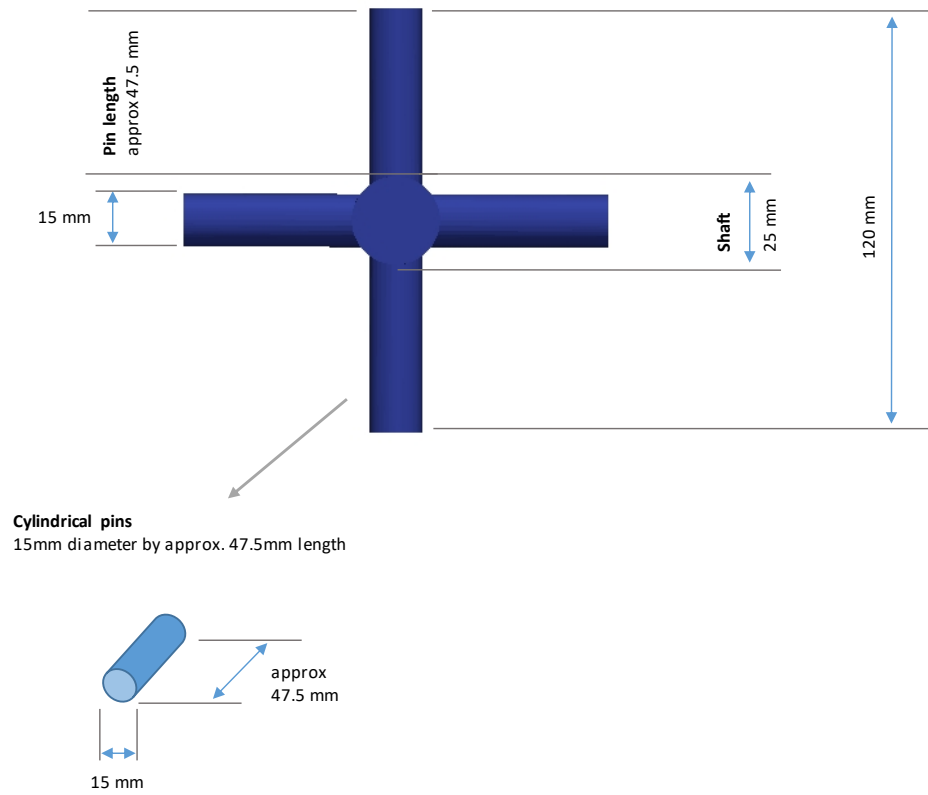


Figure 102: Existing stirrer pin detail top view

VIEW 1 - Existing Pin Stirrer Detail - Cross section slice (at center)

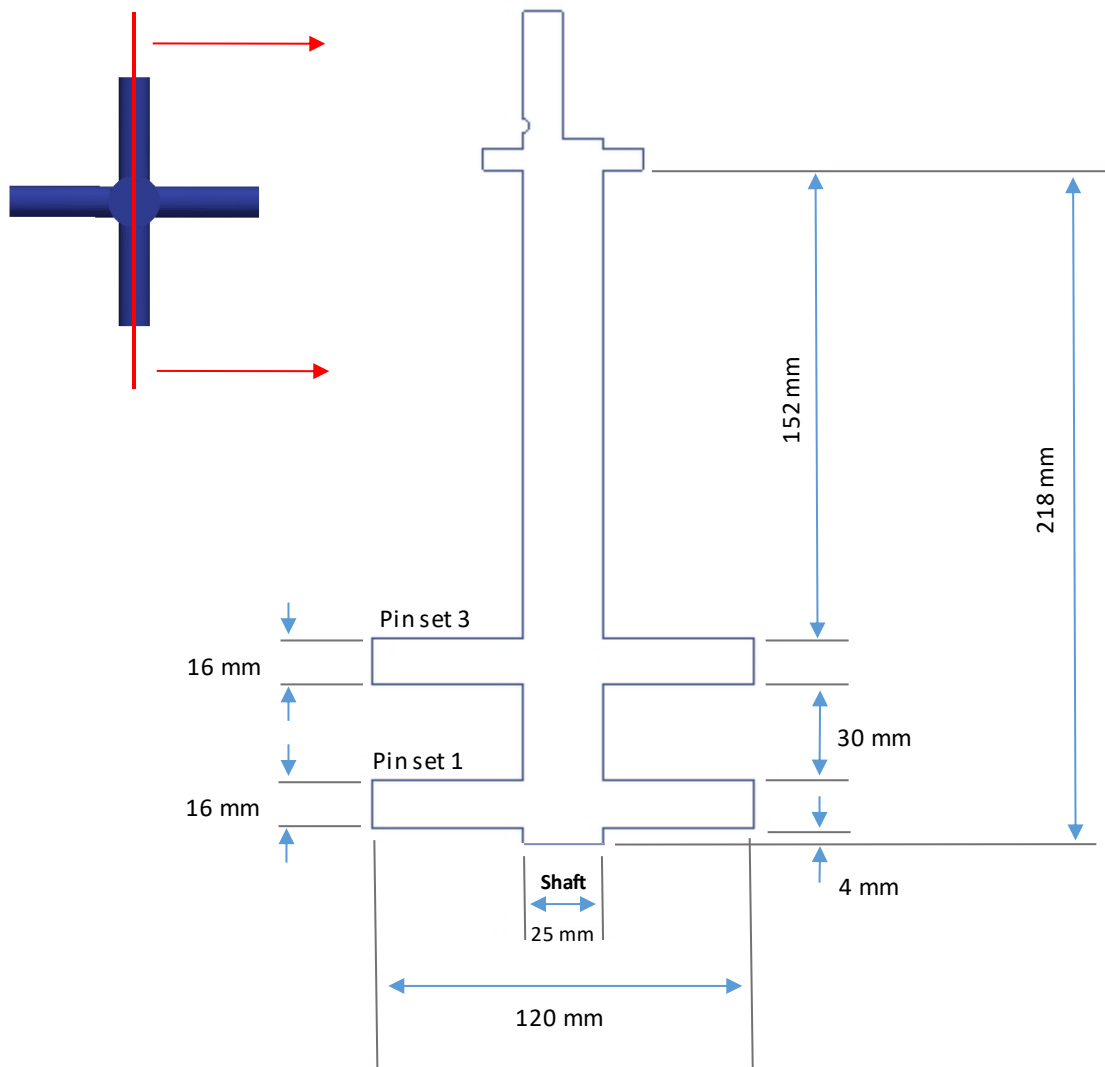


Figure 103: Existing stirrer cross section drawing – view 1

VIEW 2 - Existing Pin Stirrer Detail - Cross section slice (at center)

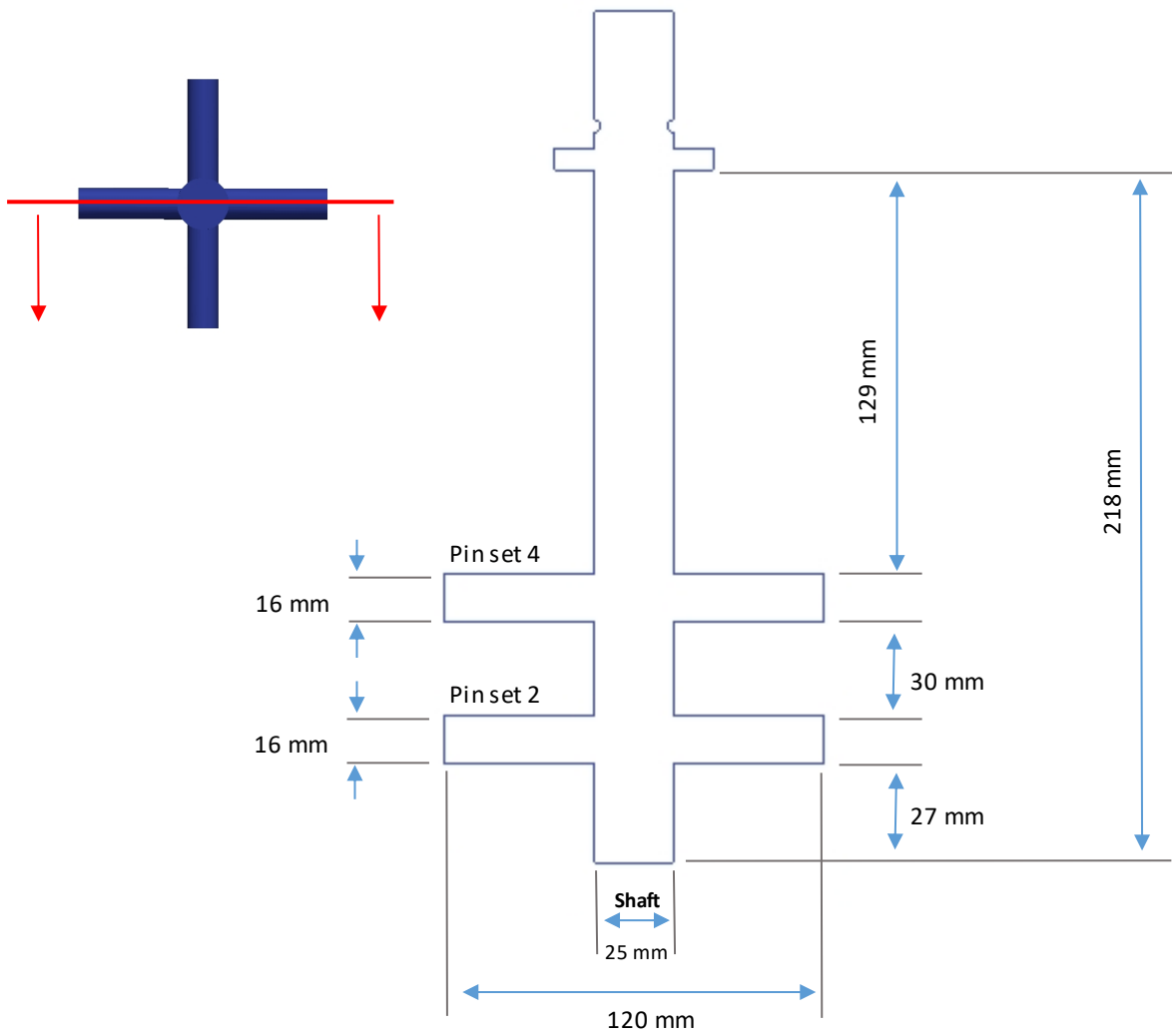
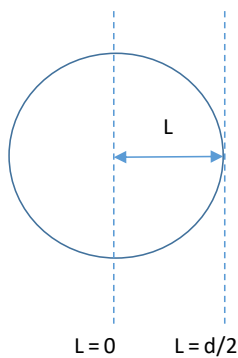


Figure 104: Existing stirrer cross section drawing – view 2

7.2 Shear Volume Formulas Derivation

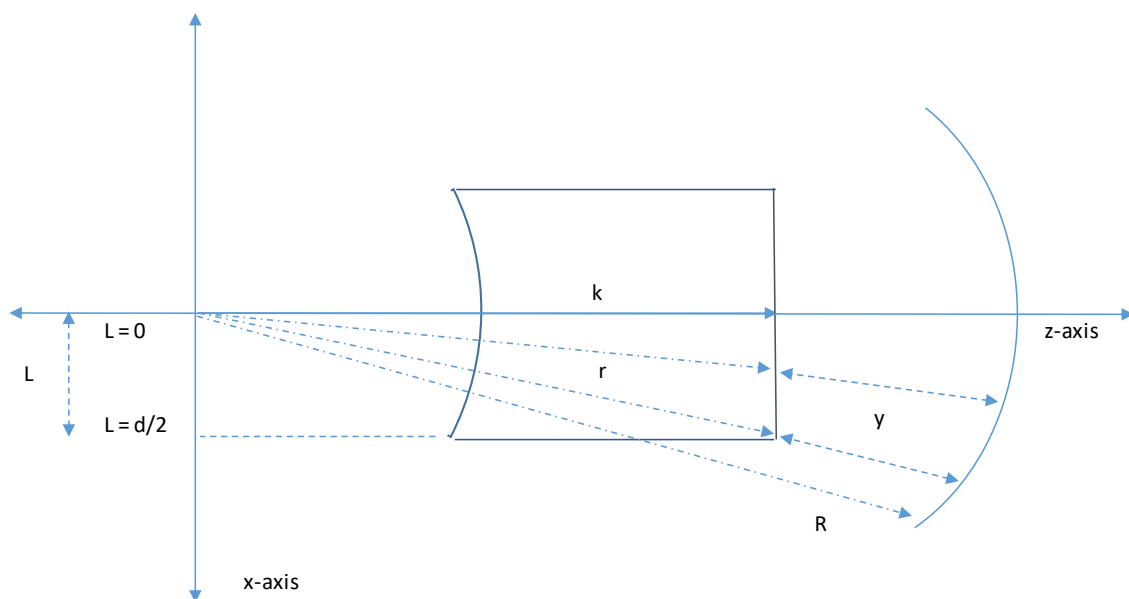
7.2.1 Shear Volume Formula Derivation for the Pin Tip



Integrate over 1/2 of pin

d = pin diameter
 L = distance from pin center
 k = distance from shaft center to pin tip center
 c = chord length
 R = radius mill vessel

$r = f(L)$
 $y = f(L)$
 $A = f(L)$



$$r = f(L)$$

$$r^2 = k^2 + L^2$$

$$r = \sqrt{k^2 + L^2}$$

$$A = f(L)$$

$$\text{chord length } c = f(L)$$

$$c = 2\sqrt{\left(\frac{d}{2}\right)^2 - L^2}$$

$$y = f(L)$$

$$y = R - r$$

$$y = R - \sqrt{k^2 + L^2}$$

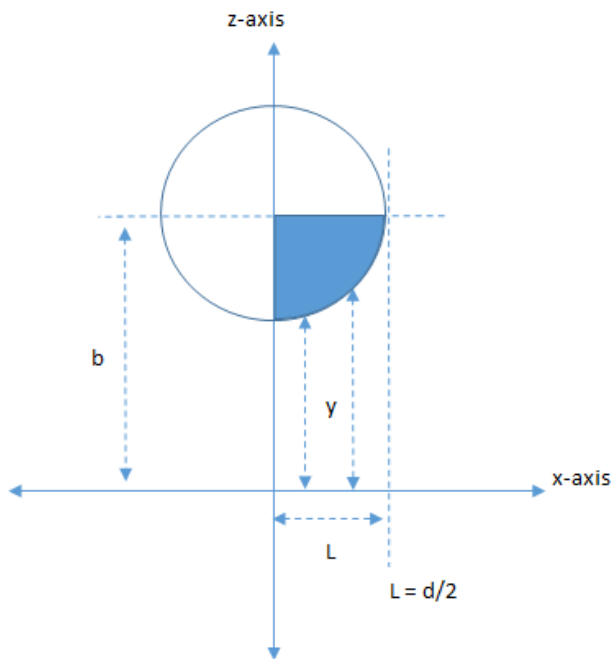
$$V_{\tau} = \frac{Ar^2}{y}$$

$$V_t = 2 \int_{L=0}^{L=\frac{d}{2}} \frac{2\sqrt{\left(\frac{d}{2}\right)^2 - L^2} * (k^2 + L^2)}{R - \sqrt{k^2 + L^2}} dL$$

$$V_t = 4 \int_{L=0}^{L=\frac{d}{2}} \frac{\sqrt{\left(\frac{d}{2}\right)^2 - L^2} * (k^2 + L^2)}{R - \sqrt{k^2 + L^2}} dL$$

Use numerical integration to solve V_t
 $d = \text{constant}$
 $R = \text{constant}$
 $k = \text{constant}$

7.2.2 Shear Volume Formula Derivation for the Pin Bottom Half



Integrate over 1/2 of pin bottom surface

$d = \text{pin diameter}$

$L = \text{distance from pin center}$

$b = \text{coordinate of pin center on z-axis}$

$y = f(L)$

Formula of circle

$$(x - a)^2 + (z - b)^2 = R^2$$

$$R = \frac{d}{2}$$

$(a,b) = \text{coordinates of center point}$

$a = 0$

b is defined by the position of the pin centre on the z-axis

$x = L$

$$L^2 + (z - b)^2 = \left(\frac{d}{2}\right)^2$$

$$z^2 - 2bz + L^2 + b^2 - \left(\frac{d}{2}\right)^2 = 0$$

Applying the quadratic formula:

$$z = \frac{-(-2b) \pm \sqrt{(-2b)^2 - 4(1) \left[L^2 + b^2 - \left(\frac{d}{2}\right)^2 \right]}}{2(1)}$$

Using only the form with the minus (-) and simplifying gives

$$z = b - \sqrt{\left(\frac{d}{2}\right)^2 - L^2}$$

$$y = z$$

$$y = b - \sqrt{\left(\frac{d}{2}\right)^2 - L^2}$$

Derivation of shear volume

$$V_{\tau} = \frac{Ar^2}{y}$$

$$V_{\tau} = 2 \int_{r_1}^{r_2} \int_{L_1}^{L_2} \frac{r^2}{b - \sqrt{\left(\frac{d}{2}\right)^2 - L^2}} dL dr$$

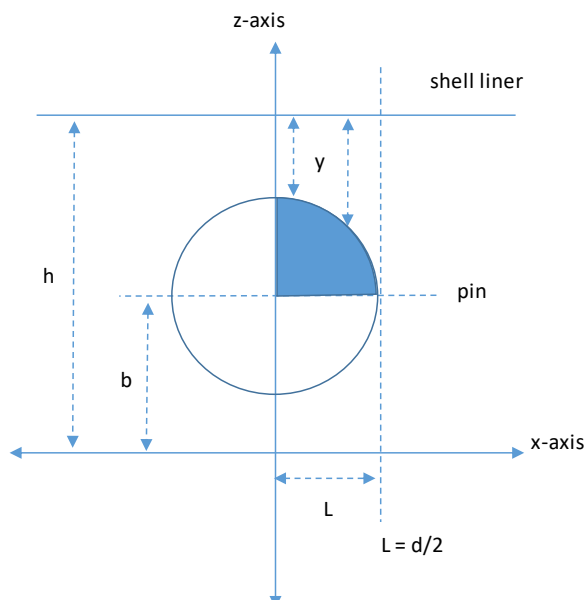
$$V_{\tau} = \frac{2}{3} * (r_2^3 - r_1^3) * \int_{L_1}^{L_2} \frac{1}{b - \sqrt{\left(\frac{d}{2}\right)^2 - L^2}} dL$$

Use numerical integration to solve V_{τ}

$d = \text{constant}$

$b = \text{constant}$

7.2.3 Shear Volume Formula Derivation for the Pin Top Half



Integrate over 1/2 of pin top surface

$d = \text{pin diameter}$

$L = \text{distance from pin center}$

$b = \text{coordinate of pin center on z-axis}$

$h = \text{coordinate of liner bottom plane on z-axis}$

$y = f(L)$

Formula of circle

$$(x - a)^2 + (z - b)^2 = R^2$$

$$R = \frac{d}{2}$$

(a,b) = coordinates of centre point

$$a = 0$$

b is defined by the position of the pin centre on the z-axis

$$x = L$$

$$L^2 + (z - b)^2 = \left(\frac{d}{2}\right)^2$$

$$z^2 - 2bz + L^2 + b^2 - \left(\frac{d}{2}\right)^2 = 0$$

Applying the quadratic formula:

$$z = \frac{-(-2b) \pm \sqrt{(-2b)^2 - 4(1) \left[L^2 + b^2 - \left(\frac{d}{2}\right)^2 \right]}}{2(1)}$$

Using only the form with the plus (+) and simplifying gives

$$z = b + \sqrt{\left(\frac{d}{2}\right)^2 - L^2}$$

$$y = h - z$$

$$y = h - b - \sqrt{\left(\frac{d}{2}\right)^2 - L^2}$$

Derivation of shear volume

$$V_\tau = \frac{Ar^2}{y}$$

$$V_\tau = 2 \int_{r_1}^{r_2} \int_{L_1}^{L_2} \frac{r^2}{h - b - \sqrt{\left(\frac{d}{2}\right)^2 - L^2}} dL dr$$

$$V_\tau = \frac{2}{3} * (r_2^3 - r_1^3) * \int_{L_1}^{L_2} \frac{1}{h - b - \sqrt{\left(\frac{d}{2}\right)^2 - L^2}} dL$$

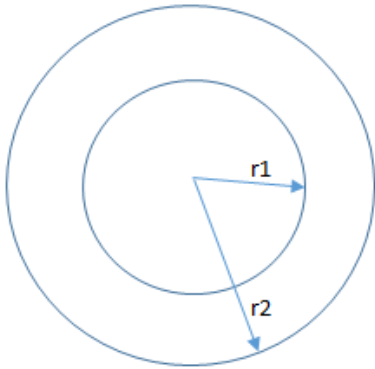
Use numerical integration to solve V_τ

d = constant

b = constant

h = constant

7.2.4 Shear Volume Formula Derivation for the Outer Ring



$$P_{\tau} = \mu\omega^2 \frac{Ar^2}{y}$$

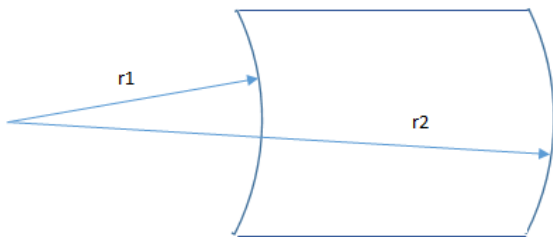
$$P_{\tau} = \mu\omega^2 \int_{r_1}^{r_2} \frac{2\pi r^3}{y} dr$$

$$P_{\tau} = \frac{2\pi\mu\omega^2}{y} \int_{r_1}^{r_2} r^3 dr$$

$$P_{\tau} = \frac{2\pi\mu\omega^2}{y} \left[\frac{r_2^4}{4} - \frac{r_1^4}{4} \right]$$

$$V_{\tau} = \frac{\pi}{2y} [r_2^4 - r_1^4]$$

7.2.5 Shear Volume Derivation for the Spoke



$$P_{\tau} = \mu\omega^2 \frac{Ar^2}{y}$$

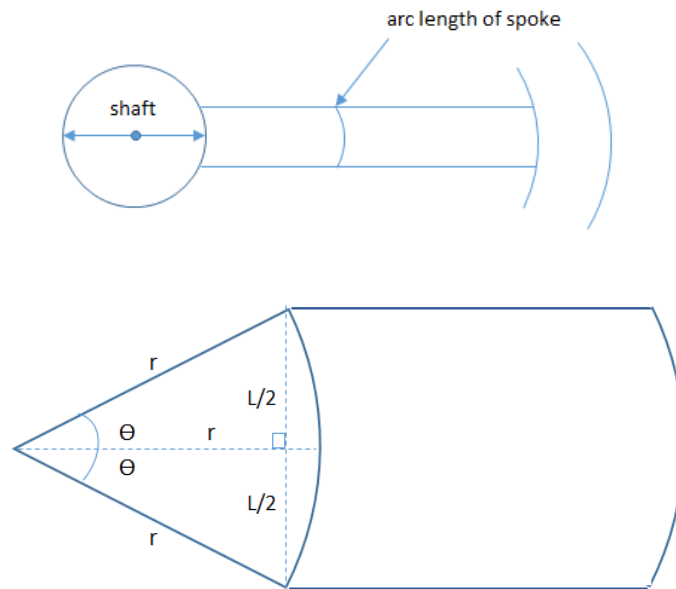
$$P_{\tau} = \mu\omega^2 \int_{r_1}^{r_2} \frac{ar^2}{y} dr \quad \text{where } a = \text{arc length, constant}$$

$$P_{\tau} = \frac{a\mu\omega^2}{y} \int_{r_1}^{r_2} r^2 dr$$

$$P_{\tau} = \frac{a\mu\omega^2}{y} \left[\frac{r_2^3}{3} - \frac{r_1^3}{3} \right]$$

$$V_{\tau} = \frac{a}{3y} [r_2^3 - r_1^3]$$

7.2.6 Formula Derivation for the Spoke Arc Length



$$\sin \theta = \frac{L}{2r}$$

$$L = 10\text{mm}$$
$$r = 12.5\text{mm}$$

$$\sin \theta = \frac{10}{2(12.5)} = 0.4$$

$$\theta = 23.578^\circ$$

$$2\theta = 47.156^\circ$$

$$\text{arc length} = \frac{47.156}{360} \times 2\pi r = 10.287\text{mm}$$

7.3 Shear Volume Calculations

Ring stirrer in smooth vessel

Between edge of rings and mill vessel

r_ring_edge	0.07200 m
y_ring_edge	0.01800 m
h_ring	0.01000 m
A_ring_edge	0.00452 m ²
Vt_per_ring_edge	0.00130 m ³
Number of rings	2
Vt_ring_edge	0.00261 m ³

Bottom of shaft and mill bottom

r1_shaft_bottom	0.0000 m
r2_shaft_bottom	0.0125 m
y_shaft_bottom	0.0200 m
Vt_shaft_bottom	0.0000019 m ³

Bottom of spokes

r1_spoke_bottom	0.0125 m
r2_spoke_bottom	0.0620 m
y_spoke_bottom	0.0200 m
Vt_per_spoke_bottom	0.00004 m ³
Number of spokes	4
Vt_spoke_bottom	0.000162122 m ³

Bottom of outer ring

r1_ring_bottom	0.0620 m
r2_ring_bottom	0.0720 m
y_ring_bottom	0.0200 m
Vt_ring_bottom	0.0009501 m ³
Vt_ring_stirrer	0.003720 m ³

Ring stirrer in disk vessel

Additional V_t due to liner - bottom surface

Top of spokes

r1_spoke_top	0.0360 m
r2_spoke_top	0.0620 m
y_spoke_top	0.0200 m
V_t _per_spoke_top	0.00003 m ³
Number of spokes	4
V_t _spoke_top	0.000131461 m ³

Top of outer ring

r1_ring_top	0.0620 m
r2_ring_top	0.0720 m
y_ring_top	0.0200 m
V_t _ring_top	0.0009501 m ³

Additional V_t due to liner - top surface

Bottom of spokes

r1_spoke_bottom	0.0360 m
r2_spoke_bottom	0.0620 m
y_spoke_bottom	0.0400 m
V_t _per_spoke_bottom	0.00002 m ³
Number of spokes	4
V_t _spoke_bottom	6.57307E-05 m ³

Bottom of outer ring

r1_ring_bottom	0.0620 m
r2_ring_bottom	0.0720 m
y_ring_bottom	0.0400 m
V_t _ring_bottom	0.0004751 m ³
V_t _liner	0.0016224 m ³
V_t _ring_in_disk	0.0053423 m ³

Pin stirrer in smooth vessel

Pin tips and shell

d - pin diameter	0.01 m
R - mill shell radius	0.09 m
k - pin length	0.072 m
L1	0 m
L2	0.005 m
number of pins	12

Integration result per pin 2.27016E-05 m³

Vt_pin_tip 0.00027242 m³

Bottom of shaft and mill bottom

r1_shaft_bottom	0.0000 m
r2_shaft_bottom	0.0125 m
y_shaft_bottom	0.0200 m

Vt_shaft_bottom 0.0000019 m³

Pin bottom and mill bottom

d - pin diameter	0.01 m
b - pin center height on z-axis	0.025 m
a - pin center position on x-axis	0 m
r1	0.0125 m
r2	0.072 m
L1	0 m
L2	0.005 m
number of pins	6

Integration result per pin 0.2379010 m³

Vt_pin_bottom_per pin 5.88876E-05 m³

Vt_pin_bottom 0.000353326 m³

Vt_total 0.0006277 m³

Pin stirrer in disk vessel

Additional Vt due to liner - top surface

d - pin diameter	0.01 m
b - pin center height on z-axis	0.045 m
a - pin center position on x-axis	0 m
r1	0.036 m
r2	0.072 m
L1	0 m
L2	0.005 m
number of pins	6

Integration result per pin 0.1218217 m³

Vt_pin_bottom_per_pin 2.6524E-05

Vt_pin_bottom 1.5914E-04 m³

Additional Vt due to liner - bottom surface

d - pin diameter	0.01 m
b - pin center height on z-axis	0.025 m
h - liner bottom plane position on z-axis	0.05 m
a - pin center position on x-axis	0 m
r1	0.036 m
r2	0.072 m
L1	0 m
L2	0.005 m
number of pins	6

Integration result per pin 0.237901 m³

Vt_pin_bottom_per_pin 5.17977E-05

Vt_pin_bottom 3.1079E-04 m³

Vt_total 0.0010976 m³

7.4 PSD of Silica Feeds

Table 28: PSD of -150 + 106 μm Mono-Sized Silica Feed

Sieve size (μm)	Sample 1			Sample 2			Average
	Mass(g)	Mass %	Cumulative % Passing	Mass(g)	Mass %	Cumulative % Passing	Cumulative % Passing
300	0.00	0.00	100.0	0.00	0.00	100.00	100.0
212	0.45	0.33	99.7	0.29	0.22	99.78	99.7
150	15.98	11.71	88.0	13.25	10.26	89.52	88.7
106	116.33	85.28	2.7	111.65	86.45	3.07	2.9
75	3.65	2.68	0.0	3.96	3.07	0.00	0.0
53	0.00	0.00	0.0	0.00	0.00	0.00	0.0
-53	0.00	0.00		0.00	0.00		
	136.41			129.15			

Table 29: PSD of -106 + 75 μm Mono-Sized Silica Feed

Sieve size (μm)	Sample 1			Sample 2			Average
	Mass(g)	Mass %	Cumulative % Passing	Mass(g)	Mass %	Cumulative % Passing	Cumulative % Passing
300	0.00	0.00	100.0	0.00	0.00	100.00	100.0
212	0.00	0.00	100.0	0.00	0.00	100.00	100.0
150	3.96	4.41	95.6	3.79	4.19	95.81	95.7
106	5.53	6.16	89.4	5.65	6.24	89.57	89.5
75	70.93	78.99	10.4	71.94	79.47	10.10	10.3
53	9.04	10.07	0.4	8.87	9.80	0.30	0.3
-53	0.34	0.38		0.27	0.30		
	89.80			90.52			

Table 30: PSD of Natural Size Silica Feed

Sieve size (μm)	Feed sample 1			Feed sample 2			Average
	Mass(g)	Mass %	Cumulative % Passing	Mass(g)	Mass %	Cumulative % Passing	Cumulative % Passing
212	0.00	0.00	100.0	0.00	0.00	100.00	100.0
150	0.05	0.07	99.9	0.00	0.00	100.00	100.0
106	0.51	0.75	99.2	0.43	0.68	99.32	99.2
75	4.92	7.26	91.9	4.44	6.98	92.35	92.1
53	9.93	14.66	77.3	9.44	14.84	77.51	77.4
38	10.55	15.57	61.7	10.12	15.91	61.60	61.6
-38	41.79	61.68		39.19	61.60		
	67.75			63.62			

7.5 XRD Results

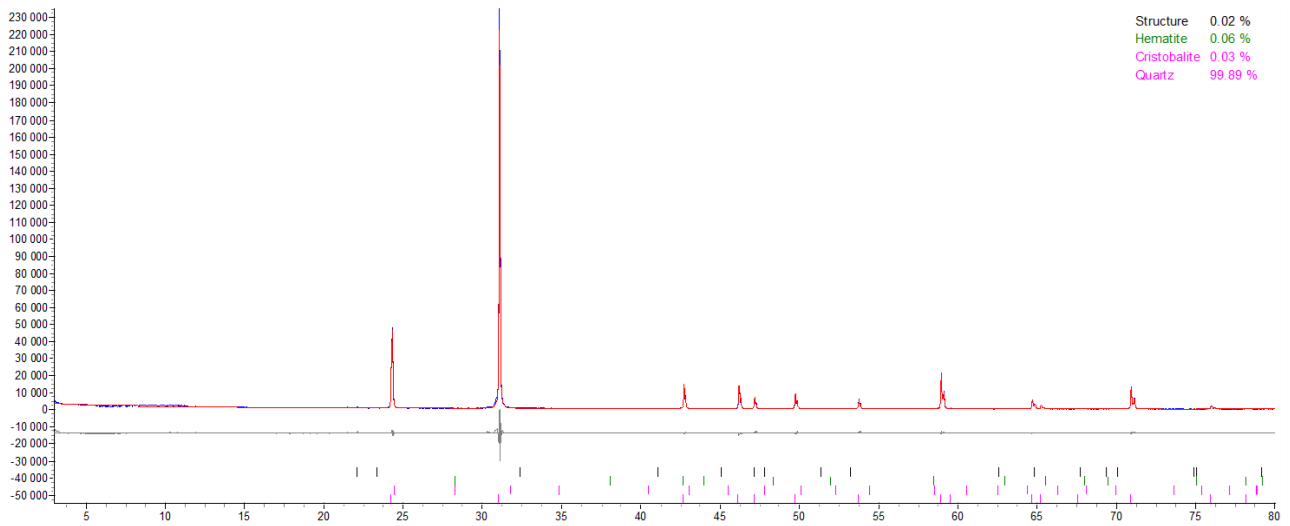


Figure 105: Quantitative XRD results of silica sand

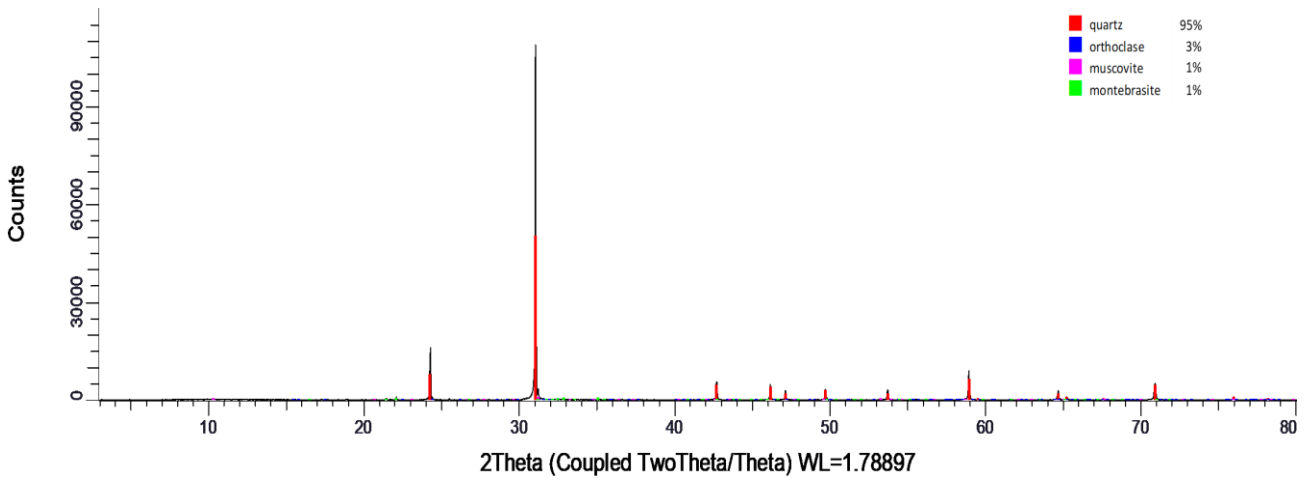


Figure 106: Quantitative XRD results of silica flour

7.6 Silica Density Measurement Results

Table 31: Specific gravity measurements - silica feed for mono-sized feed tests

Measurement Number	SG (g/cm ³)
1	2.68
2	2.66
3	2.68
Average	2.67

Table 32: Specific gravity measurements - silica feed for natural particle distribution tests

Measurement Number	SG (g/cm ³)
1	2.65
2	2.64
3	2.65
Average	2.65

7.7 Ceramic Grinding Beads Density Measurements

Table 33: Bulk density measurement on 3 mm ceramic beads

Measurement Number	Bead mass (gram)	Beaker volume (cm ³)	Bulk density (g/cm ³)
1	492.04	250	1.97
2	489.16	250	1.96
3	494.48	250	1.98
Average			1.97

Table 34: Material density measurement on 3 mm ceramic beads

Measurement Number	Total mass (gram)	Mass of water (gram)	Volume of water (cm ³)	Volume of beads (cm ³)	Bead material density (g/cm ³)
1	590.20	98.16	98.16	151.84	3.24
2	589.84	100.68	100.68	149.32	3.28
3	592.24	97.76	97.76	152.24	3.25
Average					3.25

Table 35: Beads fractional voidage calculation – 3 mm beads

Measurement Number	Volume between beads (cm ³)	Bulk volume of charge beads (cm ³)	Voidage (fraction)
1	98.16	250	0.39
2	100.68	250	0.40
3	97.76	250	0.39
Average			0.40

Table 36: Bulk density measurement on 2 mm ceramic beads

Measurement Number	Bead mass (gram)	Beaker volume (cm ³)	Bead bulk density (g/cm ³)
1	495.67	250	1.98
2	491.42	250	1.97
3	497.89	250	1.99
Average			1.98

Table 37: Material density measurement on 2 mm ceramic beads

Measurement Number	Total mass (gram)	Mass of water (gram)	Volume of water (cm ³)	Volume of beads (cm ³)	Bead material density (g/cm ³)
1	591.85	96.18	96.18	153.82	3.22
2	592.36	100.94	100.94	149.06	3.30
3	592.72	94.83	94.83	155.17	3.21
Average					3.24

Table 38: Beads fractional voidage calculation – 2 mm beads

Measurement Number	Volume between beads(cm ³)	Bulk volume of charge beads (cm ³)	Charge porosity (fraction)
1	96.18	250	0.38
2	100.94	250	0.40
3	94.83	250	0.38
Average			0.39

Table 39: Bulk density measurement on 1 mm ceramic beads

Measurement Number	Bead mass (gram)	Beaker volume (cm ³)	Bead bulk density (g/cm ³)
1	498.21	250	1.99
2	493.14	250	1.97
3	490.64	250	1.96
Average			1.98

Table 40: Material density measurement on 1 mm ceramic beads

Measurement Number	Total mass (gram)	Mass of water (gram)	Volume of water (cm ³)	Volume of beads (cm ³)	Bead material density (g/cm ³)
1	595.08	96.87	96.87	153.13	3.25
2	588.3	95.16	95.16	154.84	3.18
3	592.34	101.7	101.7	148.3	3.31
Average					3.25

Table 41: Beads fractional voidage calculation – 1 mm beads

Measurement Number	Volume between beads(cm ³)	Bulk volume of charge beads (cm ³)	Charge porosity (fraction)
1	96.87	250	0.39
2	95.16	250	0.38
3	101.7	250	0.41
Average			0.39

7.8 Experimental Results – Beads and Water Power Draw

Table 42: Test W-1 Data

Pin in Smooth - 3mm beads

Measurement set 1		Measurement set 2		Measurement set 3		Average	
Speed (rpm)	Power (W)	Speed (rpm)	Power (W)	Speed (rpm)	Power (W)	Speed (rpm)	Power (W)
271	51.0	270	49.4	270	48.9	270	49.8
307	61.5	307	59.9	307	59.3	307	60.2
344	74.5	343	72.9	343	71.7	343	73.0
382	86.6	381	85.6	381	84.2	381	85.5
401	92.8	401	91.7	401	91.0	401	91.8
419	98.2	419	97.2	419	96.4	419	97.3
456	112.7	456	111.8	456	111.0	456	111.8
493	125.8	492	124.9	492	123.3	492	124.7
530	138.8	530	137.8	530	137.9	530	138.2

Pin in Smooth - 2mm beads

Measurement set 1		Measurement set 2		Measurement set 3		Average	
Speed (rpm)	Power (W)	Speed (rpm)	Power (W)	Speed (rpm)	Power (W)	Speed (rpm)	Power (W)
270	42.6	270	41.2	270	41.2	270	41.7
307	51.6	307	50.6	307	50.2	307	50.8
343	61.7	343	60.7	343	60.5	343	61.0
381	74.5	381	74.3	381	73.6	381	74.1
400	81.7	401	80.3	401	80.1	401	80.7
418	86.6	419	85.7	419	85.9	419	86.1
456	96.9	456	96.2	457	96.1	456	96.4
492	105.8	492	105.3	492	105.4	492	105.5
529	115.8	529	115.2	530	115.2	529	115.4

Pin in Smooth - 1mm beads

Measurement set 1		Measurement set 2		Measurement set 3		Average	
Speed (rpm)	Power (W)	Speed (rpm)	Power (W)	Speed (rpm)	Power (W)	Speed (rpm)	Power (W)
269	30.6	270	29.1	271	29.8	270	29.8
307	36.4	307	35.6	307	35.9	307	36.0
343	44.3	343	43.5	344	43.7	343	43.8
381	54	382	53	382	53.6	382	53.5
401	59.7	400	58.8	401	59.1	401	59.2
419	65	419	64.8	419	64.6	419	64.8
456	75	456	75.2	455	74.5	456	74.9
492	84.4	492	81.1	492	83.6	492	83.0
530	96	530	95.3	530	96.00	530	95.8

Table 43: Test W-2 Data

Pin in Disc - 3mm beads

Measurement set 1		Measurement set 2		Measurement set 3		Average	
Speed (rpm)	Power (W)	Speed (rpm)	Power (W)	Speed (rpm)	Power (W)	Speed (rpm)	Power (W)
270	86.7	269	83.7	270	85.1	270	85.2
307	106.5	307	105.9	307	107.6	307	106.7
343	131.6	343	131.5	343	133.2	343	132.1
381	161.6	381	162	381	163.5	381	162.4
401	179.1	400	179.8	401	182.4	401	180.4
419	196.2	419	198.6	418	200.1	419	198.3
455	235.4	456	239	455	241.1	455	238.5
492	281.6	492	283.6	492	286.8	492	284.0
529	330.5	530	334.9	530	337.8	530	334.4

Pin in Disc - 2mm beads

Measurement set 1		Measurement set 2		Measurement set 3		Average	
Speed (rpm)	Power (W)	Speed (rpm)	Power (W)	Speed (rpm)	Power (W)	Speed (rpm)	Power (W)
271	75.1	269	72.4	270	71.9	270	73.1
307	95.4	306	92.4	306	91.6	306	93.1
343	117.7	343	115	344	114.9	343	115.9
381	142.1	381	139.8	381	139.4	381	140.4
401	157	401	155.1	401	153.8	401	155.3
419	169.7	419	168	419	167.9	419	168.5
456	196.3	455	195	456	195.5	456	195.6
492	223.7	492	222.4	492	221.3	492	222.5
530	257.6	529	255.6	530	255.3	530	256.2

Pin in Disc - 1mm beads

Measurement set 1		Measurement set 2		Measurement set 3		Average	
Speed (rpm)	Power (W)	Speed (rpm)	Power (W)	Speed (rpm)	Power (W)	Speed (rpm)	Power (W)
270	65.3	270	64.5	269	63.3	270	64.4
308	83.8	308	82.7	307	82.2	308	82.9
344	97.3	343	96.3	343	96.5	343	96.7
381	113.4	381	112.6	382	113.8	381	113.3
401	121.9	401	121.5	400	121.6	401	121.7
419	128.3	418	128.2	418	129.3	418	128.6
455	141.1	455	139.8	455	141.8	455	140.9
492	158.2	492	158.8	492	157.5	492	158.2
530	176.6	530	175.9	530	176.00	530	176.2

Table 44: Test W-3 Data

Ring in Smooth - 3mm beads

Measurement set 1		Measurement set 2		Measurement set 3		Average	
Speed (rpm)	Power (W)	Speed (rpm)	Power (W)	Speed (rpm)	Power (W)	Speed (rpm)	Power (W)
270	41.7	270	39.4	270	38.7	270	39.9
307	49.0	307	46.8	307	46.1	307	47.3
344	58.1	343	56	344	55.2	344	56.4
382	68.1	381	65.5	381	64.5	381	66.0
401	73.2	401	71.1	401	70.2	401	71.5
419	79.5	419	77.3	419	77.2	419	78.0
456	92.4	456	91	456	88.7	456	90.7
492	104.4	492	102.5	492	101.2	492	102.7
530	110.3	531	109.7	530	107.4	530	109.1

Ring in Smooth - 2mm beads

Measurement set 1		Measurement set 2		Measurement set 3		Average	
Speed (rpm)	Power (W)	Speed (rpm)	Power (W)	Speed (rpm)	Power (W)	Speed (rpm)	Power (W)
271	37.3	269	35.2	271	34.7	270	35.7
307	43.4	306	42	306	41.5	306	42.3
344	49.7	344	49	344	49	344	49.2
381	59.9	381	58.1	381	58.7	381	58.9
401	67.7	401	66.7	401	70.8	401	68.4
419	80.9	417	78.1	419	78.8	418	79.3
456	98.7	455	94.2	456	95.4	456	96.1
492	111.4	492	109	493	109.2	492	109.9
530	125.6	530	124.2	529	122.3	530	124.0

Ring in Smooth - 1mm beads

Measurement set 1		Measurement set 2		Measurement set 3		Average	
Speed (rpm)	Power (W)	Speed (rpm)	Power (W)	Speed (rpm)	Power (W)	Speed (rpm)	Power (W)
270	28.7	270	28.7	270	28.1	270	28.5
307	34.1	307	34.1	306	33.4	307	33.9
343	39.5	343	39.3	344	38.9	343	39.2
381	42.2	381	42.7	381	41.8	381	42.2
401	46.4	401	45.6	401	44.9	401	45.6
419	51	419	51.2	419	49.2	419	50.5
456	60.3	456	60.4	457	58.8	456	59.8
493	68.5	493	76.1	492	76.7	493	73.8
530	77.2	530	91.1	530	92.50	530	86.9

Table 45: Test W-4 Data

Ring in Disc - 3mm beads

Measurement set 1		Measurement set 2		Measurement set 3		Average	
Speed (rpm)	Power (W)	Speed (rpm)	Power (W)	Speed (rpm)	Power (W)	Speed (rpm)	Power (W)
271	61.3	270	57.5	270	57.1	270	58.6
307	73.1	307	69.2	307	68.7	307	70.3
344	86.4	343	82.1	344	81.4	344	83.3
382	102.0	382	97.8	381	96.8	382	98.9
401	111.8	401	106.7	400	105.1	401	107.9
419	120.5	419	116.2	419	114.9	419	117.2
456	140.7	456	136.7	455	135.2	456	137.5
492	162.6	492	158.8	492	158.1	492	159.8
529	188.5	529	184.9	529	183.9	529	185.8

Ring in Disc - 2mm beads

Measurement set 1		Measurement set 2		Measurement set 3		Average	
Speed (rpm)	Power (W)	Speed (rpm)	Power (W)	Speed (rpm)	Power (W)	Speed (rpm)	Power (W)
269	53.6	270	52.6	269	52.4	269	52.9
307	63.8	306	62.8	307	62.7	307	63.1
344	75.7	344	75	343	74.4	344	75.0
381	90.3	382	90.2	381	88.8	381	89.8
401	97.2	401	97.9	401	96.8	401	97.3
419	105.1	420	106.2	419	105	419	105.4
456	126.1	455	123.9	455	122.7	455	124.2
492	144.9	492	144.7	492	145.3	492	145.0
530	174.1	530	173.3	530	170.6	530	172.7

Ring in Disc - 1mm beads

Measurement set 1		Measurement set 2		Measurement set 3		Average	
Speed (rpm)	Power (W)	Speed (rpm)	Power (W)	Speed (rpm)	Power (W)	Speed (rpm)	Power (W)
270	45.6	270	44	270	43.2	270	44.3
306	56.2	306	54	307	53.3	306	54.5
343	66.7	343	64.5	343	63.5	343	64.9
381	81.4	382	80.1	382	78.5	382	80.0
401	89.6	400	89.2	401	87.7	401	88.8
420	94.8	419	92.8	419	92.7	419	93.4
455	104.1	455	103	456	102.1	455	103.1
492	117.3	492	115.3	492	114.9	492	115.8
530	134.6	531	134	530	132.30	530	133.6

Table 46: Test W-1 to W-4 Comparison

3mm beads and water

Pin in Smooth		Ring in Smooth		Pin in Disc		Ring in Disc	
Speed (rpm)	Power (W)	Speed (rpm)	Power (W)	Speed (rpm)	Power (W)	Speed (rpm)	Power (W)
270	49.8	270	39.9	270	85.2	270	58.6
307	60.2	307	47.3	307	106.7	307	70.3
343	73.0	344	56.4	343	132.1	344	83.3
381	85.5	381	66.0	381	162.4	382	98.9
401	91.8	401	71.5	401	180.4	401	107.9
419	97.3	419	78.0	419	198.3	419	117.2
456	111.8	456	90.7	455	238.5	456	137.5
492	124.7	492	102.7	492	284.0	492	159.8
530	138.2	530	109.1	530	334.4	529	185.8

2mm beads and water

Pin in Smooth		Ring in Smooth		Pin in Disc		Ring in Disc	
Speed (rpm)	Power (W)	Speed (rpm)	Power (W)	Speed (rpm)	Power (W)	Speed (rpm)	Power (W)
270	41.7	270	35.7	270	73.1	269	52.9
307	50.8	306	42.3	306	93.1	307	63.1
343	61.0	344	49.2	343	115.9	344	75.0
381	74.1	381	58.9	381	140.4	381	89.8
401	80.7	401	68.4	401	155.3	401	97.3
419	86.1	418	79.3	419	168.5	419	105.4
456	96.4	456	96.1	456	195.6	455	124.2
492	105.5	492	109.9	492	222.5	492	145.0
529	115.4	530	124.0	530	256.2	530	172.7

1mm beads and water

Pin in Smooth		Ring in Smooth		Pin in Disc		Ring in Disc	
Speed (rpm)	Power (W)	Speed (rpm)	Power (W)	Speed (rpm)	Power (W)	Speed (rpm)	Power (W)
270	29.8	270	28.5	270	64.4	270	44.3
307	36.0	307	33.9	308	82.9	306	54.5
343	43.8	343	39.2	343	96.7	343	64.9
382	53.5	381	42.2	381	113.3	382	80.0
401	59.2	401	45.6	401	121.7	401	88.8
419	64.8	419	50.5	418	128.6	419	93.4
456	74.9	456	59.8	455	140.9	455	103.1
492	83.0	493	73.8	492	158.2	492	115.8
530	95.8	530	86.9	530	176.2	530	133.6

7.9 Experimental Results – Repeatability Tests

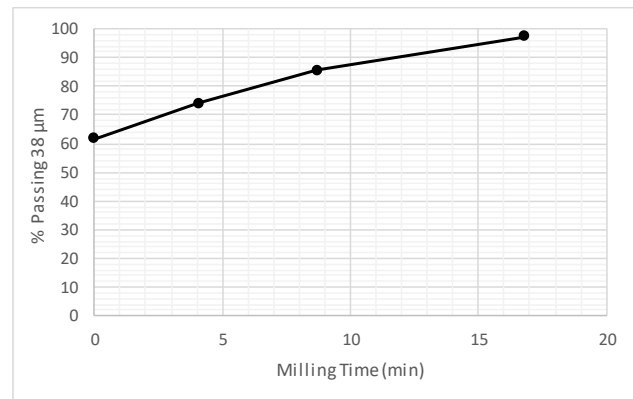
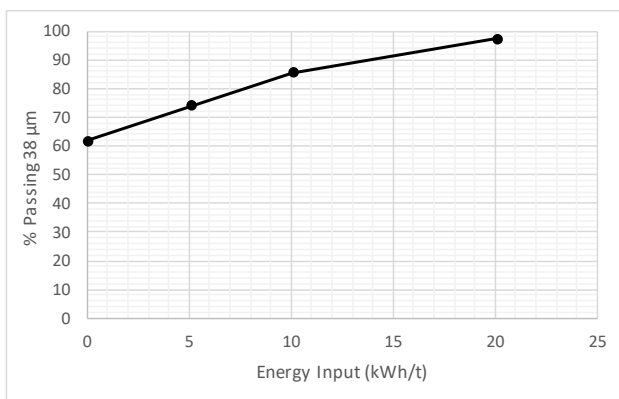
Table 47: Test R-1 Data

Test R-1: Silica Flour - Pin Smooth 400RPM

Average Power (Watt)

91.9 Watt

Energy Input	5.1 kWh/t			10.1 kWh/t			20.1 kWh/t		
Milling Time (min)	4.07 min			8.69 min			16.8 min		
Power Draw (Watt)	95.8 W			88.7 W			91.4 W		
Sieve size (µm)	Mass (g)	Mass %	Cumulative % Passing	Mass(g)	Mass %	Cumulative % Passing	Mass(g)	Mass %	Cumulative % Passing
212	0.00	0.00	100.00	0.00	0.00	100.00	0.00	0.00	100.00
150	0.00	0.00	100.00	0.00	0.00	100.00	0.00	0.00	100.00
106	0.39	0.49	99.51	0.18	0.24	99.76	0.05	0.04	99.96
75	2.29	2.89	96.62	0.71	0.96	98.79	0.27	0.22	99.74
53	7.84	9.88	86.74	3.12	4.24	94.55	0.66	0.53	99.21
38	10.02	12.63	74.11	6.61	8.98	85.58	2.27	1.84	97.37
-38	58.79	74.11		63.02	85.58		120.29	97.37	
	79.33			73.64			123.54		



Grind Size % Passing 38µm	Energy (kWh/t)	Time (min)
65	1.4	1.10
70	3.4	2.73
75	5.5	4.43
80	7.6	6.44
85	9.8	8.45

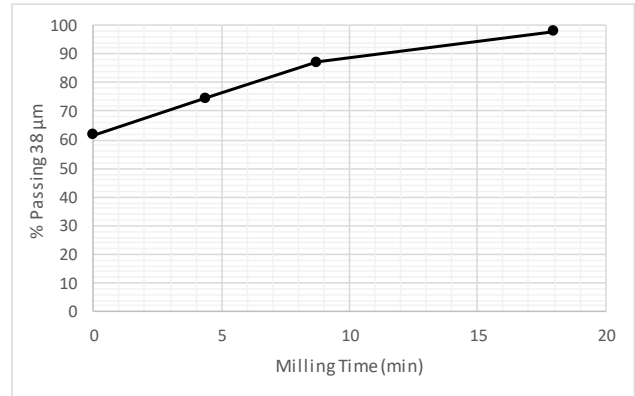
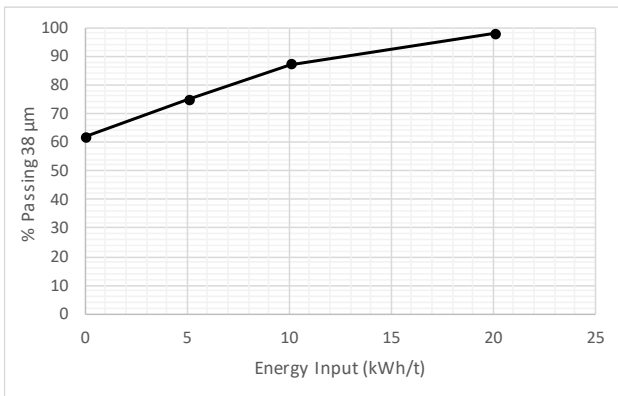
Table 48: Test R-2 Data

Test R-2: Silica Flour - Pin Smooth 400RPM

Average Power (Watt)

87.3 Watt

Energy Input	5.1 kWh/t			10.1 kWh/t			20.1 kWh/t		
Milling Time (min)	4.39 min			8.74 min			17.97 min		
Power Draw (Watt)	88.5 W			88.1 W			85.5 W		
Sieve size (µm)	Mass (g)	Mass %	Cumulative % Passing	Mass(g)	Mass %	Cumulative % Passing	Mass(g)	Mass %	Cumulative % Passing
212	0.00	0.00	100.00	0.00	0.00	100.00	0.00	0.00	100.00
150	0.00	0.00	100.00	0.00	0.00	100.00	0.00	0.00	100.00
106	0.37	0.48	99.52	0.18	0.24	99.76	0.00	0.00	100.00
75	1.96	2.53	96.99	0.70	0.93	98.83	0.21	0.17	99.83
53	6.88	8.90	88.09	2.49	3.30	95.53	0.56	0.46	99.37
38	10.36	13.40	74.69	6.40	8.48	87.05	1.85	1.52	97.85
-38	57.76	74.69		65.68	87.05		119.43	97.85	
	77.33			75.45			122.05		



Grind Size % Passing 38µm	Energy (kWh/t)	Time (min)
65	1.3	1.13
70	3.2	2.81
75	5.2	4.49
80	7.2	6.25
85	9.2	8.01

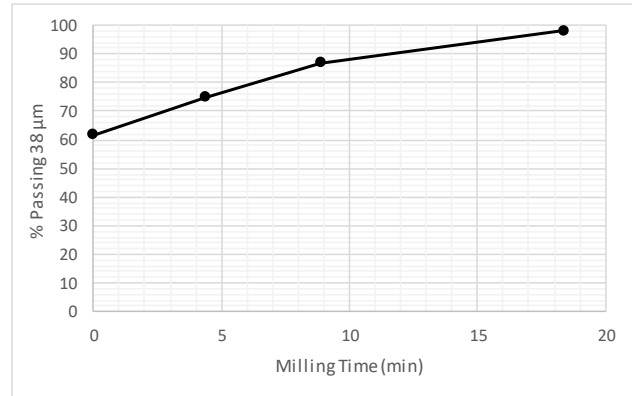
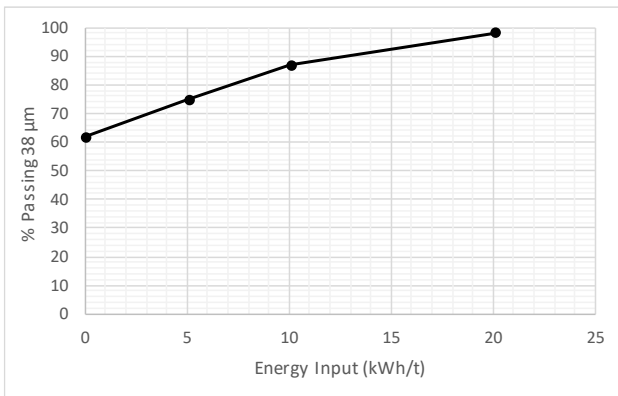
Table 49: Test R-3 Data

Test R-3: Silica Flour - Pin Smooth 400RPM

Average Power (Watt)

86.2 Watt

Energy Input	5.1 kWh/t			10.1 kWh/t			20.1 kWh/t		
Milling Time (min)	4.37 min			8.89 min			18.39 min		
Power Draw (Watt)	88.5 W			86.7 W			83.5 W		
Sieve size (µm)	Mass (g)	Mass %	Cumulative % Passing	Mass(g)	Mass %	Cumulative % Passing	Mass(g)	Mass %	Cumulative % Passing
212	0.00	0.00	100.00	0.00	0.00	100.00	0.00	0.00	100.00
150	0.00	0.00	100.00	0.00	0.00	100.00	0.00	0.00	100.00
106	0.30	0.36	99.64	0.26	0.31	99.69	0.02	0.02	99.98
75	2.15	2.61	97.03	0.63	0.74	98.95	0.23	0.19	99.80
53	7.50	9.10	87.93	2.92	3.44	95.52	0.52	0.42	99.38
38	10.78	13.08	74.85	7.34	8.64	86.88	1.69	1.36	98.02
-38	61.70	74.85		73.81	86.88		121.78	98.02	
	82.43			84.96			124.24		



Grind Size % Passing 38µm	Energy (kWh/t)	Time (min)
65	1.3	1.11
70	3.2	2.76
75	5.1	4.42
80	7.2	6.30
85	9.3	8.18

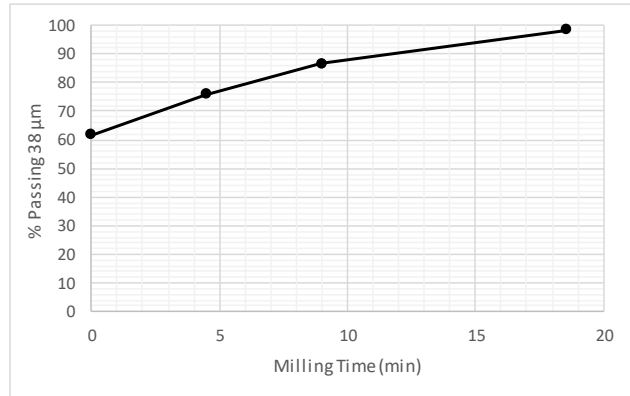
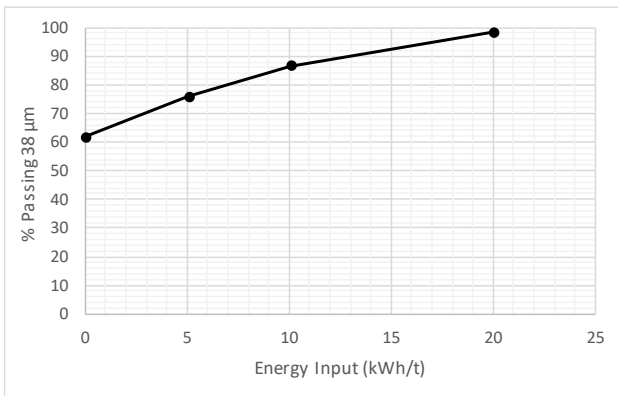
Table 50: Test R-4 Data

Test R-4: Silica Flour - Pin Smooth 400RPM

Average Power (Watt)

84.9 Watt

Energy Input	5.1 kWh/t			10.1 kWh/t			20.1 kWh/t		
Milling Time (min)	4.49 min			9 min			18.59 min		
Power Draw (Watt)	86.6 W			85.6 W			82.6 W		
Sieve size (µm)	Mass (g)	Mass %	Cumulative % Passing	Mass(g)	Mass %	Cumulative % Passing	Mass(g)	Mass %	Cumulative % Passing
212	0.00	0.00	100.00	0.00	0.00	100.00	0.00	0.00	100.00
150	0.00	0.00	100.00	0.00	0.00	100.00	0.00	0.00	100.00
106	0.04	0.05	99.95	0.12	0.15	99.85	0.03	0.03	99.97
75	1.62	2.09	97.85	0.76	0.93	98.93	0.14	0.12	99.85
53	6.53	8.44	89.41	2.89	3.52	95.40	0.42	0.36	99.49
38	10.38	13.42	75.99	7.18	8.76	86.65	1.44	1.24	98.25
-38	58.76	75.99		71.06	86.65		113.96	98.25	
	77.33			82.01			115.99		



Grind Size % Passing 38µm	Energy (kWh/t)	Time (min)
65	1.2	1.05
70	3.0	2.61
75	4.7	4.18
80	6.9	6.18
85	9.3	8.30

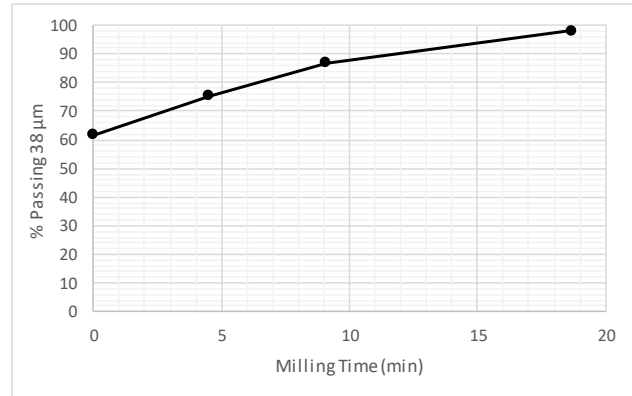
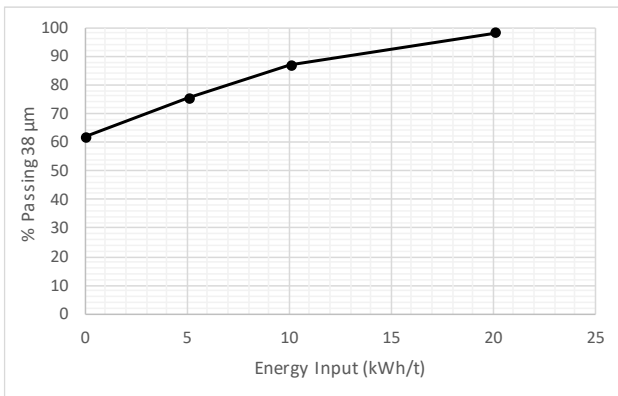
Table 51: Test R-5 Data

Test R-5: Silica Flour - Pin Smooth 400RPM

Average Power (Watt)

84.2 Watt

Energy Input	5.1 kWh/t			10.1 kWh/t			20.1 kWh/t		
Milling Time (min)	4.52 min			9.09 min			18.7 min		
Power Draw (Watt)	85.9 W			84.8 W			82.2 W		
Sieve size (µm)	Mass (g)	Mass %	Cumulative % Passing	Mass(g)	Mass %	Cumulative % Passing	Mass(g)	Mass %	Cumulative % Passing
212	0.00	0.00	100.00	0.00	0.00	100.00	0.00	0.00	100.00
150	0.00	0.00	100.00	0.00	0.00	100.00	0.06	0.05	99.95
106	0.36	0.44	99.56	0.11	0.13	99.87	0.02	0.02	99.93
75	2.08	2.52	97.04	0.84	1.01	98.86	0.18	0.15	99.78
53	7.37	8.94	88.10	3.33	4.00	94.86	0.38	0.33	99.45
38	10.55	12.80	75.30	6.65	7.98	86.88	1.43	1.22	98.23
-38	62.06	75.30		72.37	86.88		114.71	98.23	
	82.42			83.30			116.78		



Grind Size % Passing 38µm	Energy (kWh/t)	Time (min)
65	1.2	1.11
70	3.1	2.76
75	5.0	4.42
80	7.1	6.37
85	9.3	8.34

7.10 Experimental Results - Mono-size Silica Grinding Tests

Table 52: Test M-1 PSD Data

Test ID Test M-1
Feed -150 + 106 μm silica
Geometry 12-pin stirrer in smooth vessel

Sieve size(μm)	2.5 kWh/t			5 kWh/t			10 kWh/t			15 kWh/t			20 kWh/t		
	mass (g)	Mass %	Cumulative % Passing	Mass(g)	Mass %	Cumulative % Passing	Mass(g)	Mass %	Cumulative % Passing	Mass(g)	Mass %	Cumulative % Passing	Mass(g)	Mass %	Cumulative % Passing
300	0.00	0.00	100.0	0.00	0.00	100.00	0.00	0.00	100.00	0.00	0.00	100.00	0.00	0.00	100.00
212	0.19	0.15	99.9	0.03	0.02	99.98	0.12	0.09	99.91	0.10	0.09	99.91	0.00	0.00	100.00
150	1.08	0.85	99.0	0.36	0.28	99.70	0.22	0.17	99.73	0.10	0.09	99.83	0.10	0.08	99.92
106	86.53	67.76	31.3	59.74	46.44	53.25	33.27	26.05	73.69	17.20	14.83	85.00	10.60	8.71	91.21
75	22.45	17.58	13.7	35.82	27.85	25.41	36.70	28.73	44.96	27.80	23.97	61.03	23.20	19.06	72.14
53	6.65	5.21	8.5	11.89	9.24	16.16	18.30	14.33	30.63	16.20	13.97	47.07	15.70	12.90	59.24
-53	10.81	8.46		20.79	16.16		39.13	30.63		54.60	47.07		72.10	59.24	
	127.71			128.63			127.74			116.00			121.70		

Table 53: Test M-2 PSD Data

Test ID Test M-2
Feed -150 + 106 µm silica
Geometry 12-pin stirrer in disc vessel

Sieve size(µm)	2.5 kWh/t			5 kWh/t			10 kWh/t			15 kWh/t			20 kWh/t		
	mass (g)	Mass %	Cumulative % Passing	Mass(g)	Mass %	Cumulative % Passing	Mass(g)	Mass %	Cumulative % Passing	Mass(g)	Mass %	Cumulative % Passing	Mass(g)	Mass %	Cumulative % Passing
300	0.00	0.00	100.0	0.00	0.00	100.00	0.00	0.00	100.00	0.00	0.00	100.00	0.00	0.00	100.00
212	0.00	0.00	100.0	0.00	0.00	100.00	0.00	0.00	100.00	0.10	0.08	99.92	0.00	0.00	100.00
150	2.10	1.76	98.2	1.30	1.04	98.96	0.40	0.33	99.67	0.10	0.08	99.84	0.10	0.08	99.92
106	70.70	59.33	38.9	54.50	43.77	55.18	23.60	19.36	80.31	13.20	10.66	89.18	4.90	3.80	96.12
75	26.70	22.40	16.5	34.90	28.03	27.15	34.70	28.47	51.84	23.80	19.22	69.95	15.10	11.71	84.41
53	7.10	5.96	10.5	11.40	9.16	18.00	16.60	13.62	38.22	18.80	15.19	54.77	18.00	13.96	70.44
-53	12.57	10.55		22.41	18.00		46.59	38.22		67.80	54.77		90.80	70.44	
	119.17			124.51			121.89			123.80			128.90		

Table 54: Test M-3 PSD Data

Test ID Test M-3
Feed -150 + 106 μm silica
Geometry Ring stirrer in smooth vessel

Sieve size(μm)	2.5 kWh/t			5 kWh/t			10 kWh/t			15 kWh/t			20 kWh/t		
	mass (g)	Mass %	Cumulative % Passing	Mass(g)	Mass %	Cumulative % Passing	Mass(g)	Mass %	Cumulative % Passing	Mass(g)	Mass %	Cumulative % Passing	Mass(g)	Mass %	Cumulative % Passing
300	0.00	0.00	100.0	0.00	0.00	100.00	0.00	0.00	100.00	0.00	0.00	100.00	0.00	0.00	100.00
212	0.36	0.28	99.7	0.21	0.17	99.83	0.14	0.11	99.89	0.20	0.17	99.83	0.10	0.07	99.93
150	1.04	0.80	98.9	0.66	0.53	99.31	0.31	0.24	99.66	0.20	0.17	99.67	0.10	0.07	99.85
106	89.01	68.63	30.3	67.82	54.00	45.31	47.85	36.45	63.20	26.90	22.19	77.48	17.90	13.39	86.46
75	23.66	18.24	12.0	30.22	24.06	21.24	34.34	26.16	37.04	29.90	24.67	52.81	28.80	21.54	64.92
53	6.04	4.66	7.4	9.65	7.68	13.56	14.84	11.31	25.74	17.10	14.11	38.70	20.20	15.11	49.81
-53	9.58	7.39		17.03	13.56		33.78	25.74		46.90	38.70		66.60	49.81	
	129.69			125.59			131.26			121.20			133.70		

Table 55: Test M-4 PSD Data

Test ID Test M-4
Feed -150 + 106 μm silica
Geometry Ring stirrer in disc vessel

Sieve size(μm)	2.5 kWh/t			5 kWh/t			10 kWh/t			15 kWh/t			20 kWh/t		
	mass (g)	Mass %	Cumulative % Passing	Mass(g)	Mass %	Cumulative % Passing	Mass(g)	Mass %	Cumulative % Passing	Mass(g)	Mass %	Cumulative % Passing	Mass(g)	Mass %	Cumulative % Passing
300	0.00	0.00	100.0	0.00	0.00	100.00	0.00	0.00	100.00	0.00	0.00	100.00	0.00	0.00	100.00
212	0.12	0.09	99.9	0.09	0.07	99.93	0.09	0.07	99.93	0.00	0.00	100.00	0.00	0.00	100.00
150	2.35	1.83	98.1	1.82	1.41	98.52	0.65	0.51	99.42	0.36	0.31	99.69	0.23	0.18	99.82
106	88.11	68.54	29.5	77.33	60.07	38.45	48.87	38.09	61.33	21.53	18.79	80.90	13.56	10.34	89.48
75	21.27	16.54	13.0	25.14	19.53	18.92	31.72	24.72	36.61	29.87	26.07	54.83	29.51	22.50	66.98
53	5.52	4.29	8.7	7.67	5.96	12.96	12.77	9.95	26.66	15.64	13.65	41.18	19.15	14.60	52.38
-53	11.19	8.70		16.69	12.96		34.20	26.66		47.18	41.18		68.69	52.38	
	128.56			128.74			128.30			114.58			131.14		

Table 56: Test M-5 PSD Data

Test ID Test M-5
 Feed -106 + 75 μm silica
 Geometry 12-pin stirrer in smooth vessel

Sieve size(μm)	2.5 kWh/t			5 kWh/t			10 kWh/t			15 kWh/t			20 kWh/t		
	mass (g)	Mass %	Cumulative % Passing	Mass(g)	Mass %	Cumulative % Passing	Mass(g)	Mass %	Cumulative % Passing	Mass(g)	Mass %	Cumulative % Passing	Mass(g)	Mass %	Cumulative % Passing
300	0.00	0.00	100.0	0.00	0.00	100.00	0.00	0.00	100.00	0.00	0.00	100.00	0.00	0.00	100.00
212	0.00	0.00	100.0	0.00	0.00	100.00	0.00	0.00	100.00	0.00	0.00	100.00	0.00	0.00	100.00
150	3.19	2.53	97.5	1.93	1.48	98.52	0.50	0.37	99.63	0.40	0.31	99.69	0.30	0.24	99.76
106	6.46	5.13	92.3	4.78	3.67	94.85	3.10	2.30	97.32	2.30	1.78	97.91	1.00	0.79	98.97
75	71.39	56.72	35.6	50.21	38.57	56.28	29.80	22.16	75.17	14.40	11.15	86.76	5.20	4.13	94.84
53	28.31	22.49	13.1	35.62	27.36	28.91	32.40	24.09	51.08	25.80	19.97	66.80	17.10	13.57	81.27
-53	16.51	13.12		37.64	28.91		68.70	51.08		86.30	66.80		102.40	81.27	
	125.86			130.18			134.50			129.20			126.00		

Table 57: Test M-6 PSD Data

Test ID Test M-6
Feed -106 + 75 µm silica
Geometry 12-pin stirrer in disc vessel

Sieve size(µm)	2.5 kWh/t			5 kWh/t			10 kWh/t			15 kWh/t			20 kWh/t		
	mass (g)	Mass %	Cumulative % Passing	Mass(g)	Mass %	Cumulative % Passing	Mass(g)	Mass %	Cumulative % Passing	Mass(g)	Mass %	Cumulative % Passing	Mass(g)	Mass %	Cumulative % Passing
300	0.00	0.00	100.0	0.00	0.00	100.00	0.00	0.00	100.00	0.00	0.00	100.00	0.00	0.00	100.00
212	0.00	0.00	100.0	0.00	0.00	100.00	0.00	0.00	100.00	0.00	0.00	100.00	0.00	0.00	100.00
150	3.10	2.64	97.4	1.90	1.50	98.50	0.20	0.15	99.85	0.30	0.24	99.76	0.00	0.00	100.00
106	4.80	4.09	93.3	4.80	3.79	94.70	2.20	1.68	98.17	1.90	1.51	98.25	0.50	0.44	99.56
75	66.10	56.39	36.9	52.10	41.19	53.51	25.30	19.34	78.82	13.10	10.40	87.86	3.80	3.31	96.25
53	23.70	20.22	16.7	29.60	23.40	30.11	31.80	24.31	54.51	22.60	17.94	69.92	12.70	11.07	85.18
-53	19.52	16.65		38.09	30.11		71.30	54.51		88.10	69.92		97.70	85.18	
	117.22			126.49			130.80			126.00			114.70		

Table 58: Test M-7 PSD Data

Test ID Test M-7
Feed -106 + 75 µm silica
Geometry Ring stirrer in smooth vessel

Sieve size(µm)	2.5 kWh/t			5 kWh/t			10 kWh/t			15 kWh/t			20 kWh/t		
	mass (g)	Mass %	Cumulative % Passing	Mass(g)	Mass %	Cumulative % Passing	Mass(g)	Mass %	Cumulative % Passing	Mass(g)	Mass %	Cumulative % Passing	Mass(g)	Mass %	Cumulative % Passing
300	0.00	0.00	100.0	0.00	0.00	100.00	0.00	0.00	100.00	0.00	0.00	100.00	0.00	0.00	100.00
212	0.00	0.00	100.0	0.00	0.00	100.00	0.00	0.00	100.00	0.00	0.00	100.00	0.00	0.00	100.00
150	2.94	2.36	97.6	1.92	1.55	98.45	0.90	0.70	99.30	0.70	0.56	99.44	0.20	0.16	99.84
106	6.15	4.94	92.7	4.98	4.01	94.44	3.40	2.66	96.64	2.30	1.84	97.61	1.10	0.87	98.97
75	71.17	57.14	35.6	54.59	43.96	50.49	30.40	23.77	72.87	18.50	14.76	82.84	8.10	6.42	92.55
53	26.59	21.35	14.2	32.50	26.17	24.32	35.40	27.68	45.19	30.90	24.66	58.18	23.10	18.30	74.25
-53	17.70	14.21		30.20	24.32		57.80	45.19		72.90	58.18		93.70	74.25	
	124.55			124.19			127.90			125.30			126.20		

Table 59: Test M-8 PSD Data

Test ID Test M-8
Feed -106 + 75 µm silica
Geometry Ring stirrer in disc vessel

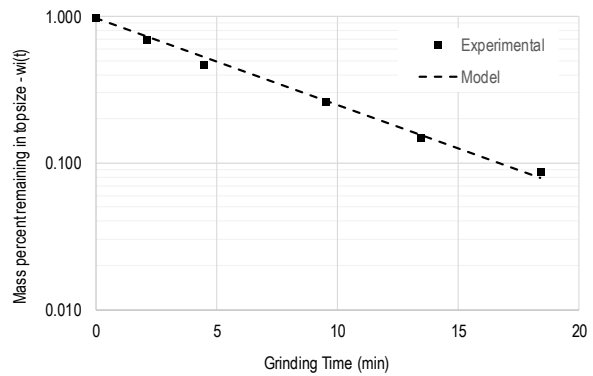
Sieve size(µm)	2.5 kWh/t			5 kWh/t			10 kWh/t			15 kWh/t			20 kWh/t		
	mass (g)	Mass %	Cumulative % Passing	Mass(g)	Mass %	Cumulative % Passing	Mass(g)	Mass %	Cumulative % Passing	Mass(g)	Mass %	Cumulative % Passing	Mass(g)	Mass %	Cumulative % Passing
300	0.00	0.00	100.0	0.00	0.00	100.00	0.00	0.00	100.00	0.00	0.00	100.00	0.00	0.00	100.00
212	0.00	0.00	100.0	0.00	0.00	100.00	0.00	0.00	100.00	0.00	0.00	100.00	0.00	0.00	100.00
150	3.19	2.65	97.3	2.11	1.63	98.37	1.06	0.80	99.20	0.37	0.28	99.72	0.19	0.15	99.85
106	7.63	6.35	91.0	5.48	4.23	94.14	3.50	2.63	96.58	1.28	0.96	98.76	1.08	0.85	99.00
75	62.86	52.28	38.7	56.22	43.39	50.75	34.08	25.59	70.98	16.83	12.61	86.15	8.02	6.34	92.66
53	20.55	17.09	21.6	27.19	20.98	29.77	34.30	25.76	45.22	29.29	21.95	64.21	21.65	17.11	75.54
-53	26.01	21.63		38.57	29.77		60.22	45.22		85.69	64.21		95.57	75.54	
	120.24			129.57			133.16			133.46			126.51		

Table 60: Test M-1 Breakage Rates

Test ID	Test M-1			w_i(0)	0.971 fraction	
Feed	-150 + 106 μm silica			S_i	0.136 min ⁻¹	
Geometry	12-pin stirrer in smooth vessel			S_i^E	0.123 kWh/t ¹	
Speed	400 RPM			Average Power	86.4 Watt	
Energy input	kWh/t	2.56	5.06	10.06	15.14	20.12
Time	seconds	126	267	568	808	1105
	minutes	2.1	4.5	9.5	13.5	18.4
Mill power	Watt	93.4	87.1	81.4	86.1	83.7
Silica feed mass	gram	1277	1277	1277	1277	1277
Sieving results						
+106 μm	gram	87.80	60.13	33.61	17.40	10.70
-106 μm	gram	39.91	68.50	94.13	98.60	111.00
Total	gram	127.71	128.63	127.74	116.00	121.70
Feed size remaining (w _i)	fraction	0.687	0.467	0.263	0.150	0.088

Fitting of Time Based Breakage Rate (S_i)

S_i (min⁻¹)		0.136		
$w_i(t) = w_i(0)\exp(-S_i t)$	t (min)	w_i(t) measured	w_i(t) model	SSQ Error
	0	0.971	0.971	0.0000
	2.1	0.687	0.730	0.0038
	4.5	0.467	0.531	0.0182
	9.5	0.263	0.268	0.0004
	13.5	0.150	0.156	0.0016
	18.4	0.088	0.080	0.0089
				0.0330



Fitting of Energy Normalised Breakage Rate (S_i^E)

S_i^E (kWh/t¹)		0.123		
$w_i(E) = w_i(0)\exp[-S_i^E E]$	E (kWh/t¹)	w_i(E) measured	w_i(E) model	SSQ Error
	0	0.971	0.971	0.0000
	2.6	0.687	0.708	0.0009
	5.1	0.467	0.520	0.0127
	10.1	0.263	0.281	0.0045
	15.1	0.150	0.150	0.0000
	20.1	0.088	0.081	0.0059
				0.0240

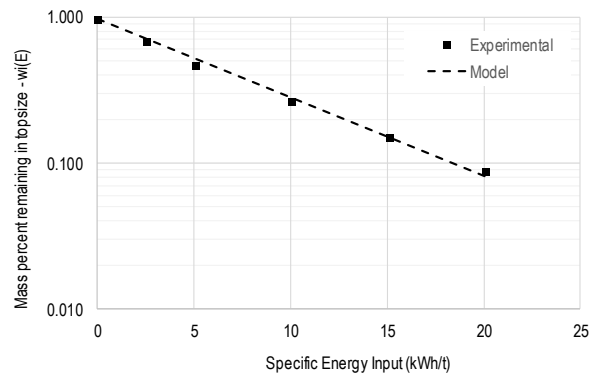


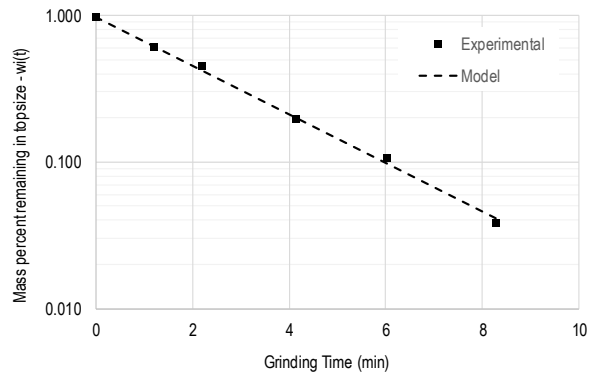
Table 61: Test M-2 Breakage Rates

Test ID	Test M-2					w_i(0)	0.971 fraction
Feed	-150 + 106 μm silica					S_i	0.382 min ⁻¹
Geometry	12-pin stirrer in disc vessel					S_i^E	0.155 kWh/t ¹
Speed	400 RPM					Average Power	184.6 Watt
Energy input	kWh/t	2.62	5.16	10.11	15.29	20.3	
Time	seconds	71	130	248	360	496	
	minutes	1.2	2.2	4.1	6.0	8.3	
Mill power	Watt	169.6	182.5	187.4	195.3	188.2	
Silica feed mass	gram	1277	1277	1277	1277	1277	
Sieving results							
+106 μm	gram	72.80	55.80	24.00	13.40	5.00	
-106 μm	gram	46.37	68.71	97.89	110.40	123.90	
Total	gram	119.17	124.51	121.89	123.80	128.90	
Feed size remaining (w _i)	fraction	0.611	0.448	0.197	0.108	0.039	

Fitting of Time Based Breakage Rate (S_i)

S_i (min⁻¹) 0.382

$w_i(t) = w_i(0)\exp(-S_i t)$	t (min)	w _i (t) measured	w _i (t) model	SSQ Error
	0	0.971	0.971	0.0000
	1.2	0.611	0.618	0.0001
	2.2	0.448	0.424	0.0029
	4.1	0.197	0.200	0.0002
	6.0	0.108	0.098	0.0090
	8.3	0.039	0.041	0.0039
				0.0161



Fitting of Energy Normalised Breakage Rate (S_i^E)

S_i^E (kWh/t¹) 0.155

$w_i(E) = w_i(0)\exp[-S_i^E E]$	E (kWh/t ¹)	w _i (E) measured	w _i (E) model	SSQ Error
	0	0.971	0.971	0.0000
	2.6	0.611	0.647	0.0035
	5.2	0.448	0.437	0.0007
	10.1	0.197	0.203	0.0009
	15.3	0.108	0.091	0.0257
	20.3	0.039	0.042	0.0061
				0.0369

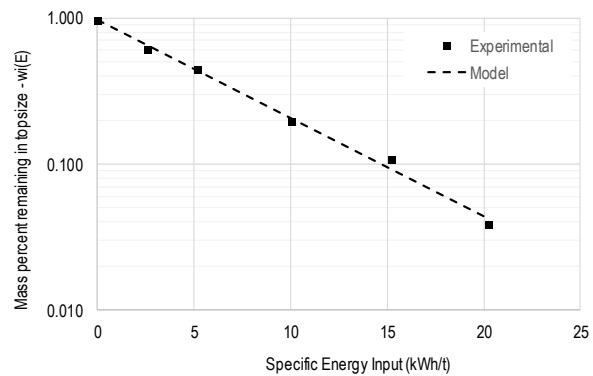


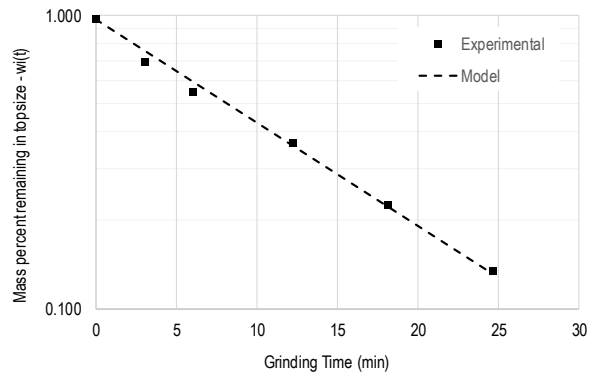
Table 62: Test M-3 Breakage Rates

Test ID	Test M-3			w_i(0)	0.971 fraction	
Feed	-150 + 106 μm silica			S_i	0.081 min ⁻¹	
Geometry	Ring stirrer in smooth vessel			S_i^E	0.098 kWh/t ¹	
Speed	400 RPM	Average Power		63.9 Watt		
Energy input	kWh/t	2.55	5.04	10.05	15.1	20.08
Time	seconds	179	361	731	1083	1477
	minutes	3.0	6.0	12.2	18.1	24.6
Mill power	Watt	65.5	64.2	63.2	64.1	62.5
Silica feed mass	gram	1277	1277	1277	1277	1277
Sieving results						
+106 μm	gram	90.41	68.69	48.30	27.30	18.10
-106 μm	gram	39.28	56.90	82.96	93.90	115.60
Total	gram	129.69	125.59	131.26	121.20	133.70
Feed size remaining (w _i)	fraction	0.697	0.547	0.368	0.225	0.135

Fitting of Time Based Breakage Rate (S_i)

S_i (min⁻¹) 0.081

$w_i(t) = w_i(0)\exp(-S_i t)$	t (min)	w _i (t) measured	w _i (t) model	SSQ Error
	0	0.971	0.971	0.0000
	3.0	0.697	0.762	0.0087
	6.0	0.547	0.596	0.0081
	12.2	0.368	0.361	0.0003
	18.1	0.225	0.225	0.0000
	24.6	0.135	0.132	0.0007
				0.0178



Fitting of Energy Normalised Breakage Rate (S_i^E)

S_i^E (kWh/t¹) 0.098

$w_i(E) = w_i(0)\exp[-S_i^E E]$	E (kWh/t ¹)	w _i (E) measured	w _i (E) model	SSQ Error
	0	0.971	0.971	0.0000
	2.6	0.697	0.755	0.0070
	5.0	0.547	0.591	0.0066
	10.1	0.368	0.361	0.0003
	15.1	0.225	0.220	0.0006
	20.1	0.135	0.135	0.0000
				0.0146

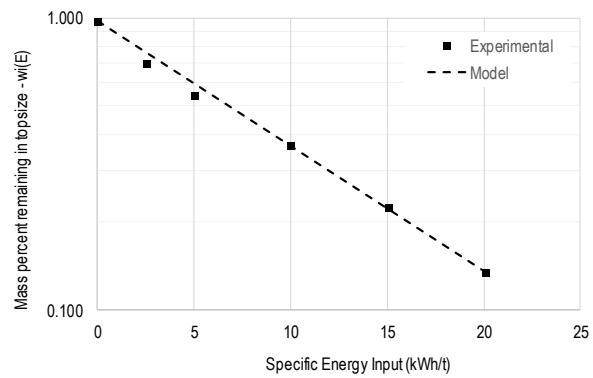
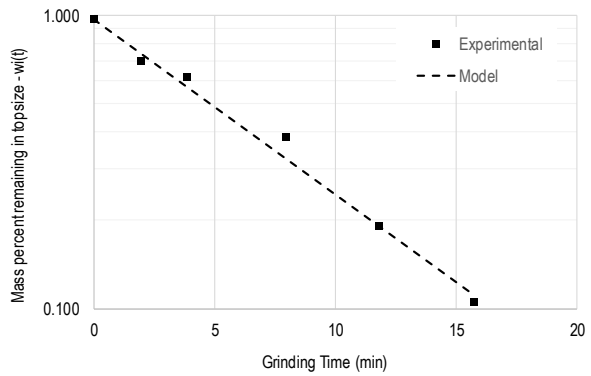


Table 63: Test M-4 Breakage Rates

Test ID	Test M-4					w_i(0)	0.971 fraction
Feed	-150 + 106 μm silica					S_i	0.137 min ⁻¹
Geometry	Ring stirrer in disc vessel					S_i^E	0.107 kWh/t ¹
Speed	400 RPM					Average Power	99.7 Watt
Energy input	kWh/t	2.58	5.08	10.07	15.15	20.15	
Time	seconds	116	229	474	707	943	
	minutes	1.9	3.8	7.9	11.8	15.7	
Mill power	Watt	102.2	102.0	97.7	98.5	98.2	
Silica feed mass	gram	1277	1277	1277	1277	1277	
Sieving results							
+106 μm	gram	90.58	79.24	49.61	21.89	13.79	
-106 μm	gram	37.98	49.50	78.69	92.69	117.35	
Total	gram	128.56	128.74	128.30	114.58	131.14	
Feed size remaining (w _i)	fraction	0.705	0.616	0.387	0.191	0.105	

Fitting of Time Based Breakage Rate (S_i)

S_i (min⁻¹)	0.137				
$w_i(t) = w_i(0)\exp(-S_i t)$	t (min)	w_i(t) measured	w_i(t) model	SSQ Error	
	0	0.971	0.971	0.0000	
	1.9	0.705	0.744	0.0032	
	3.8	0.616	0.575	0.0044	
	7.9	0.387	0.328	0.0232	
	11.8	0.191	0.192	0.0000	
	15.7	0.105	0.112	0.0041	
				0.0350	



Fitting of Energy Normalised Breakage Rate (S_i^E)

S_i^E (kWh/t¹)	0.107				
$w_i(E) = w_i(0)\exp[-S_i^E E]$	E (kWh/t¹)	w_i(E) measured	w_i(E) model	SSQ Error	
	0	0.971	0.971	0.0000	
	2.6	0.705	0.737	0.0021	
	5.1	0.616	0.564	0.0071	
	10.1	0.387	0.330	0.0212	
	15.2	0.191	0.192	0.0000	
	20.2	0.105	0.112	0.0046	
				0.0350	

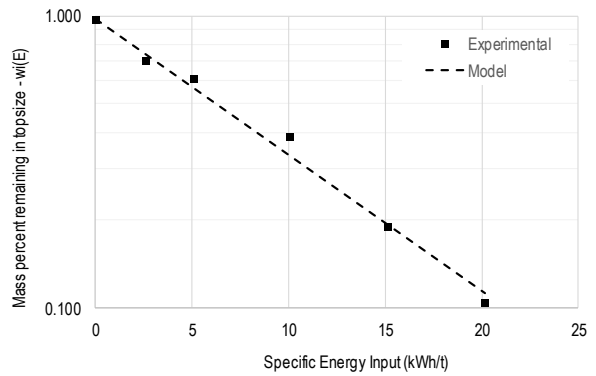
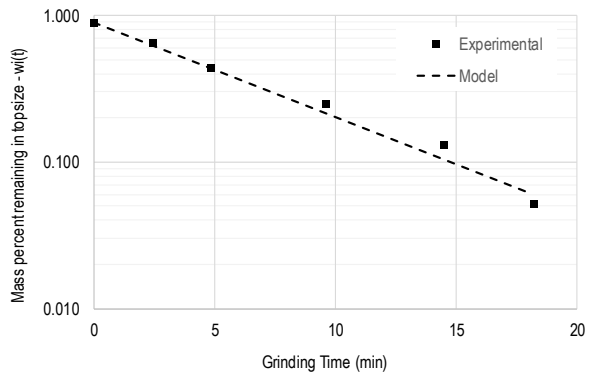


Table 64: Test M-5 Breakage Rates

Test ID	Test M-5			w_i(0)	0.897 fraction	
Feed	-106 + 75 µm silica			S_i	0.149 min ⁻¹	
Geometry	12-pin stirrer in smooth vessel			S_i^E	0.138 kWh/t ¹	
Speed	400 RPM			Average Power	81.5 Watt	
Energy input	kWh/t	2.57	5.06	10.13	15.11	19.9
Time	seconds	144	289	575	870	1090
	minutes	2.4	4.8	9.6	14.5	18.2
Mill power	Watt	82.0	80.5	81.0	79.8	83.9
Silica feed mass	gram	1277	1277	1277	1277	1277
Sieving results						
+75µm	gram	81.04	56.92	33.40	17.10	6.50
-75µm	gram	44.82	73.26	101.10	112.10	119.50
Total	gram	125.86	130.18	134.50	129.20	126.00
Feed size remaining (w _i)	fraction	0.644	0.437	0.248	0.132	0.052

Fitting of Time Based Breakage Rate (S_i)

S _i (min ⁻¹)	0.149				
$w_i(t) = w_i(0)\exp(-S_i t)$	t (min)	w_i(t) measured	w_i(t) model	SSQ Error	
	0	0.897	0.897	0.0000	
	2.4	0.644	0.628	0.0006	
	4.8	0.437	0.439	0.0000	
	9.6	0.248	0.216	0.0170	
	14.5	0.132	0.104	0.0460	
	18.2	0.052	0.060	0.0284	
				0.0921	



Fitting of Energy Normalised Breakage Rate (S_i^E)

S _i ^E (kWh/t ¹)	0.138				
$w_i(E) = w_i(0)\exp[-S_i^E E]$	E (kWh/t ¹)	w(E) measured	w(E) model	SSQ Error	
	0	0.897	0.897	0.0000	
	2.6	0.644	0.630	0.0005	
	5.1	0.437	0.447	0.0005	
	10.1	0.248	0.223	0.0107	
	15.1	0.132	0.112	0.0231	
	19.9	0.052	0.058	0.0158	
				0.0505	

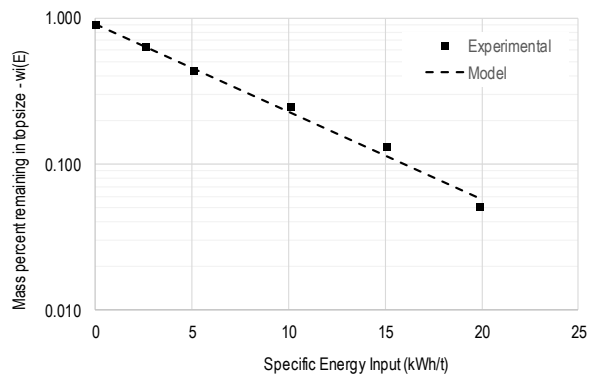


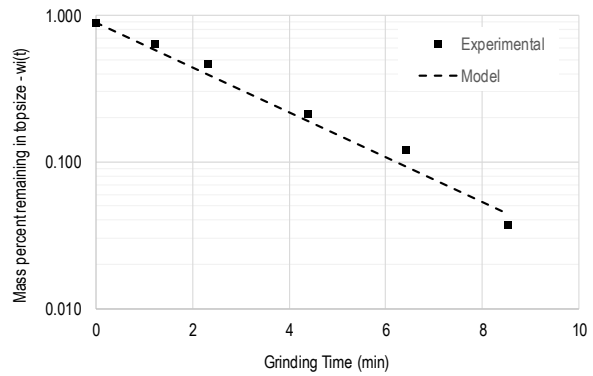
Table 65: Test M-6 Breakage Rates

Test ID	Test M-6			w_i(0)	0.897 fraction	
Feed	-106 + 75 µm silica			S_i	0.353 min ⁻¹	
Geometry	12-pin stirrer in disc vessel			S_i^E	0.148 kWh/t ¹	
Speed	400 RPM			Average Power	176.6 Watt	
Energy input	kWh/t	2.63	5.18	10.28	15.23	20.43
Time	seconds	73	139	263	384	511
	minutes	1.2	2.3	4.4	6.4	8.5
Mill power	Watt	165.6	171.3	179.7	182.3	183.8
Silica feed mass	gram	1277	1277	1277	1277	1277
Sieving results						
+75µm	gram	74.00	58.80	27.70	15.30	4.30
-75µm	gram	43.22	67.69	103.10	110.70	110.40
Total	gram	117.22	126.49	130.80	126.00	114.70
Feed size remaining (w _i)	fraction	0.631	0.465	0.212	0.121	0.037

Fitting of Time Based Breakage Rate (S_i)

S_i (min⁻¹) 0.353

$w_i(t) = w_i(0)\exp(-S_i t)$	t (min)	w _i (t) measured	w _i (t) model	SSQ Error
	0	0.897	0.897	0.0000
	1.2	0.631	0.584	0.0056
	2.3	0.465	0.396	0.0218
	4.4	0.212	0.191	0.0095
	6.4	0.121	0.094	0.0516
	8.5	0.037	0.044	0.0348
				0.1232



Fitting of Energy Normalised Breakage Rate (S_i^E)

S_i^E (kWh/t¹) 0.148

$w_i(E) = w_i(0)\exp[-S_i^E E]$	E (kWh/t ¹)	w _i (E) measured	w _i (E) model	SSQ Error
	0	0.897	0.897	0.0000
	2.6	0.631	0.608	0.0014
	5.2	0.465	0.417	0.0106
	10.3	0.212	0.196	0.0055
	15.2	0.121	0.094	0.0501
	20.4	0.037	0.044	0.0272
				0.0947

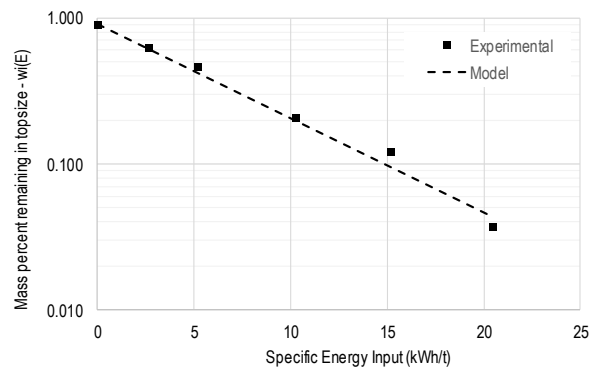
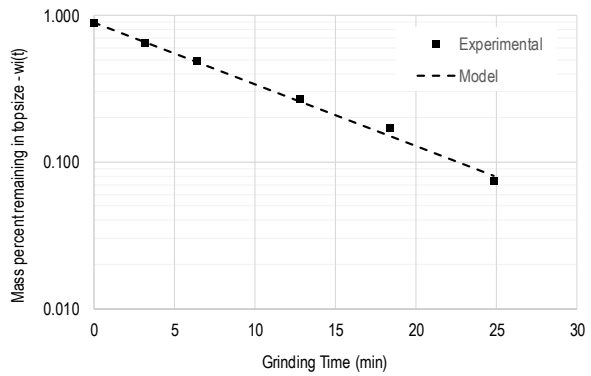


Table 66: Test M-7 Breakage Rates

Test ID	Test M-7					w_i(0)	0.897 fraction
Feed	-106 + 75 μm silica					S_i	0.097 min ⁻¹
Geometry	Ring stirrer in smooth vessel					S_i^E	0.120 kWh/t ¹
Speed	400 RPM					Average Power	61.6 Watt
Energy input	kWh/t	2.55	5.04	10.09	15.08	20.14	
Time	seconds	190	382	765	1099	1491	
	minutes	3.2	6.4	12.8	18.3	24.9	
Mill power	Watt	61.7	60.7	60.6	63.1	62.1	
Silica feed mass	gram	1277	1277	1277	1277	1277	
Sieving results							
+75μm	gram	80.26	61.49	34.70	21.50	9.40	
-75μm	gram	44.29	62.70	93.20	103.80	116.80	
Total	gram	124.55	124.19	127.90	125.30	126.20	
Feed size remaining (w _i)	fraction	0.644	0.495	0.271	0.172	0.074	

Fitting of Time Based Breakage Rate (S_i)

S_i (min⁻¹)		0.097			
$w_i(t) = w_i(0)\exp(-S_i t)$	t (min)	w_i(t) measured	w_i(t) model	SSQ Error	
	0	0.897	0.897	0.0000	
	3.2	0.644	0.660	0.0006	
	6.4	0.495	0.484	0.0005	
	12.8	0.271	0.261	0.0014	
	18.3	0.172	0.152	0.0126	
	24.9	0.074	0.081	0.0075	
				0.0226	



Fitting of Energy Normalised Breakage Rate (S_i^E)

S_i^E (kWh/t¹)		0.120			
$w_i(E) = w_i(0)\exp[-S_i^E E]$	E (kWh/t¹)	w_i(E) measured	w_i(E) model	SSQ Error	
	0	0.897	0.897	0.0000	
	2.6	0.644	0.662	0.0007	
	5.0	0.495	0.491	0.0001	
	10.1	0.271	0.269	0.0001	
	15.1	0.172	0.148	0.0190	
	20.1	0.074	0.081	0.0072	
				0.0270	

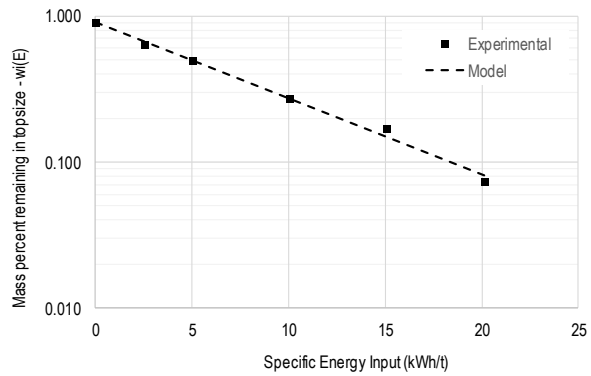
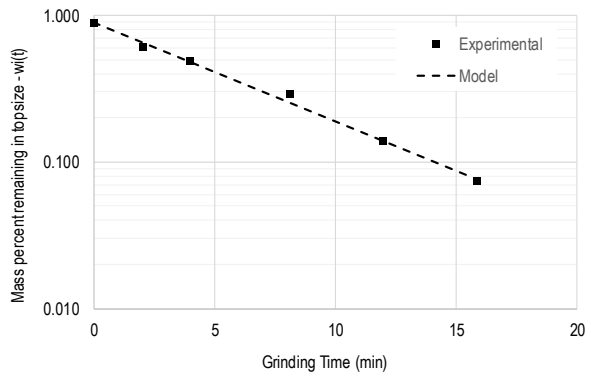


Table 67: Test M-8 Breakage Rates

Test ID	Test M-8			w_i(0)	0.897 fraction	
Feed	-106 + 75 µm silica			S_i	0.156 min ⁻¹	
Geometry	Ring stirrer in disc vessel			S_i^E	0.122 kWh/t ¹	
Speed	400 RPM			Average Power	97.5 Watt	
Energy input	kWh/t	2.57	5.07	10.14	15.14	20.22
Time	seconds	121	236	484	717	950
	minutes	2.0	3.9	8.1	12.0	15.8
Mill power	Watt	97.6	98.8	96.3	97.1	97.8
Silica feed mass	gram	1277	1277	1277	1277	1277
Sieving results						
+75µm	gram	73.68	63.81	38.64	18.48	9.29
-75µm	gram	46.56	65.76	94.52	114.98	117.22
Total	gram	120.24	129.57	133.16	133.46	126.51
Feed size remaining (w _i)	fraction	0.613	0.492	0.290	0.138	0.073

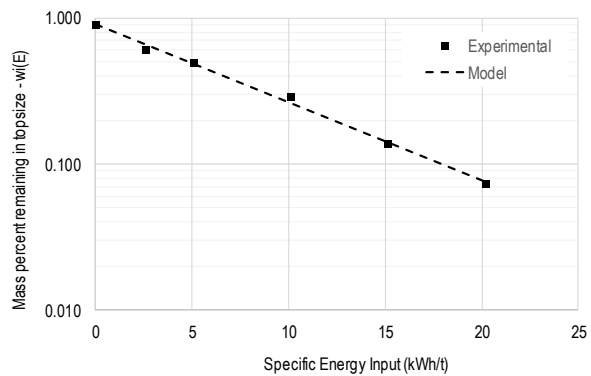
Fitting of Time Based Breakage Rate (S_i)

S _i (min ⁻¹)	0.156				
$w_i(t) = w_i(0)\exp(-S_i t)$	t	w_i(t)	w_i(t)	SSQ	
	(min)	measured	model	Error	
	0	0.897	0.897	0.0000	
	2.0	0.613	0.656	0.0049	
	3.9	0.492	0.486	0.0002	
	8.1	0.290	0.256	0.0142	
	12.0	0.138	0.140	0.0001	
	15.8	0.073	0.076	0.0015	
				0.0208	



Fitting of Energy Normalised Breakage Rate (S_i^E)

S _i ^E (kWh/t ¹)	0.122				
$w_i(E) = w_i(0)\exp[-S_i^E E]$	E	w_i(E)	w_i(E)	SSQ	
	(kWh/t ¹)	measured	model	Error	
	0	0.897	0.897	0.0000	
	2.6	0.613	0.655	0.0048	
	5.1	0.492	0.483	0.0004	
	10.1	0.290	0.259	0.0112	
	15.1	0.138	0.141	0.0003	
	20.2	0.073	0.076	0.0009	
				0.0175	



7.11 Experimental Results – Silica Flour Grinding Tests

Table 68: Test N-1 PSD Data

Test N-1: Silica Flour - Pin Smooth 270RPM

PSD Data Set 1

Sieve size (μm)	Mass (g)	Mass %	Cumulative % Passing	Mass(g)	Mass %	Cumulative % Passing	Mass(g)	Mass %	Cumulative % Passing
212	0.00	0.00	100.00	0.00	0.00	100.00	0.00	0.00	100.00
150	0.00	0.00	100.00	0.00	0.00	100.00	0.00	0.00	100.00
106	0.19	0.30	99.70	0.13	0.21	99.79	0.10	0.13	99.87
75	2.47	3.85	95.85	0.72	1.18	98.61	0.20	0.26	99.61
53	6.89	10.75	85.10	3.20	5.24	93.37	1.00	1.29	98.32
38	7.62	11.89	73.21	5.79	9.47	83.90	0.20	0.26	98.06
-38	46.92	73.21		51.27	83.90		76.00	98.06	
	64.09			61.11			77.50		

PSD Data Set 2

Sieve size (μm)	Mass (g)	Mass %	Cumulative % Passing	Mass(g)	Mass %	Cumulative % Passing	Mass(g)	Mass %	Cumulative % Passing
212	0.00	0.00	100.00	0.00	0.00	100.00	0.00	0.00	100.00
150	0.00	0.00	100.00	0.00	0.00	100.00	0.00	0.00	100.00
106	0.21	0.38	99.62	0.12	0.21	99.79	0.04	0.07	99.93
75	1.67	3.05	96.57	0.74	1.30	98.49	0.31	0.54	99.39
53	5.63	10.28	86.29	2.68	4.71	93.79	1.03	1.81	97.58
38	6.87	12.54	73.75	4.97	8.73	85.06	1.67	2.93	94.65
-38	40.41	73.75		48.45	85.06		53.94	94.65	
	54.79			56.96			56.99		

Table 69: Test N-2 PSD Data

Test N-2: Silica Flour - Pin Disc 270RPM

PSD Data Set 1

Sieve size (µm)	Mass (g)	Mass %	Cumulative % Passing	Mass(g)	Mass %	Cumulative % Passing	Mass(g)	Mass %	Cumulative % Passing
212	0.00	0.00	100.00	0.00	0.00	100.00	0.00	0.00	100.00
150	0.00	0.00	100.00	0.00	0.00	100.00	0.00	0.00	100.00
106	0.20	0.29	99.71	0.00	0.00	100.00	0.00	0.00	100.00
75	2.00	2.86	96.85	1.10	1.46	98.54	0.20	0.31	99.69
53	5.70	8.15	88.70	3.20	4.23	94.31	0.60	0.92	98.78
38	8.80	12.59	76.11	6.60	8.73	85.58	1.70	2.60	96.18
-38	53.20	76.11		64.70	85.58		62.90	96.18	
	69.90			75.60			65.40		

PSD Data Set 2

Sieve size (µm)	Mass (g)	Mass %	Cumulative % Passing	Mass(g)	Mass %	Cumulative % Passing	Mass(g)	Mass %	Cumulative % Passing
212	0.00	0.00	100.00	0.00	0.00	100.00	0.00	0.00	100.00
150	0.00	0.00	100.00	0.00	0.00	100.00	0.07	0.13	99.87
106	0.16	0.29	99.71	0.08	0.15	99.85	0.09	0.16	99.71
75	1.49	2.65	97.06	0.51	0.95	98.90	0.45	0.81	98.90
53	5.38	9.58	87.48	2.25	4.20	94.69	1.11	2.01	96.89
38	6.70	11.93	75.54	4.54	8.48	86.21	1.69	3.06	93.83
-38	42.41	75.54		46.13	86.21		51.85	93.83	
	56.14			53.51			55.26		

Table 70: Test N-3 PSD Data

Test N-3: Silica Flour - Ring Smooth 270RPM

PSD Data Set 1

Sieve size (µm)	Mass (g)	Mass %	Cumulative % Passing	Mass(g)	Mass %	Cumulative % Passing	Mass(g)	Mass %	Cumulative % Passing
212	0.00	0.00	100.00	0.00	0.00	100.00	0.00	0.00	100.00
150	0.00	0.00	100.00	0.00	0.00	100.00	0.00	0.00	100.00
106	0.17	0.30	99.70	0.12	0.22	99.78	0.09	0.16	99.84
75	1.57	2.77	96.93	0.54	1.00	98.78	0.15	0.27	99.57
53	5.74	10.14	86.78	2.98	5.52	93.25	1.03	1.86	97.71
38	7.73	13.66	73.12	5.23	9.69	83.56	1.74	3.14	94.57
-38	41.38	73.12		45.09	83.56		52.47	94.57	
	56.59			53.96			55.48		

PSD Data Set 2

Sieve size (µm)	Mass (g)	Mass %	Cumulative % Passing	Mass(g)	Mass %	Cumulative % Passing	Mass(g)	Mass %	Cumulative % Passing
212	0.00	0.00	100.00	0.00	0.00	100.00	0.00	0.00	100.00
150	0.02	0.03	99.97	0.00	0.00	100.00	0.00	0.00	100.00
106	0.30	0.50	99.46	0.13	0.24	99.76	0.06	0.11	99.89
75	2.13	3.57	95.90	0.88	1.64	98.12	0.31	0.57	99.32
53	5.97	10.00	85.90	3.06	5.69	92.43	0.81	1.48	97.84
38	8.05	13.48	72.41	5.55	10.32	82.11	1.80	3.29	94.56
-38	43.23	72.41		44.15	82.11		51.75	94.56	
	59.70			53.77			54.73		

Table 71: Test N-4 PSD Data

Test N-4: Silica Flour - Ring Disc 270RPM

PSD Data Set 1

Sieve size (µm)	Mass (g)	Mass %	Cumulative % Passing	Mass(g)	Mass %	Cumulative % Passing	Mass(g)	Mass %	Cumulative % Passing
212	0.00	0.00	100.00	0.00	0.00	100.00	0.00	0.00	100.00
150	0.00	0.00	100.00	0.00	0.00	100.00	0.00	0.00	100.00
106	0.27	0.38	99.62	0.23	0.32	99.68	0.15	0.18	99.82
75	2.12	2.99	96.63	1.26	1.76	97.92	0.63	0.76	99.05
53	6.54	9.21	87.42	3.88	5.41	92.51	1.68	2.04	97.02
38	9.82	13.83	73.59	7.24	10.10	82.41	2.70	3.28	93.74
-38	52.24	73.59		59.07	82.41		77.27	93.74	
	70.99			71.68			82.43		

PSD Data Set 2

Sieve size (µm)	Mass (g)	Mass %	Cumulative % Passing	Mass(g)	Mass %	Cumulative % Passing	Mass(g)	Mass %	Cumulative % Passing
212	0.00	0.00	100.00	0.00	0.00	100.00	0.00	0.00	100.00
150	0.00	0.00	100.00	0.00	0.00	100.00	0.00	0.00	100.00
106	0.19	0.36	99.64	0.15	0.28	99.72	0.00	0.00	100.00
75	1.53	2.89	96.75	0.98	1.81	97.91	0.10	0.21	99.79
53	4.99	9.44	87.31	3.24	5.98	91.93	0.51	1.06	98.73
38	7.25	13.72	73.59	5.39	9.95	81.98	1.55	3.23	95.50
-38	38.90	73.59		44.39	81.98		45.83	95.50	
	52.86			54.15			47.99		

Table 72: Test N-5 PSD Data

Test N-5: Silica Flour - Pin Smooth 400RPM

PSD Data Set 1

Sieve size (μm)	Mass (g)	Mass %	Cumulative % Passing	Mass(g)	Mass %	Cumulative % Passing	Mass(g)	Mass %	Cumulative % Passing
212	0.01	0.01	99.99	0.11	0.15	99.85	0.01	0.01	99.99
150	0.11	0.16	99.83	0.11	0.15	99.69	0.01	0.01	99.97
106	0.30	0.43	99.39	0.20	0.28	99.41	0.04	0.06	99.92
75	2.36	3.41	95.98	0.74	1.04	98.37	0.09	0.13	99.79
53	6.81	9.85	86.12	3.31	4.64	93.74	0.27	0.38	99.41
38	9.78	14.15	71.97	6.72	9.41	84.32	0.59	0.82	98.59
-38	49.74	71.97		60.19	84.32		70.74	98.59	
	69.11			71.38			71.75		

PSD Data Set 2

Sieve size (μm)	Mass (g)	Mass %	Cumulative % Passing	Mass(g)	Mass %	Cumulative % Passing	Mass(g)	Mass %	Cumulative % Passing
212	0.00	0.00	100.00	0.00	0.00	100.00	0.00	0.00	100.00
150	0.05	0.09	99.91	0.07	0.14	99.86	0.00	0.00	100.00
106	0.34	0.62	99.29	0.14	0.28	99.58	0.05	0.09	99.91
75	2.09	3.81	95.47	0.65	1.30	98.28	0.10	0.19	99.72
53	6.21	11.33	84.14	2.52	5.03	93.25	0.29	0.54	99.17
38	6.97	12.72	71.42	4.85	9.69	83.56	0.85	1.59	97.58
-38	39.14	71.42		41.83	83.56		52.01	97.58	
	54.80			50.06			53.30		

Table 73: Test N-6 PSD Data

Test N-6: Silica Flour - Pin Disc 400RPM

PSD Data Set 1

Sieve size (μm)	Mass (g)	Mass %	Cumulative % Passing	Mass(g)	Mass %	Cumulative % Passing	Mass(g)	Mass %	Cumulative % Passing
212	0.00	0.00	100.00	0.00	0.00	100.00	0.00	0.00	100.00
150	0.00	0.00	100.00	0.00	0.00	100.00	0.00	0.00	100.00
106	0.30	0.40	99.60	0.10	0.13	99.87	0.00	0.00	100.00
75	2.80	3.77	95.82	1.00	1.31	98.56	0.20	0.28	99.72
53	7.00	9.43	86.39	3.30	4.31	94.26	0.50	0.69	99.03
38	9.10	12.26	74.12	5.20	6.79	87.47	1.30	1.80	97.23
-38	55.00	74.12		67.00	87.47		70.30	97.23	
	74.20			76.60			72.30		

PSD Data Set 2

Sieve size (μm)	Mass (g)	Mass %	Cumulative % Passing	Mass(g)	Mass %	Cumulative % Passing	Mass(g)	Mass %	Cumulative % Passing
212	0.00	0.00	100.00	0.00	0.00	100.00	0.00	0.00	100.00
150	0.07	0.11	99.89	0.00	0.00	100.00	0.00	0.00	100.00
106	0.27	0.43	99.46	0.07	0.12	99.88	0.00	0.00	100.00
75	2.12	3.38	96.08	0.39	0.67	99.21	0.08	0.14	99.86
53	6.45	10.28	85.81	2.64	4.55	94.65	0.37	0.65	99.20
38	8.37	13.33	72.47	4.93	8.50	86.15	1.13	2.00	97.21
-38	45.49	72.47		49.96	86.15		54.97	97.21	
	62.77			57.99			56.55		

Table 74: Test N-7 PSD Data

Test N-7: Silica Flour - Ring Smooth 400RPM

PSD Data Set 1

Sieve size (μm)	Mass (g)	Mass %	Cumulative % Passing	Mass(g)	Mass %	Cumulative % Passing	Mass(g)	Mass %	Cumulative % Passing
212	0.00	0.00	100.00	0.00	0.00	100.00	0.07	0.09	99.91
150	0.00	0.00	100.00	0.07	0.14	99.86	0.07	0.09	99.81
106	0.41	0.59	99.41	0.06	0.12	99.73	0.09	0.12	99.69
75	2.28	3.29	96.12	0.49	1.01	98.72	0.17	0.23	99.47
53	8.23	11.87	84.25	2.66	5.51	93.21	0.59	0.78	98.68
38	9.52	13.73	70.52	4.74	9.82	83.39	1.91	2.54	96.14
-38	48.90	70.52		40.27	83.39		72.31	96.14	
	69.34			48.29			75.21		

PSD Data Set 2

Sieve size (μm)	Mass (g)	Mass %	Cumulative % Passing	Mass(g)	Mass %	Cumulative % Passing	Mass(g)	Mass %	Cumulative % Passing
212	0.00	0.00	100.00	0.00	0.00	100.00	0.00	0.00	100.00
150	0.00	0.00	100.00	0.10	0.21	99.79	0.00	0.00	100.00
106	0.24	0.44	99.56	0.13	0.27	99.52	0.00	0.00	100.00
75	2.04	3.71	95.85	0.65	1.35	98.18	0.12	0.29	99.71
53	6.58	11.98	83.87	2.53	5.25	92.93	0.40	0.98	98.73
38	6.53	11.89	71.99	4.93	10.22	82.71	1.12	2.75	95.98
-38	39.55	71.99		39.89	82.71		39.16	95.98	
	54.94			48.23			40.80		

Table 75: Test N-8 PSD Data

Test N-8: Silica Flour - Ring Disc 400RPM

PSD Data Set 1

Sieve size (µm)	Mass (g)	Mass %	Cumulative % Passing	Mass(g)	Mass %	Cumulative % Passing	Mass(g)	Mass %	Cumulative % Passing
212	0.03	0.05	99.95	0.00	0.00	100.00	0.00	0.00	100.00
150	0.06	0.09	99.86	0.00	0.00	100.00	0.00	0.00	100.00
106	0.22	0.34	99.52	0.22	0.28	99.72	0.00	0.00	100.00
75	2.18	3.36	96.16	0.97	1.23	98.49	0.13	0.17	99.83
53	6.67	10.29	85.87	3.95	5.01	93.48	0.53	0.68	99.16
38	8.94	13.79	72.08	7.81	9.90	83.58	1.83	2.34	96.82
-38	46.72	72.08		65.91	83.58		75.83	96.82	
	64.82			78.86			78.32		

PSD Data Set 2

Sieve size (µm)	Mass (g)	Mass %	Cumulative % Passing	Mass(g)	Mass %	Cumulative % Passing	Mass(g)	Mass %	Cumulative % Passing
212	0.00	0.00	100.00	0.00	0.00	100.00	0.00	0.00	100.00
150	0.14	0.29	99.71	0.06	0.10	99.90	0.00	0.00	100.00
106	0.30	0.62	99.09	0.17	0.30	99.60	0.00	0.00	100.00
75	1.56	3.21	95.88	0.73	1.27	98.33	0.09	0.17	99.83
53	4.99	10.28	85.61	3.00	5.21	93.12	0.35	0.65	99.18
38	6.14	12.64	72.96	4.93	8.57	84.55	1.20	2.24	96.94
-38	35.43	72.96		48.64	84.55		51.88	96.94	
	48.56			57.53			53.52		

Table 76: Test N-9 PSD Data

Test N-9: Silica Flour - Pin Smooth 530RPM

PSD Data Set 1

Sieve size (µm)	Mass (g)	Mass %	Cumulative % Passing	Mass(g)	Mass %	Cumulative % Passing	Mass(g)	Mass %	Cumulative % Passing
212	0.00	0.00	100.00	0.00	0.00	100.00	0.00	0.00	100.00
150	0.07	0.10	99.90	0.10	0.13	99.87	0.03	0.04	99.96
106	0.19	0.26	99.65	0.10	0.13	99.75	0.01	0.01	99.95
75	1.70	2.31	97.33	1.00	1.25	98.50	0.02	0.03	99.92
53	5.78	7.87	89.47	3.20	4.01	94.49	0.09	0.12	99.80
38	10.14	13.80	75.67	6.20	7.77	86.72	0.59	0.79	99.01
-38	55.60	75.67		69.20	86.72		74.13	99.01	
	73.48			79.80			74.87		

PSD Data Set 2

Sieve size (µm)	Mass (g)	Mass %	Cumulative % Passing	Mass(g)	Mass %	Cumulative % Passing	Mass(g)	Mass %	Cumulative % Passing
212	0.00	0.00	100.00	0.00	0.00	100.00	0.00	0.00	100.00
150	0.05	0.08	99.92	0.00	0.00	100.00	0.00	0.00	100.00
106	0.21	0.36	99.56	0.10	0.18	99.82	0.00	0.00	100.00
75	1.63	2.76	96.80	0.55	1.02	98.80	0.00	0.00	100.00
53	5.48	9.28	87.51	2.34	4.32	94.48	0.11	0.20	99.80
38	7.69	13.03	74.49	4.39	8.11	86.37	0.45	0.81	98.99
-38	43.97	74.49		46.78	86.37		54.80	98.99	
	59.03			54.16			55.36		

Table 77: Test N-10 PSD Data

Test N-10: Silica Flour - Pin Disc 530RPM

PSD Data Set 1

Sieve size (μm)	Mass (g)	Mass %	Cumulative % Passing	Mass(g)	Mass %	Cumulative % Passing	Mass(g)	Mass %	Cumulative % Passing
212	0.00	0.00	100.00	0.00	0.00	100.00	0.00	0.00	100.00
150	0.10	0.13	99.87	0.03	0.04	99.96	0.00	0.00	100.00
106	0.10	0.13	99.75	0.01	0.01	99.94	0.00	0.00	100.00
75	2.40	3.03	96.72	0.32	0.47	99.47	0.10	0.13	99.87
53	6.80	8.59	88.13	1.62	2.39	97.08	0.30	0.38	99.49
38	9.10	11.49	76.64	5.53	8.17	88.91	1.30	1.65	97.84
-38	60.70	76.64		60.21	88.91		77.00	97.84	
	79.20			67.72			78.70		

PSD Data Set 2

Sieve size (μm)	Mass (g)	Mass %	Cumulative % Passing	Mass(g)	Mass %	Cumulative % Passing	Mass(g)	Mass %	Cumulative % Passing
212	0.00	0.00	100.00	0.00	0.00	100.00	0.00	0.00	100.00
150	0.04	0.07	99.93	0.06	0.12	99.88	0.00	0.00	100.00
106	0.24	0.44	99.49	0.05	0.10	99.77	0.00	0.00	100.00
75	1.48	2.71	96.78	0.26	0.54	99.23	0.06	0.10	99.90
53	4.93	9.03	87.75	1.29	2.67	96.56	0.37	0.60	99.30
38	5.79	10.61	77.14	3.75	7.76	88.80	1.35	2.20	97.10
-38	42.11	77.14		42.91	88.80		59.66	97.10	
	54.59			48.32			61.44		

Table 78: Test N-11 PSD Data

Test N-11: Silica Flour - Ring Smooth 530RPM

PSD Data Set 1

Sieve size (μm)	Mass (g)	Mass %	Cumulative % Passing	Mass(g)	Mass %	Cumulative % Passing	Mass(g)	Mass %	Cumulative % Passing
212	0.00	0.00	100.00	0.01	0.01	99.99	0.00	0.00	100.00
150	0.10	0.18	99.82	0.05	0.07	99.91	0.01	0.01	99.99
106	0.16	0.28	99.54	0.12	0.18	99.73	0.01	0.01	99.97
75	1.21	2.14	97.40	0.72	1.07	98.66	0.07	0.09	99.88
53	5.64	9.97	87.43	2.69	3.99	94.67	0.26	0.35	99.53
38	7.49	13.24	74.19	5.22	7.75	86.92	1.16	1.54	97.99
-38	41.97	74.19		58.56	86.92		73.70	97.99	
	56.57			67.37			75.21		

PSD Data Set 2

Sieve size (μm)	Mass (g)	Mass %	Cumulative % Passing	Mass(g)	Mass %	Cumulative % Passing	Mass(g)	Mass %	Cumulative % Passing
212	0.00	0.00	100.00	0.00	0.00	100.00	0.00	0.00	100.00
150	0.06	0.11	99.89	0.00	0.00	100.00	0.00	0.00	100.00
106	0.24	0.42	99.47	0.05	0.10	99.90	0.11	0.21	99.79
75	1.67	2.96	96.51	0.48	1.01	98.89	0.14	0.27	99.52
53	5.56	9.84	86.67	1.95	4.08	94.81	0.15	0.29	99.24
38	7.86	13.92	72.75	4.13	8.65	86.16	0.71	1.35	97.89
-38	41.09	72.75		41.14	86.16		51.47	97.89	
	56.48			47.75			52.58		

Table 79: Test N-12 PSD Data

Test N-12: Silica Flour - Ring Disc 530RPM

PSD Data Set 1

Sieve size (μm)	Mass (g)	Mass %	Cumulative % Passing	Mass(g)	Mass %	Cumulative % Passing	Mass(g)	Mass %	Cumulative % Passing
212	0.00	0.00	100.00	0.00	0.00	100.00	0.00	0.00	100.00
150	0.05	0.07	99.93	0.00	0.00	100.00	0.00	0.00	100.00
106	0.38	0.50	99.43	0.09	0.12	99.88	0.00	0.00	100.00
75	2.73	3.61	95.82	0.64	0.88	98.99	0.00	0.00	100.00
53	8.05	10.66	85.16	3.14	4.33	94.66	0.33	0.42	99.58
38	9.19	12.17	72.99	6.78	9.36	85.30	1.37	1.73	97.85
-38	55.12	72.99		61.79	85.30		77.52	97.85	
	75.52			72.44			79.22		

PSD Data Set 2

Sieve size (μm)	Mass (g)	Mass %	Cumulative % Passing	Mass(g)	Mass %	Cumulative % Passing	Mass(g)	Mass %	Cumulative % Passing
212	0.00	0.00	100.00	0.00	0.00	100.00	0.00	0.00	100.00
150	0.06	0.12	99.88	0.00	0.00	100.00	0.00	0.00	100.00
106	0.18	0.35	99.53	0.08	0.14	99.86	0.00	0.00	100.00
75	1.41	2.74	96.80	0.44	0.76	99.11	0.00	0.00	100.00
53	5.05	9.80	87.00	2.17	3.72	95.38	0.19	0.36	99.64
38	6.82	13.24	73.76	4.95	8.50	86.89	0.79	1.52	98.12
-38	38.01	73.76		50.62	86.89		51.13	98.12	
	51.53			58.26			52.11		

Table 80: Test N-1 Milling Data

Test N-1: Silica Flour - Pin Smooth 270RPM

Average Power (Watt)

43.8 Watt

Energy Input	5.1 kWh/t	10.1 kWh/t	20.1 kWh/t
Milling Time (min)	8.7 min	17.77 min	34.9 min
Power Draw (Watt)	44.4 W	43.2 W	44 W
Sieve size (µm)	Cumulative % Passing	Cumulative % Passing	Cumulative % Passing
212	100.00	100.00	100.00
150	100.00	100.00	100.00
106	99.66	99.79	99.90
75	96.21	98.55	99.50
53	85.70	93.58	97.95
38	73.48	84.48	96.36

% Passing 38µm	Energy (kWh/t)	Time (min)
65	1.4	2.47
70	3.6	6.14
75	5.7	9.95
80	8.0	14.07
85	10.5	18.52

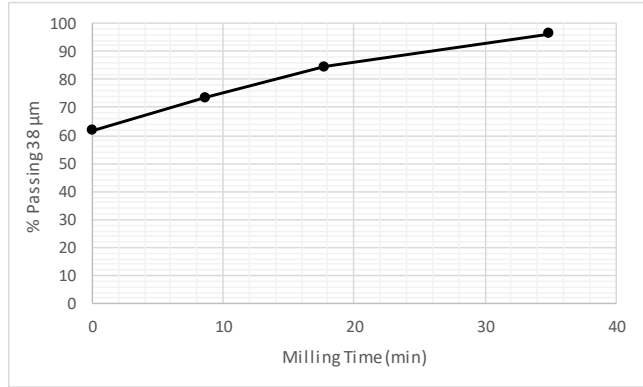
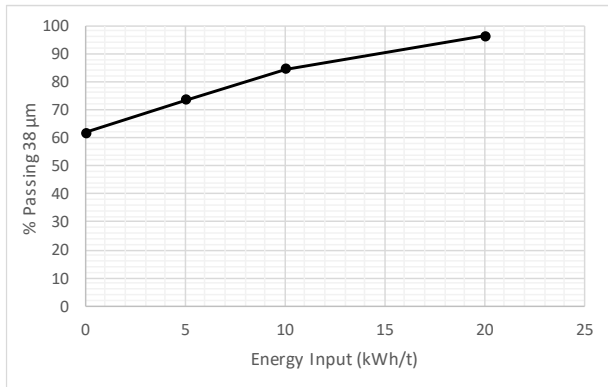


Table 81: Test N-2 Milling Data

Test N-2: Silica Flour - Pin Disc 270RPM

Average Power (Watt)

82.3 Watt

Energy Input	5.1 kWh/t	10.1 kWh/t	20.1 kWh/t
Milling Time (min)	4.59 min	9.19 min	19.37 min
Power Draw (Watt)	84.2 W	83.7 W	79.2 W
Sieve size (µm)	Cumulative % Passing	Cumulative % Passing	Cumulative % Passing
212	100.00	100.00	100.00
150	100.00	100.00	99.94
106	99.71	99.93	99.86
75	96.96	98.72	99.30
53	88.09	94.50	97.83
38	75.83	85.90	95.00

Grind Size % Passing	Energy (kWh/t)	Time (min)
65	1.2	1.09
70	3.0	2.70
75	4.7	4.32
80	7.1	6.49
85	9.6	8.77

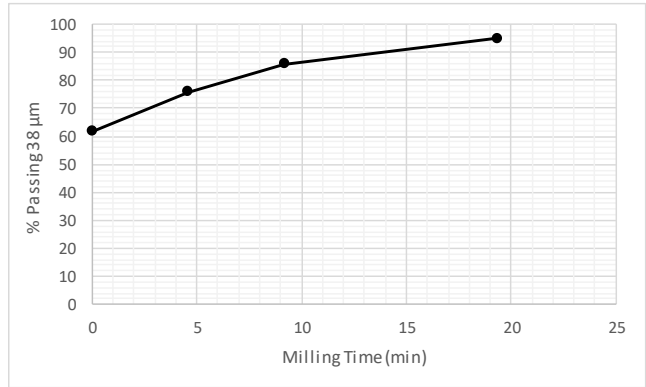
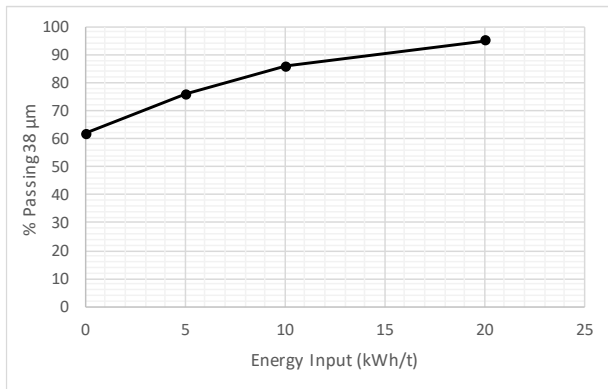


Table 82: Test N-3 Milling Data

Test N-3: Silica Flour - Ring Smooth 270RPM

Average Power (Watt)

31.9 Watt

Energy Input	5.1 kWh/t	10.1 kWh/t	20.1 kWh/t
Milling Time (min)	11.67 min	24.07 min	49.52 min
Power Draw (Watt)	33 W	31.9 W	31 W
Sieve size (µm)	Cumulative % Passing	Cumulative % Passing	Cumulative % Passing
212	100.00	100.00	100.00
150	99.98	100.00	100.00
106	99.58	99.77	99.86
75	96.41	98.45	99.45
53	86.34	92.84	97.78
38	72.77	82.84	94.56

Grind Size % Passing	Energy (kWh/t)	Time (min)
65	1.5	3.52
70	3.8	8.76
75	6.1	14.42
80	8.6	20.57
85	11.9	28.76

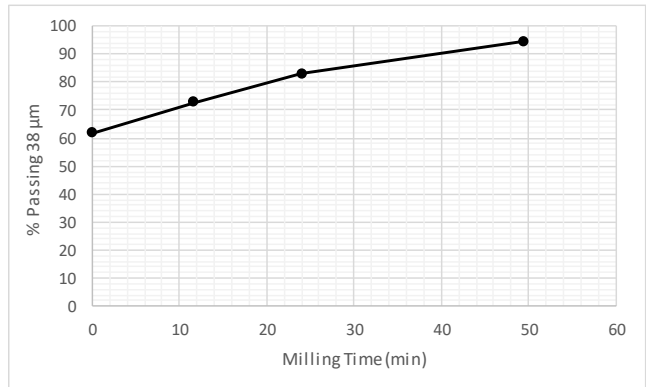
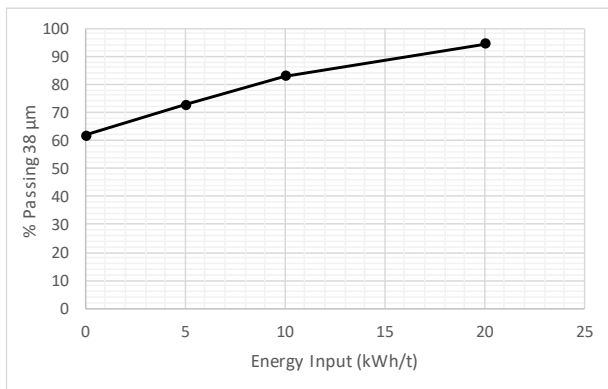


Table 83: Test N-4 Milling Data

Test N-4: Silica Flour - Ring Disc 270RPM

Average Power (Watt)

48.9 Watt

Energy Input	5.1 kWh/t	10.1 kWh/t	20.1 kWh/t
Milling Time (min)	7.79 min	15.65 min	31.64 min
Power Draw (Watt)	49.4 W	49.1 W	48.5 W
Sieve size (µm)	Cumulative % Passing	Cumulative % Passing	Cumulative % Passing
212	100.00	100.00	100.00
150	100.00	100.00	100.00
106	99.63	99.70	99.91
75	96.69	97.92	99.42
53	87.36	92.22	97.87
38	73.59	82.19	94.62

Grind Size % Passing	Energy (kWh/t)	Time (min)
65	1.4	2.19
70	3.5	5.45
75	5.8	9.07
80	8.8	13.65
85	12.3	19.26

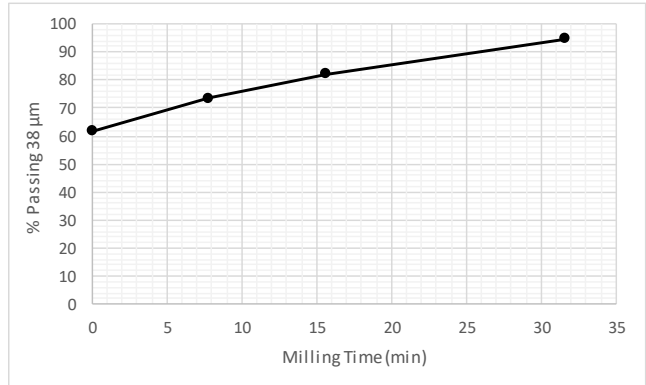
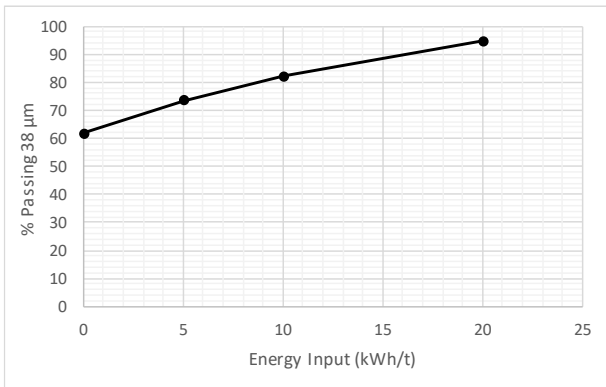


Table 84: Test N-5 Milling Data

Test N-5: Silica Flour - Pin Smooth 400RPM

Average Power (Watt)

82.3 Watt

Energy Input	5.1 kWh/t	10.1 kWh/t	20.1 kWh/t
Milling Time (min)	4.62 min	9.3 min	19.17 min
Power Draw (Watt)	84.1 W	82.7 W	80.2 W
Sieve size (µm)	Cumulative % Passing	Cumulative % Passing	Cumulative % Passing
212	99.99	99.92	99.99
150	99.87	99.78	99.99
106	99.34	99.50	99.91
75	95.73	98.33	99.75
53	85.13	93.49	99.29
38	71.70	83.94	98.09

Grind Size % Passing	Energy (kWh/t)	Time (min)
65	1.7	1.54
70	4.2	3.84
75	6.4	5.88
80	8.4	7.79
85	10.8	10.04

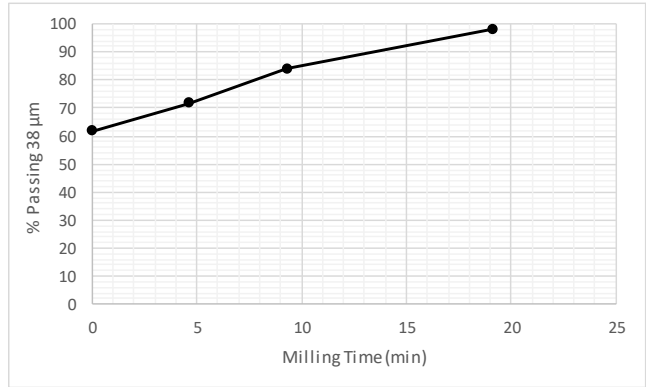
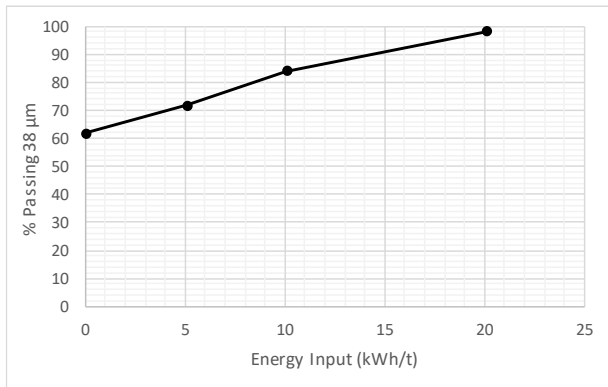


Table 85: Test N-6 Milling Data

Test N-6: Silica Flour - Pin Disc 400RPM

Average Power (Watt)

171.4 Watt

Energy Input	5.2 kWh/t	10.2 kWh/t	20.2 kWh/t
Milling Time (min)	2.3 min	4.5 min	9.02 min
Power Draw (Watt)	171.3 W	172.1 W	171 W
Sieve size (µm)	Cumulative % Passing	Cumulative % Passing	Cumulative % Passing
212	100.00	100.00	100.00
150	99.94	100.00	100.00
106	99.53	99.87	100.00
75	95.95	98.89	99.79
53	86.10	94.46	99.12
38	73.30	86.81	97.22

% Passing 38µm	Energy (kWh/t)	Time (min)
65	1.5	0.66
70	3.7	1.65
75	5.8	2.58
80	7.6	3.39
85	9.5	4.21

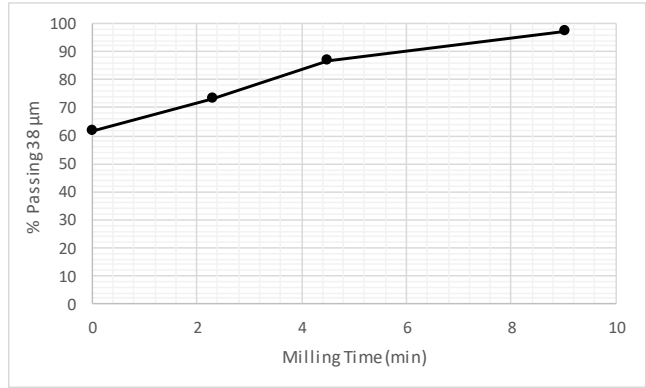
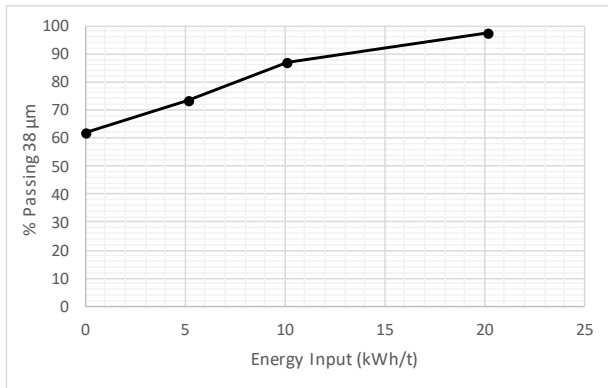


Table 86: Test N-7 Milling Data

Test N-7: Silica Flour - Ring Smooth 400RPM

Average Power (Watt)

60.2 Watt

Energy Input	5.1 kWh/t	10.1 kWh/t	20.1 kWh/t
Milling Time (min)	6.3 min	12.89 min	25.8 min
Power Draw (Watt)	61.4 W	59.7 W	59.5 W
Sieve size (μm)	Cumulative % Passing	Cumulative % Passing	Cumulative % Passing
212	100.00	100.00	99.95
150	100.00	99.82	99.91
106	99.49	99.63	99.85
75	95.99	98.45	99.59
53	84.06	93.07	98.70
38	71.25	83.05	96.06

Grind Size % Passing	Energy (kWh/t)	Time (min)
65	1.8	2.20
70	4.4	5.48
75	6.6	8.39
80	8.8	11.18
85	11.6	14.82

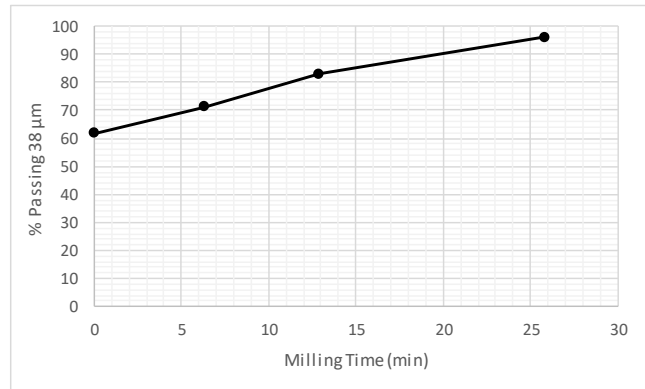
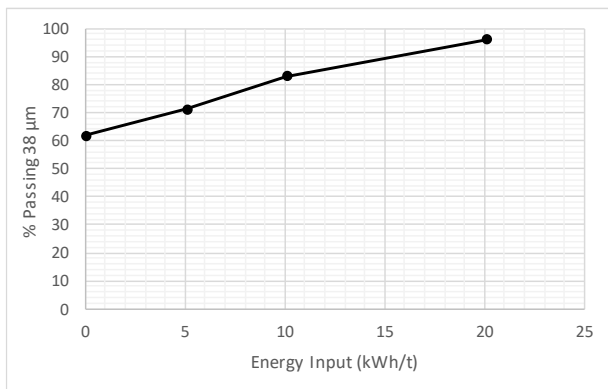


Table 87: Test N-8 Milling Data

Test N-8: Silica Flour - Ring Disc 400RPM

Average Power (Watt)

102.7 Watt

Energy Input	5.1 kWh/t	10.1 kWh/t	20.1 kWh/t
Milling Time (min)	3.74 min	7.49 min	15.24 min
Power Draw (Watt)	104.3 W	103 W	100.8 W
Sieve size (µm)	Cumulative % Passing	Cumulative % Passing	Cumulative % Passing
212	99.98	100.00	100.00
150	99.79	99.95	100.00
106	99.31	99.66	100.00
75	96.02	98.41	99.83
53	85.74	93.30	99.17
38	72.52	84.06	96.88

% Passing 38µm	Energy (kWh/t)	Time (min)
65	1.6	1.15
70	3.9	2.87
75	6.2	4.54
80	8.3	6.16
85	10.8	8.05

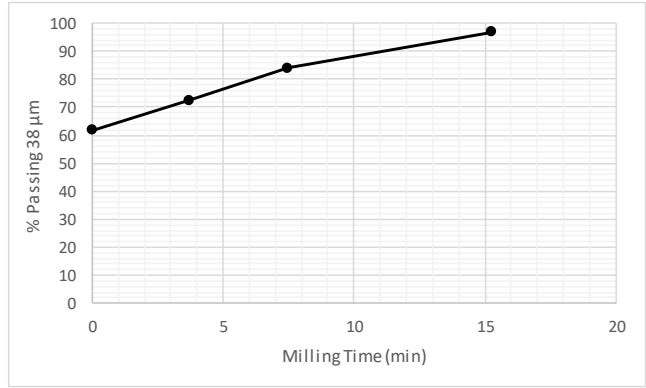
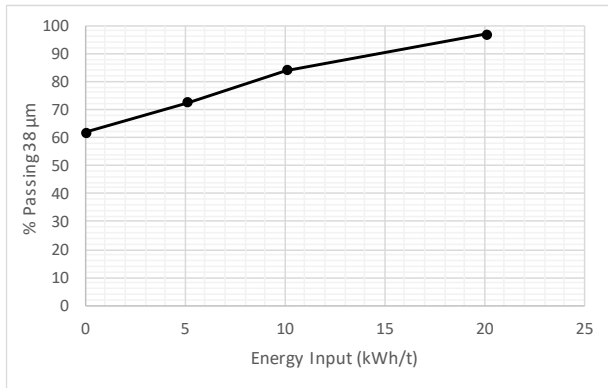


Table 88: Test N-9 Milling Data

Test N-9: Silica Flour - Pin Smooth 530RPM

Average Power (Watt)

112.7 Watt

Energy Input	5.2 kWh/t	10.2 kWh/t	20.1 kWh/t
Milling Time (min)	3.52 min	6.79 min	13.62 min
Power Draw (Watt)	111.2 W	114.1 W	113 W
Sieve size (µm)	Cumulative % Passing	Cumulative % Passing	Cumulative % Passing
212	100.00	100.00	100.00
150	99.91	99.94	99.98
106	99.60	99.78	99.97
75	97.07	98.65	99.96
53	88.49	94.48	99.80
38	75.08	86.55	99.00

% Passing 38µm	Energy (kWh/t)	Time (min)
65	1.3	0.88
70	3.2	2.19
75	5.1	3.50
80	7.3	4.92
85	9.4	6.34

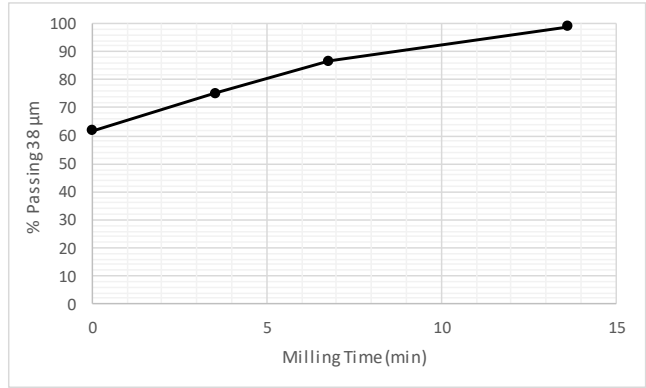
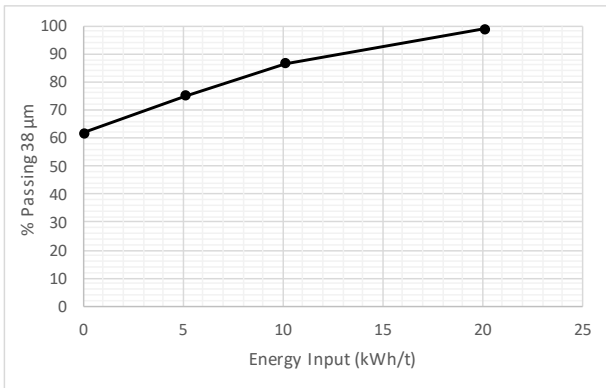


Table 89: Test N-10 Milling Data

Test N-10: Silica Flour - Pin Disc 530RPM

Average Power (Watt)

305.0 Watt

Energy Input	5.5 kWh/t	10.4 kWh/t	20.3 kWh/t
Milling Time (min)	1.4 min	2.59 min	4.95 min
Power Draw (Watt)	296.2 W	305.4 W	313.6 W
Sieve size (µm)	Cumulative % Passing	Cumulative % Passing	Cumulative % Passing
212	100.00	100.00	100.00
150	99.90	99.92	100.00
106	99.62	99.86	100.00
75	96.75	99.35	99.89
53	87.94	96.82	99.40
38	76.89	88.86	97.47

Grind Size % Passing	Energy (kWh/t)	Time (min)
65	1.2	0.31
70	3.0	0.77
75	4.7	1.23
80	6.7	1.71
85	8.7	2.20

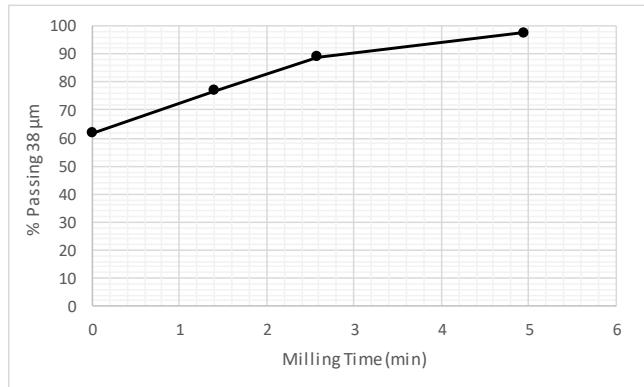
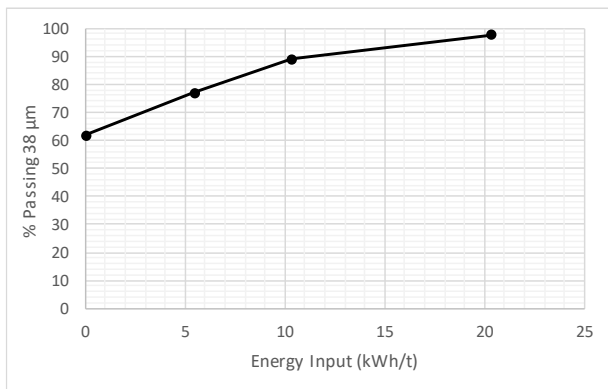


Table 90: Test N-11 Milling Data

Test N-11: Silica Flour - Ring Smooth 530RPM

Average Power (Watt)

94.3 Watt

Energy Input	5.1 kWh/t	10.1 kWh/t	20.1 kWh/t
Milling Time (min)	4.37 min	7.9 min	16.07 min
Power Draw (Watt)	89.4 W	97.8 W	95.8 W
Sieve size (µm)	Cumulative % Passing	Cumulative % Passing	Cumulative % Passing
212	100.00	99.99	100.00
150	99.86	99.96	99.99
106	99.50	99.81	99.88
75	96.96	98.78	99.70
53	87.05	94.74	99.39
38	73.47	86.54	97.94

Grind Size % Passing	Energy (kWh/t)	Time (min)
65	1.4	1.24
70	3.6	3.09
75	5.7	4.78
80	7.6	6.13
85	9.5	7.48

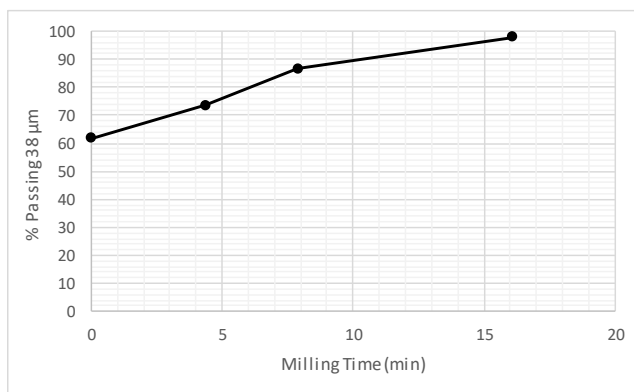
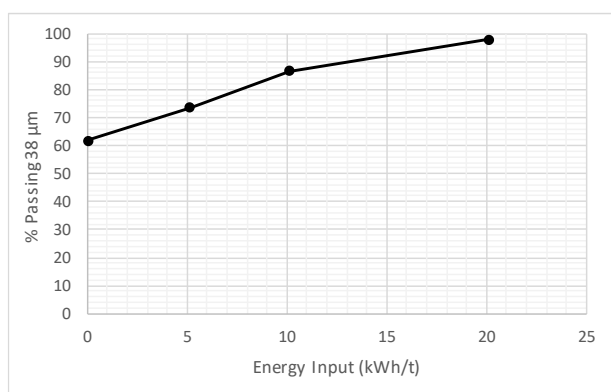


Table 91: Test N-12 Milling Data

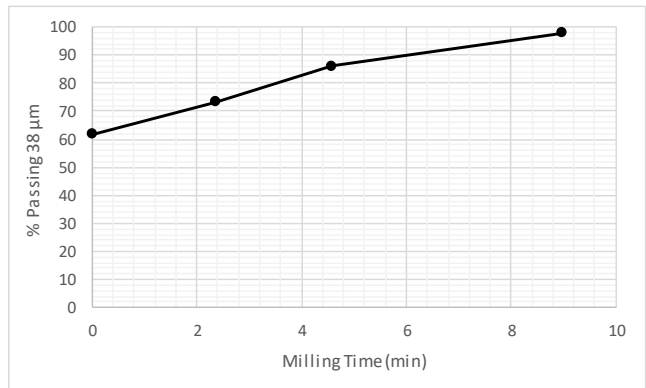
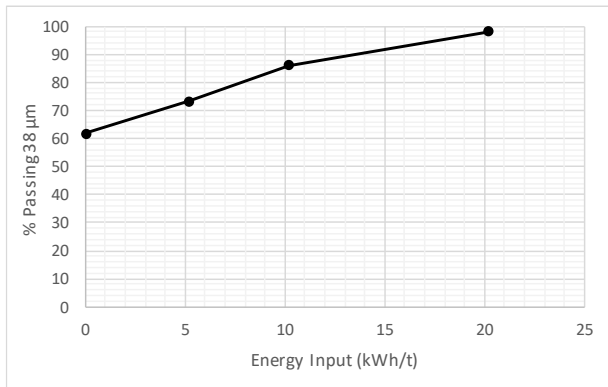
Test N-12: Silica Flour - Ring Disc 530RPM

Average Power (Watt)

170.1 Watt

Energy Input	5.2 kWh/t	10.2 kWh/t	20.2 kWh/t
Milling Time (min)	2.35 min	4.59 min	8.97 min
Power Draw (Watt)	168.3 W	170 W	172.1 W
Sieve size (µm)	Cumulative % Passing	Cumulative % Passing	Cumulative % Passing
212	100.00	100.00	100.00
150	99.91	100.00	100.00
106	99.48	99.87	100.00
75	96.31	99.05	100.00
53	86.08	95.02	99.61
38	73.38	86.09	97.99

% Passing 38µm	Energy (kWh/t)	Time (min)
65	1.5	0.67
70	3.7	1.67
75	5.8	2.64
80	7.8	3.51
85	9.7	4.39



7.12 DEM Virtual Prototyping

7.12.1 DEM Calibration Model Torque

Sim 1
COR 0.380
Friction 0.250

Time (sec)	Average Torque (N.m)
1	-2.070
2	-2.181
3	-2.248
4	-2.204
5	-2.086
6	-2.155
7	-2.061
8	-2.049
9	-2.046
10	-2.070
11	-2.075
12	-1.945
13	-2.070
14	-2.028
15	-2.126
16	-2.009
17	-1.972
18	-2.047
19	-2.109

Average	-2.082
---------	--------

Sim 2
COR 0.380
Friction 0.475

Time (sec)	Average Torque (N.m)
1	-2.372
2	-2.438
3	-2.481
4	-2.538
5	-2.487
6	-2.453
7	-2.510
8	-2.464
9	-2.518
10	-2.522
11	-2.511
12	-2.529
13	-2.547
14	-2.540
15	-2.440
16	-2.509
17	-2.409
18	-2.475
19	-2.399

Average	-2.481
---------	--------

Sim 3
COR 0.380
Friction 0.700

Time (sec)	Average Torque (N.m)
1	-2.673
2	-2.705
3	-2.746
4	-2.725
5	-2.619
6	-2.725
7	-2.649
8	-2.844
9	-2.602
10	-2.589
11	-2.739
12	-2.659
13	-2.668
14	-2.598
15	-2.570
16	-2.661
17	-2.620
18	-2.734
19	-2.622

Average	-2.671
---------	--------

Sim 4
COR 0.630
Friction 0.250

Time (sec)	Average Torque (N.m)
1	-2.094
2	-2.215
3	-2.033
4	-2.328
5	-2.064
6	-2.074
7	-2.123
8	-2.004
9	-1.996
10	-2.014
11	-2.007
12	-2.092
13	-2.159
14	-2.034
15	-1.999
16	-2.057
17	-1.938
18	-2.145
19	-1.956

Average	-2.070
---------	--------

Sim 5
COR 0.630
Friction 0.475

Time (sec)	Average Torque (N.m)
1	-2.369
2	-2.530
3	-2.471
4	-2.466
5	-2.439
6	-2.445
7	-2.444
8	-2.362
9	-2.355
10	-2.399
11	-2.478
12	-2.466
13	-2.478
14	-2.397
15	-2.472
16	-2.442
17	-2.396
18	-2.439
19	-2.409

Average	-2.435
---------	--------

Sim 6
COR 0.630
Friction 0.700

Time (sec)	Average Torque (N.m)
1	-2.509
2	-2.699
3	-2.654
4	-2.639
5	-2.682
6	-2.541
7	-2.677
8	-2.692
9	-2.571
10	-2.658
11	-2.607
12	-2.549
13	-2.628
14	-2.610
15	-2.670
16	-2.559
17	-2.631
18	-2.652
19	-2.671

Average	-2.626
---------	--------

Sim 7
COR 0.880
Friction 0.250

Time (sec)	Average Torque (N.m)
1	-2.017
2	-1.956
3	-2.066
4	-1.997
5	-1.994
6	-1.970
7	-1.938
8	-2.087
9	-2.074
10	-2.032
11	-1.947
12	-2.085
13	-1.954
14	-2.071
15	-1.945
16	-1.951
17	-2.011
18	-1.890
19	-1.836

Average	-1.991
---------	--------

Sim 8
COR 0.880
Friction 0.475

Time (sec)	Average Torque (N.m)
1	-2.255
2	-2.427
3	-2.451
4	-2.489
5	-2.414
6	-2.337
7	-2.390
8	-2.372
9	-2.430
10	-2.269
11	-2.297
12	-2.352
13	-2.326
14	-2.332
15	-2.307
16	-2.363
17	-2.455
18	-2.373
19	-2.460

Average	-2.374
---------	--------

Sim 9
COR 0.880
Friction 0.700

Time (sec)	Average Torque (N.m)
1	-2.438
2	-2.479
3	-2.451
4	-2.466
5	-2.561
6	-2.668
7	-2.530
8	-2.451
9	-2.404
10	-2.550
11	-2.388
12	-2.547
13	-2.453
14	-2.502
15	-2.544
16	-2.585
17	-2.490
18	-2.507
19	-2.433

Average	-2.497
---------	--------

Sim 10
COR 0.950
Friction 0.200

Time (sec)	Average Torque (N.m)
1	-1.809
2	-1.814
3	-1.867
4	-1.966
5	-1.881
6	-1.811
7	-2.135
8	-1.844
9	-1.806
10	-1.832
11	-1.716
12	-1.761
13	-1.852
14	-1.866
15	-1.814
16	-1.753
17	-1.836
18	-1.937
19	-1.735

Average	-1.844
---------	--------

Sim 11
COR 0.950
Friction 0.150

Time (sec)	Average Torque (N.m)
1	-1.610
2	-1.632
3	-1.677
4	-1.631
5	-1.632
6	-1.570
7	-1.669
8	-1.636
9	-1.627
10	-1.584
11	-1.573
12	-1.623
13	-1.689
14	-1.585
15	-1.609
16	-1.607
17	-1.666
18	-1.567
19	-1.615

Average	-1.621
---------	--------

Sim 12
COR 0.950
Friction 0.050

Time (sec)	Average Torque (N.m)
1	-1.096
2	-0.854
3	-0.870
4	-0.854
5	-0.801
6	-0.820
7	-0.878
8	-0.954
9	-0.903
10	-0.803
11	-0.860
12	-0.769
13	-0.903
14	-0.945
15	-0.914
16	-0.923
17	-0.856
18	-0.927
19	-0.830

Average	-0.882
---------	--------

Sim 13
COR 0.950
Friction 0.120

Time (sec)	Average Torque (N.m)
1	-1.537
2	-1.508
3	-1.459
4	-1.558
5	-1.468
6	-1.510
7	-1.530
8	-1.534
9	-1.459
10	-1.533
11	-1.476
12	-1.501
13	-1.443
14	-1.566
15	-1.509
16	-1.470
17	-1.539
18	-1.502
19	-1.470

Average	-1.504
---------	--------

Sim 14
COR 0.950
Friction 0.100

Time (sec)	Average Torque (N.m)
1	-1.544
2	-1.351
3	-1.327
4	-1.458
5	-1.425
6	-1.357
7	-1.435
8	-1.423
9	-1.334
10	-1.380
11	-1.465
12	-1.338
13	-1.435
14	-1.325
15	-1.333
16	-1.324
17	-1.459
18	-1.362
19	-1.389

Average	-1.393
---------	--------

Sim 15
COR 0.950
Friction 0.080

Time (sec)	Average Torque (N.m)
1	-1.264
2	-1.304
3	-1.408
4	-1.178
5	-1.126
6	-1.281
7	-1.224
8	-1.222
9	-1.208
10	-1.289
11	-1.214
12	-1.233
13	-1.232
14	-1.170
15	-1.214
16	-1.271
17	-1.292
18	-1.221
19	-1.207

Average	-1.240
---------	--------

7.12.2 DEM Calibration Model Charge Profiles

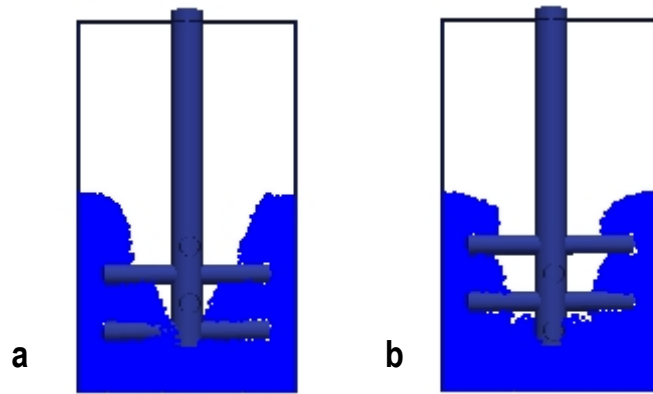


Figure 107: Simulation 1 Charge Profile a) view of x-axis b) view of y-axis

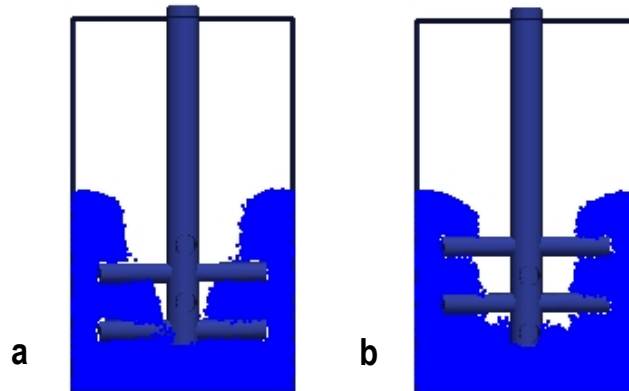


Figure 108: Simulation 2 Charge Profile a) view of x-axis b) view of y-axis

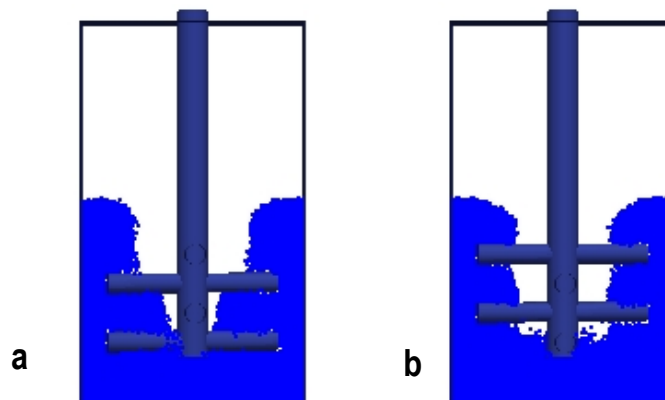


Figure 109: Simulation 3 Charge Profile a) view of x-axis b) view of y-axis

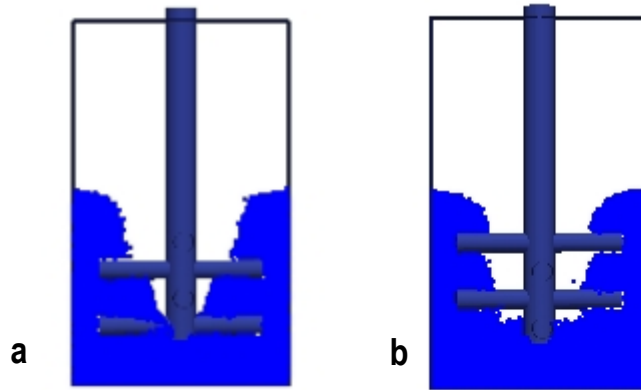


Figure 110: Simulation 4 Charge Profile a) view of x-axis b) view of y-axis

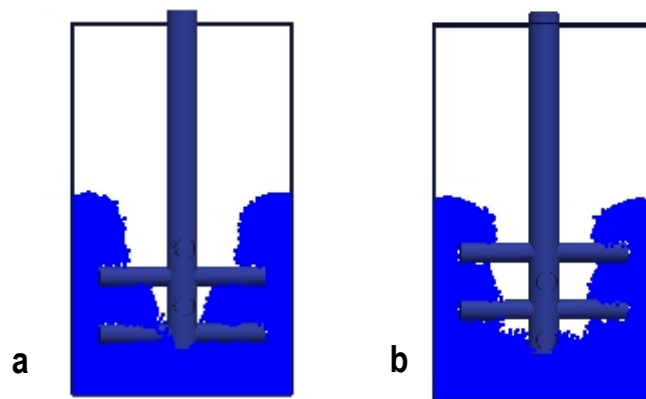


Figure 111: Simulation 5 Charge Profile a) view of x-axis b) view of y-axis

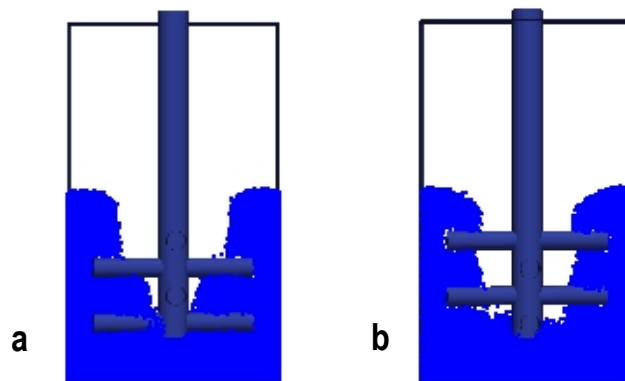


Figure 112: Simulation 6 Charge Profile a) view of x-axis b) view of y-axis

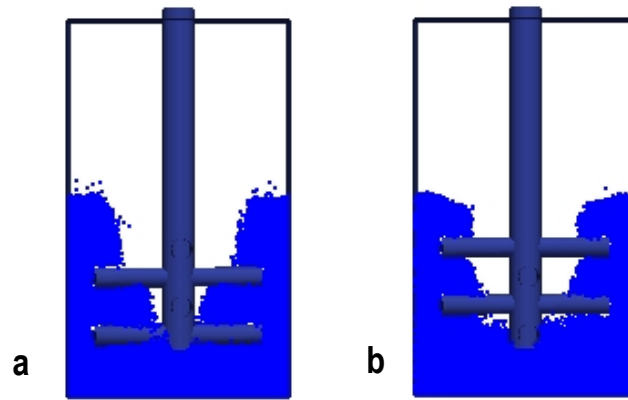


Figure 113: Simulation 7 Charge Profile a) view of x-axis b) view of y-axis

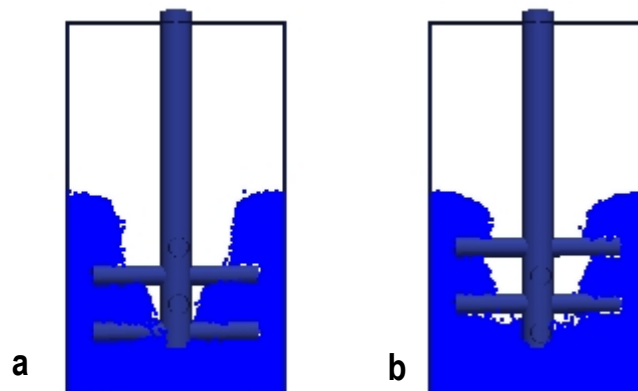


Figure 114: Simulation 8 Charge Profile a) view of x-axis b) view of y-axis

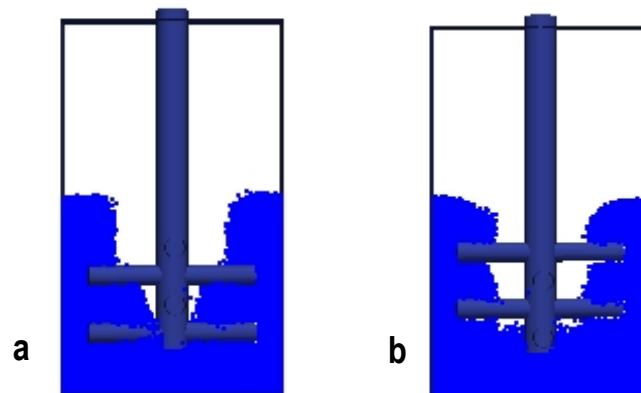


Figure 115: Simulation 9 Charge Profile a) view of x-axis b) view of y-axis

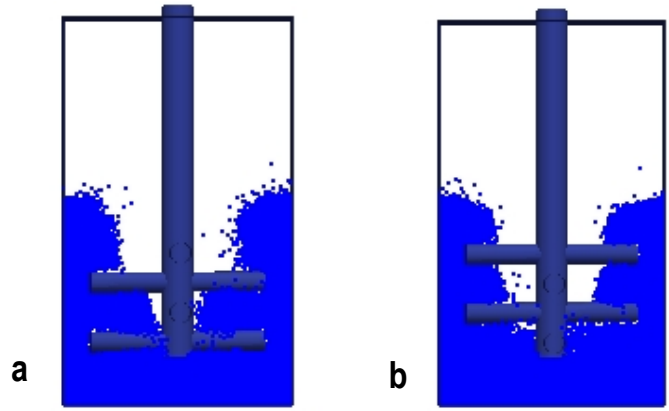


Figure 116: Simulation 10 Charge Profile a) view of x-axis b) view of y-axis

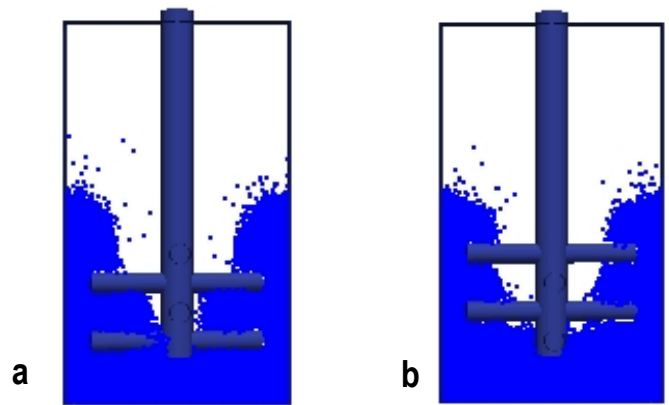


Figure 117: Simulation 11 Charge Profile a) view of x-axis b) view of y-axis

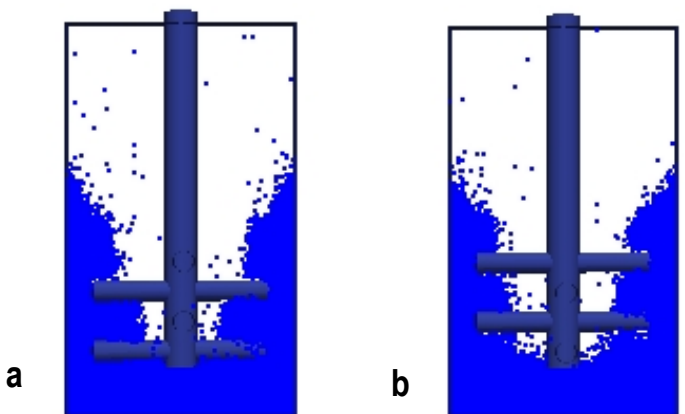


Figure 118: Simulation 12 Charge Profile a) view of x-axis b) view of y-axis

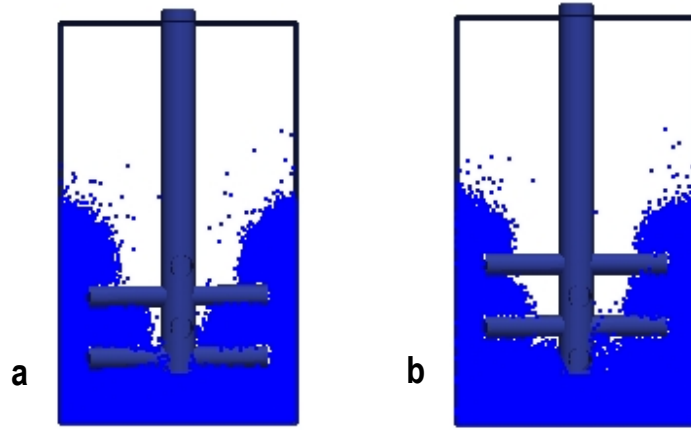


Figure 119: Simulation 13 Charge Profile a) view of x-axis b) view of y-axis

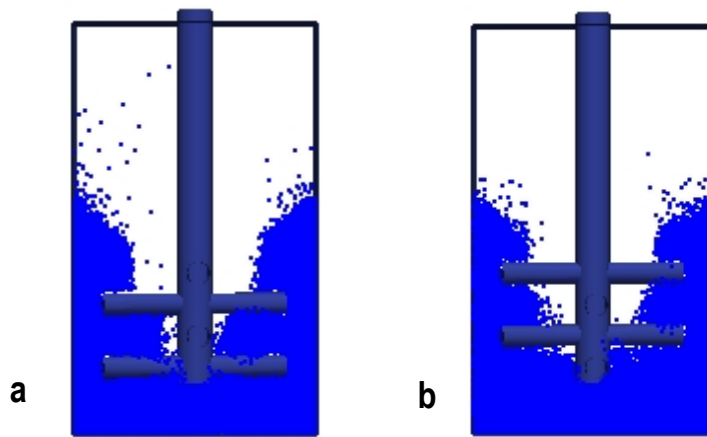


Figure 120: Simulation 14 Charge Profile a) view of x-axis b) view of y-axis

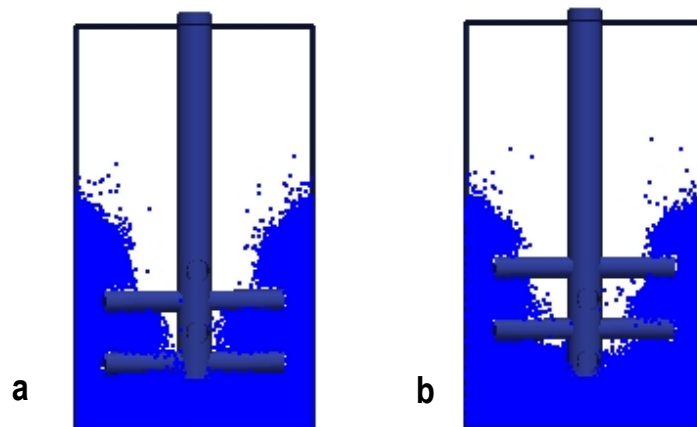


Figure 121: Simulation 15 Charge Profile a) view of x-axis b) view of y-axis

7.12.3 DEM Virtual Prototyping Simulations Model Torque

12 Pin Stirrer in Smooth Vessel

COR 0.950
Friction 0.090

Time (sec)	Average Torque (N.m)
1	-1.977
2	-2.001
3	-1.917
4	-1.869
5	-1.889
6	-1.780
7	-1.880
8	-1.831
9	-1.812
10	-1.928
11	-1.903
12	-1.802
13	-1.857
14	-1.907
15	-1.873
16	-1.874
17	-1.877
18	-1.916
19	-1.882

Average	-1.883
---------	--------

12 Pin Stirrer in Disc Vessel

COR 0.950
Friction 0.090

Time (sec)	Average Torque (N.m)
1	-1.983
2	-3.227
3	-3.210
4	-3.263
5	-3.448
6	-3.315
7	-3.390
8	-3.284
9	-3.250
10	-3.276
11	-3.374
12	-3.291
13	-3.292
14	-3.379
15	-3.391
16	-3.416
17	-3.325
18	-3.151
19	-3.376

Average	-3.244
---------	--------

Ring Stirrer in Smooth Vessel

COR 0.950
Friction 0.090

Time (sec)	Average Torque (N.m)
1	-1.247
2	-1.234
3	-1.284
4	-1.241
5	-1.208
6	-1.232
7	-1.270
8	-1.200
9	-1.264
10	-1.260
11	-1.194
12	-1.216
13	-1.224
14	-1.272
15	-1.268
16	-1.240
17	-1.333
18	-1.230
19	-1.277

Average	-1.247
---------	--------

Ring Stirrer in Disc Vessel

COR 0.950
Friction 0.090

Time (sec)	Average Torque (N.m)
1	-1.244
2	-1.749
3	-1.754
4	-1.742
5	-1.801
6	-1.853
7	-1.683
8	-1.789
9	-1.800
10	-1.825
11	-1.851
12	-1.799
13	-1.772
14	-1.864
15	-1.810
16	-1.800
17	-1.811
18	-1.812
19	-1.777

Average	-1.765
---------	--------

7.12.4 DEM Virtual Prototyping Simulations Charge Profiles

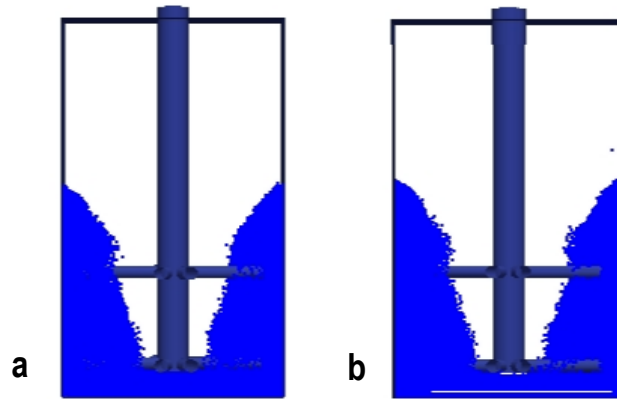


Figure 122: Pin in Smooth Virtual Prototyping Simulation a) view of x-axis b) view of y-axis

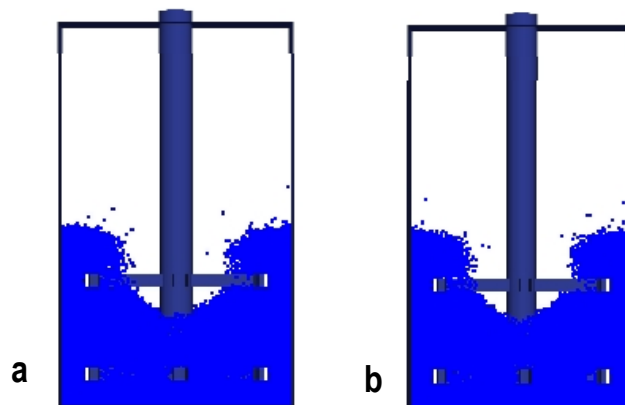


Figure 123: Ring in Smooth Virtual Prototyping Simulation a) view of x-axis b) view of y-axis

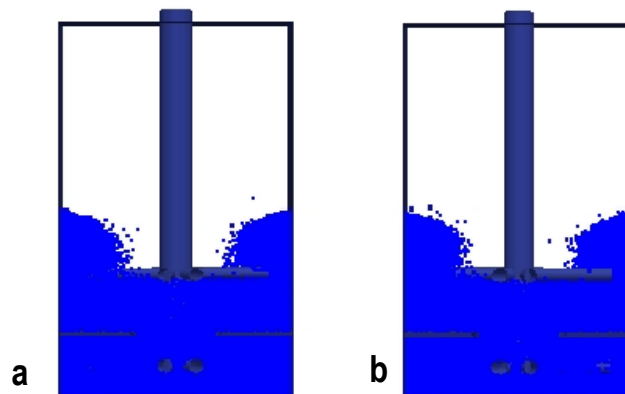


Figure 124: Pin in Disc Virtual Prototyping Simulation a) view of x-axis b) view of y-axis

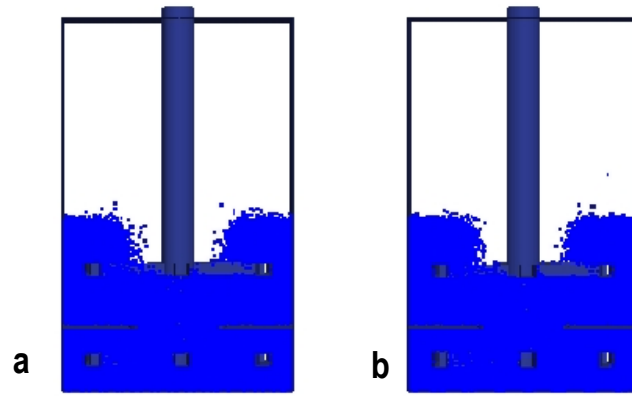


Figure 125: Ring in Disc Virtual Prototyping Simulation a) view of x-axis b) view of y-axis

7.13 DEM Re-calibrated Model

7.13.1 DEM Re-calibrated Model Simulations Torque

12 Pin Stirrer in Smooth Vessel

COR 0.950
Friction 0.450

Time (sec)	Average Torque (N.m)
1	-3.173
2	-3.150
3	-3.232
4	-3.184
5	-3.333
6	-3.367
7	-3.144
8	-3.189
9	-3.357
10	-3.202
11	-3.236
12	-3.160
13	-3.216
14	-3.322
15	-3.218
16	-3.306
17	-3.304
18	-3.294
19	-3.366

Average	-3.250
---------	--------

12 Pin Stirrer in Disc Vessel

COR 0.950
Friction 0.450

Time (sec)	Average Torque (N.m)
1	-2.821
2	-4.630
3	-4.728
4	-4.754
5	-4.708
6	-4.902
7	-4.992
8	-4.756
9	-4.859
10	-4.831
11	-4.678
12	-4.782
13	-4.741
14	-4.750
15	-4.900
16	-4.771
17	-5.034
18	-4.945
19	-4.821

Average	-4.705
---------	--------

Ring Stirrer in Smooth Vessel

COR 0.950
Friction 0.450

Time (sec)	Average Torque (N.m)
1	-2.484
2	-2.633
3	-2.652
4	-2.708
5	-2.579
6	-2.626
7	-2.620
8	-2.608
9	-2.581
10	-2.644
11	-2.623
12	-2.655
13	-2.643
14	-2.531
15	-2.501
16	-2.573
17	-2.495
18	-2.590
19	-2.548

Average	-2.594
---------	--------

Ring Stirrer in Disc Vessel

COR 0.950
Friction 0.450

Time (sec)	Average Torque (N.m)
1	-2.225
2	-3.671
3	-3.724
4	-3.868
5	-3.954
6	-3.965
7	-3.873
8	-3.884
9	-3.912
10	-3.831
11	-3.926
12	-3.857
13	-3.948
14	-3.897
15	-3.890
16	-3.934
17	-3.971
18	-3.817
19	-4.042

Average	-3.799
---------	--------

7.13.2 DEM Re-calibrated Model Simulations Charge Profiles

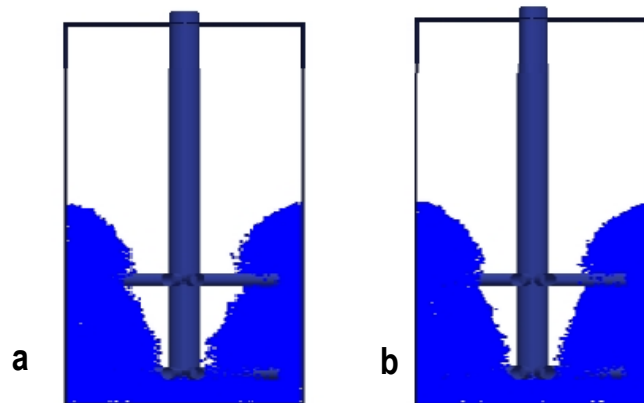


Figure 126: Pin in Smooth DEM Charge Profile a) view of x-axis b) view of y-axis

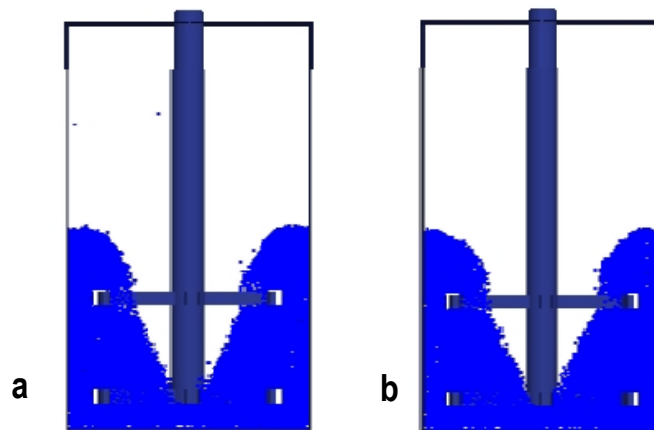


Figure 127: Ring in Smooth DEM Charge Profile a) view of x-axis b) view of y-axis

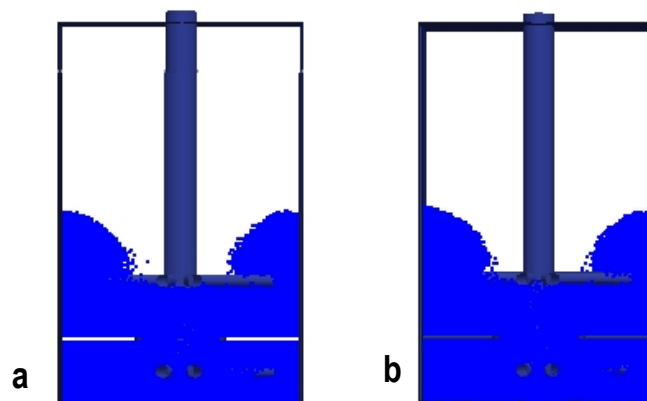


Figure 128: Pin in Disc DEM Charge Profile a) view of x-axis b) view of y-axis

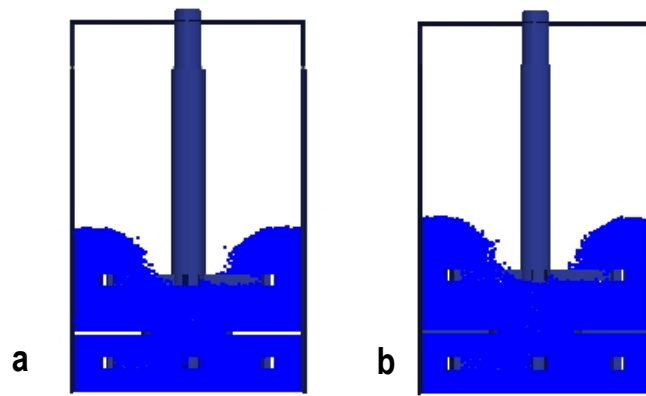


Figure 129: Ring in Disc DEM Charge Profile a) view of x-axis b) view of y-axis

7.14 Custom Post Processing Computer Codes Written for DEM modelling

7.14.1 Code for Calculating Per Second Average Torque

```
#include <fstream>
#include <ostream>
#include <istream>
#include <string>
#include <sstream>
#include <iostream>
#include <vector>
#include <cmath>
#include <sys/stat.h>
#include <unistd.h>
#include <math.h>

using namespace std;

//FUNCTION PROTOTYPES

double StrToDbl(string);           //converts string to double

int main () {

int counter = 0;
int length, position, max, time_int;
double T_sum,T_average, time_max, count_T;

vector <double> Torque(1);
vector <double> Time(1);

string a;

ifstream inputdata;
ofstream outputdata;

string word, infilename,outfilename;
infilename = "torque.txt";
outfilename = "seconds.txt";

//Determine number of entries and set up storage vectors

inputdata.open(infilename.c_str());

inputdata.seekg(0L,ios::beg);

    while (inputdata >> word)
    {
        // displaying content

        counter = counter + 1;

    }

inputdata.close();

cout << counter << endl;

length = (counter-5)/2;

Torque.resize(length);
Time.resize(length);
```



```

//Read data from file into storage

inputdata.open(infile.c_str());
inputdata.seekg(0L,ios::beg);

    for (int n = 0; n < 5; n++ ) {
        inputdata >> a;
        cout << a << endl;
    }

    for (int p = 0; p < length; p++ ) {
        inputdata >> a;
        Time[p] = StrToDbl(a);
        inputdata >> a;
        Torque[p] = StrToDbl(a);

        cout << Time[p] << " " << Torque[p]<< endl;
    }

inputdata.close();

//Determine the max time (sec) to calculate per second average to

time_max = floor(Time[length-1]);

max = static_cast<int>(time_max);

cout << time_max << endl;
cout << max << endl;

//Calculate and dump out average torque per second

outputdata.open(outfile.c_str());

outputdata << "Time (sec)" << " " << "Average Torque (N.m)" << "\n";

position = 0;
T_sum = 0;
count_T = 0;

time_int = static_cast<int>(Time[position]);

    for (int k = 0; k < max; k++ ) {

        if (time_int < (k+1)) {

            while(time_int < (k+1))
            {

                T_sum = T_sum + Torque[position];

                position = position + 1;

                count_T = count_T + 1;

                time_int = static_cast<int>(Time[position]);
            }
        }
    }

```

```

        T_average = T_sum /count_T;

        outputdata << k + 1 << " " << T_average << "\n";

        T_sum = 0;
        count_T = 0;

    } // end of if loop
} // end k for loop

outputdata.close();

return 0;
}

//FUNCTION DECLARATIONS

double StrToDbl(string si) {
    double i;
    stringstream ss(si); //turn the string into a stream
    ss >> i; //convert
    return i;
}

```

7.14.2 Code for Calculating Velocity Histograms

```
#include <fstream>
#include <ostream>
#include <istream>
#include <string>
#include <sstream>
#include <iostream>
#include <vector>
#include <math.h>

using namespace std;

//FUNCTION PROTOTYPES

int StrToInt(string);           //converts a string to an integer
string IntToStr(int);          //converts integer to string
double StrToDbl(string);       //converts a string to a double
string DblToStr(double);       //converts double to string

int main () {

//variables used in main

    double no_atoms;
    double vx,vy,vz,vsqr,v,v_avg;
    double v_totaliser=0;

    string infilename;
    ifstream infile;
    string outfilename;
    ofstream outfile;

    string a;

    vector <double> v_bead(1,0);
    vector <double> v_bin(1,0);
    vector <double> v_bin_count(1,0);

    double v_max = 4; //maximum velocity (m/s)
    double v_min = 0; //minimum velocity (m/s)
    double no_bins = 41; //number of bins
    double bin_inc = (v_max - v_min)/(no_bins-1); // calculates the
increment size for the bins

    string no_bins_s;
    int no_bins_i;

    no_bins_s = DblToStr(no_bins);
    no_bins_i = StrToInt(no_bins_s);

    v_bin.resize(no_bins_i);
    v_bin_count.resize(no_bins_i);

    v_bin[0] = v_min;

    for (int n = 1; n < no_bins_i; n++) //initialise the v_bin storage
vector with bin bottom velocities
    {
```

```

        v_bin[n] = v_bin[(n-1)]+bin_inc;
        v_bin_count[n] = 0;
    }

//DUMP OUT TO CHECK BINS ARE CORRECT

    outfilename = "velocity_bins.txt";
    outfile.open((outfilename.c_str()),std::ios_base::out);
    outfile <<"Velocity_bins_(m/s)"<< "\n";

    for (int p = 0; p < no_bins_i; p++)    //dump out values of all velocity
bins to text file
    {
        outfile << v_bin[p] << "\n";
    }

    outfile.close();

//read in data from bead.txt file that contains bead data for a specific
timestep

    infilename = "beads.txt";
    infile.open(infilename.c_str());
    infile.seekg(0L,ios::beg);

    infile >> a;
    infile >> a;
    infile >> a;
    infile >> a;
    infile >> a;
    infile >> a;
    infile >> a;
    infile >> a;

    no_atoms = StrToDbl(a);    // number of beads

    string no_atoms_s;
    int no_atoms_i;

    no_atoms_s = DblToStr(no_atoms);
    no_atoms_i = StrToInt(no_atoms_s);

    v_bead.resize(no_atoms_i);

    for (int n = 0; n < 30; n++)    //read in for 30 entries to pass the
headings section
    {
        infile >> a;
    }

    outfilename = "velocity_bead_xyz.txt";
    outfile.open (outfilename.c_str());
    outfile <<"vx"<< " " << "vy" << " " << "vz" << "\n";

```

```

    for (int n = 0; n < no_atoms_i; n++) //read in velocity data for each
bead
    {

        for (int k = 0; k < 5; k++) //read in for 5 entries to
get to velocities
        {
            infile >> a;
        }

        infile >> a;
        vx = StrToDbl(a); // velocity component along x-axis
        infile >> a;
        vy = StrToDbl(a); // velocity component along y-axis
        infile >> a;
        vz = StrToDbl(a); // velocity component along z-axis

        //DUMP TO CHECK VELOCITY IS READ IN CORRECTLY

        outfile << vx << " " << vy << " " << vz << "\n";

        vsqr = (vx*vx)+(vy*vy)+(vz*vz);
        v = sqrt(vsqr);

        v_bead[n] = v;

        for (int j = 0; j < 8; j++) //read in for 8 entries to
get to end of data
        {
            infile >> a;
        }

    } // end read in for loop

    outfile.close();
    infile.close();

    outfilename = "velocity_bead.txt";
    outfile.open (outfilename.c_str());
    outfile <<"Velocity_ (m/s)"<< "\n";

    for (int p = 0; p < no_atoms_i; p++) //dump out values of all bead
velocities
    {
        outfile << v_bead[p] << "\n";
    }

    outfile.close();

//Calculate average velocity

    for (int n = 0; n < no_atoms_i; n++) //calculate average velocity
    {
        v_totaliser = v_totaliser + v_bead[n];
    }

    v_avg = v_totaliser/no_atoms;

```

```

outfilename = "average_velocity.txt";
outfile.open (outfilename.c_str());
outfile <<"Average_velocity" << "\n";
outfile << v_avg << "\n";
outfile.close();

//loop through all velocity bins and bead data and "count" bead velocities to
bins

    for (int z = 0; (z < (no_bins_i-1)); z++)    //loop through all bins
    {
        for (int n = 0; n < no_atoms_i; n++)    //loop through beads
        {
            if ((v_bead[n] >= v_bin[z])&&(v_bead[n] < v_bin[z+1]))
            {
                v_bin_count[z] = v_bin_count[z] + 1;
            }
        }
    }

//for the last bin that only has a lower limit

        for (int n = 0; n < no_atoms_i; n++)    //loop through beads
        {
            if (v_bead[n] >= v_bin[(no_bins_i-1)])
            {
                v_bin_count[(no_bins_i-1)] =
v_bin_count[(no_bins_i-1)] + 1;
            }
        }

    outfilename = "velocity_histogram.txt";
    outfile.open (outfilename.c_str());
    outfile <<"Velocity_(m/s)"<< " " << "count" << "\n";

    for (int p = 0; p < no_bins_i; p++)    //dump out values of all bead
velocities
    {
        outfile << v_bin[p] << " " << v_bin_count[p] << "\n";
    }

    outfile.close();

return 0;
}

//FUNCTION DEFINITIONS
int StrToInt(string si) {
    int i;
    stringstream ss(si); //turn the string into a stream
    ss >> i; //convert
    return i;
}

string IntToStr(int a) {
    stringstream ss;
    ss << a;

```

```
string str = ss.str();  
return str;  
}
```

```
double StrToDbl(string sd) {  
    double d;  
    stringstream ss(sd); //turn the string into a stream  
    ss >> d; //convert  
    return d;  
}
```

```
string DblToStr(double a) {  
    stringstream ss;  
    ss << a;  
    string str = ss.str();  
    return str;  
}
```

7.15 Silica Flour Data Sheet



OMEGA FINE PRODUCTS (PTY) LTD

ADDRESS: 128 Pebble Street, Clayville ext 14,
 Olifantsfontein, 1666, Gauteng, South Africa.
 POSTAL: P.O. Box 1239, Olifantsfontein, 1665, South Africa
 TELEPHONE: 011 316 2064 / 5727

PRODUCT SPECIFICATION SHEET

SILICA 150 (S15) (-150 MICRON)

CHEMICAL ANALYSIS	%
Calcium CaO	0.00
Magnesium MgO	0.00
Silicon SiO ₂	98.50
Sodium Na ₂ O	0.03
Potassium K ₂ O ₂	0.05
Titanium TiO ₂	0.14
Alumina Al ₂ O ₃	0.80
Iron Fe ₂ O ₂	0.09
L.O.I	0.25
PHYSICAL PROPERTIES	NORM
pH	6.30
Moisture	< 0.20%
Oil Absorption	16g/100g
Hardness moh	7.00
Specific Gravity	2.7
PARTICLE SIZING	NORM
250 MICRON	0.00%
150 MICRON	99.80%
75 MICRON	85.00 -87.00%
45 MICRON	63.00 – 73.00%
25 MICRON	40.00 – 44.00%

This information is a guidance only. No guarantee is given or implied. Company disclaims any liability arising from damage or consequential loss.